AD NUMBER

AD833232

LIMITATION CHANGES

TO:

Approved for public release; distribution is unlimited.

FROM:

Distribution authorized to U.S. Gov't. agencies and their contractors; Critical Technology; APR 1968. Other requests shall be referred to Air Force Flight Dynamics Laboratory, Attn: FDTS, Wright-Patterson AFB, OH 45433. This document contains export-controlled technical data.

AUTHORITY

AFFDL ltr, Jan 1974

AFFDL-TR-68-75

HYDROGEN TANKAGE APPLICATION TO MANNED AEROSPACE SYSTEMS PHASES II & III

Volume I. Design and Analytical Investigations

John H. Heathman, et al

Convair Division of General Dynamics

Technical Report AFFDL-TR-68-75 , Volume I
April 1968

Air Force Flight Dynamics Laboratory
Air Force Systems Command
Wright-Patterson Air Force Base, Ohio, 45433

171

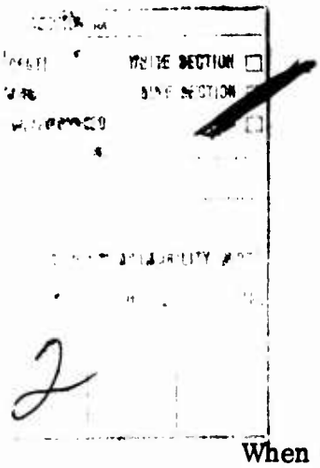

NOTICES

When Government drawings, specifications, or other data are used for any purpose other than in connection with a definitely related Government procurement operation, the United States Government thereby incurs no responsibility nor any obligation whatsoever; and the fact that the Government may have formulated, furnished, or in any way supplied the said drawings, specifications, or other data is not to be regarded by implication or otherwise as in any manner licensing the holder or any person or corporation, or conveying any rights or permission to manufacture, use, or sell any patented invention that may in any way be related thereto.

This document is subject to special export controls and each transmittal to foreign governments or foreign nationals may be made only with prior approval of the Air Force Flight Dynamics Laboratory.

Copies of this report should not be returned unless return is required by security considerations, contractual obligations, or notice on a specific document.

HYDROGEN TANKAGE APPLICATION TO MANNED AEROSPACE SYSTEMS PHASES II & III

Volume I. Design and Analytical Investigations

John H. Heathman, et al

FOREWORD

This is Volume I of three volumes prepared as the Final Report on Phases II and III of a three phase program, performed by Convair division of General Dynamics, San Diego, California, under Contract AF33(615)-2048 during the period from September 1965 to March 1968. Final Report for the Phase I period, July 1964 to September 1965, was AFFDL-TR-65-230. This report was submitted April 1964 under Report No. GDC-DCB68-008 for approval.

AFFDL-TR-68-75	Hydrogen Tankage Application to Manned Aerospace Systems
Volume I	Design and Analytical Investigations
Volume II	Manufacturing
Volume III	Structural Acceptance and Flight Simulation Testing

The work was administered under the direction of the Air Force Flight Dynamics Laboratory, Structures Division, by Mr. L. R. Phillips, FDTS, Project Engineer.

Project leader for Convair on this program was Mr. J. H. Heathman, under the administration of Mr. R. A. Nau, Manager of Advanced Launch and Reentry Systems. Task leaders were Mr. J. L. Lester, Testing, and Mr. J. C. Hopkins, Manufacturing Operations. Others who contributed in studies and preparation of report include Messrs: G. Yates, Thermodynamics; W. Egli, Fuel and Insulation Systems; A Fujimoto, Structural Design; and J. F. Fischer, Structural Analysis.

This technical report has been reviewed and approved.

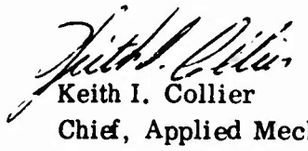

Keith I. Collier
Chief, Applied Mechanics Branch
Structures Division
Air Force Flight Dynamics Laboratory

ABSTRACT

This is Volume I of three volumes of the final report of Phases II and III of a three phase program to design, fabricate and experimentally verify non-integral, insulated, liquid hydrogen tankage for advanced aerospace systems. The vehicle, mission data, fuel quantity and usage rates, and tankage configuration were supplied by the Structures Division of the Air Force Flight Dynamics Laboratory. This volume presents the design criteria and ground rules, design of the tankage systems structure, insulation and fuel system together with analytical investigations supporting these designs. The design of this 6,000 gallon liquid hydrogen tank is representative of a half-scale version of that which might be employed for a Mach 6 hypersonic cruise vehicle application and incorporates most of the significant aspects of the tankage system which have influence on its overall performance. The tank has a "Siamese" configuration; consisting of a main shell, 20 feet in length, with a cross-section of two intersecting circles, 64 inches in diameter and an 8-foot total width, enclosed by ellipsoidal dome bulkheads. The structure is of pressure membrane construction, aligned to a maximum operating pressure of 30 psig, with frame stiffening of the cylindrical shells to prevent collapse under the unpressurized condition. Skins are allowed to buckle elastically. The tank support system, located at the main frames, allows for the movement of the tank around a single fixed point within the vehicles hot structure. The tanks thin gage, 0.016, structural material is Alloy 718, a nickel-base heat resistant superalloy, employed primarily in the aged condition. The insulation employed is an all-Microquartz system in a helium environment, distributed around the tank in such a manner as to provide maximum protection of the fuel. The fuel system employs a booster pump to handle saturated fuel conditions and a vent manifold system to ensure good distribution of the boiloff gas for upper tank wall cooling. The designing requirements were established as a result of the Phase I work which included the development of a thermal performance and weight synthesis computer program employed for system optimization. This computer program was updated and used to provide evaluation of slush-hydrogen, thermal performance of the designed tank, and optimization of a vehicle-size tankage system.

TABLE OF CONTENTS

LIST OF ILLUSTRATIONS

LIST OF ILLUSTRATIONS (CONTINUED)

LIST OF ILLUSTRATIONS (CONTINUED)

LIST OF TABLES

1

INTRODUCTION

Studies on advanced aerospace vehicles employing liquid hydrogen as a fuel have clearly pointed up the tankage system as a major problem area in the establishing of realistic weight penalties for storage and feasibility of fabrication. The problems arise as a direct result of some of the unusual characteristics of liquid hydrogen, which include its extremely low density, highly volatile nature, low boiling temperature, and high coefficient of thermal expansion. Little knowledge existed on hydrogen's thermal behavior under the adverse environmental conditions involved or for horizontal tankage applications. This technology area significantly influences the tankage system design and thermal performance.

In 1964, the Air Force Flight Dynamics Laboratory contracted the Convair division of General Dynamics to design, fabricate, and functionally demonstrate a large volume, lightweight, non-integral LH_2 tankage system applicable to a Mach 6 manned hypersonic cruise vehicle, Reference 1. The program was organized in such a manner that the tankage concepts and optimization procedures developed could be applied to all classes of hydrogen fueled hypersonic vehicles capable of sustained cruising in the sensible atmosphere or re-entry from orbital altitudes. The major obstacle to attaining the goals of this effort was the design and fabrication of a leak-tight tankage system capable of withstanding the severe environment associated with the flight simulation testing and, at the same time, achieve the light weight, thermal efficiency, and high reliability required to perform 500 repeated mission cycles.

This volume presents the design criteria and groundrules; design of the tankage systems structure, insulation and fuel system together with the analytical investigations supporting these designs. The design of this 6,000 gallon liquid hydrogen tank is representative of a half-scale version of that which might be employed for a Mach 6 hypersonic cruise vehicle application and incorporates most of the significant aspects of the tankage system which have influence on its overall performance. The tank has a "Siamese" configuration; consisting of a 20-foot main shell, with a cross-section of two intersecting circles, 64 inches in diameter and an 8-foot total width, enclosed by ellipsoidal dome bulkheads. The structure

is of pressure membrane construction, aligned to a maximum operating pressure of 30 psig, with frame stiffening of the cylindrical shells to prevent collapse under the unpressurized condition. Skins are allowed to buckle elastically. The tank support system, located at the main frames, reacts all inertia loading on the tankage system while reducing structural and thermal redundancy between the tank and vehicle structure to a minimum. The tank structural material is thin gage, 0.016, Alloy 718, a nickel base heat-resistant superalloy, employed primarily in the aged condition. The insulation employed is a permeable all-quartz system in a helium environment, distributed around the tank in a manner to provide maximum protection of the fuel. The fuel system employs a booster pump to handle saturated fuel conditions and a vent manifold system to ensure good distribution of the boiloff gas for upper tank wall cooling. Design requirements were established as a result of the Phase I work which included the development of a thermal performance and weight synthesis computer program employed for system optimization. This computer program was updated and used to evaluate slush-hydrogen, the thermal performance of the test tank, and the optimization of a vehicle-size tankage system. These studies are documented in this volume.

Phase I of this work, Reference 2, was reported on in AFFDL-TR-65-230, "Hydrogen Tankage for Hypersonic Cruise Vehicles - Phase I", dated August 1966. Manufacturing and testing are reported on in Volumes II and III respectively of this report.

2

DESIGN CRITERIA AND GROUND RULES

2.1 VEHICLE CONFIGURATION AND MISSION DATA

Vehicle configuration and mission data were supplied by the AFFDL and are typical of a Mach 6 manned hypersonic cruise vehicle. The representative vehicle is shown in Figure 1. The non-integral, insulated tankage system is shown located in the forward fuselage section at a given station of 40 feet back from the nose. This forward section of the fuselage is described as an elliptical cone with an 8 degree half angle in the profile view and a 10 degree half angle in the plan view. The flight angle of attack during cruise was given as 5 degrees.

The velocity and altitude profiles associated with this vehicle are given in Figure 2. The vehicle was to have a 30 minute ground-hold time after being disconnected from the fuel supply and a 90 minute flight time. The vehicle climbs to an altitude of 100,000 feet and then cruises at Mach 6 for a total range of 5000 nautical miles. The letdown and landing portions of the flight were not considered. The atmospheric pressure and temperature associated with the altitude profile was determined from the 1962 standard atmosphere tables. The tankage system fuel usage rate was scaled from the vehicle requirements and are shown in Figure 3. Depletion of usable fuel occurred at the end of cruise.

2.2 TEMPERATURE TRAJECTORY

Based on the above mission data and vehicle geometry, equilibrium skin temperatures were calculated along the trajectory on the top, bottom, and side of the fuselage. Equilibrium temperatures at Station 40 are shown in Figure 4. Temperatures from Station 30 to 50 vary by only about 30°; since this variation is not considered significant, a constant temperature along the fuselage length was assumed. The fuselage was divided into upper and lower zones for the purpose of analysis and test. The upper and lower temperature profiles as a function of time are shown in Figure 5. Since the fuselage structure is assumed to be an all metal honeycomb with no insulation, temperature drop through the fuselage structure was assumed to be negligible.

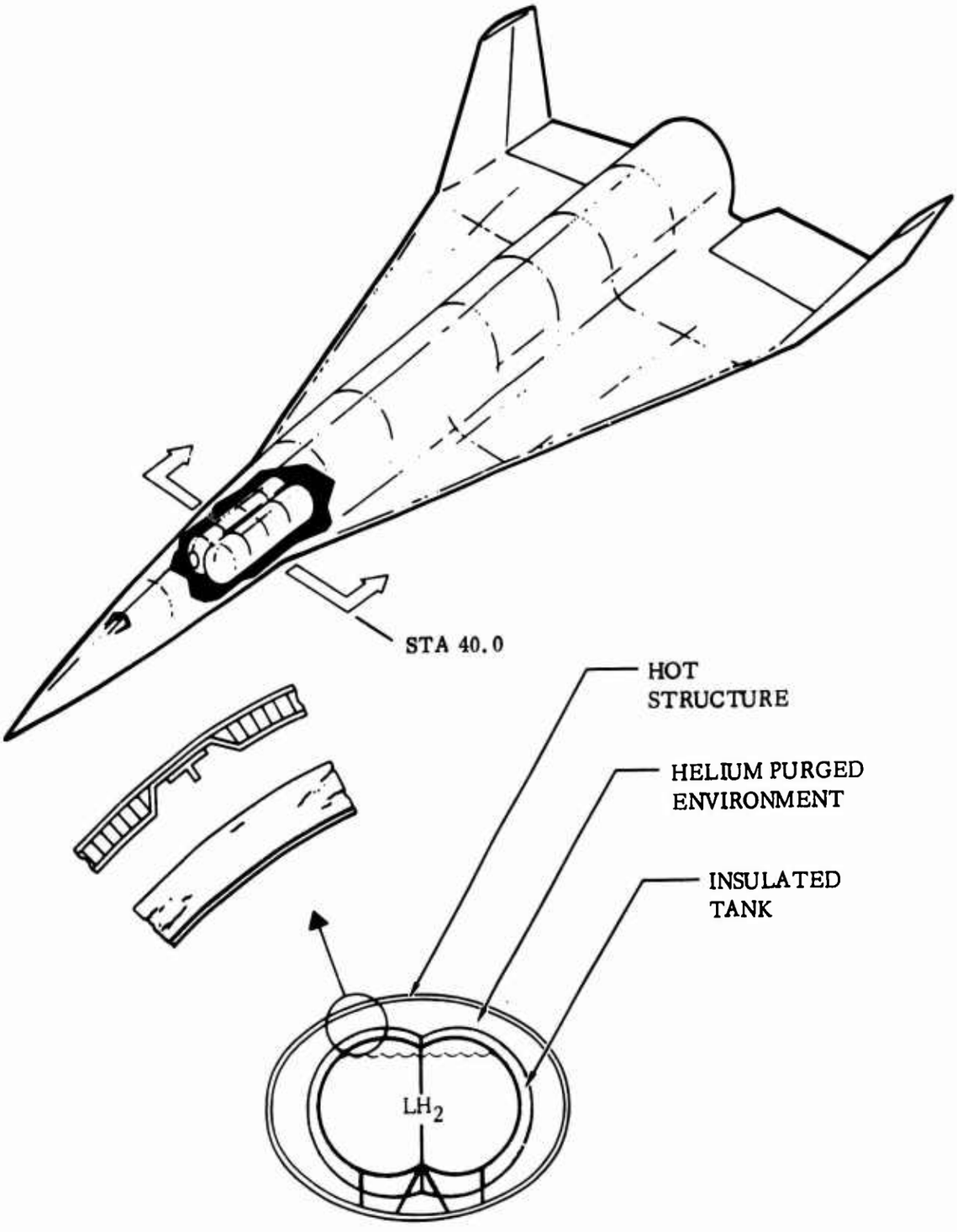

Figure 1. Representative Vehicle Configuration

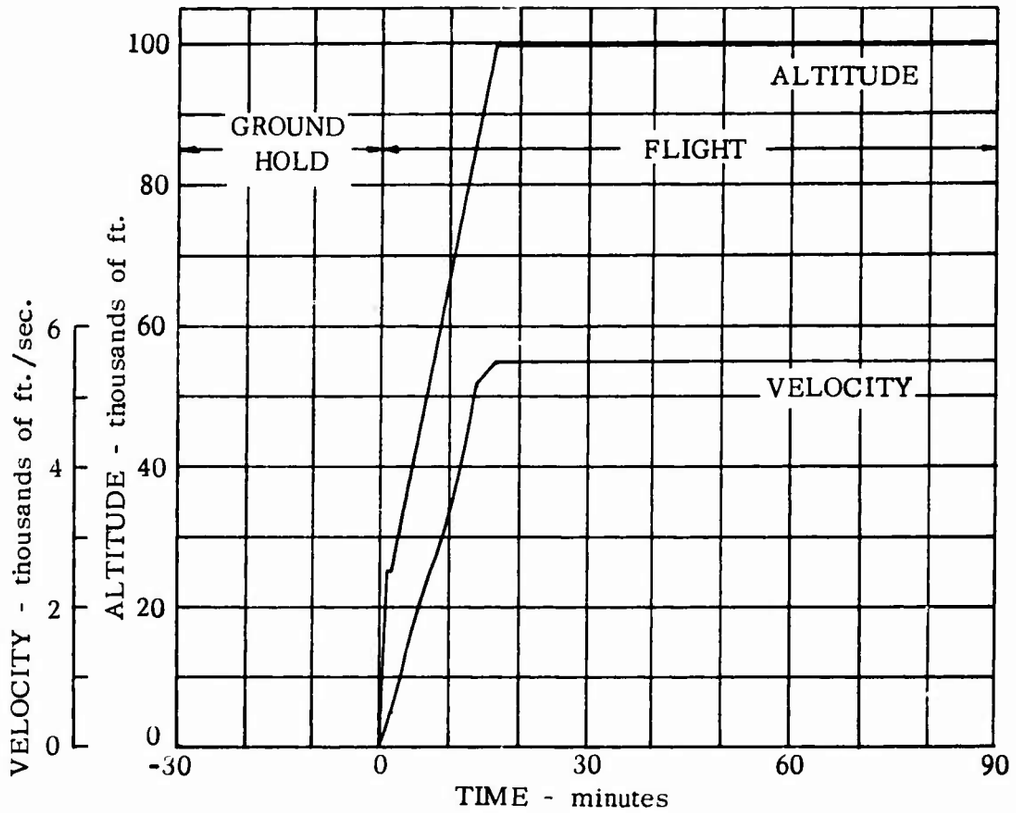

Figure 2. Velocity and Altitude Profile

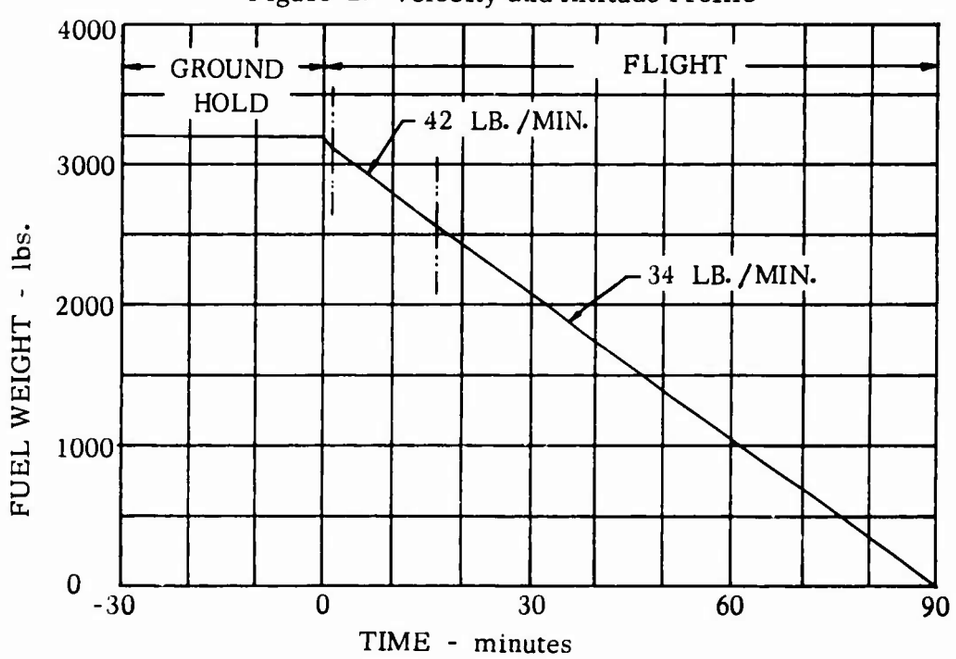

Figure 3. Tankage System Fuel Usage

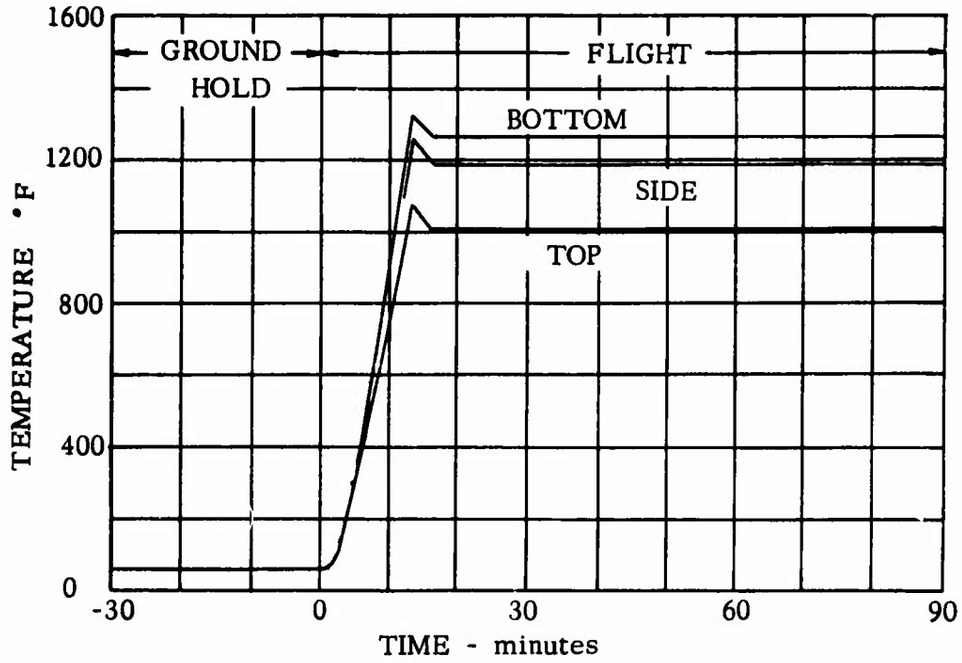

Figure 4. Equilibrium Skin Temperatures

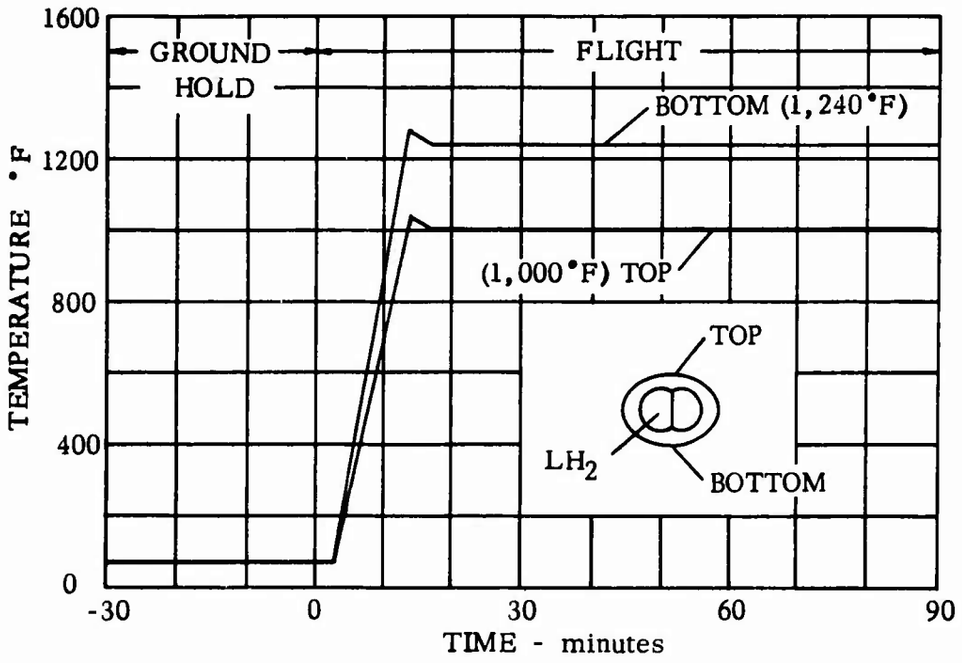

Figure 5. Simulated Temperature Profile

Heat is transferred from the fuselage to the tank insulation primarily by convection during ground-hold and by radiation during the cruise portion of the flight. A dry inert environment of helium is contained between the tank and vehicle structure and assumed to be at the same pressure as the outside environment.

2.3 TANK SIZE AND CONFIGURATION

The tankage system is a 6,000 gallon half-scale version of a vehicle size tank and is non-integral with the vehicle structure. It has a "Siamese" configuration consisting of a main shell, 20 feet in length, with a cross-section of two intersecting circles, 64 inches in diameter and a 8 foot total width, enclosed by ellipsoidal dome bulkheads. This configuration, Figure 6, provides for high volume utilization within the vehicle while maintaining an efficient pressure vessel shape.

2.4 STRUCTURAL CRITERIA

The tank supports and fittings were designed to withstand the critical ground, flight, and test conditions specified below.

2.4.1 BASIC GROUND RULES. Supplied ground rules from AFFDL were as follows:

a. The tankage shall be non-integral.

b. Internal pressurization shall not be required to support any of the applied loads during fueling, ground-hold, and taxi operations.

c. Material allowable strength values shall be based on room temperature properties except where elevated temperatures are encountered. That is, no advantage shall be taken of increased material strength at temperatures below room temperature.

d. The structure shall endure a service life of 500 missions without any failure.

2.4.2 OPTIMUM PARAMETERS AND CONDITIONS. From the results of studies, testing, and an optimization program on the overall system performed in Phase I the following parameters and conditions were established as optimum for this specific tankage system application:

a. Alloy 718 as the structural material.

b. A maximum operating pressure of 30 psig.

c. A frame stiffened structural concept for the tank cylindrical sections.

d. Elastic instability of any structural component shall not be regarded as a failure so long as the applied loading can redistribute into alternative load paths having sufficient strength to prevent them from yielding under limit load and from failure under ultimate load.

2.4.3 LOADS AND TEMPERATURES. The design loading and temperature conditions are given below. Unless otherwise specified for any particular condition, the indicated load factors can act together in all possible combinations. The sign convention used here is depicted in Figure 6.

a. LIMIT LOADS shall be defined as the maximum loads to which the structure will actually be subjected at any time during service. There must not be any yielding of the structure when limit loading is applied.

b. ULTIMATE LOADS shall be defined as the product obtained through the multiplication of limit loads by the appropriate factor of safety. The structure must not experience any failure when subjected to ultimate loads.

c. ULTIMATE FACTOR OF SAFETY shall be 1.5 except for the burst pressure condition for which it shall be 2.0.

d. FATIGUE - the structure shall endure a service life of 500 missions without failure.

2.4.3.1 Handling, Fill, Ground-Hold and Taxi.

a. HANDLING	LIMIT CONDITION
Liquid Content:	Empty
Temperature:	Room ($70^{o}F$)
Pressure:	0 psig
N_x =	± 1.0
N_y =	± 1.0
N_z =	0, -2.0

These load factors act independently.

b. TANK FILL AND GROUND-HOLD	LIMIT CONDITION
Liquid Content:	Empty to full of LH_2
Temperature:	-420 to $40^{o}F$ (see Figure 7)
Pressure:	$0 - 15^{+2}_{-1}$ psig
N_x =	0
N_y =	0
N_z =	-1.0

c. TAXI — LIMIT CONDITION

Liquid Content:	Full to empty of LH_2
Temperature:	-420 to 60°F (see Figure 7)
Pressure:	$0 - 15^{+2}_{-1}$ psig
N_x =	+0.5, -0.8
N_y =	± 0.5
N_z =	0, -2.0

2.4.3.2 Flight and Crash Conditions.

a. FLIGHT — LIMIT CONDITION

Liquid Content:	Full to empty of LH_2
Temperature:	-420 to 400°F (see Figure 7)
Pressure:	$15^{+2}_{-1} - 30^{+2}_{-1}$ psig
N_x =	± 0.5
N_y =	± 0.5
N_z =	0, -2.0

b. CRASH — ULTIMATE CONDITION (only for the supports and related carry-through structure)

Liquid Content:	Full to empty of LH_2
Temperature:	-420 to 400°F (see Figure 7)
Pressure:	15^{+2}_{-1} psig
N_x =	+1.5, -3.0
N_y =	± 1.5
N_z =	+2.0, -4.5

These load factors act independently.

2.4.3.3 Maximum Pressure Loading Condition

a. BURST PRESSURE — ULTIMATE CONDITION

Liquid Content:	Full to empty of LH_2
Temperature:	Room (70°F)
Pressure:	60 psig

N_x =	0
N_y =	0
N_z =	-1.0

2.4.3.4 Test Conditions. Evaluation of suitable test methods resulted in the choice of the following:

a. PROOF-PRESSURE TEST

Liquid Content:	Full of water (in addition, the entire tank is immersed in water)
Temperature:	Room ($70^{\circ}F$)
Pressure:	40 psig
N_x =	0
N_y =	0
N_z =	-1.0

b. UNPRESSURIZED TANK BENDING CAPABILITY TEST

Liquid Content:	0 to 12.1 inches of water
Temperature:	Room ($70^{\circ}F$)
Pressure:	0
N_x =	0
N_y =	0
N_z =	-1.0

c. CRYOGENIC SHOCK AND PRESSURE CYCLING*

Liquid Content:	0 to 8 inches of liquid nitrogen
Temperature:	$-320^{\circ}F$
Pressure:	0 to 30 psig*
N_x =	0
N_y =	0
N_z =	-1.0

*Repeated six times, five of the pressure cycles had a pressure hold-time of 5 minutes and the last cycle 90 minutes.

2.4.3.5 Temperatures, Liquid Levels and Pressure Variation. The temperature gradients, liquid levels, and pressure variations associated with a nominal mission cycle are shown in Figures 7 and 8.

2.5 INSULATION SYSTEM CRITERIA

The insulation system shall conform to the following design criteria:

a. The insulation system shall have a service life of 500 normal missions without refurbishment or major repair.

b. The insulation must be removable and capable of withstanding flexing of the tank and loads introduced by thermal effects.

c. Localized damage to the insulation must be repairable in the field without disturbing the undamaged portion of the system.

d. All supports and connections to the tanks are to be capable of connection or disconnection without disturbance of the basic tank insulation.

2.6 FUEL SYSTEM CRITERIA

Significant criteria for fuel system design are:

a. Operational Requirements

1. 30-minute ground-hold while disconnected from any ground support facilities.
2. Fuel flow schedule (scaled from Reference 1) to meet 90 minutes of usable fuel flow to engine (Figure 8)
3. 3245 lbs of usable fuel
4. 500 flight minimum system life

b. Environment

1. Ambient pressure vs. time to conform to vehicle trajectory using ARDC Model Atmosphere.
2. Inert helium gas atmosphere in space between tank and vehicle structure.
3. Compartment temperature range from below ambient to 1300°F (Figure 5).
4. Tank internal environment temperature: from -420°F to upper temperature limit of 400°F (Figure 7).
5. Pressure: 0 to 30 psig.

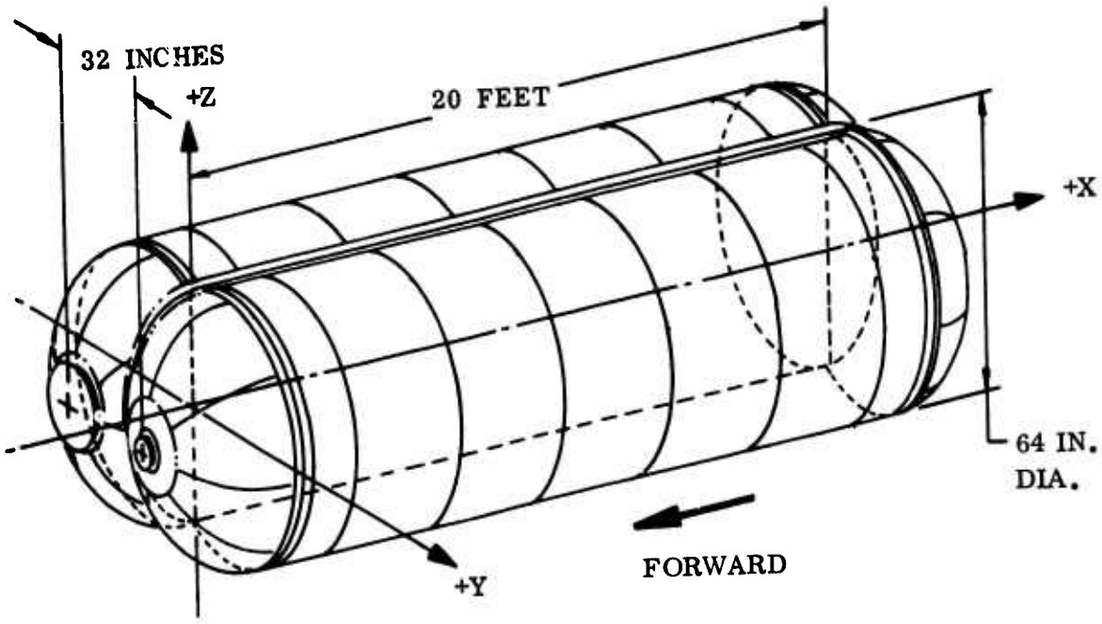

Figure 6. Tankage Configuration and Sign Convention

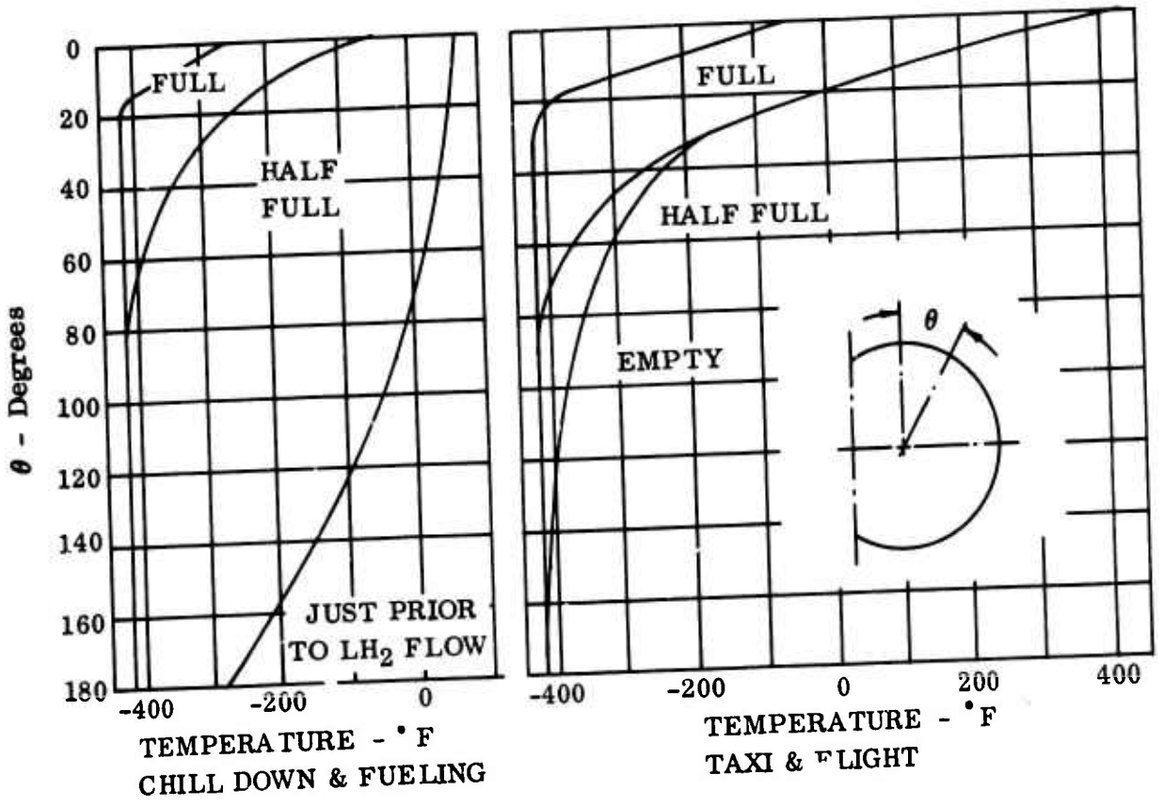

Figure 7. Temperature vs. θ for Various Design Condition

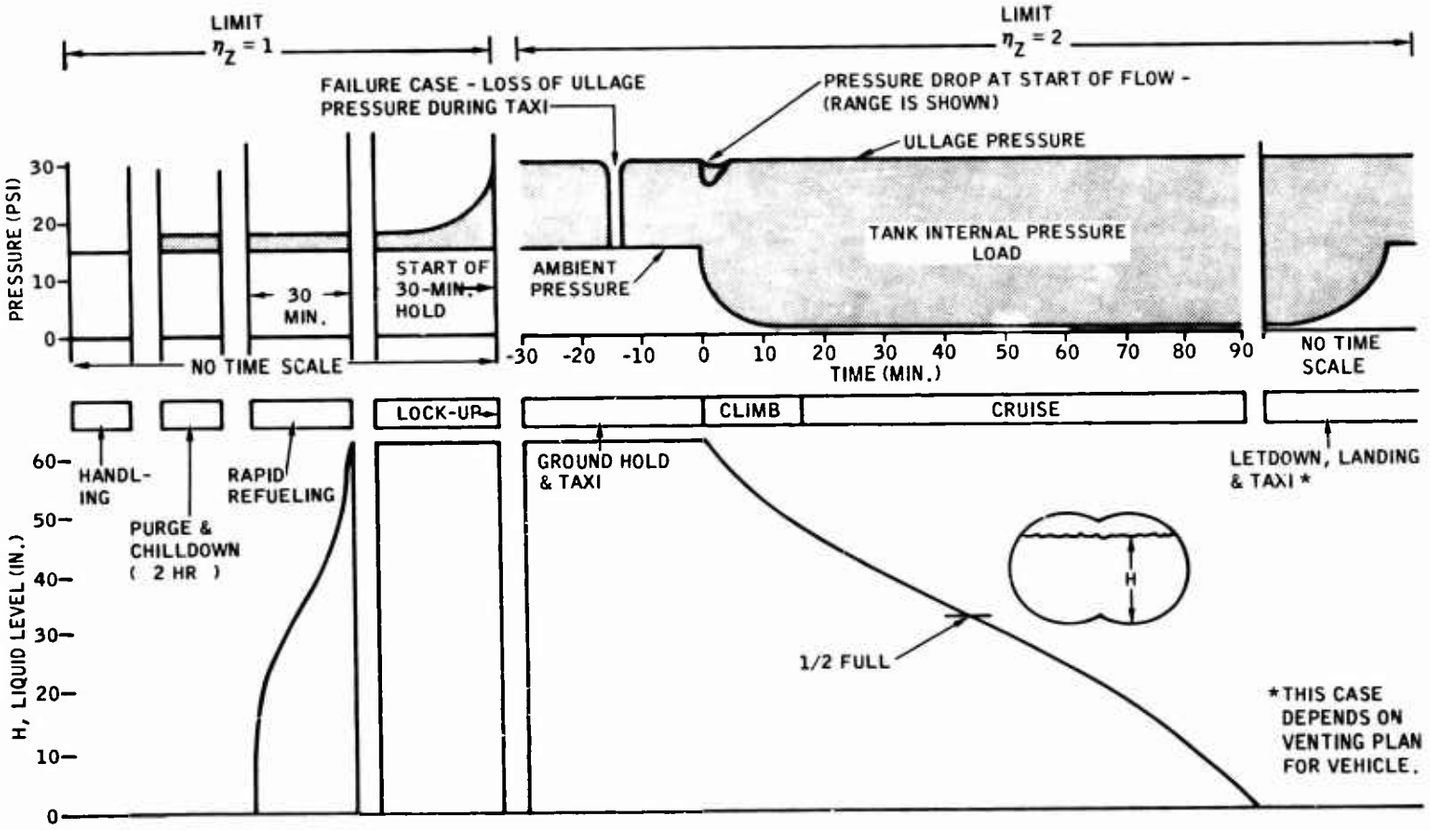

Figure 8. Liquid Level and Pressure vs. Time

3

STRUCTURAL MATERIAL - ALLOY 718

Alloy 718, a nickel-base heat-resistant superalloy, was chosen as the tank structural material on the basis of evaluation studies carried out in Phase I. This age-hardenable wrought alloy was introduced by the Huntington Division of the International Nickel Co., in 1959, to fill the need for a wrought material having medium high temperature capability with good weldability. This alloy was also found to have good properties at cryogenic temperatures. The sluggish response of the alloy to age-hardening permits welding without spontaneous hardening as a result of the heating and cooling cycles. This characteristic is also advantageous in other fabrication processes. The material condition determined as most suitable for this tankage application was 30 percent cold-rolled plus aged, but restrictions on its availability from the mill due to the short procurement lead times and limited quantities involved precluded its application on this program. The aged hardened condition of Alloy 718 was primarily employed in the tank design with some limited application of the solution-annealed condition. The age-hardening heat treatment employed was that determined as optimum for cryogenic applications. This alloy has excellent strength and toughness throughout the associated temperature range and good fabricability once correct procedures have been established.

3.1 METALLURGY

The chemical composition of this alloy differs from other nickel-base superalloys in its class by the addition of columbium and iron and reduction in its aluminum and titanium content. This provides for increased weldability with some loss in its high temperature capability. The properties and microstructure of this alloy are sensitive to the chemical composition and heat treatment employed and is still being studied in order to provide optimum heat treat procedures and chemical composition control for specific applications and fabricability requirements.

3.1.1 HEAT TREATMENT. The solution-anneal and age-hardening heat treatments determined as optimum for this application were established by extensive in-house evaluation studies, performed in 1964 (Reference 3), and are covered by GD/Convair specifications, 0-71038 for sheet, strip and plate; and 0-71037 for bars and forgings. These heat treatments are similar to and now replaced by AMS Specifications 5597 and 5664, which were developed for applications "requiring high strength at cryogenic temperatures and short time use up to 1000° F."

The heat treatments employed were:

Annealing -

Heating to 1950° F, holding this temperature for sufficient time to obtain uniform temperature in the material, followed by cooling to room temperature at a rate equivalent to air cool or faster.

Age-Hardening -

(a) heating to 1350° F
(b) holding at 1350° F ±25° F for 8 hours
(c) furnance cooling to 1200° F (cooling rate not critical)
(d) holding at 1200° F ±25° F until the total of (b), (c), (d) is 18 hours
(e) air cool

A large amount of the existing material data on Alloy 718 was not truly applicable to this program due to the differing heat treatments employed. The early development work done with this material employed a simplified single temperature age-hardening heat treatment which has now been replaced by improved duplex heat treatment procedures. Also, the solution anneal heat treatment temperature is significantly different which again influences the resulting material data. To identify the heat treatment involved with any given physical and mechanical properties data the following abbreviated callouts will be employed.

Ann. 1950° F + AGE 1350° F/1200° F

Alloy 718 is also susceptible to attack by elements such as sulphur, lead, bismuth, etc., during heat treatment and requires good cleaning measures to be taken to remove foreign materials such as grease, oils, paints, etc. Cleanliness is also important during welding operations.

3.1.2 DIMENSIONAL STABILITY. This alloy contracts during the process at a linear rate of approximately 0.001 inch per inch dependent upon the initial material condition.

3.2 AVAILABILITY AND PROCUREMENT

The Alloy 718 material was available and procured in the form of sheet, strip, plate, bar and forgings. The small quantities required of any gage, size or form and the fact that this alloy was still in the development stage made procurement of this material a difficult task. In order to support the tank fabrication task within the scheduled time span the majority of the material ordering was made on an off-the-shelf basis. This resulted in many differing material heats, adverse sheet and bar stock sizes, and severe limitations on the desired tolerance control on thickness and surface finish.

Choice of an 0.016 inch gage as minimum for fabrication purposes and its use in an aged condition were the result of an early evaluation of material procurement limitations.

Material evaluation studies had shown the 30% CR (cold-rolled) and aged condition of the Alloy 718 had the best attributes as the tank structural material but extended material procurement lead time, limited quantity requirements and the lack of sufficient material data to support good material specifications precluded its consideration for this program. Whereas, an 0.010 inch material gage in the 30% CR and aged condition is considered applicable to a production program the reduction in material strength associated with the aged condition and present limitations on surface finish and tolerance control on thickness resulted in the choice of an 0.016 inch minimum fabrication gage.

Tolerance control less than the AISI standard, ±10% of nominal for thin gages, does not appear feasible with the annealed and aged conditions of this material neither does improvement in the surface finish. Both improvement in tolerance control and surface finish are accomplished by cold roll passes using polished rolls which naturally cold works the material. The Atlas and Centaur programs, both of which employ thin gage material, require a tolerance control on an 0.016 gage of ±0.0005 which is obtained through the use of a Sendzimir Mill, whereas, the procured material for this program had a deviation from nominal of ±0.002. The normal fabrication difficulties associated with thin gages was further compounded by this limitation.

Restricted lengths of sheet material available, 96 inches instead of the desired 144 inches, also adversely affected the design and consequent fabrication of the tank. This required the intermediate frames and cylindrical skins lengths be obtained by fusion buttwelding together shorter lengths of the material.

The Alloy 718 material for this program was procured under GD/Convair specifications: 0-71038, for sheet, strip and plate; and 0-71037, for bars and forgings. These have now been replaced by equivalent Specifications AMS 5597 and AMS 5664 respectively. These specifications cover both the annealed and annealed plus age-hardened heat treat conditions specified in Section 3.1 as well as the guaranteed mechanical properties.

		F_{ty} - psi	F_{tu} - psi	e - %
Annealed	<0.187	80,000 Max.	140,000 Max.	30 Min.
	>0.187	90,000 Max.	150,000 Max.	40 Min.
Age Hardened		150,000 Min.	180,000 Min.	15 Min.

The history and chemical analysis of the procured material for this program is given in Table I along with size, quantity and part application. Table II summarizes the "certificate of test" room temperature mechanical properties of this material which conformed to both Convair and AMS specifications.

Considerably more material was required than originally anticipated in order to support the development of acceptable weld schedules, provide test specimens for verification of tooling and weld procedures and have sufficient spare subassemblies and parts to circumvent schedule delays. A total of 4812 lbs of Alloy 718 material was procured and used to support the fabrication of a tank structure whose final weight was 985 lbs. Whereas, over 1700 lbs of this excess weight was involved in machining the bar stock and forgings and 550 lbs in obtaining gore details and a spare dome assembly at least 900 lbs of material was required to support the development of weld schedules.

The desired material finish (2B) for this program required by ordering specification on the thin gages, could not be provided by present mill-processing. Photo micrographs of the "as-received" sheet material at a magnification of 500X revealed considerable surface roughness, Figure 9, and slight intergranular attack. None of the methods used to improve the surface finish, which included vapor honing, pickling and hand sanding, resulted in any significant improvement in this finish. In addition, it was necessary to take mixed lots of sheet material from various existing stocks in order to meet schedule. A variety of scratches, dings, canned and abraded areas were found in the material, "as-delivered," probably due to off-the-shelf buying method and its limited supply.

3.3 PHYSICAL PROPERTIES

Considerable physical property data for Alloy 718 was required to support the tank design. Much of this required data was not available at the time of the design and assumed values on the basis of similar materials was employed. As correct data became available its influence was determined and the information updated. Thermal conductivity (K) and specific heat (c_p) data for Alloy 718 was required to support the structural and thermal analysis of the tankage system.

Thermal expansion data were used to determine the relative movement of the tank with respect to the vehicle structure under the extreme temperature differentials and the magnitude of thermal stresses that develop in the tank structure as a result of temperature gradients. Figure 10 gives the thermal expansion (α) to temperature relationship that was employed during this program.

The density of Alloy 718 has been given as 0.296 lbs/cu.in. for the solution-annealed condition and 0.297 lbs/cu.in. for the age-hardened temper. The slight difference between the two material conditions is credited to a 0.001 in/in linear

Table I. History and Chemical Analysis of Alloy 718 Material as Received

Material Use	Tank Cyl, Center Web and Frames					Bulk-head	Main Frame "Y" Ring Splice		
Gage/Size	.016					.018	.040		
Quantity (lbs) Used	635	189	135	15	15	759	487	124	111
Supplier*	(1)	(1)	(2)	(2)	(2)	(1)	(3)	(3)	(2)
Heat No.	8006E	7950EV	E96034	E95348	E96155	8008EV	C50217	C50216	5995
Spec.**	(5)	(6)	(5)	(5)	(5)	(5)	(5)	(5)	(5)
Chemistry (Wt %)									
C	.04	.04	.056	.043	.060	.04	.04	.04	.033
Mn	.19	.15	.02	.05	.02	.17	.06	.05	.09
Fe	19.19	19.01	Bal	Bal	Bal	19.16	Bal	Bal	Bal
S	.007	.007	.003	.004	.008	.007	.01	.01	.006
Si	.30	.28	.14	.30	.07	.32	.07	.07	.20
Cu	.06	.05	.03	.03	.02	.05	.08	.07	.02
Ni	51.92	52.13	52.47	53.80	53.58	52.02	51.82	51.88	52.70
Cr	18.63	18.57	18.33	18.60	18.22	18.64	19.05	18.82	18.95
Al	.45	.55	.43	.47	.46	.43	.48	.46	.47
Ti	.86	.95	1.03	1.06	1.08	.95	1.00	.97	.87
Co	.07	.06	.05	.05	.06	.07	.13	.15	.06
Mo	3.14	3.05	2.96	2.09	2.95	3.08	2.98	3.04	3.03
Cb+Ta	5.12	5.12	5.04	5.01	5.03	5.04	5.21	5.17	5.10
P	.009	.008	.004	.004	.012	.009	.005	.004	.009
B	.0027	.003	.0033	.0031	.0030	.0024	.005	.004	.004

*Suppliers: (1) A. M. Castle & Co.
(2) Alloy Specialties
(3) Techalloy
(4) Carlton Forge

**Specifications: (7) GDC 0-71037 Bar and Forging
(5) GDC 0-71038 Sheet, Strip & Plate
(6) RBO-70-039 Rev. E

Table I. History and Chemical Analysis of Alloy 718 Material as Received (continued)

Material Use	Tank Door	Tank Door Doublers	"Y" Ring Splice			"Y" Ring/Support Fittings		Tank Door	Door
Gage/Size	.020	.032	.048			2x2 Bar		23.2OD x 19.2ID x 1.7	21.40Dx 16.5IDx1.0
Quantity Used (lbs)	28	135	56	189.5	101.3	913	588	202	128.5
Supplier*	(2)	(2)	(3)	(2)	(2)	(2)	(2)	(4)	(4)
Heat No.	5618	5953	C50216	5995	5748	6028	6042	50805	50805
Spec. **	(5)	(5)	(5)			(7)		(7)	
Chemistry (Wt %)									
C	.043	.038	.04	.033	.047	.034	.038	.04	
Mn	.13	.09	.05	.09	.08	.12	.10	.06	
Fe	Bal	Bal	Bal	Bal	Bal	Bal	Bal	Bal	
S	.001	.004	.01	.006	.005	.002	.002	.003	
Si	.16	.12	.07	.20	.16	.08	.13	.15	
Cu	.02	.03	.07	.02	.02	.02	.03	.03	
Ni	52.40	52.50	51.88	52.7	52.80	52.40	52.30	51.20	
Cr	18.50	18.90	18.82	18.95	18.90	18.50	19.45	18.27	
Al	.45	.50	.46	.47	.50	.49	.50	.65	
Ti	.94	.92	.97	.87	1.00	.89	.92	1.10	
Co	.20	.30	.15	.06	.60	.09	.09	.20	
Mo	3.06	3.10	3.04	3.03	3.02	3.10	2.98	3.07	
Cb+Ta	5.22	5.10	5.17	5.10	5.17	5.17	5.19	5.31	
P	.004	.005	.004	.009	.003	.003	.005	-	
B	.003	.004	.004	.004	.004	.003	.004	-	

*Suppliers: (1) A. M. Castle & Co
(2) Alloy Specialties
(3) Techalloy
(4) Carlton Forge

**Specifications: (5) GDC 0-71038 Sheet, Strip and Plate
(6) RBO-70-039 Rev. "E"
(7) GDC 0-71038 Bar and Forging

Table II. Room Temperature Mechanical Properties of Alloy 718

	Tank Cylinder, Center Web and Frames					Bulkhead	Main Frame, "Y" Ring Splice		
Gage/Size	.016					.018	.040		
Heat No.	8006EV	7950EV	E96034	E95348	E96155	8008EV	C50217	C50216	5995
Supplier***	(1)	(1)	(2)	(2)	(2)	(1)	(3)	(3)	(2)
UTS (KSI)	123.5	117.0	124.0	122.0	122.4	124.5	117.0	118.0	119.0
Annealed*	123.0	-	121.3	122.1	123.3	117.0	-	-	-
Aged**	198.0	198.0	207.8	203.6	202.6	197.0	-	-	206.0
	200.5	-	210.6	204.7	203.8	193.5	-	-	-
2% Yield (KSI)	54.0	48.5	62.7	62.5	56.5	51.5	52.0	54.5	55.0
Annealed*	50.3	-	64.0	56.9	59.4	52.0	-	-	-
Aged**	160.0	164.0	179.3	186.4	185.6	168.0	-	-	181.5
	160.0	-	181.2	191.5	189.4	165.5	-	-	-
Elongation(%)	49	50	49	46	45	53	55	53	50
Annealed*	49	-	57	48	47	54	-	-	-
Aged**	20	19	17	17	17	20	-	-	18
	20	-	17	17	16	20	-	-	-
Hardness	15T086	15T088	15T88	15T79	15T81	15T086	45T59	45T59	RC-9
Annealed*	15T086	-	15T87	15T80	15T79	15T086	-	-	-
Aged**	15N084	15N084	15N80	15N80	15N81	15N085	-	-	RC-44
	15N084	-	15N81	15N81	15N81	15N085	-	-	-

* Mill annealed 1950°F **Age 1350°F, for 8 hrs., FC to 1200°F, hold @ 1200°F until a total aging time of 18 hrs., A.C.

*** Suppliers: (1) A. M. Castle and Company; (2) Alloy Specialties, Ltd.; (3) Techalloy Co., Inc.; (4) Carlton Forge Works

Table II. Room Temperature Mechanical Properties of Alloy 718 (continued)

	Tank Door	Tank Door Doublers	"Y" Ring Splice			"Y" Ring/ Support Fittings		Tank Door	Door
Gage/Size	.020	.032	.048			2x2xRL Bar		23.2OD x 19.2ID x 1.7	21.4OD x 16.5ID x 1.0
Supplier***	5618 (2)	5953 (2)	C50216 (3)	5995 (2)	5748 (2)	6028 (2)	6042 (2)	50805	
UTS (KSI)	111.7	122.3	125.0	118.8	123.0	-	122.8	129.9	
Annealed*	-	-	-	-	120.4	-	-	118.6	
Aged**	192.7	204.8	-	200.0	202.0	189.5	189.8	198.0	
	-	-	-	-	202.2	-	-	192.8	
2% Yield (KSI)	57.2	59.9	56.75	54.1	55.0	-	61.5	77.3	
Annealed*	-	-	-	-	55.2	-	-	69.0	
Aged**	168.6	170.4	-	174.0	181.8	164.5	162.3	175.5	
	-	-	-	-	182.9	-	-	169.3	
Elongation (%)	40	48	55	53	53.0	-	62.1	55.0	
Annealed*	-	-	-	-	50.0	-	-	71.0	
Aged**	17	18	-	17.5	18.0	23.4	26.3	20.0	
	-	-	-	-	20.0	-	-	18.5	
Hardness	15T82	30T70	B-90	RC-7	30T75	-	RB89.5	170 Bhn	
Annealed*	-	-	-	-	30T74	-	-	170 Bhn	
Aged**	15N83	30N63	-	RC-43	30N62	RB90-94	RB42.5	415 Bhn	
	-	-	-	-	30N62	-	-	415 Bhn	

*Mill annealed 1950°F **Age 1350°F, for 8 hrs., FC to 1200°F, hold @ 1200°F until a total aging time of 18 hrs., A.C.

***Suppliers: (1) A. M. Castle and Company; (2) Alloy Specialties, Ltd.; (3) Techalloy Co., Inc.; (4) Carlton Forge Works

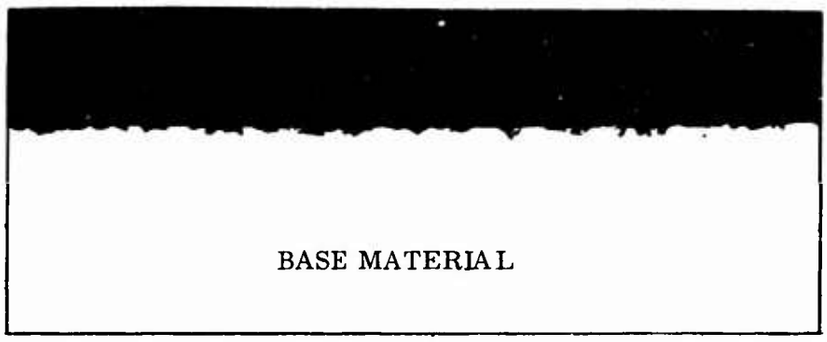

Magnification 500X
Alloy 718 "as received" finish "2D"

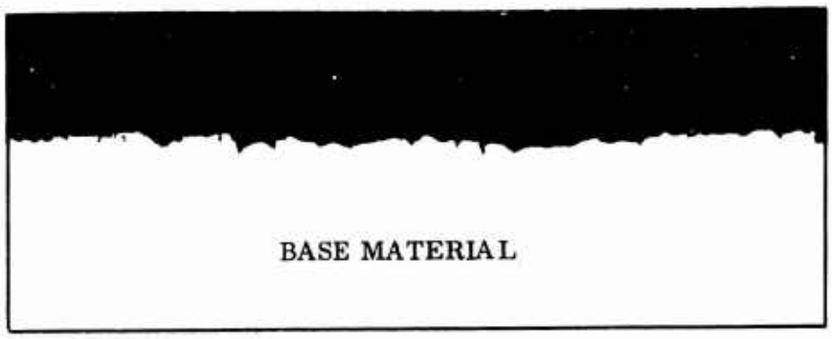

Magnification 500X
Alloy 718 Hand Sanded, Pickled and Passivated

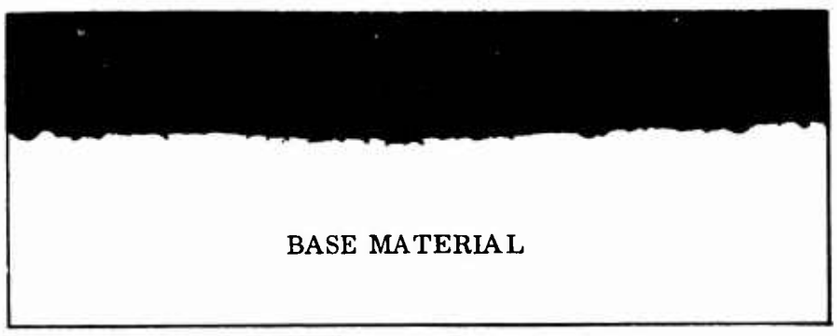

Magnification 500X
Alloy 718 Vapor Honed, Pickled and Passivated

Figure 9. Photomicrographs of Alloy 718

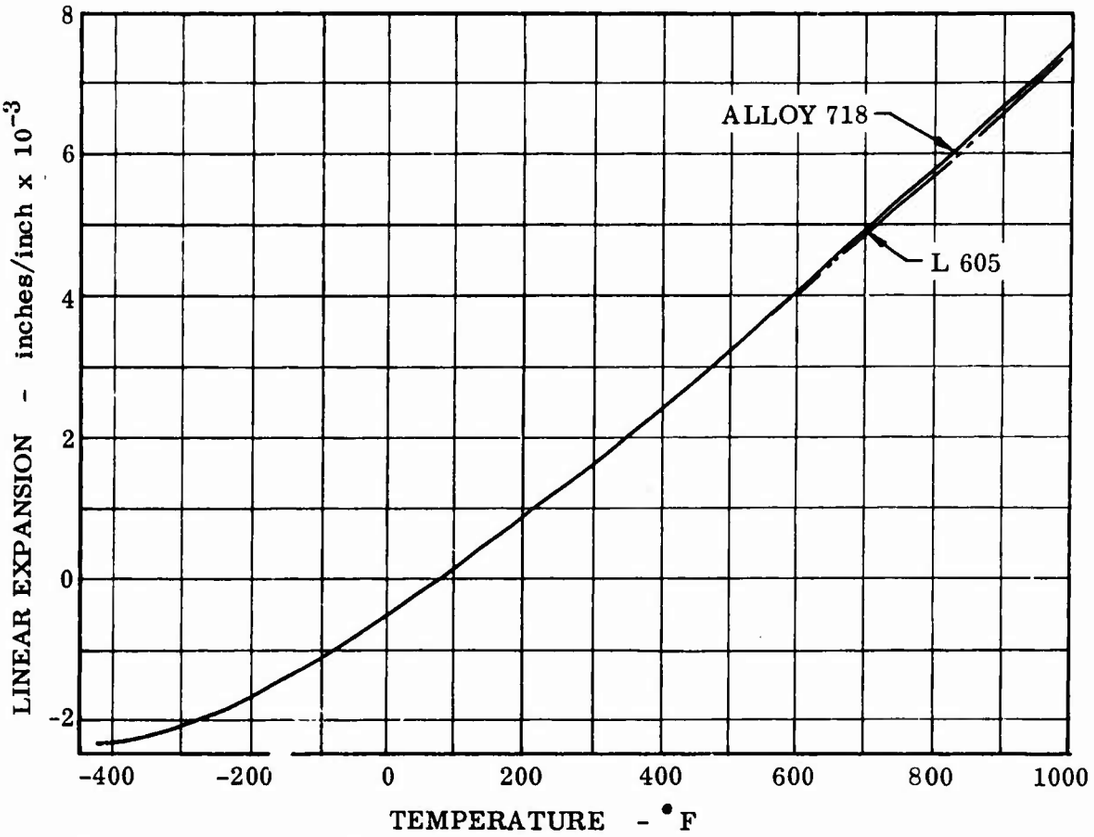

Figure 10. Thermal Expansion Characteristic of Structural Materials

contraction the material undergoes during the aging process. Consideration of this linear contraction was an important factor in the design and fabrication phases of this program. The amount of shrinkage was also found to vary with the amount of cold work the material had experienced prior to heat treating.

3.4 MECHANICAL PROPERTIES OF BASE MATERIAL

The base material mechanical properties employed on this program for the solution annealed condition and the age-hardened temper which is recommended for future production programs. This data is presented in the format employed by MIL-HDBK-5A. The room temperature properties values, Table III, are stated and their variation with temperature given as percentages of these values, Figures 11, 12, 13, and 14. The room temperature F_{tu}, F_{ty} and e values of Table III are those guaranteed by both Convair and AMS procurement specifications. All of the remaining data were established by reviewing the available literature on the Alloy 718, including vendor data, results from testing performed at Convair, data published by government agencies, etc. The mechanical properties specified are considered to be adequate for design purposes. Increased material strength at cryogenic temperatures was not employed in the tank design and is shown to qualify the base materials good cryogenic properties and for reference purposes.

Table III. Alloy 718 - Room Temperature Design Allowables

Mechanical Properties Condition	F_{tu}, ksi	F_{ty}, ksi	e, %	E, 10^6 psi
Annealed	110	50	48	29.6
Annealed & Aged	180	150	15.0	29.6
30% CR + Aged	220	200	12.0	29.6

SPECIFICATIONS: GD/A 0-71037 Bars and Forgings, AMS 5596A

GD/A 0-71038 Sheet, Strip and Plate, AMS 5664

HEAT TREAT: Mill Annealed - 1950°F, AGE 1350°F for 8 hrs., F.C. to 1200°F, hold @ 1200°F for a total aging time of 18 hrs., A.C.

30% CR + Aged: AGE 1250°F, 8 hrs., F.C. @ 20°F/hr. to 1150°F, hold @ 1150°F for a total aging time of 18 hrs., F.C.

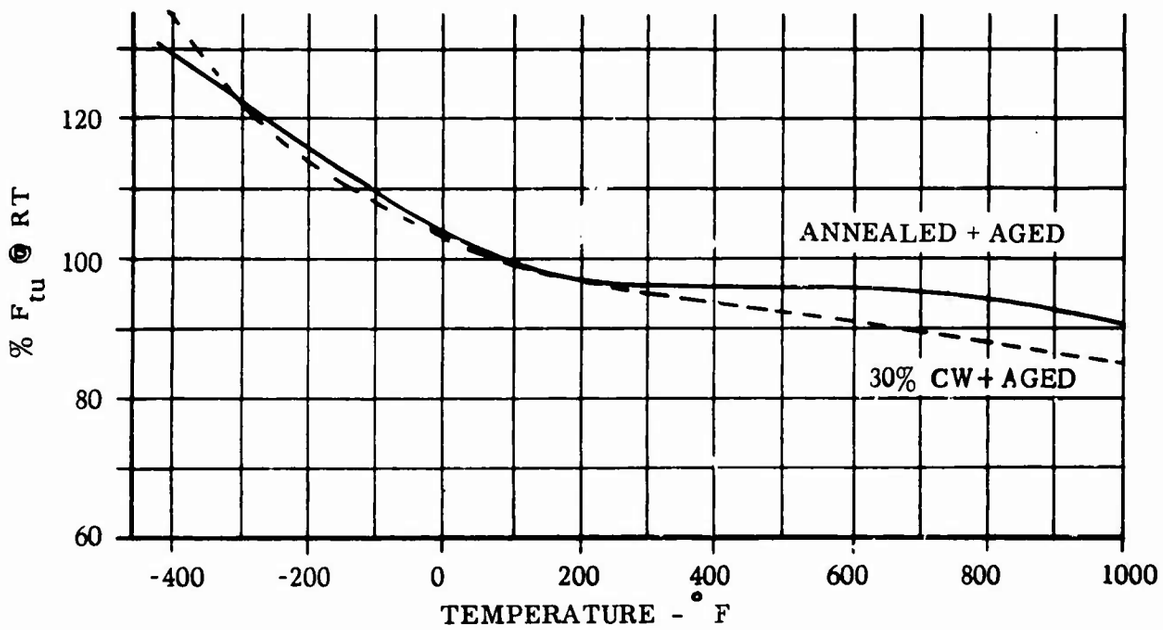

Figure 11. Effects of Temperature on Ultimate Strength (F_{tu}) of Alloy 718

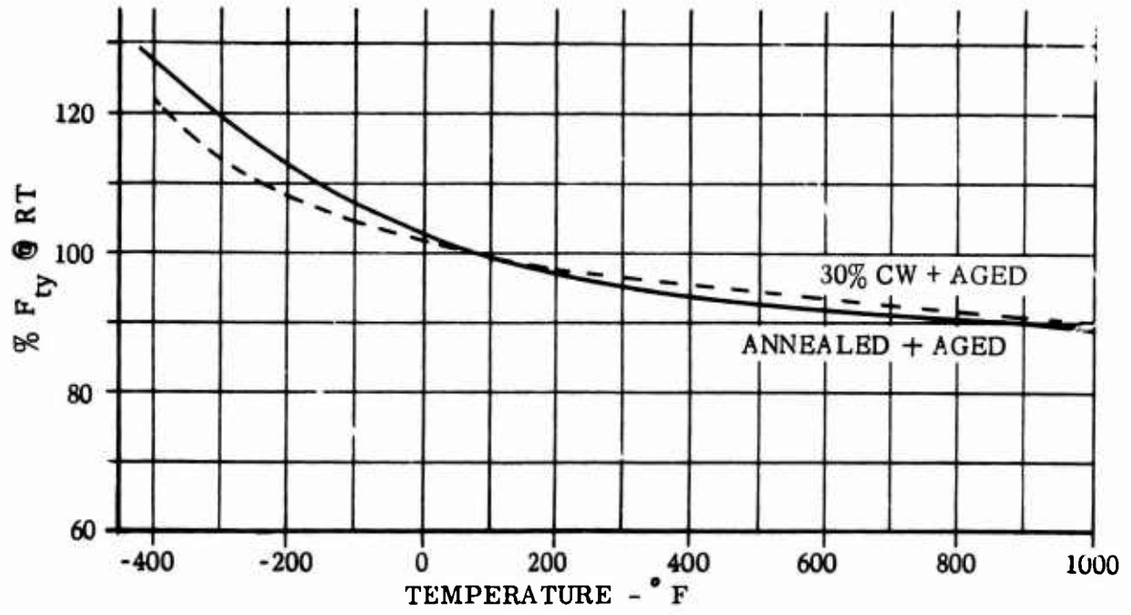

Figure 12. Effects of Temperature on Yield Strength (F_{ty}) of Alloy 718

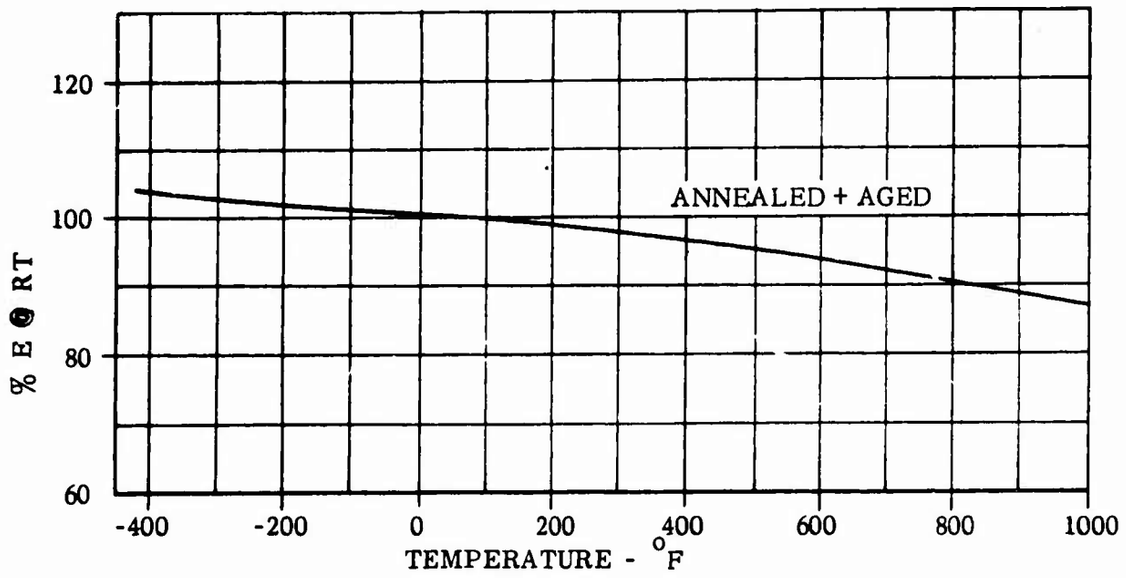

Figure 13. Effects of Temperature on Tensile Modulus (E) - Alloy 718

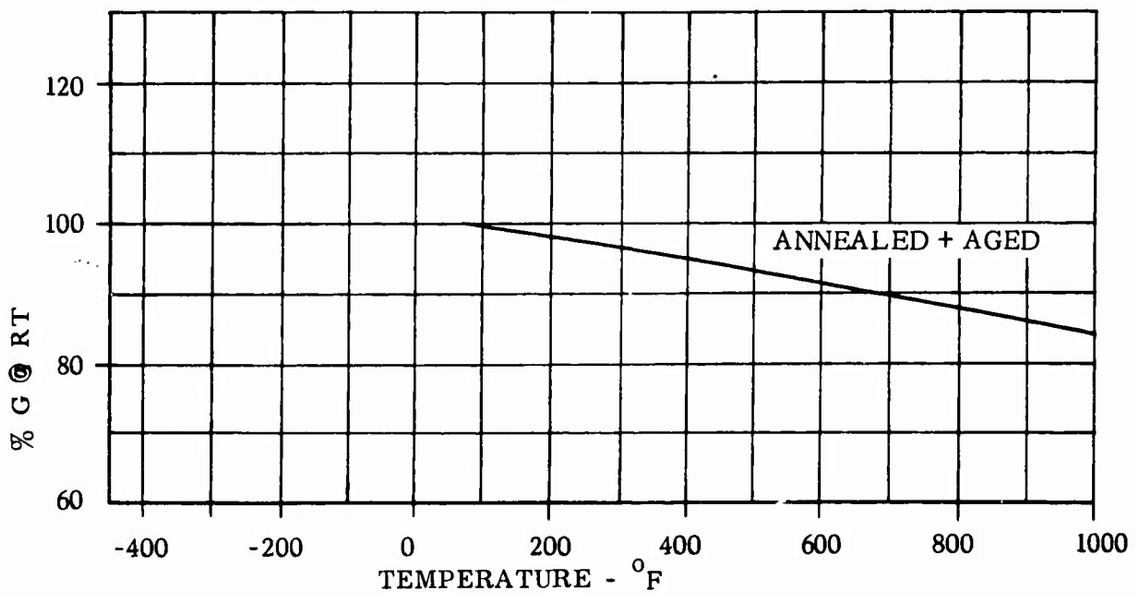

Figure 14. Effects of Temperature on Modulus of Rigidity (G) - Alloy 718

In addition to the conventional mechanical properties of ultimate stress, yield stress, Young's modulus, etc., the suitability of a material for pressure vessel applications is heavily dependent upon its toughness (resistance to brittle fracture) over the range of operating temperatures. For the tankage of the present program, these temperatures range from -423° F up to +440° F. Several different criteria may be applied to evaluate a materials toughness, one of the most common being the notched/unnotched ultimate tensile stress ratio. This ratio is affected by the type of notch used on the actual test specimens. However, experimental investigations performed at Convair have shown that a notch configuration with a stress concentration factor of 6.3 provides a reliable basis for toughness evaluation. Notched/unnotched tensile ratios obtained from such specimens are listed in Figure 15. The curves are based on the average value of several data points given in Reference 3. This data covers the 718 material in the annealed plus double aged condition and also the 30% cold rolled plus double aged condition. It can be seen that, in both cases, the material exhibits excellent notched/unnotched tensile ratios for temperatures range of +75° F to -423° F, indicating the material to have good toughness characteristics for the intended application of this program. Although no values are given here for elevated temperatures, it is expected that excellent ratios would likewise be obtained at the relatively moderate upper design level of +440° F.

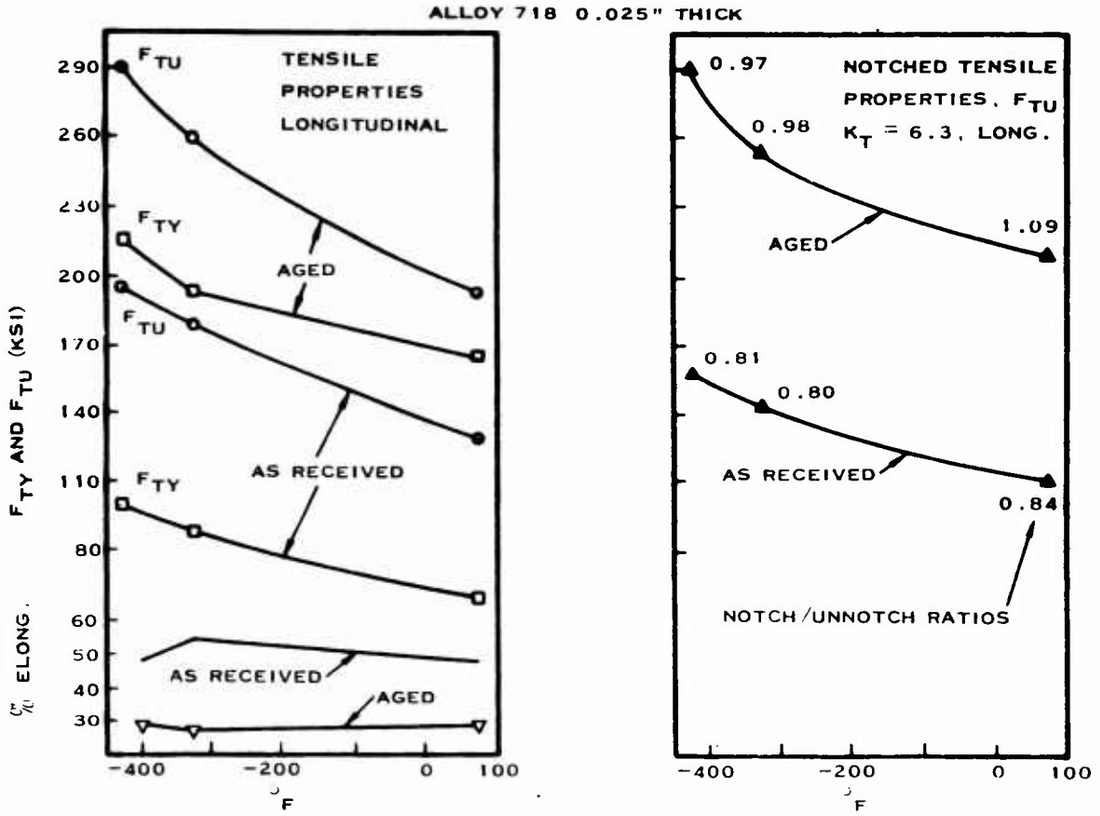

Figure 15. Tensile and Notched Tensile Properties of Alloy 718

In addition to the notched/unnotched tensile ratios, evaluation of material toughness was determined from fracture mechanics data for center-notched tensile specimens, References 4 and 5 . By using this type of data, the curves of Figures 16 and 17 were drawn which show relationships between gross stress and critical crack length. For a given stress level, cracks having lengths equal to or greater than the critical value are self-propagating and, in pressure vessels, will lead to explosive-type failures. This mode of failure is frequently referred to as fragmentation and is dependent upon the fact that severe stress concentrations exist at the ends of any sharp crack. Self-propagation occurs whenever the energy released by the crack growth equals or exceeds the energy required to create the fractured surfaces.

3.5 WELD STRENGTH

A primary objective in the tank design was to employ fusion buttwelds wherever possible. Despite this objective many joints were made using a spotweld process due to the influences of cost and scheduling. Spotwelding does not represent an optimum joining method for this application since each spot is a local stress raiser and hence has greater sensitivity to failure under the pressure fatigue cycling. The tungsten-inert-gas (TIG) process was the primary weld method employed for accomplishing fusion buttwelding. A limited amount of electron beam (EB) welding was also employed. Both these weld processes have the same weld strength requirements and allowables. In limited access areas where spotwelding could not be accomplished by the resistance method a TIG fusion spotweld process was employed. This process is an advanced state-of-the-art welding method and limited data existed on its use and associated strength values. The design requirements were that it have the same strength as the resistance spotwelds.

3.5.1 FUSION BUTTWELD JOINTS. Determination of an allowable design stress for the weld joint was required for two material conditions: (a) welded solution-annealed material which was then aged, and (b) aged material in the as-welded condition was determined from literature research and in-house testing performed under company and government sponsored programs, (Reference 3). The results of this research indicated that the welded annealed and subsequently aged material condition had strength values close to that of the parent aged material of 180,000 psi ultimate and the as-welded aged material had a weld material strength close to the solution annealed material strength of 110,000 psi ultimate. The value specified in procurement specifications of 140,000 psi ultimate is a maximum value and is only stated in order to ensure high ductility and no cold working at the mill. These values were employed for material weld strengths of the two welded condition. MIL-HDBK-5A requires that a weld strength allowable should be no greater than 85 percent of the weld material strength. The problems of potential mismatch and thinning at the weld joint in fusion buttwelding such a large thin-gage structure and poor tolerance control on sheet gage

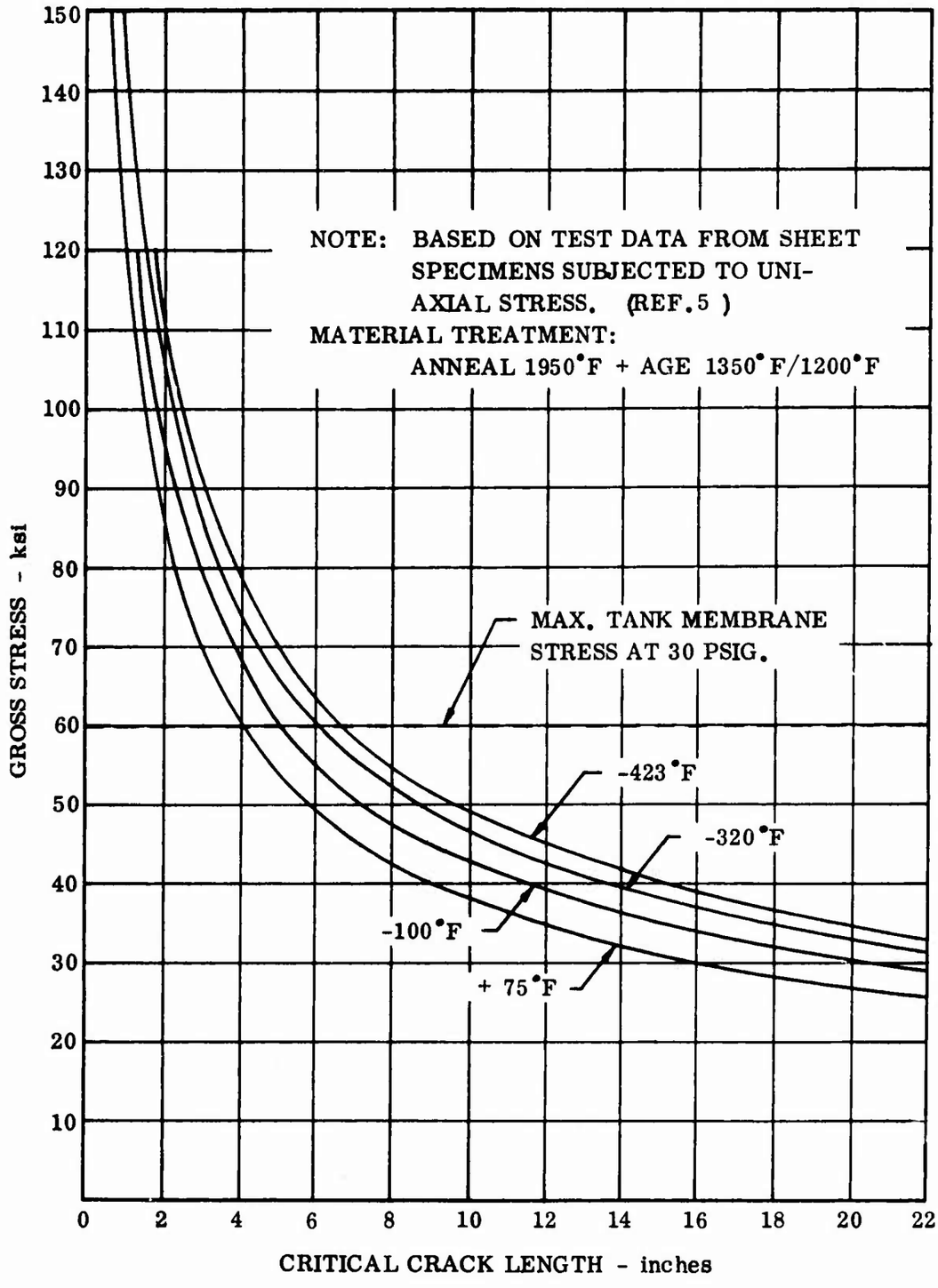

Figure 16. Gross Stress vs. Critical Crack Length for Alloy 718 (Annealed + Aged)

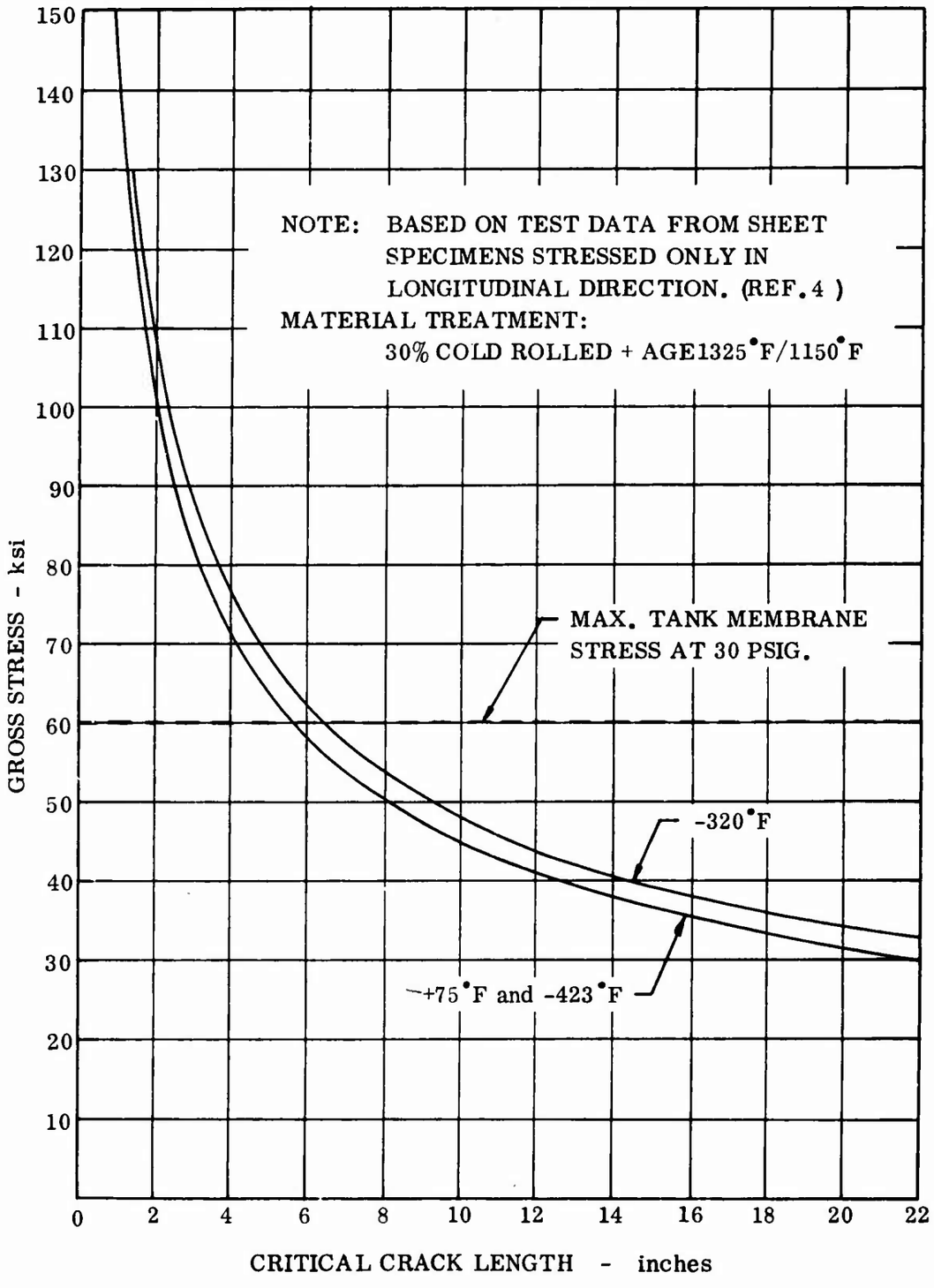

Figure 17. Gross Stress vs. Critical Crack Length of Alloy 718 (30% Cold Rolled + Aged)

available, ±10% of nominal, led to the choice of a design strength allowable 75 percent of the indicated weld material strength. Much of the procured 0.016 inch sheet material was found to be on the low side of nominal, i.e. 0.014 inch, when examined.

Design allowable stresses at the weld joints were:

Aged + Weld

110,000 x 0.75 = 82,500 psi ultimate
50,000 x 0.75 = 37,500 psi yield

Annealed + Weld + Aged

180,000 x 0.75 = 135,000 psi ultimate
150,000 x 0.75 = 112,500 psi yield

The extremely low yield strength of the solution annealed condition gives rise to a seemingly critical stress situation under limit loading for the as-welded aged material. Although tests have substantiated the ultimate strength of the weld material no data exists on the yield strength and it can only be assumed equivalent to the parent material.

The maximum design limit stress experienced across these joints in the tank design is 40,000 psi which would indicate a negative margin of safety. However, this condition is only experienced once in the life of the tank and if yielding would occur it would increase the strength of the weld due to strain hardening influences. This joint design was originally reinforced with spot welded doublers but were removed due to concern they would not survive pressure cycling.

Design weld joint allowable stresses at elevated temperature were based on equivalent loss in parent material strength (Figures 11 and 12).

3.5.2 SPOT AND SEAM WELD JOINTS. The design allowables for shear and cross-tension strengths of individual spots in the Alloy 718 material were based upon the values required for nickel-base alloys in MIL-HDBK-5A, with a parent material strength greater than 150,000 psi. These values are 80 percent of the minimum values required by the welding Specification MIL-W-6858. The design allowable on the tensile strength of spotwelds is 25 percent of the shear strength. The spotweld shear strengths determined from in-house testing and weld certification are shown plotted against the design allowables and requirements of MIL-W-6858 in Figure 18. The same design allowables were used for both resistance and fusion spotwelding processes. Comparison of actual shear strength of spots for each process when compared to the design allowables can be seen in Figure 19. Efficiency of the sheet

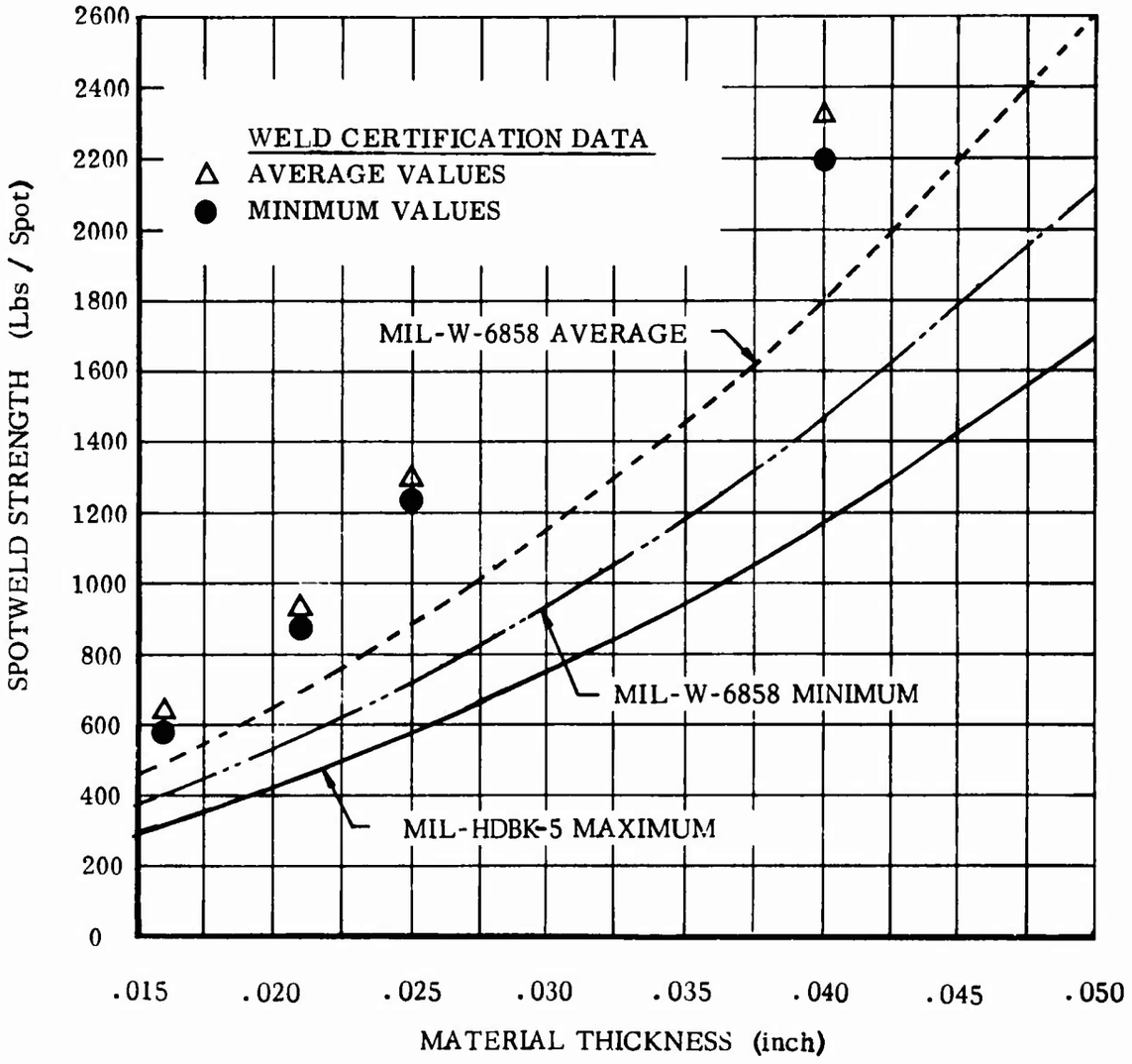

Figure 18. Resistance Spotweld Shear Strength of Alloy 718

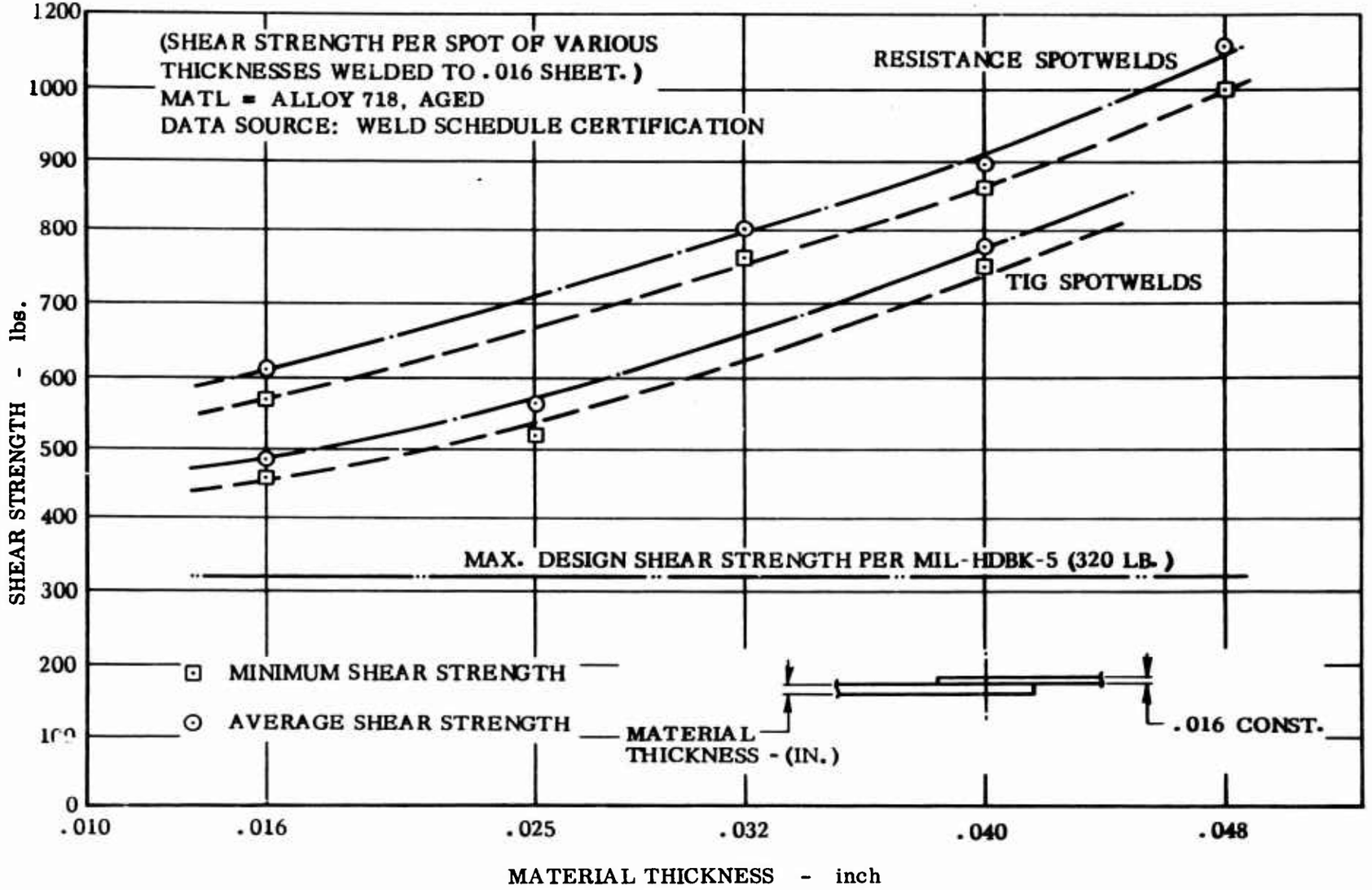

Figure 19. Comparative Shear Strength of TIG and Resistance Spotwelds

material in a spot welded was obtained by use of the curves in MIL-HDBK-5A for the AISI 301-H stainless steel material.

Design strength of spotwelds at elevated temperature were based on equivalent loss in the parent material strength (Figures 11 and 12).

4

TANK STRUCTURAL CONCEPT

The tank is of thin gage, pressure membrane construction and consists of two internally frame stiffened cylindrical segments joined to a center beam and closed out by ellipsoidal bulkheads, Figures 20 and 21. This unique configuration of tank was found to provide high structural efficiency in handling the unpressurized tank bending condition without compromising the pressurized considerations. The tank skins are allowed to buckle elastically in the unpressurized condition and under the high thermal loading induced during simulated flight. These conditions result in an inherently redundant structure for the unpressurized condition which is subject to even further redundancy as a result of its sensitivity to fabrication variations and imperfections due to its large-size, thin-gage, and unique shape. A computer program was developed to handle these redundancies along with suitable knock-down factors to cover for the potential manufacturing imperfections. In some areas alternative load paths were provided. Alloy 718, a nickel-base heat-resistant superalloy, is the tank structural material and is employed primarily in the aged condition. The basic design approach in joining methods was to provide a structure as free of resistance welds as possible within the limitations of cost and scheduling. Resistance spot welds represent stress risers and are hence prone to fatigue failure. The tank support system, located at the main frames, was designed to react all inertia loading on the tankage system while at the same time reducing the structural and thermal redundancy between the tank and vehicle structure to a minimum. The maximum tank operating pressure is 30 psig, aligned to a 30 psia maintained condition of the fuel from lock-up to the end of flight.

4.1 MAIN SHELL

The main shell consists of two frame stiffened cylindrical sections joined to a center beam. It has a length of 240 inches and a cross-section of two intersecting 64 inch diameter circles that join together to provide a 90 inch width. This configuration provides a good pressure vessel shape when a vertical center web is placed at the intersection. Under pressurization the loading intensities are the same in both the shell and web and no discontinuity stresses occur at the intersection as a result of its geometry. The cross-section of two intersecting soap bubbles have a similar geometry.

The main shell was required to resist unpressurized tank bending. This is accomplished by the internal frame stiffening of the cylindrical sections and vertical stiffening of the center web. The required stiffening of the center web to react the frame loading and design requirements for a build-up at the intersection in order to join the cylindrical sections to the center web provided a naturally stiff beam for shear

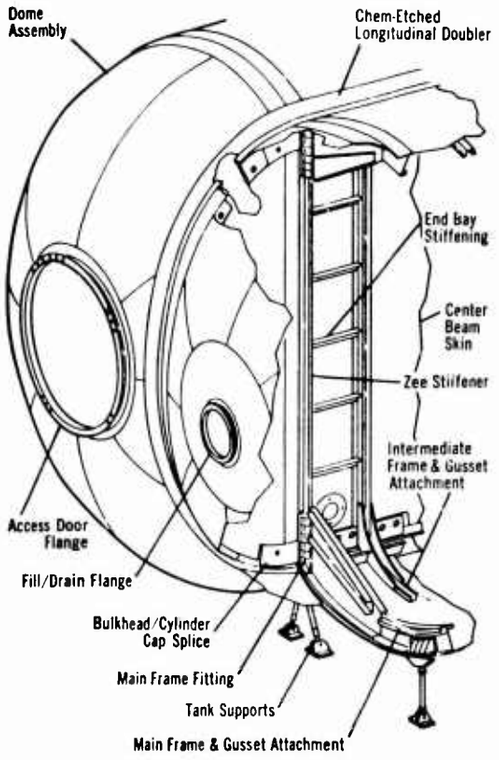

Figure 20. Tank Structural Concept

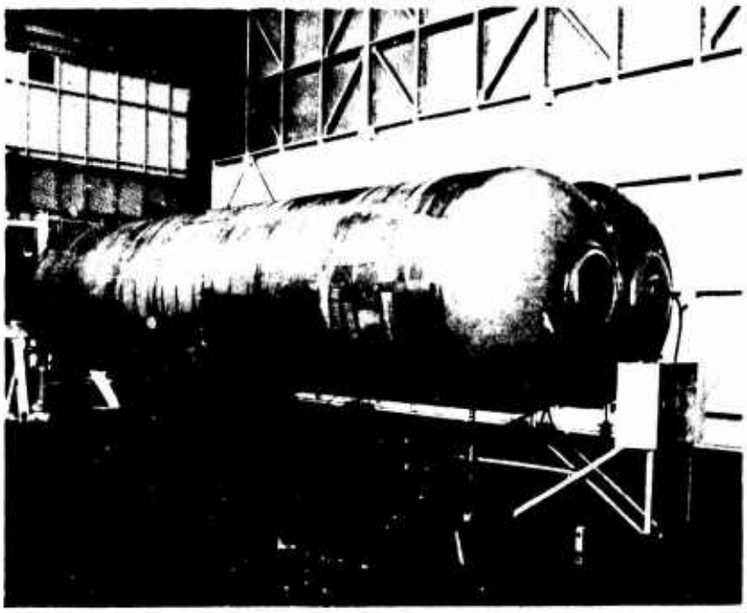

Figure 21. Completed Tank Structure

transfer and tank bending reaction. By allowing elastic buckling of the cylindrical skins advantage was taken of the existence of this natural beam.

The cylinder sections are joined to the center beam by the fusion buttwelding of doublers on the cylinder sections to the machined "Y" section caps of the center beam. The ends of the main shell skin have similar resistance welded doublers that provide for attachment to the bulkhead assemblies by means of fusion buttwelding. The intermediate and main frames are joined to the center beam by gussets that attach to the center beams vertical stiffeners. The limited access available to make these attachments made it necessary to employ a TIG fusion spotweld process.

The tank shell is supported at its two extreme ends by two rigid main frames which redistribute the localized reactions of the supports.

One of the principal analytical tasks was concerned with the skin buckling phenomena resulting from the combined influences of tank pressures, inertia loading, and temperature. The center beam prevents the overall collapse of the tank shell in the presence of buckled skins. Whenever the cylindrical skins experience instability, load paths are transferred into the center beam to maintain the main shell structural integrity. In order to analyze this redundant structure a digital computer program was employed which evaluated stresses in the center beam caps, degree of buckling and the distribution of shear in the skin, see Appendix I. The results of the analysis indicated that some skin will be buckled for all conditions, both pressurized and unpressurized. The most severe buckling case was indicated to occur during the unpressurized taxi condition when the full tank of liquid hydrogen fuel experiences a 2-g limit inertia loading at which time the entire upper half of the tank cylindrical skins near the midsections buckle elastically. Significant shear buckling of the cylindrical skins was also indicated, adjacent to the tank vertical support members. Concern that the shear buckling of the cylindrical skins might be greater than the analysis had indicated, as a result of manufacturing imperfections and variations, resulted in the placing of an internal longeron at the horizontal centerline of the tank. This member provides a reaction to inward rotation of the closing bulkheads about the center beam in the event that any excessive buckling would try to develop.

4.1.1 CYLINDRICAL SECTIONS - The cylindrical sections are 0.016 inch gage cylindrical skins which are stiffened by internal frames on 10 centers along their 240 inch lengths. Main frames are provided at the extreme ends of the section and a longeron runs the entire length of each section located at the horizontal centerline. The cylindrical skins are bordered on all four sides by 0.048 inch thick doublers which provide for attachment to the center beam machined "Y" section cap and the bulkhead doublers. These doublers are attached to the skin by means of resistance spot and seam welding.

The longitudinal lap joints are the most critical weld joints in the tank from a stress standpoint and experience the full membrane hoop stress coupled with influences of

the local discontinuity stresses. This joint is also required to withstand the pressure fatigue cycling associated with 500 flights. Insufficient schedule time and funding precluded the possibility of a test program being performed on joint designs and the only course of action open was to exercise great care in the design of the joint in order to reduce the local discontinuities to a minimum and avoid high loading on individual spot welds. It would have been desirable to have obtained weld lands by chem-milling the basic skins from increased gage material but the associated cost and schedule time would have been exorbitant. By providing two chem-milled steps in the doubler, 0.048-0.032-0.016, reduction in the development of local discontinuity stresses was achieved also the avoidance of high loading on the first row of resistance spots. This gives increased fatigue capability to the joint.

Complete removal of resistance spot welds from such a critical weld joint is obviously desirable since each spot weld, despite any design innovations, present a local stress raiser and hence has greater sensitivity to cracking as a result of pressure cycling. In order to provide full assurance that this joint, or any of those employing spot welds, have sufficient structural integrity to survive the pressure fatigue cycling requirements associated with 500 missions would require an extensive test program.

4.1.1.1 Cylinder Skins - The cylindrical skins are 0.016 gage and in complete form measure 134 inches circumferentially and 240 inches in length. The length is obtained by the fusion buttwelding together of nine (9) sections, the first and last sections are 15 inches wide and the remainder 30 inches. This arrangement of lengths provide consistency in location of the welds with respect to the 10 inch spacing of the intermediate frames. This made for common frame/skin assemblies in the fabrication phase and assured that no seam weld would fall in a location where resistance welding is required or stress discontinuities exist. Restrictions in sheet sizes available from the mill, 36" wide x 96" length, required that the circumferential length be obtained by fusion buttwelding lengths together. These welds are subject to maximum loading conditions and were consequently welded in the annealed condition and then aged. This produced a weld joint material strength close to that of the parent material. The circumferential welds were made with the material in the aged condition and left as welded. Heat treating of the complete large-size thin-gage structure would have been impractical. Critical loading of these welds are given below.

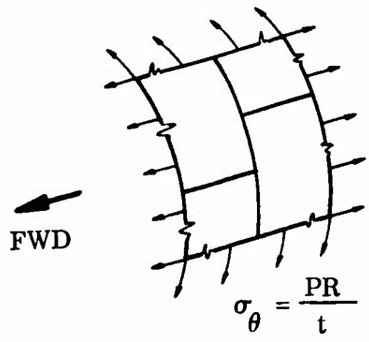

CIRCUMFERENTIAL WELD JOINTS

MATERIAL CONDITION: Aged + Weld

Burst Condition - Ultimate

P = 60 psig

σ = 60,000 psi ultimate

Weld strength allowable = 82,500 psi (Section 3.5.1)

MS = 0.38

Proof Pressure - Limit

p = 40 psig

σ = 40,000 psi

Weld strength allowable = 37,500 psi (Section 3.5.1)

MS = - 0.06

This negative margin of safety was originally covered for in the design by the addition of spot welded doublers at all circumferential splices. However, the increased task of adding the doublers, potential loss in fatigue strength as a result of discontinuity influences and presence of resistance spots, and the loss in some of the tank leak-tight integrity due to potential cracking in any one of the 22,000 additional spotwelds that would have been involved led to the doublers removal. Removal of the doublers was not made until it had been assured that the joint strength of production parts was greater than the design strength. All circumferential joints were roll-planished during fabrication which brought up the strength of the as-welded material condition.

HORIZONTAL WELD JOINTS

MATERIAL CONDITION: Annealed + Weld + Aged

Burst Condition - Ultimate

$p = 60$ psig $\quad \sigma = 120,000$ psig

Weld strength allowable = 135,000 psi

MS = 0.13

Proof pressure test is less critical due to the ultimate/yield strengths associated with the aged material condition.

4.1.1.2 Frames - The main frames provide for redistribution of the localized support reactions and are located close to the main-shell/bulkhead intersections. They also provide the only true hard points on the tank structure. The main frames are relatively stiff; having a zee cross-section, a 3 inch height and employ a 0.040 inch sheet gage of an aged material condition. The main frames are locally reinforced at the vertical load supports by reinforcing angles that backup the inner lipped flange of the main frames. Load transfer to the opposite frame and center beam is accomplished by reinforced sheet metal gussets that terminate in machined fittings. The final load transfer is made through a bolted joint in the two opposing machined fittings.

The primary function of the intermediate frames is to stiffen the cylindrical skins against collapse under the unpressurized loading conditions. These frames are internal, have a thin gage (.016), open cross-section, low height and are located on 10 inch centers along the 240 inch main shell length. Shear transfer to the center beam is accomplished by back-to-back gussets that tie through to channel-section vertical stiffeners on the center beam.

They are internal to reduce heat leaks into the tank, minimize the development of thermal stresses and simplify the insulation installation. An open cross-section, inverted-hat, provides for good venting capability and reduced ullage stagnation. The low height, 0.74 inches, affords close installation of the vent manifold system to the upper tank surface thereby offering maxiumum utilization of fuel boiloff cooling capability and at the same time provide minimum restriction to longitudinal flow of boiloff across the top of the tank.

Both the intermediate and main frames were analyzed by use of a digital computer program, (Reference 6), based upon Castigliano's Theorem with the use of a matrix formulation to reduce algebraic complexities. Only in-plane deformations were considered. Solutions obtained accounted for the inertia loading on the structure, insulation and fuel together with the influences of internal pressure and localized load reaction. A typical output for the intermediate frames, is shown in Figure 22 which relates solely to the influences of hydrostatic pressure for a half-full tank of fuel. Maximum loading

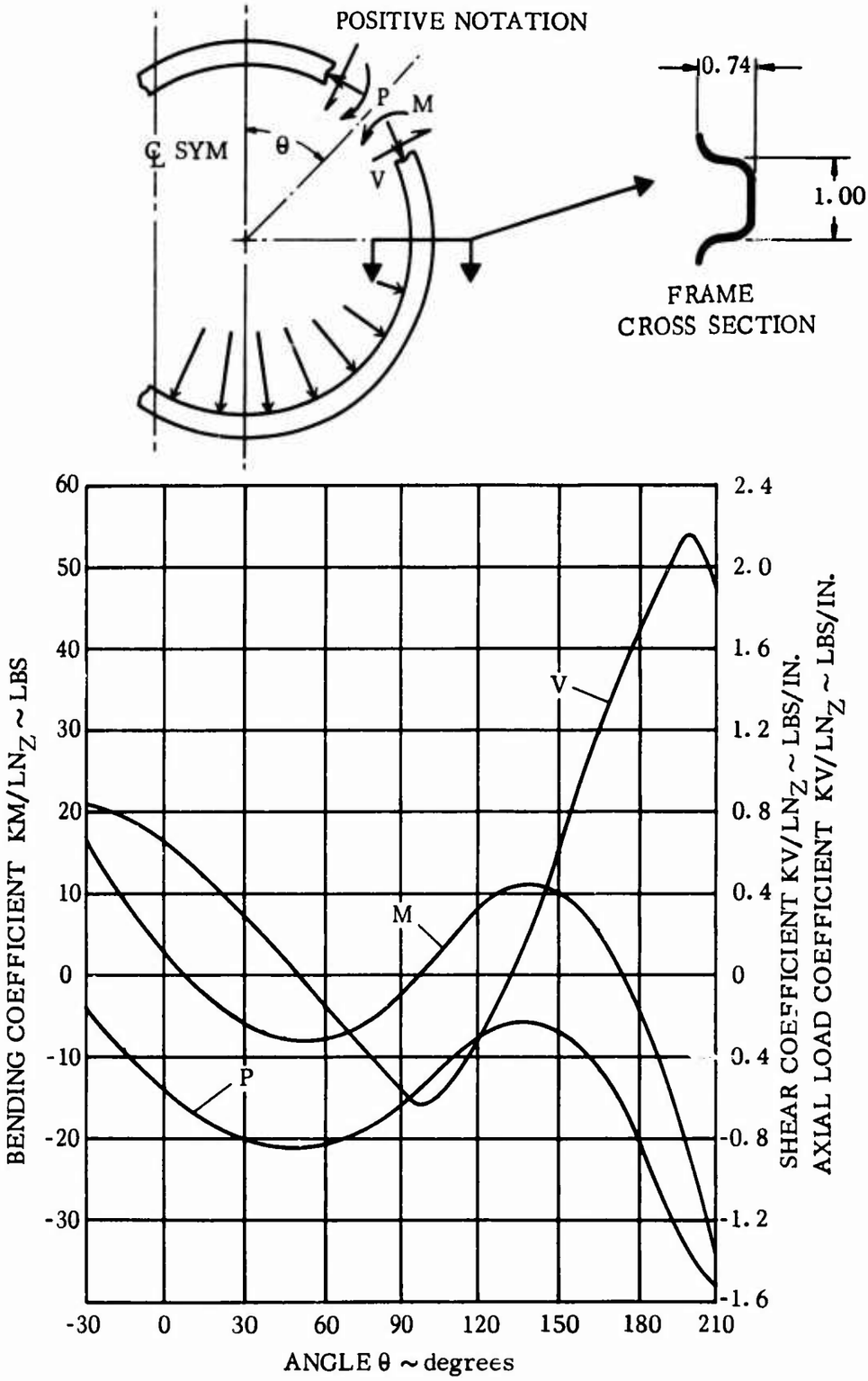

Figure 22. Loading of Intermediate Frames - Half-Full Fuel Condition

cases were determined by superimposing all associated conditions for a specified loading case. The corresponding stresses were computed from the standard expression:

$$\sigma = \frac{P}{A} + \frac{Mc}{I}$$

The case of internal pressure acting alone provided an interesting loading case for the intermediate frames when in-plane bending was found to develop as depicted in Figure 23. From this figure it can be seen that the free-body of the pressurized skin is not concentric with that of the frame. This is due to the position of the vertical plane of the symmetry. Insofar as displacements of the horizontal deflections are concerned the plane of symmetry is a rigid wall. The non-uniform displacement results from this condition. Structural acceptance testing confirmed this finding from the results obtained during the proof-pressure testing.

The load carrying capability of the intermediate frames was found to be very sensitive to variation in the sheet material thickness associated with its thin-gage cross-section. The final gage on many of the as-fabricated frames was found to be 0.012 compared to the nominal design gage of 0.016, as a result of receipt of material on the extreme low side of the standard AISA gage tolerance, ±0.002, and greater thinning than anticipated during the forming operation. The design of the frames were based on the local crippling strength allowable for the inner frame caps and the associated stress level. With the reduction in gage the crippling allowable drops by 44 percent and the stress increases by 33 percent. This loss in load-carrying capability resulted in local reinforcing of all frames in the area of maximum loading, close to upper frame gussets. This points up a significant problem area associated with the use of thin gages. Materials should be procured from the mill with a tolerance control a third of that specified by the standard AISI tolerance; and the forming, cleaning and other fabrication procedures influencing gage change must be capable of prediction within close limits. These influences must also be fully recognized in the design phase. The Atlas and Centaur programs require the procured material in the gage considered here, 0.016, to have a ±0.0005 inch tolerance on thickness. This was accomplished by a special mill-rolling process.

4.1.1.3 Longerons - Two longerons were incorporated into the tank structure to provide restraint against potential inward rotation of the domes as a result of main shell elastic shear buckling during the unpressurized tank bending conditions. These longerons are internal and run the entire length of the cylinder sections. They are located on the tank horizontal centerline to minimize being loaded by tank bending moments. Attachment is made to each intermediate frame, and to the main shell skin only in the last two bays where long legged angle gussets are employed with sufficient flexibility in their connections to minimize load introduction during the pressurized condition. The longeron has a hat cross-section, similar to the intermediate frames, and an 0.016 gage. The longerons were considered as column members in their analysis

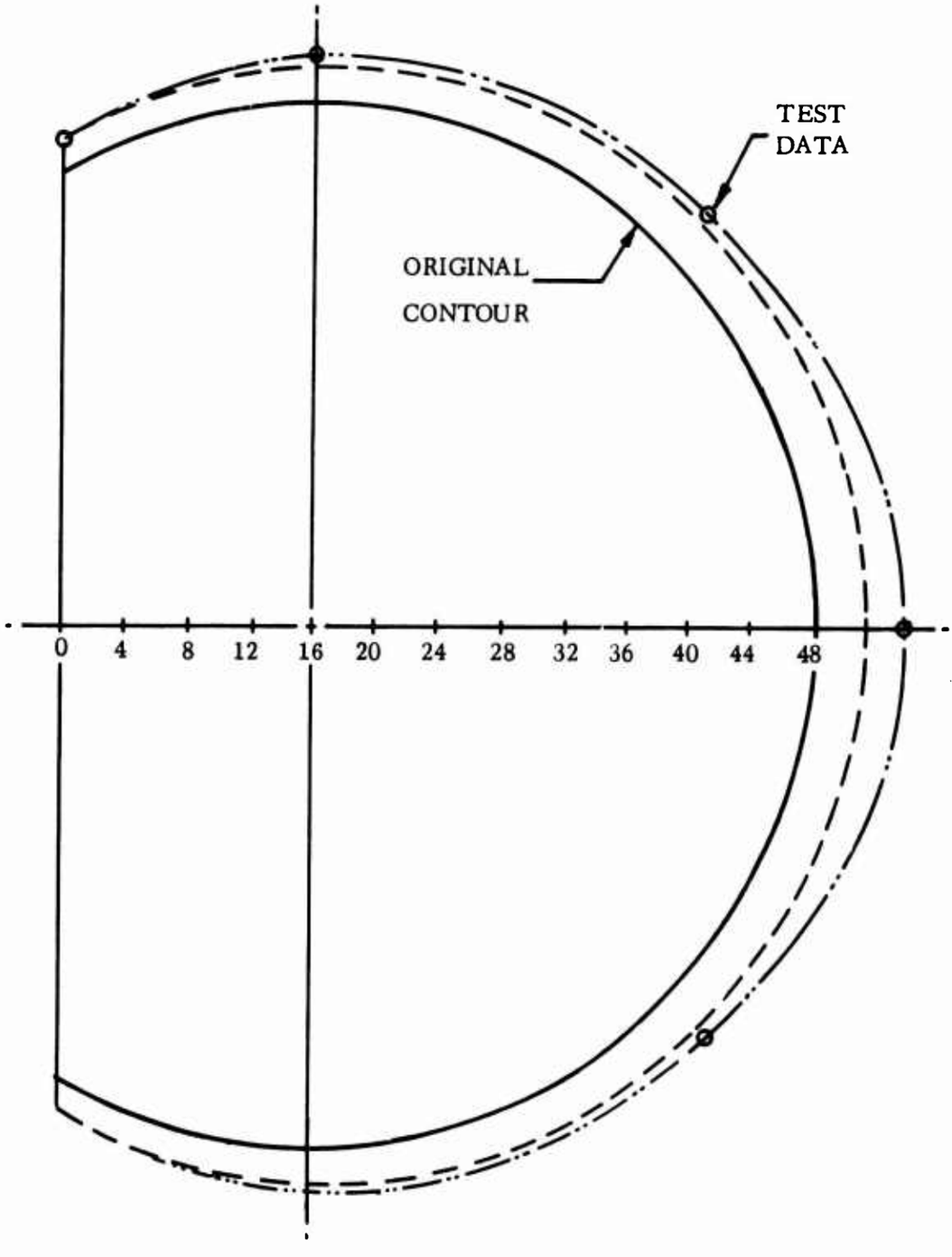

Figure 23. Radial Deformation Pattern

which were fixed at their ends and elastically supported at the intermediate frames, the spring constants being determined from a conventional energy solution. The redundancy of the tank structural concept and its inherent sensitivity to manufacturing variations and imperfections precluded any capability to accurately predict the full extent of the outside main shell shortening as a result of shear buckles. The inclusion of the longerons was made to cover this limitation with its actual effectiveness to be determined during the testing program. Results of the unpressurized tank bending test (Ref. Volume II) based on strain gage readings and visual inspection of the buckling developed, showed the longerons play an important role in resisting buckling with a compressive force of 1,000 pounds being developed in this member.

4.1.2 Center Beam - A naturally stiff center beam results from the need to handle the tank pressurized condition and to provide an attachment means for joining the cylinder sections, and its intermediate frames. The resulting beam was found to be capable of handling a large proportion of the total loading from the unpressurized tank bending condition without any significant increase in weight. A truss-type structural arrangement was also investigated for the center beam and was indicated to have good potential for providing minimum weight. This concept provides for increased accessability and unrestricted fuel flow between tank lobes. However, concern over its susceptibility to damage during fabrication and handling, and the reduction in available load paths to handle the tank structural redundancies led to the choice of the web concept. The truss concept should be further investigated for actual flight applications.

The center web, which experiences the same pressure membrane loading intensities as the main shell, employed the same material sheet gage of 0.016 inches. The web was built up in a similar manner to the cylinder skins and involved the same joint designs. One significant difference between the center web and the cylindrical skins is that the center web does not experience any pressure differential across it when the tank is pressurized. This raised the question as to whether it would react its proportion of longitudinal pressure loading if anything but a drum-tight construction was involved, or the dome intersection construction lacked the capability to transmit this loading. The tank was designed to provide as much control as possible in obtaining the required drum-tight construction of the web during the fabrication phase in order to prevent these adverse conditions developing but did not rely on it to carry its full share of the pressure loading. If significant buckling had been allowed to exist in the as-fabricated web, transverse bending of the vertical stiffeners and uneven distribution of the vertical load reaction could have resulted causing possible critical loading conditions.

The center beam caps were required to be machined fittings in order to handle a three directional loading condition and provide for practical assembly sequencing and fabrication procedures. The cap has a "Y" cross section, 120 degree angle between each leg, with legs of sufficient length to satisfy the minimum requirements for

accomplishment of the associated welding methods. The leg thickness of 0.048 was based on minimum machining requirements for such a long section, 120 inches, and the need of a close tolerance part. This thickness is also well suited to the strength requirements for a fusion buttweld joint in the hoop direction. Attachment to the cylinder sections is made by fusion buttwelding the outstanding legs to doublers on the cylindrical skins. The vertical leg of the cap is spliced to the center web by means of doublers that are resistance spot welded directly to the fitting and through fillers to the center web. These doublers have 3/4 inch diameter holes on 2 inch centers along the full length of the tank in order to provide cross flow of liquid and ullage gas between the two lobes of the tank.

Stiffening of the web is supplied by two back-to-back vertical channel members at 10 inch spacing along the tank. These stiffeners align with and provide attachment for the intermediate frames through the use of frame gussets that are spotwelded to both frames and stiffeners. The attachment of the stiffeners to the center web is by resistance spotwelding except at the extreme ends where they attach to the longitudinal doublers and a bolted connection is made. This bolt pattern allows for transfer of the frame moment to the opposite frame. The end bays of the center beam are stiffened by horizontal members to increase their shear carrying capability.

4.2 END BULKHEADS

The end bulkheads consist of two intersecting ellipsoidal domes joined to a center vertical web. The ellipsoidal domes have a major/minor (a/b) axis ratio of 1.38 which provides efficient volume utilization while still maintaining an unstiffened membrane construction. Openings are provided at the apex of all domes to allow access of personnel to either side of the tank and for the penetration of fuel system lines.

It was desirable to choose the flattest dome possible within minimum weight considerations in order to provide maximum utilization of the volume within the vehicle shell and at the same time present the smallest surface area of tank to the incoming heat fluxes for the volume contained. From the basic stress equations associated with a pressurized condition of ellipsoidal domes, given below, it can be seen that in an aspect ratio of the major/minor axis greater than $\sqrt{2}$ (1.414) will result in the development of compressive stresses

$$\sigma_{\phi} = p \frac{R_2}{t} \tag{1}$$

$$\sigma_{\theta} = \frac{p}{t} \left(R_2 - \frac{R_2^2}{2R_1} \right) \tag{2}$$

where:

σ_{ϕ} = Meridional membrane stress - psi

p = Internal pressure - psig

R_1 = Radius of curvature in the plane of the meridian

R_2 = Radius of curvature perpendicular to the meridian

σ_{θ} = Hoop membrane stress - psi

t = Membrane thickness - inches

At the equator the equation for hoop stress can be written as:

$$\sigma_{\theta} = \frac{pa}{t}\left(1 - \frac{a^2}{2b^2}\right) \tag{3}$$

where a = major semi-axis b = minor semi-axis

when ratio of $a/b < \sqrt{2}$ σ_{θ} is positive

at $a/b = \sqrt{2}$ σ_{θ} is zero

at $a/b > \sqrt{2}$ σ_{θ} is negative

An a/b ratio of 1.38 was chosen for the dome design, which allows a small margin for manufacturing tolerance and was well suited to easy modification of an existing weld fixturing arrangement. The hoop and meridional load intensity distribution for this dome configuration is given in Figure 24 for the burst pressure, 60 psig, case. The hoop stresses developed in the dome are very small at the equator which reduces stress discontinuities to a minimum when attachment is made to a frame. Readily usable analytical tools to account for the non-axisymmetrical conditions such as temperature gradients and hydrostatic heads were not found available. By the use of much simplified analytical methods and employing suitable knock-down factors to account for potential manufacturing variances and deviations it was determined that the vehicle conditions did not produce buckling. However, a structural acceptance test, simulating a 2g limit loading condition on a full unpressurized tank of liquid hydrogen fuel, was found by this same analysis to result in elastic buckling of the dome. This condition is of greater severity than the actual flight case due to the more localized nature of the loadings and reduction in the stabilizing influence of higher liquid levels.

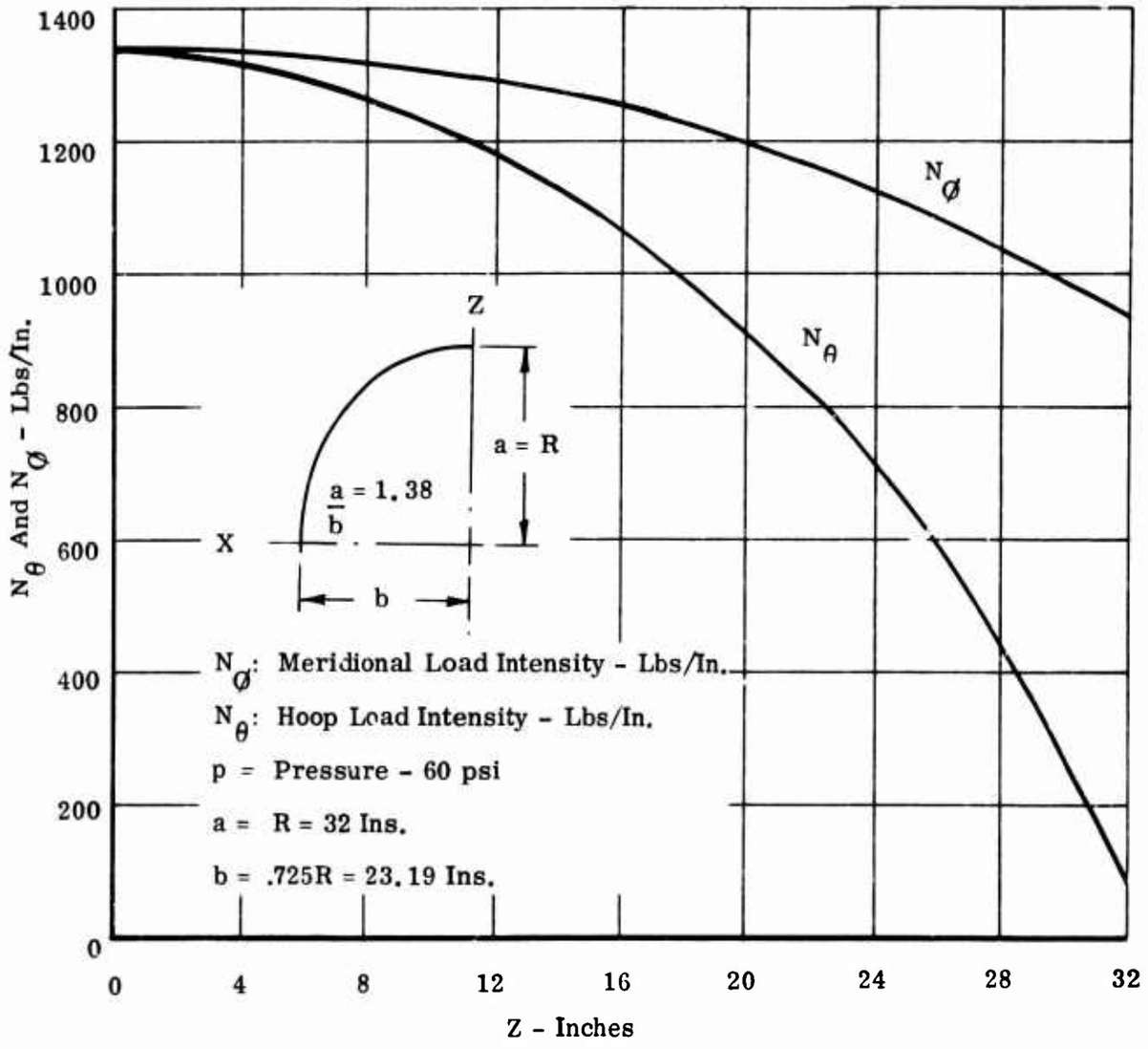

Figure 24. Ellipsoidal Dome (R/b = 1.38) - Meridian and Hoop Load Intensities

The thin gage, 0.018, and large size, 64 inch diameter, of the domes precluded the consideration for a single-piece construction. The design chosen was a build-up dome assembly of eight gore sections fusion butt-welded together. Whereas, an 0.016 gage had been chosen as a minimum fabrication gage for the main shell an 0.018 gage was used for the domes in order to account for thinning during the forming operation and potential weld mismatch at the joints.

Openings were provided at the apex of all domes for personnel access to both lobes of the tank and for the penetration of fuel system lines. The door access rings and covers were based on an existing Atlas design with consideration for the increased strength of the Alloy 718 material and a 20-inch diameter opening instead of a 24-inch diameter. This smaller access opening was necessary in order to provide sufficient distance between the edge of the door ring stiffening and the bulkheads center web. This opening was found to be sufficiently large to allow the free access of a 230 pound welder during the final tank assembly phases. Metallic "O" rings fitting into a "V" groove was the sealing method employed for all removable covers. This is a proven sealing technique and is employed on both the Atlas and Centaur vehicles. The door and cover rings were machined from ring forgings in the solution annealed condition of the Alloy 718 material in order to provide sufficient ductility to accommodate the high strains that result from localized pressure deflections at these fittings.

The center beam assembly that joins the two domes and forms a complete bulkhead consists of a web and a machined "Y" section that is formed around the elliptical shape. The machined ring is joined to the web by means of resistance spotwelded doublers which have holes around their perifery to allow free cross-flow of liquid and ullage gas between the two lobes of the tank. Actual load distribution within this item of the tankage structure is very dependent upon the manufacturing variances and imperfections that are involved, especially from the influence of the longitudinal pressure loading. Theoretically the longitudinal pressure loading component is reacted by the total cross-section of the tank structure. However, should any of the center web have buckles or something less than drum-tight construction, load redistribution will occur, causing a greater amount of the load to be reacted by the formed "Y" section. The center web is not stabilized like the main skins by a pressure differential. The large web size and thin gage made assurity of a drum-tight construction after fabrication questionable. Such variances could have produced significant discontinuity stresses at the dome intersection so an alternative load path was provided. The fabrication requirements for joining and the need for venting holes between the two tank lobes had already provided a significant curved beam construction at the intersection and this was reinforced and spliced through to the main center beam in order to provide sufficient load carrying capability and preclude any adverse load redistributions within reasonable limits of web buckling.

The domes join to the center web and main shell through the fusion butt-welding of 0.048 inch thick doublers attached to the trimmed edges of the dome by resistance spot and seam welding. In a production tank design this could be accomplished by the chem-milling of lands on the basic dome skins. The presense of these doublers and the reinforcement around the tank openings produce discontinuity stresses under the pressurized condition. The magnitude of these stresses were determined through the use of a digital computer program (Reference 7). This program accounted carry-over influences between adjacent discontinuities as well as the coupled effects of meridional loads. Figure 25 shows a bulkhead assembly ready for mating with the main shell assembly.

4.3 TANK SUPPORT SYSTEM

The tank support system was designed with the objective of efficiently reacting all inertia loading on the tankage system and at the same time reduce the structural and thermal redundancies between the tank and vehicle structure to a minimum. If all redundancies were removed, the tank and vehicle would be free to undergo their respective thermal and elastic deformations without any imposed restraint from one another. On the basis of design studies accomplished in Phase I, (Reference 2), the support system design shown in Figure 26 was chosen for the tankage system. This concept locates the six points of support on the lower surface of the tank at the main frames, a natural hard point.

The forward support system, Station 101.75 consists of two vertical load members, located at BL 31.70 left and right, and a tripod at the tank centerline to react side load and drag. The vertical load members are pinjointed, spherical ball-bearings, to allow free transverse thermal and elastic deformation between the tank and vehicle structure. The tripod supplies the only fixed point on the tank relative to the vehicle structure, and then only in the longitudinal and transverse directions. A pin bearing slide at the apex of the tripod allows free movement of the tank in the vertical direction under any induced loading from the side supports. The drag member of the tripod is inclined to the vertical at an angle of 60°. This angle was chosen in order that the resulting kick-load on the bipod members for the drag loading case was no greater than that produced by the side-loading case. An optimum angle from the vertical for the bipod members of 24° was based upon equating column compressive allowable and axial load as a function of column length and then determining length for minimum weight.

The aft support system, Station 338.25, is similar to the forward except that the tripod is replaced by a bipod and is capable of rotation in the forward and aft directions, again with the capability of free movement for the tank in the vertical direction under any induced loading conditions. The system allows for longitudinal movement between the tank and vehicle structure.

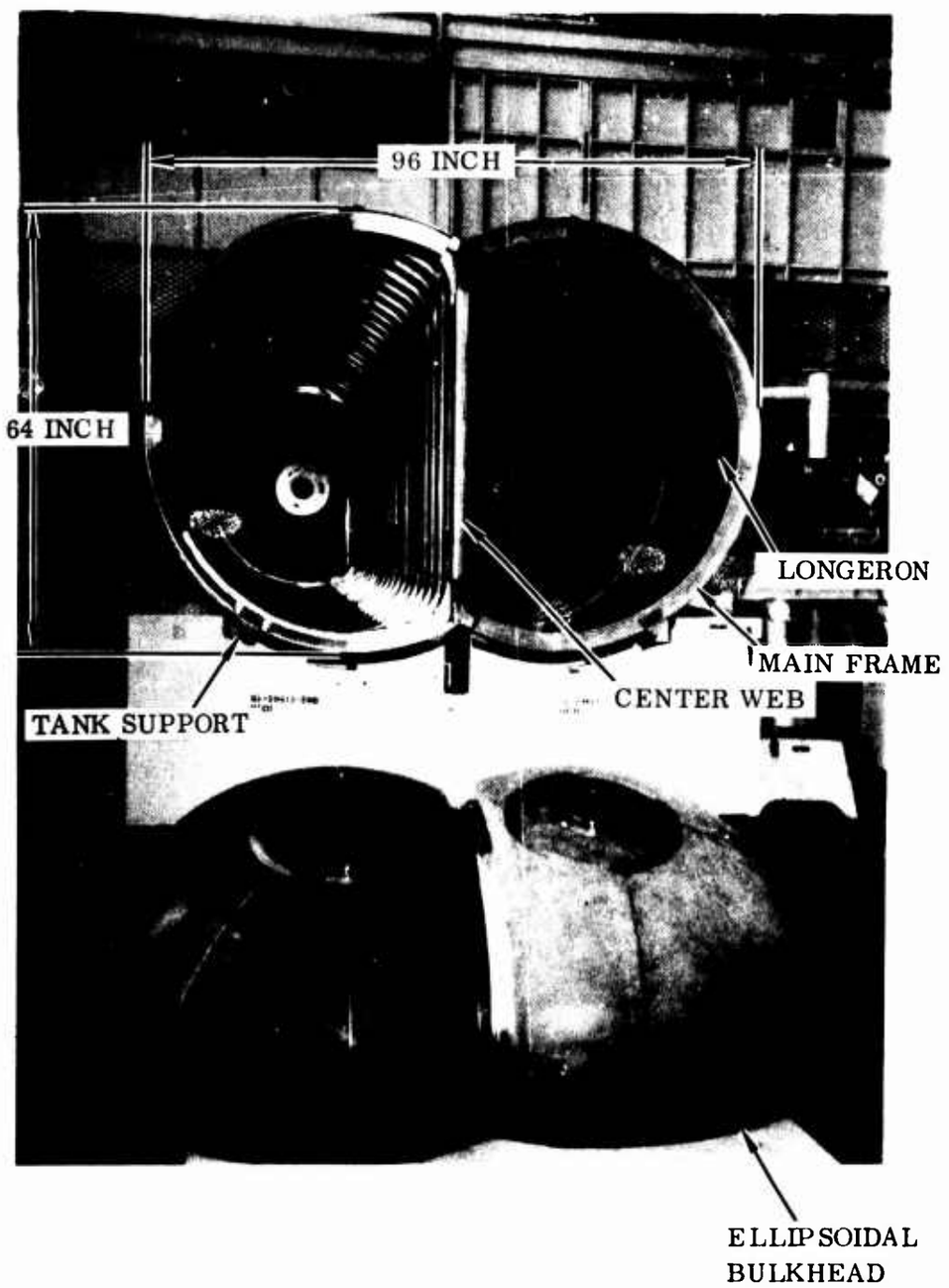

Figure 25. Bulkhead Assembly and Main Shell

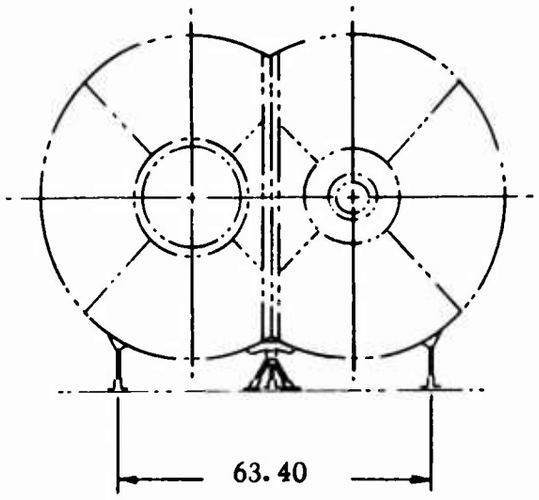

VIEW LOOKING AFT

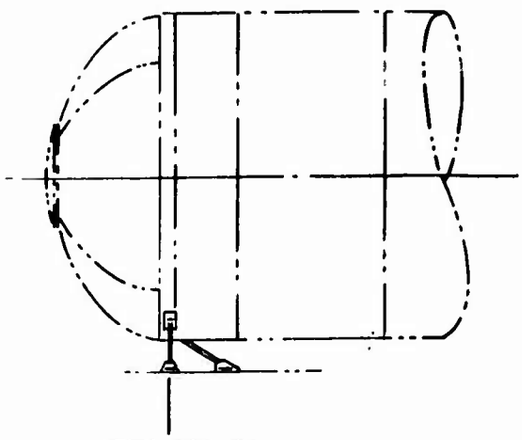

SIDE V

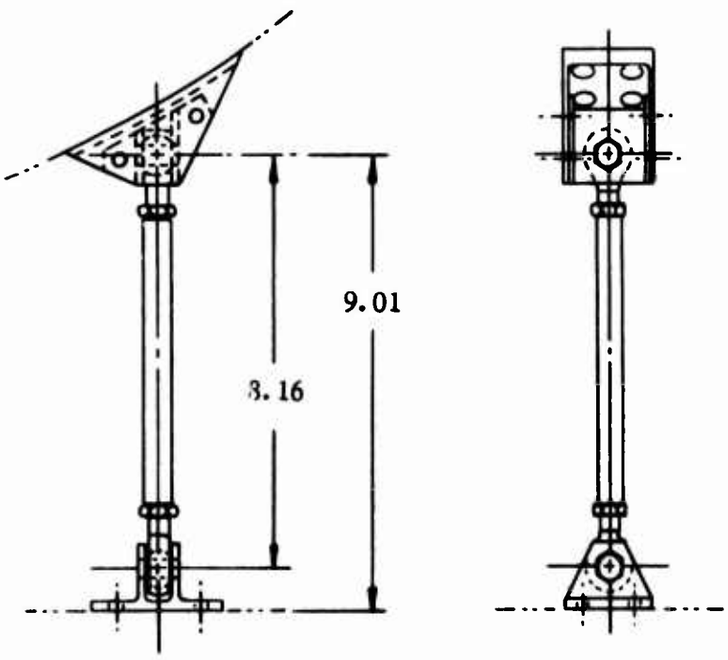

SIDE SUPPORT (4) - VERTICAL LOAD

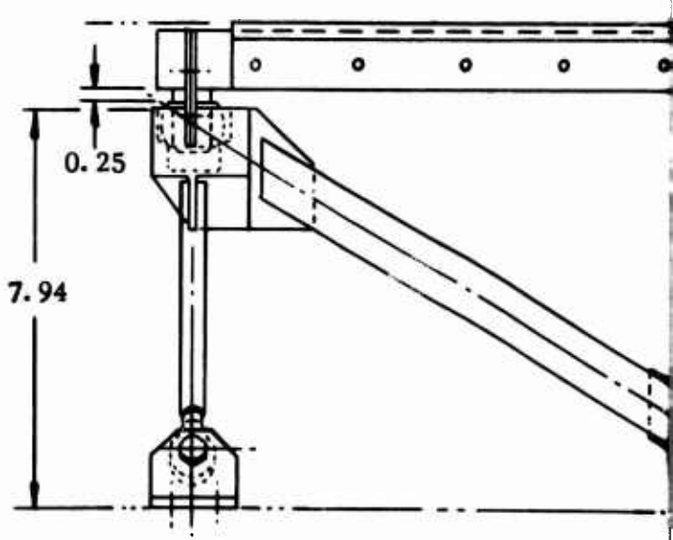

FWD. TRIPOD SUPPORT - SIDE & DR

A.

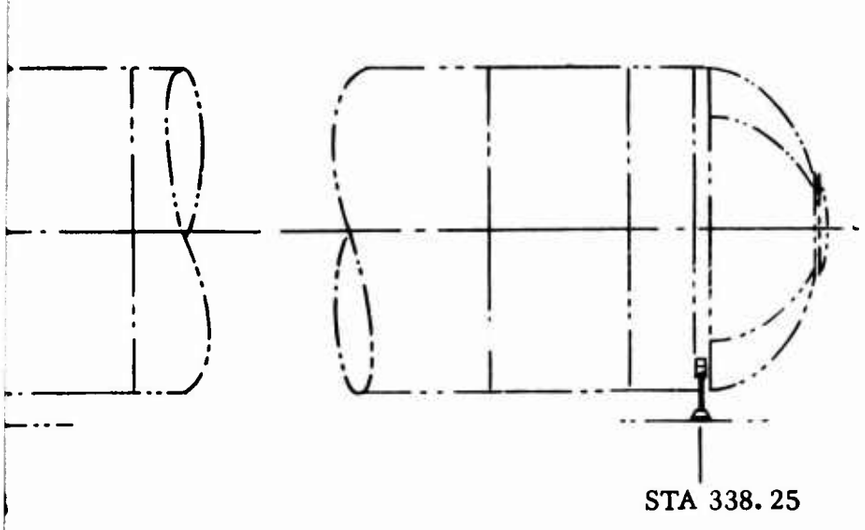

SIDE VIEW

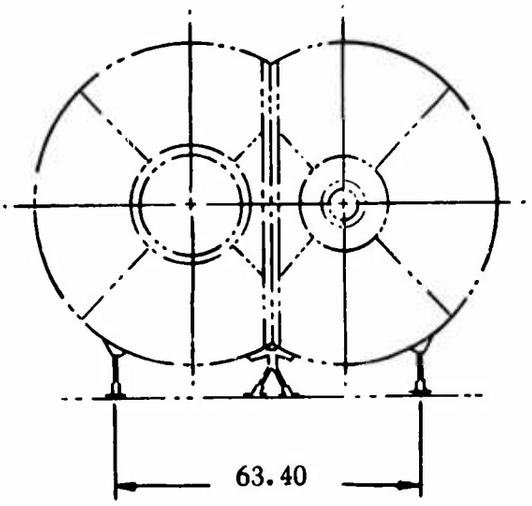

VIEW LOOKING FWD

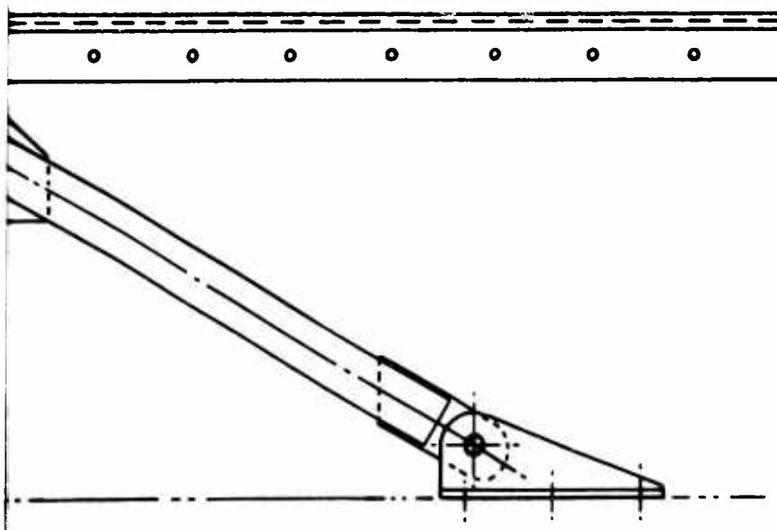

TRIPOD SUPPORT - SIDE & DRAG LOAD

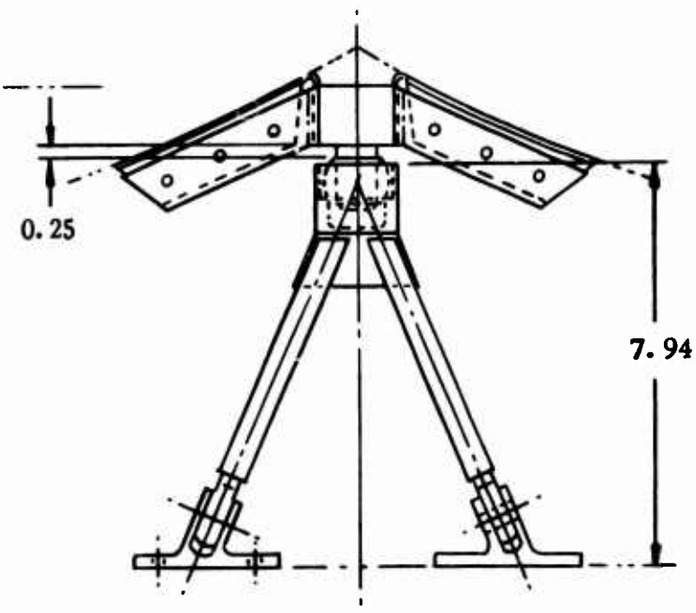

AFT BIPOD SUPPORT - SIDE LOAD

Figure 26. Tank Support System

B.

The magnitude of the relative thermal and elastic deformations that occur between the tank and vehicle structure during the flight cycle were significant considerations in the tank support system design. This is due to the different extremes of temperature the tank and vehicle structure experience and influences of pressure loading on the tank. The vehicle structure was assumed fabricated from the L605 material. Its coefficient of thermal expansion was found to be quite similar to that of the Alloy 718 tankage material (Figure 10). The pertinent deformations involved are given below. The transverse measurements are those occurring between the tank centerline and the vertical supports, the longitudinal are those occurring between the forward tripod and the aft support system. Deformations producing an inward for forward rotation of the supports in respect to the vehicle structure are negative while those producing opposite rotation are positive.

Tanking with liquid hydrogen (-423°F) in an unpressurized condition produces -2.64×10^{-3} (338.25 - 101.75) = -0.624 inches longitudinally and $-2.64 \times 10^{-3} \times 31.70$ = -0.084 inches transversely. Pressurizing the tank produces only longitudinal elastic deformations, since the transverse deformations are restrained by the main frames.

Ground Hold - 15.3 psig

$$\epsilon \times 236.5 = \frac{p\,R \times 236.5}{2tE} = \frac{15.3 \times 32 \times 236.5}{2 \times 0.016 \times 29.4 \times 10^{6}} = 0.123 \text{ inches}$$

Flight - 30 psig

$$0.123 \times \frac{30.0}{15.3} = 0.241 \text{ inches}$$

The maximum temperature reached by the lower vehicle structure during flight is 1300°F

$-10.4 \times 10^{-3} \times 236.50 = -2.460$ inches longitudinally

$-10.4 \times 10^{-3} \times 31.70 = 0.330$ inches transversely

Maximum deformations occur during flight

$-0.624 + 0.241 - 2.460 = -2.843$ inches longitudinally

$-0.084 - 0.330 = -0.418$ inches transversely

Heat leaks through the tankage support system were not found to be a significant problem area for hypersonic cruise vehicles. These losses relate to the thermal efficiency of the insulation system, and represents less than one percent of the total boiloff. Design of a low-conductivity support system did not warrant consideration. All items of the tank support system, except the spherical bearings, were designed using Alloy 718 as the structural material which was employed in the aged condition.

5

INSULATION SYSTEM

The primary functions of the insulation system are to limit boil-off of the liquid hydrogen fuel and avoid liquification of the surrounding atmosphere on the tank surface. A secondary function is to limit the temperature of the upper tank surface as the fuel level recedes. The insulation was required to be lightweight thermally efficient and capable of withstanding the extreme temperature environment imposed for 500 vehicle missions with high reliability. The system found to have the best compromise of thermal efficiency, reliability, and fabricability was a permeable all-quartz fiber insulation employed in a helium atmosphere. This insulation system was arrived at on the basis of extensive studies and supporting test programs performed in Phase I,(Reference 2).

The insulation is installed on the tank in the form of removable blankets, contained in a wire cloth envelope, and secured by means of wire lacing between studs on the tank and blanket assemblies, Figure 27 . This design provided a system with uncompromised high temperature capability. The insulation thickness varies from 1.3 inches at the top of the tank to 4.00 inches at the bottom with a gradual transition taking place at the side. Essentially this provides an optimum thickness for all locations on the tank, and was based upon the length of time the liquid and associated environment were at a given point. Insulation distribution was found to be one of the more important considerations in obtaining a minimum weight tankage system.

A stainless steel foil convection barrier, located under the first outside felt layer of insulation, covers the upper two-thirds of the tank surface area. This barrier impedes convection flow of warm helium gas through the insulation during ground hold, and also serves as a radiation barrier during flight. An experimental test program carried out without such a barrier in Phase I showed increased heat leaks to the liquid as a result of helium gas convection currents.

Helium, the required environmental gas, is introduced into the annular gap between the tank and the outer vehicle structure and allowed to diffuse into the insulation. Helium is required in this permeable system since it is the only gas which does not condense at liquid hydrogen temperatures. By inerting this space with helium, safety hazards due to potential hydrogen leakage from the tank and propellant lines are minimized. The disadvantages of this gas are its high conductivity and shortage in supply, but until more advanced insulation systems are developed it remains the only choice for such applications as the hypersonic cruise vehicle.

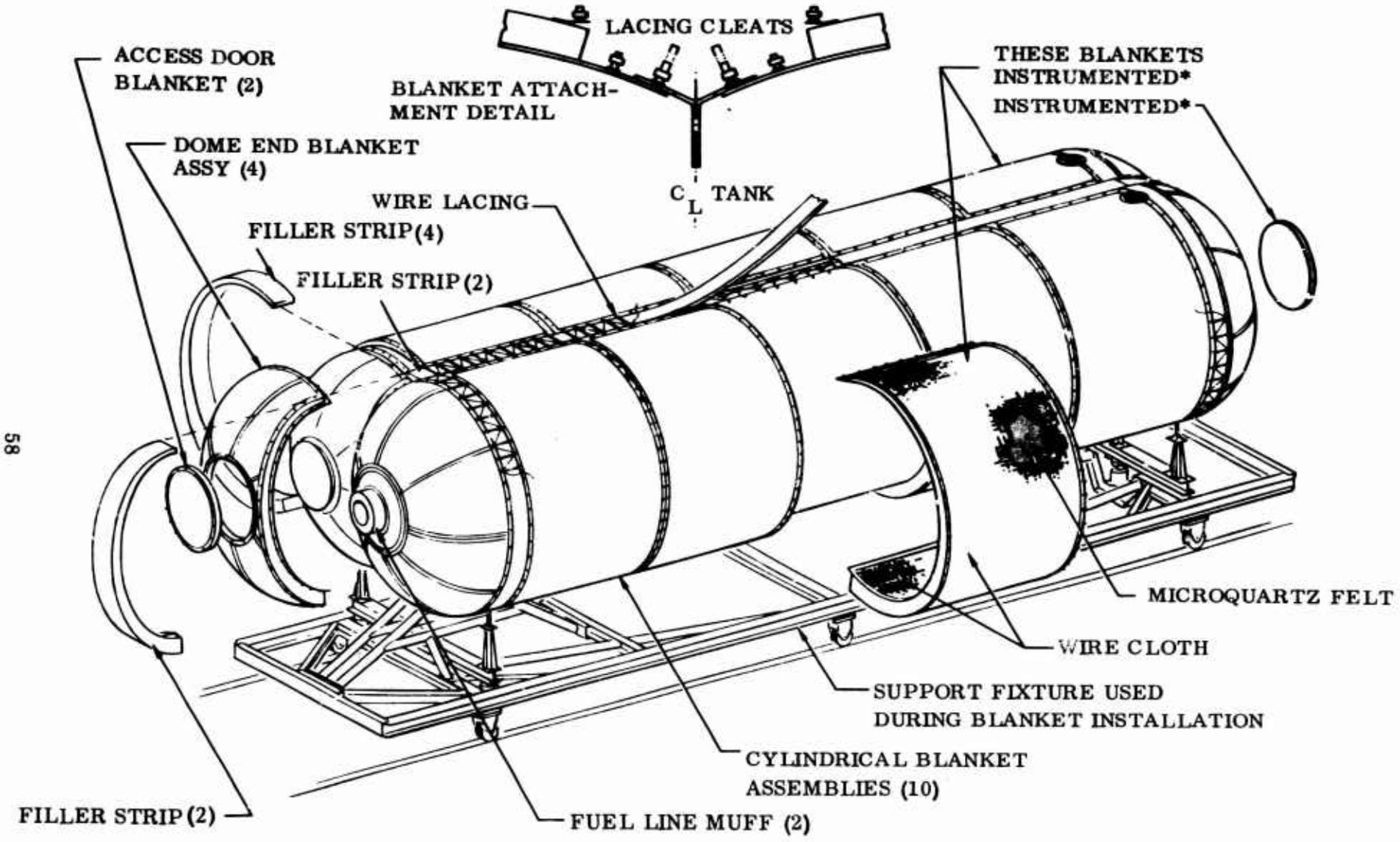

Figure 27. Insulation Installation

5.1 INSULATION MATERIAL - MICRO-QUARTZ

The basic insulation material employed was MICRO-QUARTZ felt, a Johns-Manville product trade name. This permeable all-quartz fiber material is supplied in the form of felts which have an off-white color, are flexible, and without a binder of any kind. Further details on the properties of this material are given in Table IV , References 8 and 9 . This material was chosen during Phase I on the basis of its low conductivity and density, good temperature capability, available thermal data, and excellent fabrication qualities which are due to its inherent flexibility.

5.1.1 THERMAL CONDUCTIVITY. Thermal conductivity data (K) for Micro-Quartz in a helium atmosphere was derived from a test program performed in Phase I (Reference 2) using a cryotherm test apparatus. Figure 28 shows the thermal conductivity for 1 inch and 3 inch blankets at 760 mm Hg and 8 mm Hg in a helium environment. The manner in which conductivity varies with pressure is shown in Figure 29 . This data is specifically aligned to this tankage systems environmental conditions and the test specimens were actual blanket assemblies. An exception was that the test specimens used a quartz cloth covering and quartz thread stitching rather than the wire cloth and thread used on the present insulation system. This difference was not anticipated to significantly change the conductivity values.

5.1.2 SHRINKAGE AND WEIGHT LOSS. Due to the amorphous nature of the silica fibers in Micro-Quartz there is a loss of chemically-held water accompanied by linear and thickness shrinkage when used at elevated temperatures. The extent to which this occurs is dependent upon the temperature, installed conditions, and soak time. Data established from in-house testing is shown in Figure 30 , Reference 10. Although this data does not cover the specific temperature conditions, 1240°F, involved on this program a reasonable estimate can be made from these results. A linear and thickness shrinkage of 2 percent is indicated with a loss in weight of possibly 6 percent. When the shrinkage value is considered for a 240 inch length a 4. 8 inch shortening is indicated. This led to a consideration for prefiring all the individual felts at the maximum operating temperature or above in order to stabilize the material. However, the time and cost involved was found prohibitive. The actual conditions the insulation would experience are quite different from that which a test sample undergoes. Only one face of the insulation would be exposed to high temperatures, the shrinkage of these outer layers is restrained by adjacent cooler layers which are also mechanically tied through and sandwiched by wire mesh. It was decided to proceed without any temperature stabilizing of the felts and provide for residual compression in all joints to take up localized shrinkage effects. Later flight simulation testing, five one hour runs at 1240°F, showed this approach valid. No gaps occurred in the insulation or any evidence of adverse shrinkage.

5.1.3 PROCUREMENT. Both 3/16 and 1/2 inch thick felts, with associated densities of 3.0 and 3.5 lbs/cu ft respectively, were purchased in widths of 36 inches and in both the 60 and 120 inch lengths.

Table IV. Microquartz - Material Properties

Chemical Composition			Physical Properties	
SiO_2	98.5%	(minimum)	Color:	An off-white.
Boron	0.01	(maximum)	Density:	Supplied in nominal densities of 3.0, 3.5, and 6.0 lb/ft^3.
Fe	0.06	"	Size:	Nominal thickness - 3/16" and 1/2" Sheet length - 60" and 120" Sheet width - 36"
Al_2O_3	0.50	"	Fiber Diameter:	1.3 microns (nominal). Other fiber diameters are available for specific applications.
Ca 0	0.35	"	Maximum Using Temp:	1600° F.
Mg 0	0.35	"	Thermal Conductivity:	(See Figure 28)
Na_2 0	0.15	"		

Description:

Micro-Quartz felts are made by the water deposition of fine 98.5% pure silica fibers. The felt is clean, flexible, and without a binder of any kind. It is sufficiently handleable for effective application and possesses the thermo-physical properties and chemical stability of pure silica. It is unaffected by moisture and will not accelerate or cause corrosion. It is inert to most acids.

Manufacturer: Johns-Manville, 22 East 40th Street, New York 16, New York.

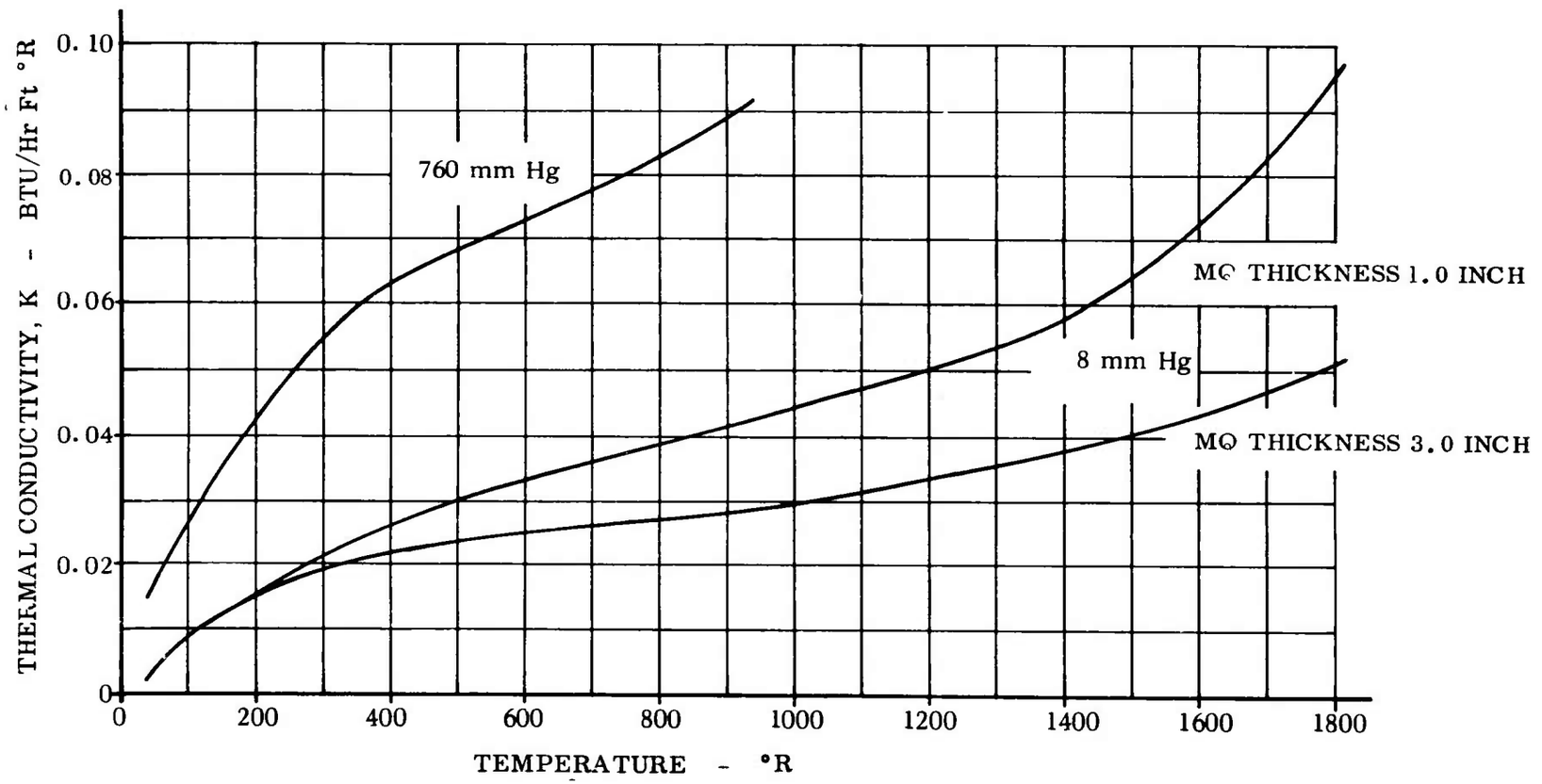

Figure 28. Thermal Conductivity of Micro-Quartz in Helium

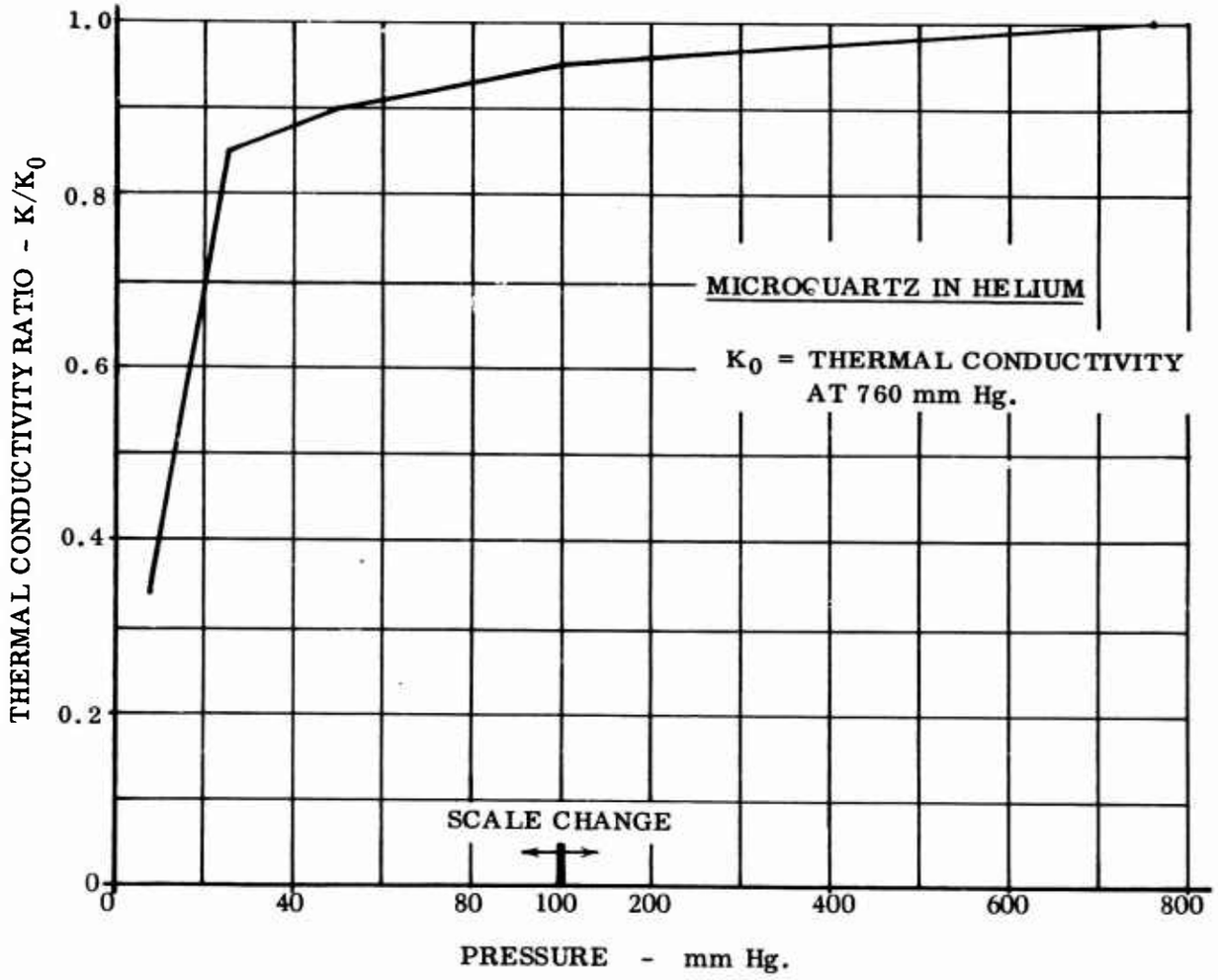

Figure 29. Typical Thermal Conductivity as a Function of Pressure

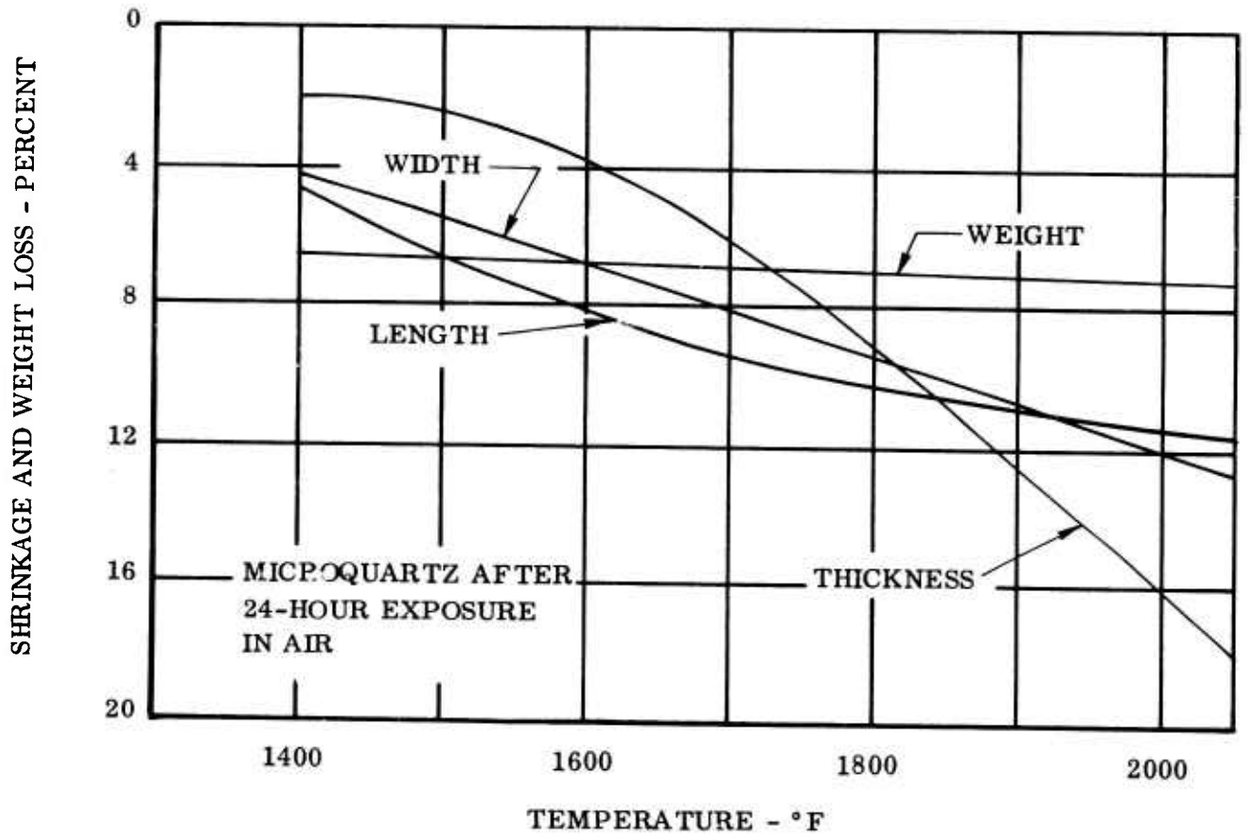

Figure 30. Shrinkage Rate Weight Change Vs. Temperature

Standard Sizes	Nominal Density and Weight (Based on single, standard sheets)		
Nominal Thickness - 3/16" & 1/2"	Density	Thickness	Weight
Sheet Length - 60" & 120" + 1/2" - 0"	(lb/cu ft)	(inches)	(lb/sq ft + 10%)
Sheet Width - 36" + 1/2" - 0"	3.0	3/16	.047
Note: Other thicknesses down to 1/8" and	3.5	1/2	.146
up to 1" are available on special	6.0	3/16	.094
order.	6.0	1/2	.250

5.2 BLANKET DESIGN

The insulation system was designed to be installed on the tank in the form of removable blankets which could be readily repaired without disturbing the undamaged sections. All penetrations through the insulation such as supports, vent and fuel lines, and access hatches are provided with individual blankets or cutouts for free access without disturbing the basic tank insulation. Figure 31 shows completed insulation installation.

The insulation system consists of ten (10) cylindrical blankets, four (4) dome blankets, two (2) access cover blankets, two (2) fuel line muffs, and joint blankets. The joint blankets provide for the filling of gaps at the tie-down areas, good fit around the tank supports, and for adjustment means on the final fit-up of the cylindrical and dome end blankets.

Blanket thickness varies from 1.30 inches at the top of the tank to 4.00 inches at the bottom with a 60 degree uniform transition at the midsection. This distribution also applies to the end dome blanket installations with slight modification for good design and fabricability.

All blanket assemblies have a similar construction which consists of layers of quartz felt build-up to the desired total thickness, sandwiched between wire cloth and then tufted with wire on 4 inch centers to provide good handling capability. During this tufting or stitching operation the quartz felts are compressed from their original 3.5 lb/cu ft density to approximately 4.5 lbs/cu ft. This compression imparts resiliency to the finished blanket which provides for good fabricability and handling considerations. The wire cloth has a 60 x 60 square weave mesh, an 0.0045 wire diameter and is fabricated from the 321 CRES alloy. The tight weave was selected to contain the quartz fiber without causing any undue localized loading which could result in powdering. Each individual wire cloth is framed on all four sides with thin-gage stainless steel strips to retain its shape and allow for attachment to the tank. The strips sandwich the mesh and are joined by means of a resistance spot weld process. Studs are installed on the strips, 4 inch centers, by means of a capacitor discharge stud weld process. These studs, No. 10 thread 3/8 inch long, with A-286 nuts provide the means for wire lacing the individual blanket assemblies to the tank structure or adjacent blankets. Similar studs are provided in the valley sections of the tank structure and in the area of the main frames. The framed edges

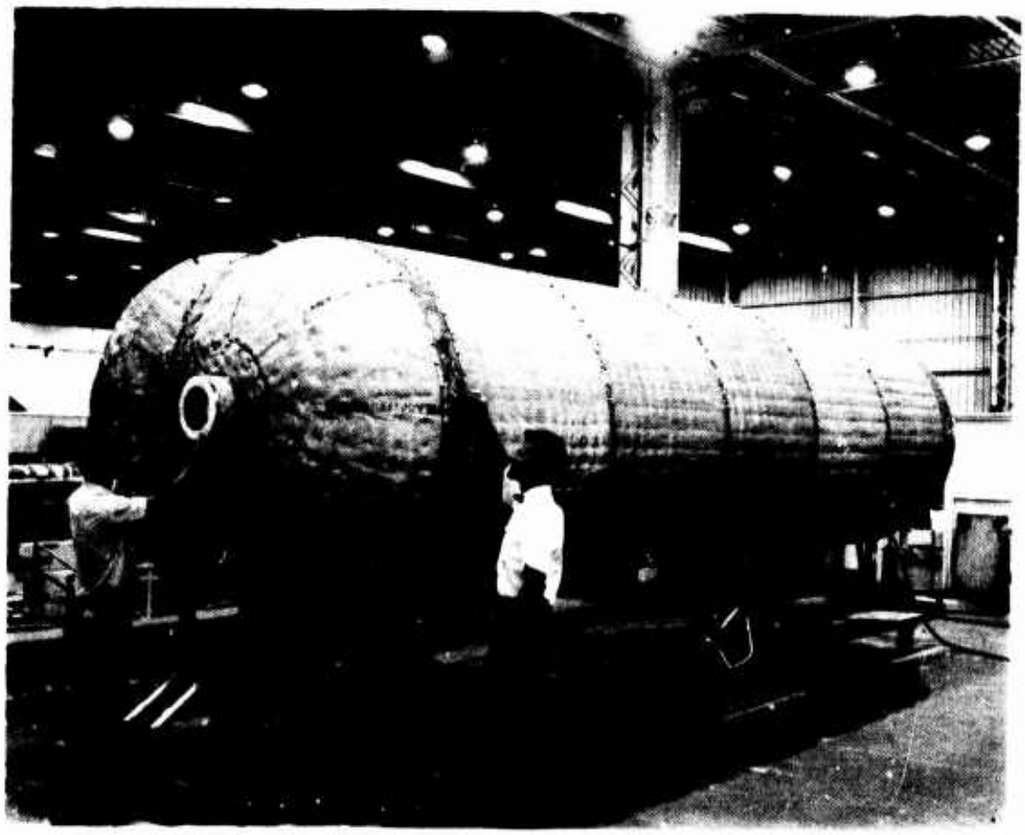

Figure 31. Completed Insulation Installation.

of the mesh provide for load redistribution from the studs into the basic mesh when the balnkets are installed. The handling capability of individual blankets when fabricated was excellent and the sensitivity of the quartz fiber to being permanently deformed by any local application of load was significantly reduced by the use of the wire mesh covering. The dome end blankets have a single-piece construction with individual access door blankets, or fuel line muffs at their apex. The wire cloth assemblies have a formed gore construction with joining accomplished by slight overlapping of the mesh reinforced by spot welded radial metal strips. The lacing and tufting wire was standard locking wire made from the heat resistant Inconel 600 alloy material.

A convection barrier, consisting of a layer of stainless steel foil, covers the upper two-thirds of the tank and is located under the first outside felt of the insulation blankets. The purpose of this barrier is to impede the flow of warm helium into the insulation, which would otherwise result in increased heat leaks to the tank at ground hold. This convection process is the suspected cause of heat fluxes exceeding predicted values during Phase I testing. The barrier weight, based on 0.0005 inch foil, is approximately 9 pounds, while the equivalent boil-off loss due to convection is 15 to 25 pounds of hydrogen. The barrier was actually fabricated from 0.001 inch stainless steel in this application due to the increased cost and procurement difficulties with the thinner gage. The convection barrier also reduces boil-off losses by serving as a radiation barrier during the flight condition.

An important consideration in the insulation system design and subsequent fabrication was to avoid any gaps in the insulation joints or construction. Some initial difficulties were experienced with tufting the blankets, due to the thickness and inclusion of a metal foil convection shield. The holes in the blanket resulting from the stitching operation were required to be no greater than the wire thread. If this was not accomplished loss in the insulation thermal efficiency would have resulted together with local hot spots on the tank structure. Use of special tools and proven procedures resolved this problem area. Sizing and forming tools were used to provide for accurate dimensional control of the blankets and a good fit to the tank surface. Extreme care was taken in the fitup of the blankets during installation in order to circumvent gaps and provide sufficient residual compression in the blanket edges to take up the effects of shrinkage that occurs when exposed to the high temperature environment of the simulated flight testing.

The integrity of the insulation system was established after the flight simulation testing when no deterioration or loss of thermal efficiency occurred from four tests and the capability to survive many additional flight cycles clearly indicated.

6

FUEL AND VENT SYSTEMS

The fuel and vent systems consist of the equipment and provisions necessary to chill-down and fill the fuel tank, transfer fuel from the tank and control pressures to the desired values. The fuel and vent systems' components associated directly with and installed in the large scale test tank are illustrated in Figure 32 . The fuel system includes a fill/drain line and submersible electric driven boost pump. The vent system includes two distribution manifolds connected to vent ports in each cylinder section of the tank and an emergency pressure relief standpipe. These components were used as illustrated for the LH_2 flight simulation tests. Three external valves were used for pressure and flow control. A vent valve was used which could be set to any regulated absolute pressure. An emergency mechanical vent valve was used to relieve at fixed gage pressure. A throttle valve was used to regulate liquid flow rate from the boost pump.

6.1 DESIGN APPROACH

The simplest fuel system would consist of a fill and drain pipe to fill the tank and drain the fuel to the engine pumps. The vent would be an open pipe to carry the fuel vapor overboard. However, a low boiling point cryogenic fluid in a flight weight tankage installation requires careful, predetermined pressure control. Pressurization must be considered in the following areas:

Structural Design. Thin gage construction requires that negative differential pressures not be permitted to develop. Pressure stabilized structures in many cases offer the minimum weight, whereas excessively high pressures introduce a structural weight penalty.

Tanking. Effective volume utilization involves filling the tank with maximum density fuel. This is especially true with liquid hydrogen where there is a 2.5 percent density decrease from the quiescent to the boiling condition plus a large coefficient of thermal expansion. Boiling suppression by pressurization permits a greater mass of fuel to be tanked into a given volume.

Fuel Transfer. High pressure ratio engine fuel pumps must be fed with subcooled fuel so that there is a net positive suction head at the pump inlet. This can be accomplished by pressurizing the tank as the fuel heats to keep it in a

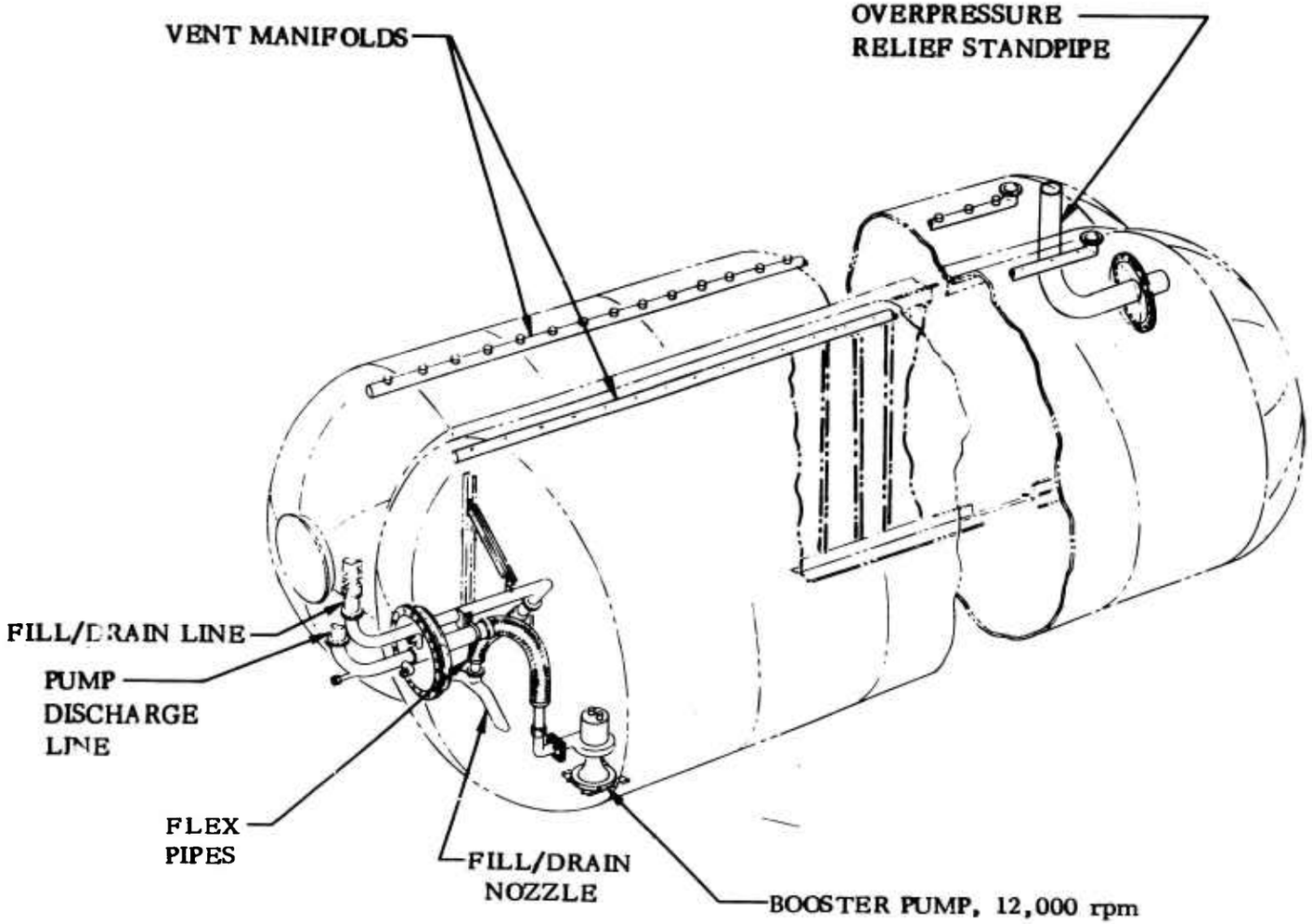

Figure 32. Fuel and Vent Systems Configuration - Large Scale Test Tank

subcooled condition for transfer or by pressurizing the fuel with a low pressure ratio tank mounted boost pump which can handle boiling fuel.

Boil-Off Losses. Pressurization subcools the fuel and permits it to absorb sensible heat. The heat thus absorbed by the fuel reduces boil-off losses.

All of the above criteria were considered in establishing the fuel and vent system design. It is apparent that the interrelating factors listed above must be considered simultaneously in order to determine an optimum tank installation. Tank size and structural weight, insulation weight and performance, and liquid thermal conditions, when evaluated together, involve a complex optimization process in order to select the best tankage installation. A detailed thermal performance and weights analysis is given in Appendix IV. Included in the appendix is a sample optimization of a full scale vehicle tank. A similar optimization was performed on the large scale tank tested during this program. Those optimization results were reported in Reference [2], Phase I of this program. A ground rule for this particular tank structure is unpressurized tanking and ground taxi. Pressure stabilized construction was not considered a parameter in this analysis. The optimum operating pressure for the large scale test tank was 30 psia. At this pressure the fuel starts boiling early in the flight. Thus, the optimization eliminated tank pressurization as a means of fuel transfer to the engines. Considerably more thermal protection (more insulation) and higher pressures (increased structure weight) would be required to effectively use pressurized fuel transfer. Thus, a boost pump is the recommended minimum weight approach for liquid hydrogen tanked at atmospheric pressure utilizing this particular insulation system. If the fuel were subcooled or possibly slush, or if a high efficiency thermal protection system were available where the fuel could be maintained subcooled at a reasonable pressure, pressurized fuel transfer might be an optimum system. However, liquid hydrogen tends to quickly stratify and develop a deep boiling layer so that for long flight times such as the cruise mission being considered here, pressurized fuel transfer is not likely to be an optimum system approach. Slush hydrogen was evaluated and compared with the liquid hydrogen. The results are given in Appendix III. The slush hydrogen tankage installation is lighter and occupies less volume than the liquid installation. However, the development of the stratified boiling layer of liquid in the slush tank still leads to the requirement for a boost pump fuel transfer system.

The evaluation of the slush system invoked another of the pressurization criteria; preventing negative pressure differentials on the tank structure. Even though a stratified boiling layer developed, there was insufficient boiling liquid to flash and prevent a significant ullage pressure drop when liquid outflow started so that pressurization is required for the slush system. The recommended pressurization system is helium stored and used at cryogenic temperature. The pressurization system selection is explained in Appendix III.

The large scale test tank used in this program employs self-pressurization. The particular pressure in this case, 30 psia, is the optimum for sensible heat absorption by the fuel. Pressurization is also used to suppress boiling and achieve a maximum density when the tank is topped during the fill operation. The tanking procedure is illustrated in Figure 33. Self-pressurization involves closing the tank vent permitting the ullage to heat up and increase the pressure. In this particular tank, self-pressurization occurred at the rate of 3 psi per minute. This is based on test results reported in Volume III. This pressurization rate is rapid and no external pressure is required. Here again, a tank with more efficient insulation would pressurize less rapidly and, depending on operational requirements, might require external pressurization. The tank pressure is held at 30 psia during ground hold by a pressure regulator valve. During this time a stratified boiling layer of liquid develops at the top surface and venting occurs. When the pump outflow starts at the beginning of simulated flight, the ullage expands and the pressure drops. The maximum pressure drop during the tests, Volume III of this report, was from 30 to 28.5 psia and the time below 30 psia was about two minutes. Ullage heating and flash-off from the boiling liquid layer resist the pressure drop. The only concern at this point is negative tank differential pressure. So long as the tank operating pressure is about 2 psi above ambient, there is no problem with a negative pressure differential. These tests were run with a 3 per cent ullage space at the end of ground hold and the pump outflow rates were scaled from actual flight requirements. The ullage expansion is therefore representative of an operational tank installation.

6.2 FUEL AND VENT SYSTEM COMPONENTS

6.2.1 FUEL SYSTEM. The fuel system employed a tank-mounted, submersible, electric driven boost pump which could handle saturated or boiling liquid hydrogen. The pump was designed and built for the Air Force by Pesco Products division of Borg-Warner Corporation, Reference 11 . The unit has a centrifugal impeller and a 3-phase, 120 volt, 400 cycle, 12,000 rpm motor. The pump is located at the forward end of the tank in the left hand lobe. This end of the tank has a fixed location in relation to the supporting structure and the need for flexible connections in the external fill/drain and pump discharge lines is thus minimized. The high pressure fuel discharge line (1-1/2 inches diameter) is vacuum-jacketed from the pump to the tank pierce point in order to avoid heat transfer from the warmer outflowing liquid to the hydrogen in the tank. The discharge line is divorced from the fuel fill/drain line to avoid backflowing through the impeller. The fill operation could cause excessive reverse rpm and centrifugal force on the pump rotor. The design maximum pump flow rate is 120 gpm and the fill rate was about 200 gpm. The fill/drain line (2 inches diameter) enters the tank through the same cover flange as the pump discharge line. The fill/drain line includes a Y inside the tank so that both lobes of the tank were filled and chilled down simultaneously. No vacuum jacket was required on the fill/drain line inside the tank. All liquid hydrogen lines were vacuum-jacketed inside the chamber up to the tank connection.

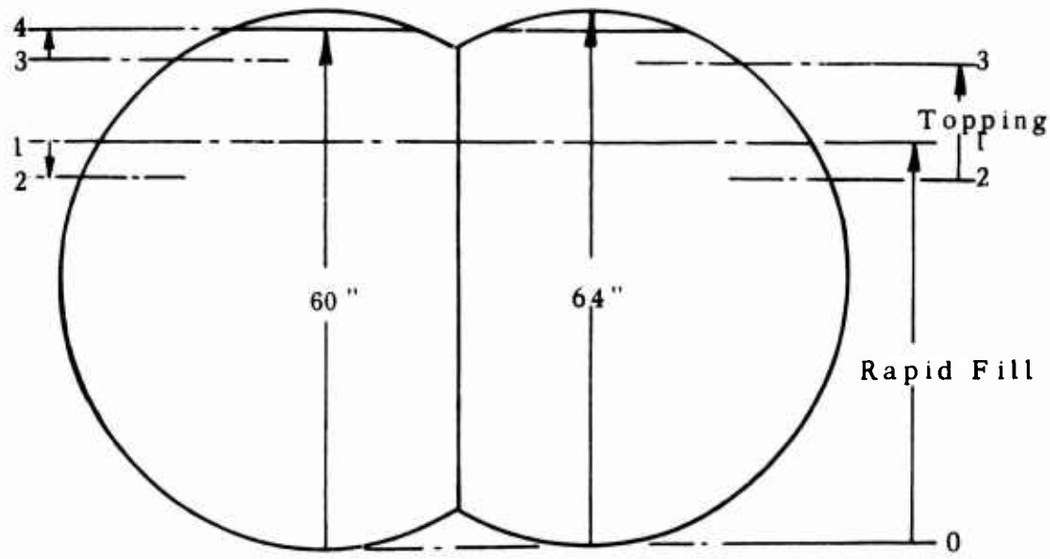

Level

0 - 1 Rapid refueling to 90% useful capacity with vent open. Fuel is boiling.

1 - 2 Set vent pressure control to 2 psig to suppress boiling and reduce bulk volume.

2 - 3 Topping-up under 2 psig pressure to a pre-determined level that will prevent liquid rise above 60 inches during ground hold.

3 - 4 Liquid expansion due to density decrease as bulk temperature rises during 30-minute ground hold. The final fill level at the end of ground hold is to be 60 inches. Insulation system performance predicts topping level required to meet this condition.

Figure 33. Tank Fill and Ground-Hold Fuel Levels

6.2.2 VENT SYSTEM. The vent system consists of two 3-inch diameter internal piccolo manifolds and an overpressure relief standpipe. The piccolo tube is provided with vent holes, decreasing in size in the downstream direction as a function of the upstream pressure drop, uniformly spaced along the full length of each cylinder section. These holes were sized to uniformly distribute the boil-off gas along and cool the dry upper tank surface. The vent and hole sizing analysis is given in Appendix II. The tank is vented through this system during all normal fill and simulated flight operations. The vent pipes from each lobe were externally connected to flexible 2-inch lines which went up through the furnace and the top of the chamber then connected together at the 2-inch vent pressure regulator valve. The tank drawings with 2-inch vent ports were released and fabrication started before the detail analysis on the piccolo vent manifold was complete. The 3-inch internal vent manifolds were transitioned to 2 inches with a rounded bell mouth to minimize pressure losses. An auxiliary vent system was incorporated in the form of a 3-inch diameter standpipe connected to an external pressure relief valve. In the case of tank overpressure, the valve will open preventing damage to the tank structure. The auxiliary system is necessary since the piccolo manifold pressure drop could become large in case of inadvertent liquid overfill, or increased boil-off due to failure of the radiant furnace control or insulation system in the test setup.

6.3 FLIGHT SYSTEMS

An actual aircraft fuel system will have two boost pumps in a tank of this type. They are required for redundancy and reliability. In this tank, 70 pounds of otherwise usable fuel was trapped in the lobe with no pump. The liquid was pumped down to three inches; five and one-half inches was trapped in the other lobe. The pump installation weight is 37 pounds, so that a simple weight tradeoff would indicate the second pump should be installed.

An actual aircraft vent system installation will probably necessitate the installation of both fore and aft vent ports in the tank to provide for sloshing effects. As aircraft angle of attack and flight accelerations are considered, it will be possible for either the forward or aft ports to be covered with liquid. Thus, the dual vent will be necessary. In addition, a safety vent relief which is not part of the piccolo vent system will also be needed. This is especially true during tanking and chilldown, where vent flow rates will be high.

The effects of pressure loss in the dual vent system are illustrated in Figure 34 . In this case, there are 12 holes in each manifold carrying only one-fourth of the total flow (90 lb/hr). The pressure losses are reduced by about a factor of 4 for a given vent manifold size. This design will naturally be complicated by external manifolding which ties it all together into the aircraft vent system. Careful manufacture and assembly, as well as good total system calibration, will be required to assure uniform flow and adequate internal cooling for which the piccolo vent system is designed.

MANIFOLD FLOW RATE, 180 lbs/hr @ 520°R, HYDROGEN GAS

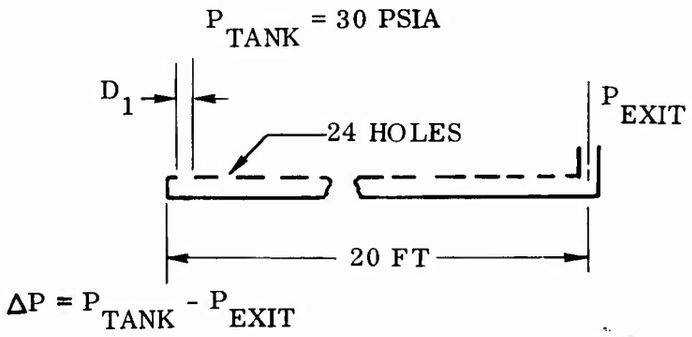

MANIFOLD FLOW RATE, 90 lbs/hr @ 520°R, HYDROGEN GAS

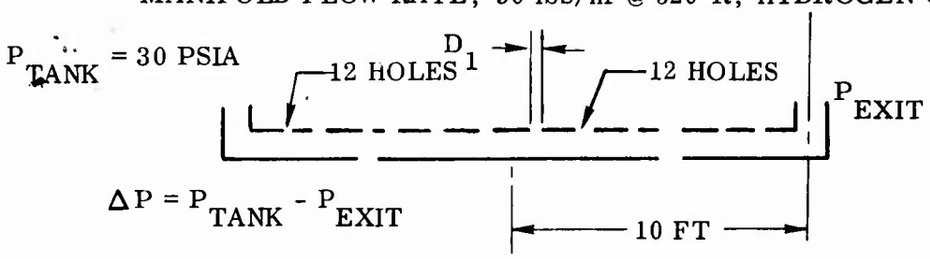

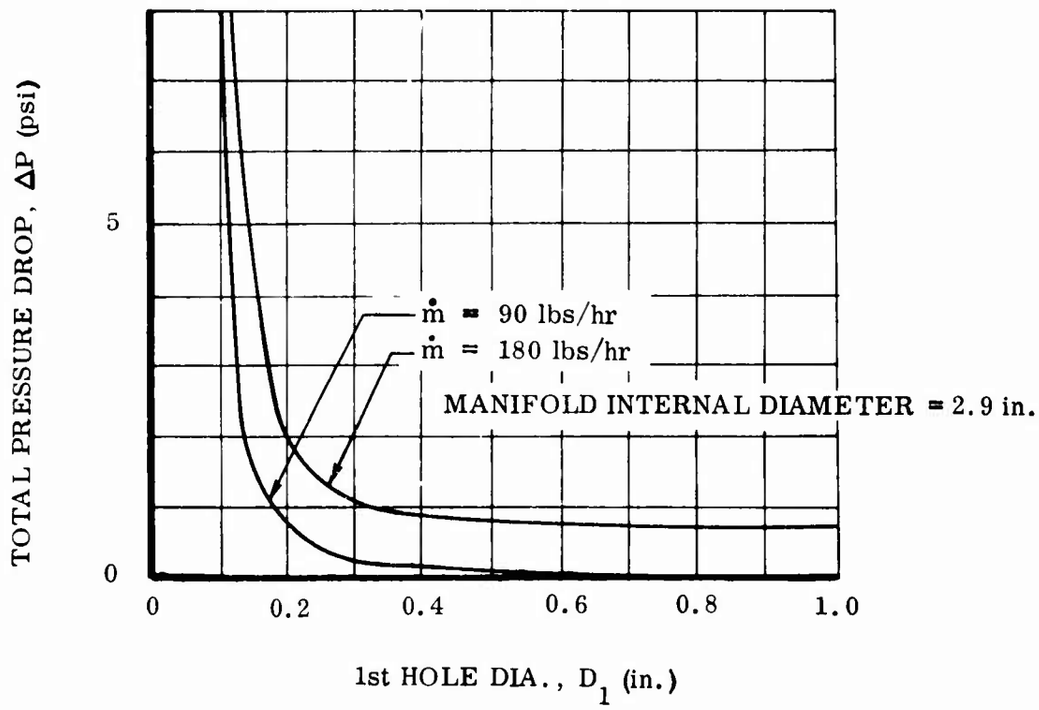

Figure 34. Pressure Loss in Vent System

Two possible conditions could exist in an aircraft where liquid may be introduced into the vent manifold. These are: (1) during tanking where a loss of liquid level sensing might result in an inadvertent overfill and (2) boost pump start-up may induce liquid sloshing which could dump liquid into the manifold. Once liquid enters the manifold, it is trapped and can only get out by boiling and exiting through the vent. While liquid remains in the manifold, it reduces the gas flow area and increases the pressure loss.

The large scale tank has been designed with vent ports in the aft end only, where the piccolo vents were attached. No forward vent ports were installed. A pressure relief standpipe was incorporated to preclude the possibility of an overpressure situation.

7

CONCLUSIONS AND RECOMMENDATIONS

Significant progress as a result of this program has been made in establishing the feasibility of liquid hydrogen tankage systems in application towards advanced aerospace vehicles. Most of the significant aspects of the overall-all tankage system aspects were investigated, evaluated and interrelated to provide minimum weight, high efficiency and integrity. One area not considered was the influence of fuel sloshing on the tankage system integrity, performance and fuel system requirements. Sloshing is the most significant problem area remaining to be researched and will require some analytical research before proceeding into test application.

1. The tank configuration employed was seen to have desirable attributes other than its volumetric efficiency within the elliptical fuselage cross-section. With this configuration, an extremely efficient structural concept was possible. The center web, by only a small amount of additional stiffening, provided the capability for handling the majority of the unpressurized bending requirements of the tank. This allowed a simple frame stiffening concept to be used for the tank cylindrical sections instead of longitudinal stiffeners. Stiffeners would have involved significant weight penalties due to influences of pressure and induced thermal loading. The configuration also provided an efficient pressure vessel shape.

2. The structural material, Alloy 718, proved an excellent choice for the tank once its initial fabrication difficulties were overcome. The initial problems with the material are to be credited more to its recent development and limited usage than any inherent limitations. Although in this specific application it was not directly exposed to extremely high temperatures, for an early emptying tank it would become subject to steady state temperatures approaching those of the outer vehicle surface. This material has excellent high temperature strength to handle such considerations.

3. Heat leaks through the tank support system are negligible and certainly not a problem area for hypersonic cruise vehicle applications. The significance of such heat leaks relate to the efficiency of the over-all insulation system and represent an extremely small percentage of the total boiloff.

4. Efficiency of a tankage system was found to be very dependent upon the rate of fuel usage and the time it contains the fuel. This is primarily due to the fact that an optimum insulation thickness exists for any given location, depending upon the time that point sees the liquid and associated environment. Further study is recommended on the significance of maximum efficiency in regard to other fueled conditions, especially early emptying tanks. The insulation system functioned well in its fabricated form, but it still remains desirous to seek a more efficient insulation system and a means of circumventing the need for helium.

5. The need of a boost pump to handle saturated fuel conditions was clearly evident and all that now remains is to develop a flightweight model with the capability to handle the higher temperature environment associated with earlier emptying tanks.

6. Optimum tank pressures are low for hypersonic cruise vehicle applications. Good venting control is required if structural weight penalties are to be avoided. Use of the boiloff gas will increase the venting control problem.

7. The significance of ullage stratification on upper tank wall temperatures, determined to be a problem in an earlier phase of this work, was reduced by the vent manifold system. This system took greater advantage of cooling effects of the boiloff by forced circulation. The system as designed would not, however, be applicable to a flight tank since sloshing and changes in liquid level angle would choke the vent and produce over-pressures and potential tank rupture. A dual vent system would be required that allows one vent to become covered with liquid while allowing the other to vent the gas condition.

8. The presence of moisture in the insulation system poses a problem for a flight article since there is less capability of removing it inside a fuselage than there was in the environmental test chamber. A fuselage has little capability of accepting negative pressures and purging is not an efficient method for drying the tank insulation.

9. Spray cooling was not required in the specific application considered, but for earlier emptying tanks or a higher temperature environment, as would be experienced with Mach 8 to 12 vehicle, it would appear necessary that trade-off studies be performed to determine the relative structural weight/fuel loss involvements.

10. Boiloff occurred even during the ground-hold period, despite an essentially sub-cooled condition of the fuel, due to surface boiling conditions. The liquid stratifies with rapid increase in the depth of the boiling layer. The influence of bottom heating did not appear to have any real influence on providing circulation of the liquid condition.

11. The influence of fuel sloshing was not researched in this work despite its obvious significance except as an area of some analytical interest. This was due to the complexity of the associated dynamic and thermal analysis for horizontal tank applications and potential safety hazards in testing without sufficient background experience.

8

REFERENCES

1. Air Force Contract AF33(615)-2048, "Design, Fabrication and Experimental Verification of Cryogenic Tankage Applicable to Manned Aerospace Systems," dated 1 July 1964.

2. Heathman, J. H., et. al., "Hydrogen Tankage for Hypersonic Cruise Vehicles - Phase I," Contract No. AF33(615)-2048, Technical Report AFFDL-TR-65-230, August 1966.

3. Girton, L. D., "Evaluation of Sheet Alloy 718 for Formed and Welded Missile Parts," GD/A-ERR-AN-656, December 1964.

4. Christian, J. L., Yang, C. T., and Witzell, W. E., "Physical and Mechanical Properties of Pressure Vessel Materials for Application in a Cryogenic Environment," Contract No. AF33(657)-11289, General Dynamics Convair Division Report No. GD/A-DDG-002, December 1964.

5. Witzell, W. E., "Fracture Data for Materials at Cryogenic Temperatures," Contract No. AF33(615)-3779, General Dynamics Convair Division Report No. GDC-ZZL67-017, July 1967.

6. Lloyd, J. R., "Analysis of a General Shell-Supported Frame," General Dynamics Convair Report No. AE 62-0490, 31 December 1962.

7. Smith, G. W., "Analysis of Multiple Discontinuities in Shells of Revolution Including Coupled Effects of Meridional Load," General Dynamics Convair Report GD/A 63-1044, 31 July 1963.

8. Johns-Manville Corp., New York Bulletin IN-414A, dated January 1962, "Micro-Quartz Felt."

9. Pettyjohn, R. R., "Thermal Properties Investigation of High Temperature Fibrous Insulating Materials," General Dynamics Convair Division Report GDC-ERR-AN-996, 31 December 1966.

10. Ryan, J. M., et. al., "The Optimization of Thermal Composites," Contract AF33(615)-1672, Technical Report AFML-TR-65-244, December 1965.

11. Caine, G. H., et. al., "Design Fabrication and Tests of a Liquid Parahydrogen Booster Pump," WADC TR-58-680, December 1958, by Pesco Products, division of Borg-Warner Corporation for Wright Air Development Center, WPAFB.

12. Haerter, A. A., "Flow Distribution and Pressure Change Along Slotted or Branched Ducts," ASHRAE Transactions, Vol. 69, 1963.

13. Healy, J. H., Patterson, M. N., Brown, E. J., "Pressure Losses through Fittings Used in Return Air Duct Systems," ASHRAE Journal, Vol. 4, May 1962.

14. American Institute of Physics Handbook, 2nd Edition, 1963, Chap. 2 u., McGraw-Hill.

15. Epstein, M., "Prediction of Liquid Hydrogen and Oxygen Pressurant Requirements," International Advances in Cryogenic Engineering, pp 303-307, Plenum Press, New York, 1965.

16. Perkins, C. K., and Wilburn, R. D., SAE/ASME Air Transport and Space Meeting, "Capacitance Mass Sensing of Boiling Propellants," Paper No. 859A, New York, April 1964.

APPENDIX I

DIGITAL COMPUTER PROGRAM FOR THERMAL STRESS AND BUCKLING ANALYSIS

This appendix presents the basic outline of a digital computer program which was developed for the structural analysis of a cryogenic tank subjected to the loading effects of pressure, inertia, and temperature gradients.

This analysis was directed to the selected double-bubble tankage configuration which has a center beam and stabilizing frames. This structural arrangement allows the skin to buckle, thus reducing its meridional stress due to the thermal gradient, while the center beam provides restraint from total collapse.

Bending capability is maintained by utilizing the center member as a beam. This member has significant cap areas, and its web structure is capable of transmitting shear. By slightly increasing the bending capability of the intermediate stabilizing frames, they are able to transmit shear from the outer shells into the center beam, as the outer shells lose shear capability due to buckling.

The theory employed in this program constitutes a strength-of-material approach which is well within the state-of-the-art. Therefore, no derivations of formulae are presented here. Emphasis is placed on the sequence of operations and the final equations actually used in the solution. Figure 35 shows program geometry and sign convention. A flow chart of this program is given in Figure 36.

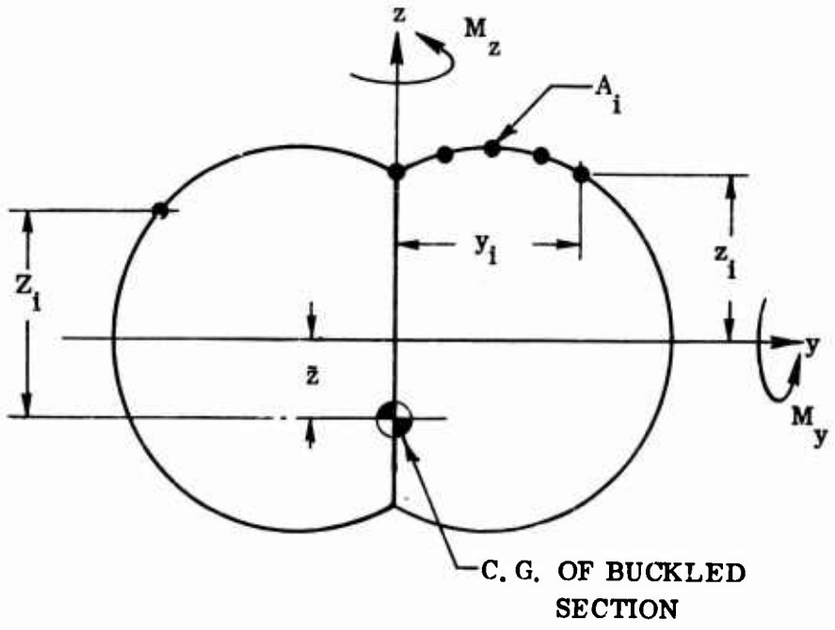

Figure 35. Sign and Geometry Convention

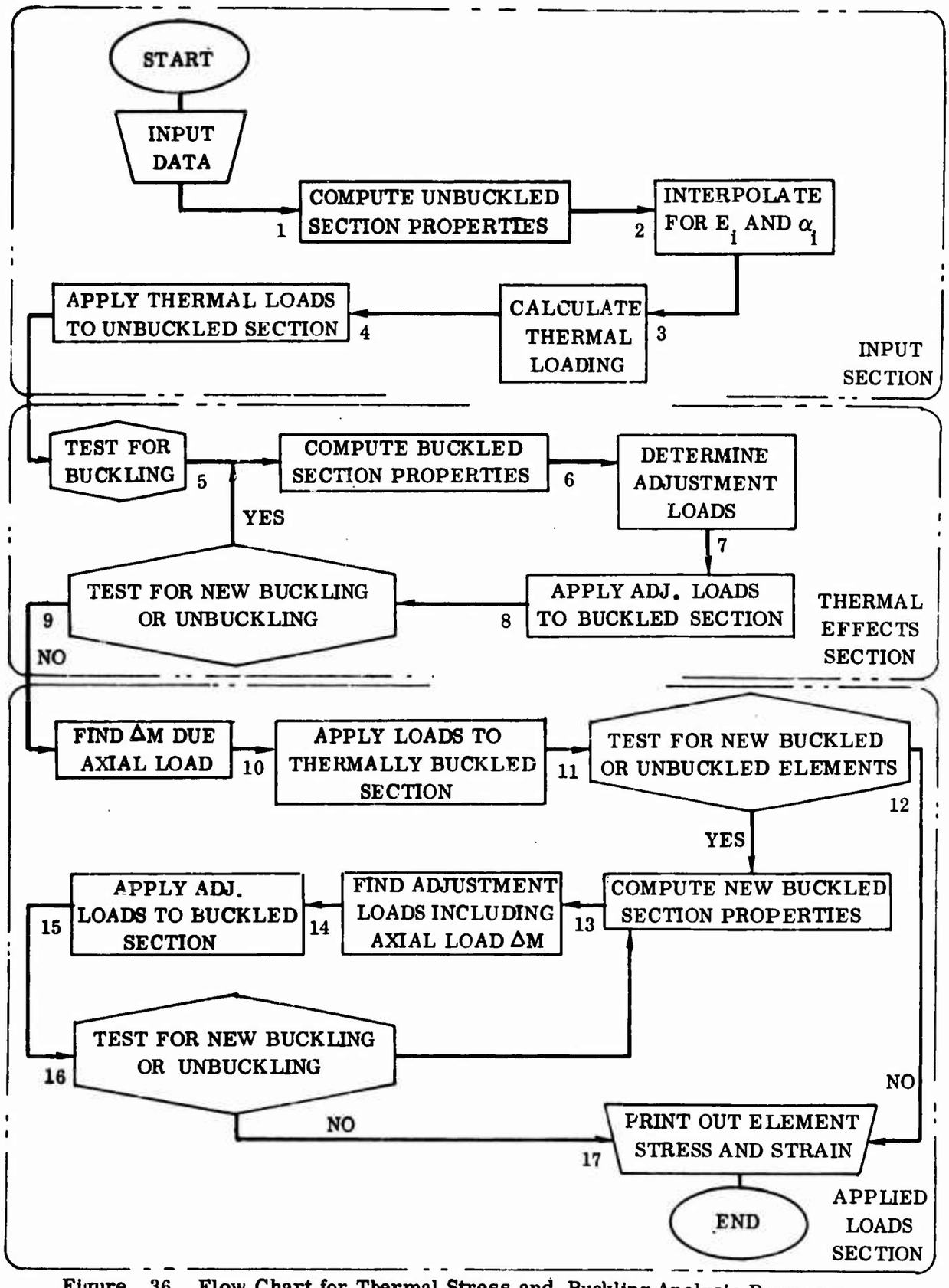

Figure 36. Flow Chart for Thermal Stress and Buckling Analysis Program

1 NOMENCLATURE

The nomenclature and subscripts used in the program are as follows:

NOMENCLATURE

A	=	Area, sq in.
E	=	Young's Modulus, psi
I	=	Moment of inertia or product of inertia, $in.^4$
M	=	Moment, in.-lb
P	=	Axial load, lb
T	=	Temperature, °R
Y	=	Coordinate from buckled section c.g., in.
Z	=	Coordinate from buckled section c.g., in.
f	=	Stress, psi
y	=	Coordinate along y axis, in.
z	=	Coordinate along z axis, in.
Δ	=	Value of change
Σ	=	Value of summation
α	=	Coefficient of thermal expansion, in./in./R
ϵ	=	Strain, in./in.

SUBSCRIPTS

ADJ	=	Adjustment
B	=	Buckled section
L	=	Load induced
NS	=	No stress induced
T	=	Temperature induced, or of unbuckled section
b	=	Index of buckled elements
i	=	Index of all elements
k	=	Index of unbuckled elements
p	=	Center of pressure
y	=	About y axis
yz	=	About y and z axes
z	=	About z axis

2 INPUT DATA

The total cross section is divided into discrete elements which are assigned values for A, y, z, ϵ_c, and T. It is assumed that the divisions will be sufficiently small to permit neglect of each element's moment of inertia about its own centroidal axis. Material property data are furnished in the form of a table which gives both Young's modulus and the coefficient of thermal expansion as functions of temperature.

Applied loads are specified in the input, that is, moments for the two axes and an axial load with the coordinates of its resultant.

The temperature input are those at which no thermal stresses are induced.

Input List

A_i	Element Input Data
y_i	
z_i	
ϵ_{ci}	
T_i	
M_y	Applied Loads
M_z	
P	
y_p	Ordinates
z_p	
T_{NS}	Temperature

Material Properties

$T_1 \quad \alpha_1 \quad E_1$

$T_2 \quad \alpha_2 \quad E_2$

$T_3 \quad \alpha_3 \quad E_3$

$\downarrow$

$T_{10} \quad \alpha_{10} \quad E_{10}$

3 GOVERNING EQUATIONS AND PROGRAM LOGIC

Step 1 - Compute unbuckled section properties.

$$A_T = \Sigma_{i=1}^{ALL} A_i$$

$$\bar{y} = (\Sigma_{ALL} A_i y_i)/A_T$$

$$\bar{z} = (\Sigma_{ALL} A_i z_i)/A_T$$

$$I_y = \Sigma_{ALL} (z_i^2 A_i - A_T \bar{z}^2)$$

$$I_z = \Sigma_{ALL} (y_i^2 A_i - A_T \bar{y}^2)$$

Coordinates from neutral axis:

$$Y_i = Y_i - \bar{y}$$

$$Z_i = z_i - \bar{z}$$

$$I_{yz} = \Sigma_{ALL}\, Y_i Z_i A_i$$

Step 2 - Interpolate for E_i and α_i . Follow Table lookup procedure.

Step 3 - Calculate thermal loading.

$$P_T = \Sigma_{ALL}\, \alpha_i E_i\, (T_i - T_{NS})\, A_i$$

$$M_{yT} = -\Sigma\, \alpha_i\, E_i\, (T_i - T_{NS})\, Z_i\, A_i$$

$$M_{zT} = \Sigma\, \alpha_i\, E_i\, (T_i - T_{NS})\, Y_i\, A_i$$

Step 4 - Apply thermal loads to unbuckled section properties.

$$f_{Ti} = -\alpha_i E_i\, (T_i - T_{NS}) + \frac{P_T}{A_T}$$

$$+ \left(\frac{I_y M_{zT} + I_{yz} M_{zT}}{I_y I_z - I_{yz}^2} \right) Y_i$$

$$- \left(\frac{I_z M_{yT} + I_{yz} M_{zT}}{I_y I_z - I_{yz}} \right) Z_i \quad \text{and}$$

$$\epsilon_{Ti} = f_{Ti}/E_i$$

Step 5 - Test for buckling and adjust stresses of buckled elements.

For buckled elements:

$$\epsilon_{Ti} \leq \epsilon_{ci} \text{ reset } f_{Ti} = \epsilon_{ci} E_i$$

i is removed from k list and put in b list.

For unbuckled elements:

$$\epsilon_{Ti} > \epsilon_{ci} \qquad f_{Ti} \text{ as found in step 4}$$

All unbuckled elements make k list. Note:

$$\Sigma_b + \Sigma_k = \Sigma_i$$

Step 6 - Compute buckled section properties.

$$A_B = \Sigma_{ALL\,k}\, A_k$$

$$\bar{y}_B = (\Sigma_{ALL\,k}\, A_k y_k)/A_B$$

$$\bar{z}_B = (\Sigma_{ALL\,k}\, A_k z_k)/A_B$$

$$I_{yB} = \Sigma_{ALL\,k}\, z_k^2 A_k - A_B (\bar{z}_B)^2$$

$$I_{zB} = \Sigma_{ALL\,k}\, y_k^2 A_k - A_B (\bar{y}_B)^2$$

Coordinates from new neutral axis:

$$Y_i = y_i - \bar{y}_B$$

$$Z_i = z_i - \bar{z}_B$$

$$I_{yzB} = \Sigma_{ALL\,k}\, Y_k Z_k A_k$$

Step 7 - Determine adjustment loads.

$$P_{TADJ} = \Sigma_{ALL\,b} (\epsilon_{Tb} - \epsilon_{cb})\, E_b A_b$$

$$M_{yTADJ} = \Sigma_{ALL\,b} (\epsilon_{Tb} - \epsilon_{cb})\, Z_b E_b A_b$$

$$M_{zTADJ} = \Sigma_{ALL\,b} (\epsilon_{Tb} - \epsilon_{cb})\, Y_b E_b A_b$$

Step 8 - Apply adjustment loads to buckled section and determine revised stresses and strains.

Change in strain:

$$\Delta\epsilon_{Ti} = -\frac{P_{TADJ}}{E_i A_B} + \left(\frac{I_{yB} M_{zTADJ} + I_{yzB} M_{yTADJ}}{I_{yB} I_{zB} - I_{yzB}^2}\right)\frac{Y_i}{E_i}$$

$$-\left(\frac{I_{zB} M_{zTADJ} + I_{yzB} M_{zTADJ}}{I_{yB} I_{zB} - I_{yzB}^2}\right)\frac{Z_i}{E_i}$$

New strain:

$$\epsilon_{Ti_{new}} = \epsilon_{Ti_{old}} + \Delta\epsilon_{Ti}$$

Change in stress:

$$\Delta f_{Tk} = E_k (\Delta\epsilon_{Tk}) \qquad \Delta f_{tb} = 0$$

New stress:

$$f_{Ti_{new}} = f_{Ti_{old}} + \Delta f_{Ti}$$

Step 9 - Test for new buckling or unbuckling. Test buckled elements. If $\epsilon_{Tb} > \epsilon_{cb}$, element has unbuckled, element is newly unbuckled and is placed in k list and set:

$$f_{Ti} = \epsilon_{Ti} E_i$$

Test unbuckled elements. If $\epsilon_{Tk} \leq \epsilon_{ck}$, element has buckled, element is newly buckled and is placed in b list and set $f_{ti} = \epsilon_{ci} E_i$. If either test in step 9 finds a change in the buckled status, a reiteration through steps 6 - 9 is performed. When no change in the buckled status is found, the calculation of thermal effects is complete.

Step 10 - Find ΔM due to the axial load. Because the center of gravity does not generally coincide with the center of pressure of the axial load caused by gas and hydrostatic pressures, a bending effect is caused.

$$\Delta M_y = P(z_p - \bar{z}) \text{ and } M_{Ly_{new}} = M_{Ly_{old}} + \Delta M_y$$

$$\Delta M_z = P(y_p - \bar{y}) \text{ and } M_{Lz_{new}} = M_{Lz_{old}} + \Delta M_z$$

Step 11 - Apply the applied loads to the thermally buckled section:

$$\epsilon_{Li} = \left[\frac{P}{A_B} + \left(\frac{I_{yB} M_{Lz} + I_{yzB} M_{Ly}}{I_{yB} I_{zB} - I_{yzB}^2} \right) Y_i - \left(\frac{I_{zB} M_{Ly} + I_{yzB} M_{Lz}}{I_{yB} I_{zB} - I_{yzB}^2} \right) Z_i \right] \frac{1}{E_i}$$

$$\epsilon_i = \epsilon_{Li} + \epsilon_{Ti}$$

Step 12 - Test for new buckled or unbuckled elements and adjust stresses. Test buckled elements.

If $\epsilon_b > \epsilon_{ci}$ element has unbuckled, element is newly unbuckled and is placed in k list. Set stress:

$$f_i = \epsilon_i E_i$$

If $\epsilon_k \leq \epsilon_{ck}$ element has buckled, element is newly buckled and is placed in b list. Set stress

$$f_i = \epsilon_{ci} E_i$$

Step 13 - Compute new buckled section properties same as step 6.

Step 14 - Find adjustment loads and ΔM due to change in center of gravity position. The adjustment loads:

$$P_{LADJ} = -\Sigma_{ALL\ b} (\epsilon_b - \epsilon_{cb}) E_b A_b$$

$$M_{yLADJ} = -\Sigma_{ALL\ b} (\epsilon_b - \epsilon_{cb}) Z_b E_b A_b + \Delta M_y$$

$$M_{zLADJ} = -\Sigma_{ALL\ b} (\epsilon_b - \epsilon_{cb}) Y_b E_b A_b + \Delta M_z$$

where ΔM_y, ΔM_z are:

$$\Delta M_y = P (\bar{z}_{old} - \bar{z}_{new})$$

$$\Delta M_z = P (\bar{y}_{old} - \bar{y}_{new})$$

Step 15 - Apply adjustment loads to buckled section and determine revised strains. Change in strain:

$$\Delta \epsilon_i = \left[-\frac{P_{LADJ}}{A_B} + \left(\frac{I_{yB} M_{zLADJ} + I_{yzB} M_{yLADJ}}{I_{yB} I_{zB} - I_{yzB}^2} \right) Y_i - \left(\frac{I_{zB} M_{zLADJ} + I_{yzB} M_{zLADJ}}{I_{yB} I_{zB} - I_{yzB}^2} \right) Z_i \right] \frac{1}{E_i}$$

$$\epsilon_{i_{new}} = \epsilon_{i_{old}} + \Delta \epsilon_i$$

Step 16 - Test for new buckling or unbuckling (same as step 12). If there is a change in the buckled status, a reiteration through steps 13 - 16 is performed. If no change in the buckling is found, the calculation is complete.

Step 17 - Output. The final values for stress and strain at each element are printed.

APPENDIX II

VENT MANIFOLD SIZING ANALYSIS

1 INTRODUCTION

The vent system for the large scale tank consists of two internal piccolo manifolds and an overpressure relief standpipe. The piccolo tube is provided with vent holes uniformly spaced along the full length of each cylinder section. These holes are facing upwards and are located at the mid point between each internal frame to cause the boil-off gas to uniformly distribute along and cool the dry upper tank surface. The tank is vented thru this manifold during all normal fill and flight operations.

A small scale tank was tested in the horizontal position during Phase I of this contract, Reference 2. The vent pipe extended vertically upward in one end of the tank and terminated with the open end about 1.5 inches from the upper surface. The upper surface was smooth with no frames or projections to impede horizontal gas flow. The vent installation in this test tank demonstrated two significant problem areas. One problem which resulted was the development of a significant circumferential temperature gradient in the tank skin from the vent level to the top. Gradients greater than 50°R per inch were recorded. Gradients of lesser magnitude also developed in the axial direction along the top.

2 LIST OF SYMBOLS

- A Area, ft^2
- C Coefficient in entrance loss equation
- D Diameter, ft.
- f Friction factor
- g Acceleration of gravity, 32.2, ft/sec^2
- K Coefficient in mixing loss equation
- L Length of pipe between holes, ft.
- N Coefficient in entrance loss equation
- P Pressure - absolute, lbs/ft^2
- ΔP Pressure differential, lbs/ft^2
- q Velocity head, lbs/ft^2
- R Gas constant, ft/°R
- Re Reynolds Number
- T Temperature, °R
- v Velocity, ft/sec
- $\dot{W}$ Flow rate, lbs/sec
- ρ Gas density, lbs/ft^3
- μ Viscosity, lbs/ft-sec

Subscripts

d	Downstream of hole in manifold
h	Hole
m	Manifold
u	Upstream of hole in manifold
13	Hole entrance pressure loss (see Figure 37)
23	Mixing pressure loss (see Figure 37)
34	Friction pressure loss (see Figure 37)

3 SIZING ANALYSIS

The large scale tank has internal belt frames which will tend to trap hot gas at the top and prevent horizontal movement. The best method to minimize gas entrapment and to provide maximum cooling is to put a vent port flush with the tank skin between each frame and collect the gas in an external manifold. This, however, is impractical with the thin gage membrane type tank construction. An internal collector manifold has been selected. The internal pipe takes up potential fuel space. The larger the pipe diameter, the more fuel space is lost,but a small pipe diameter increases the vent system pressure losses. Space, cooling effectiveness and pressure drop must all be considered in the final vent design.

A literature search was made to obtain analytical information and test data on which to base the pressure losses in the sizing analysis. Surprisingly little data is available on a return or collector type manifold. The only published work found in this area has been compiled since 1962. This work is based on large diameter, relatively low velocity air conditioning type ducting. Ample data is available on supply type piccolo manifolds. These have been used for years to provide effective air conditioning for pilots in one and two place aircraft cabins over wide extremes of pressure, temperature and flow velocity. This data, unfortunately, is not applicable to return type manifolds. Reference 12 presents a one-dimensional solution to the momentum and continuity differential equations for a return type manifold. This solution has practical limitations and does not necessarily account for all the turning and mixing losses. Reference 13 presents some test data and evaluates the coefficients in classical incompressible flow equations which relate velocity head, q, to pressure losses in return flow manifold systems. The velocity in a duct is given by the equation:

$$v = \dot{W}/A\rho \qquad (1)$$

and the velocity head is given by

$$q = \rho v^2/2g \qquad (2)$$

A return type manifold system for which loss coefficients were measured is illustrated schematically in Figure 37 below. Two ducts are joined at right angles with the manifold duct having both upstream and downstream flow. The pressure losses are

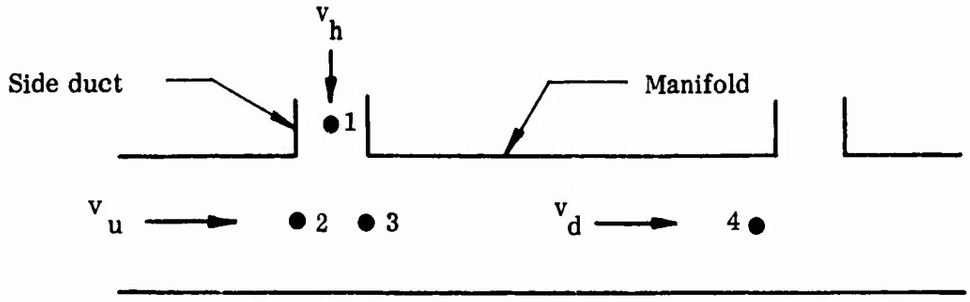

Figure 37. Schematic Diagram of Return Type Manifold

represented by the following equations (Reference 13):

$$\text{Mixing Loss in Manifold} \quad \frac{\Delta P_{23}}{q_d} = K \left(1 - \frac{v_u}{v_d}\right)^2 \tag{3}$$

$$\text{Entering Loss from Side Duct} \quad \frac{\Delta P_{13}}{q_h} = C\left(\frac{v_h}{v_d}\right)^N - 1 \tag{4}$$

$$\text{Friction Loss in Manifold} \quad \frac{\Delta P_{34}}{q_d} = f\left(\frac{L}{D_m}\right) \tag{5}$$

The tests in Reference 13 used an actual duct for the flow stream entering the manifold. Since the manifold under consideration in the test tank is a typical sharp-edged orifice entrance, a sudden contraction loss of 0.45 was added to Equation (4), resulting in a total entering loss of:

$$\text{Entering Loss thru Hole} \quad \frac{\Delta P_{13}}{q_u} = C\left(\frac{v_h}{v_d}\right)^N - 1 + 0.45 \tag{6}$$

The test data points from Reference 13 for the coefficients K, C, N are shown in Figure 38 , 39 and 40 respectively. Also shown are the curve fit equations used to describe the coefficients for computer solution of the manifold sizing analysis. The friction factor, f, was evaluated for a smooth pipe according to the equations:

$$f = 64/Re \qquad Re < 2500 \tag{7a}$$

$$f = 0.316/Re^{1/4} \qquad 2500 \leq Re \leq 10^5 \tag{7b}$$

$$f = (2 \log_{10}(Re\, f^{1/2}) - 0.8)^{-1/2} \qquad Re > 10^5 \tag{7c}$$

where $Re = \rho v_d D_m/\mu$

A computer solution was developed using the equations described above to size the holes and determine the pressure losses for equal flow per hole at constant inlet gas temperature. The holes are uniformly spaced in a constant diameter manifold. The solution also permits calculating the flow rate through each hole and the pressure losses in a manifold with known hole sizes. In this case, provision was made to vary the local inlet gas temperature at each hole. The viscosity used for Reynolds Number is calculated using Keyes equation (Reference 14):

$$\mu = \frac{a_o\, T^{1/2}}{1 + (a/T)\, 10^{-a_1/T}} \tag{8}$$

where the coefficients a, a_o, a_1 are constants which are different for each gas.

The vent design point was selected as a flow rate of 0.1 lbs/sec at 520°R. This is estimated to be the maximum boil-off rate and vent gas temperature which will be encountered in the large scale tank testing. This is 360 lbs/hr total or 180 lbs/hr through each of the piccolo vent manifolds. The vent was evaluated parametrically as a function of manifold diameter and first (upstream) hole diameter at uniform flow (equal flow per hole). The results are shown in Figure 41 . The vent pressure loss varies significantly with manifold diameter as would be expected. However, the pressure loss is generally insensitive to first hole diameter until the first hole size is decreased to a value sufficiently small that the flow approaches a 'plenum-to-plenum' effect where the hole velocity is much greater than the manifold velocity all the way along the manifold. The hole size variation with first hole diameter is shown in Figure 42 for the 2.9 inch I.D. manifold at the design flow rate. The diameter of the last hole varies only a small amount as the first hole diameter is increased from 0.2 to 1.0 inch.

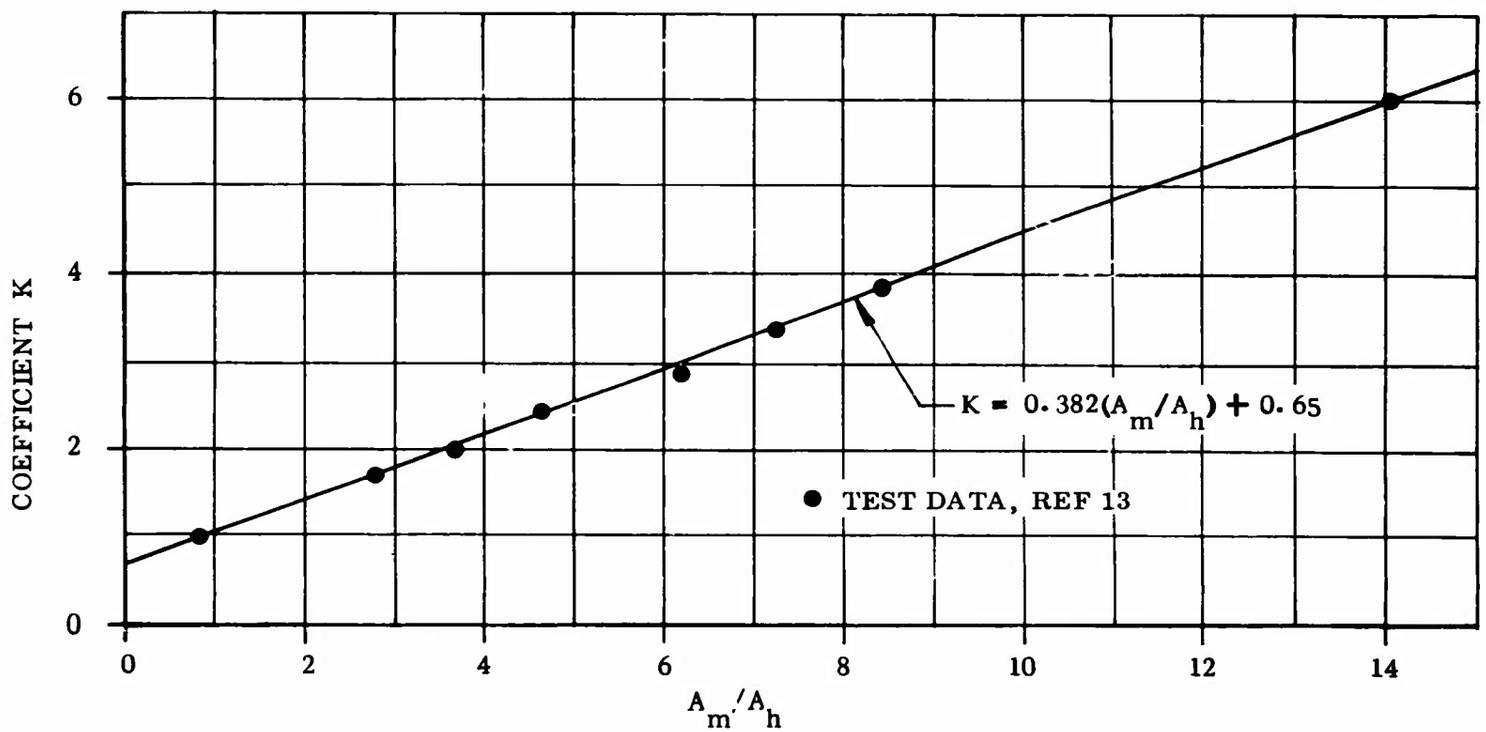

Figure 38. Coefficient K as a Function of Manifold-to-Hole Area Ratio

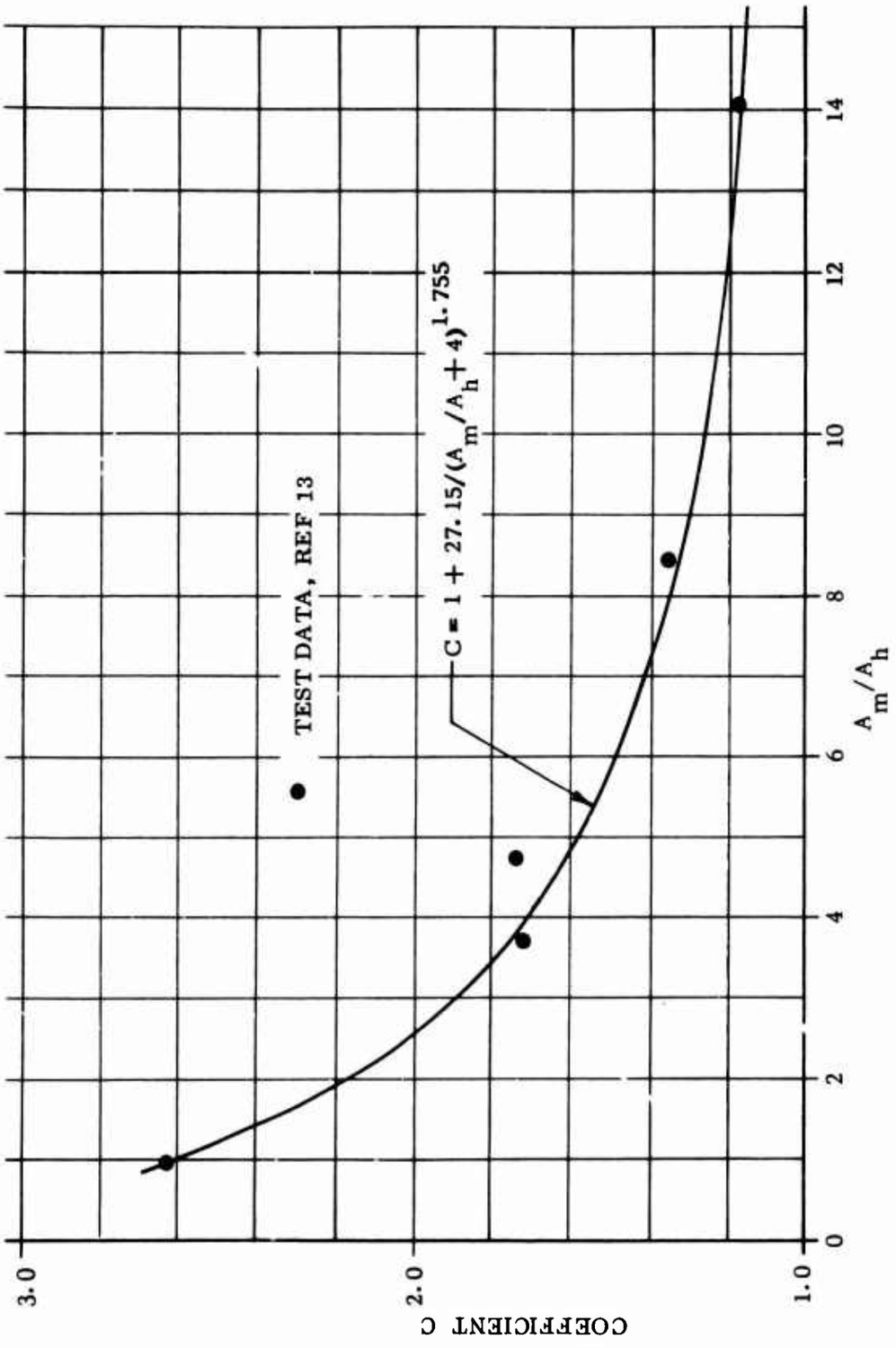

Figure 39. Coefficient C as a Function of Manifold-to-Hole Area Ratio

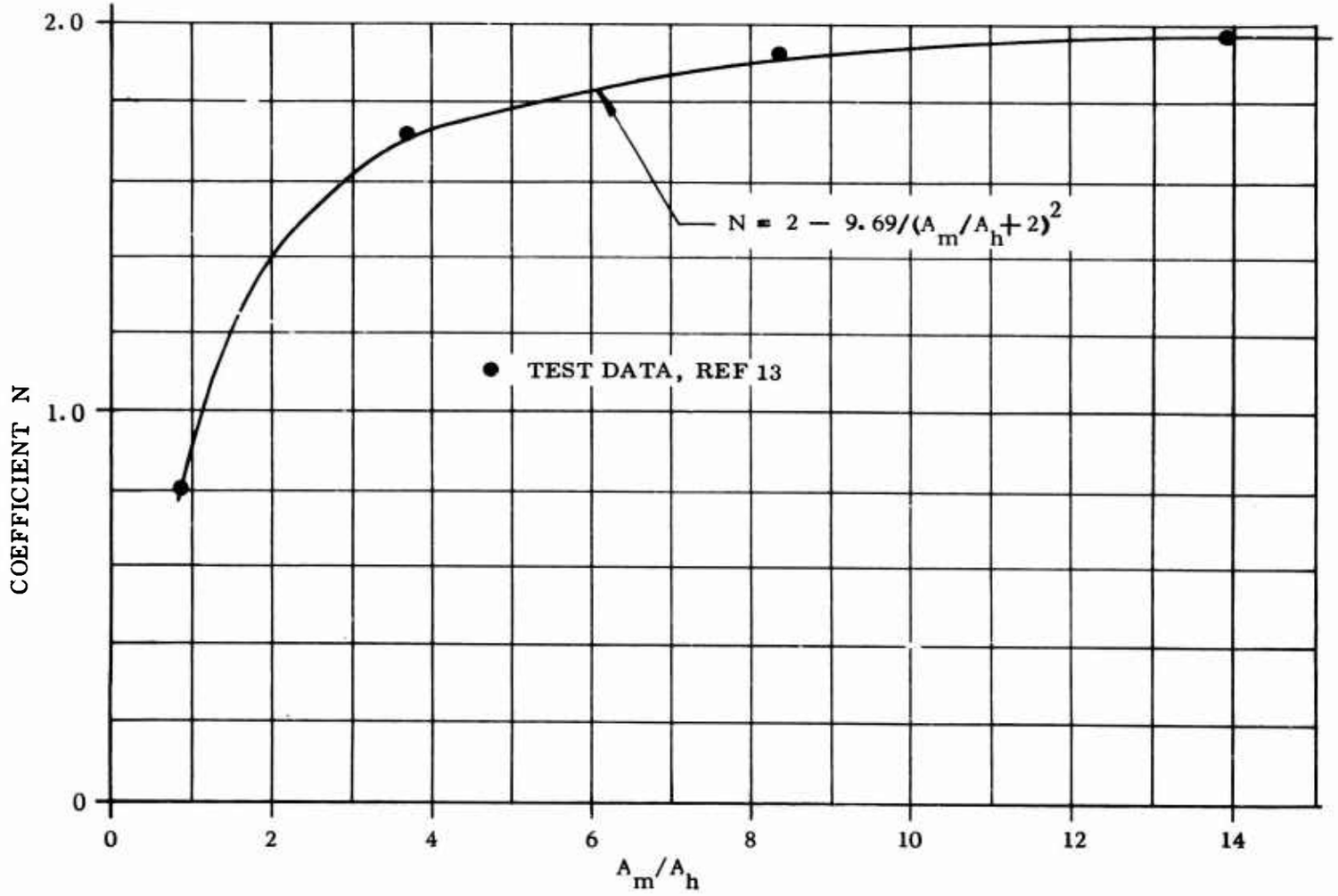

Figure 40. Coefficient N as a Function of Manifold-to-Hole Area Ratio

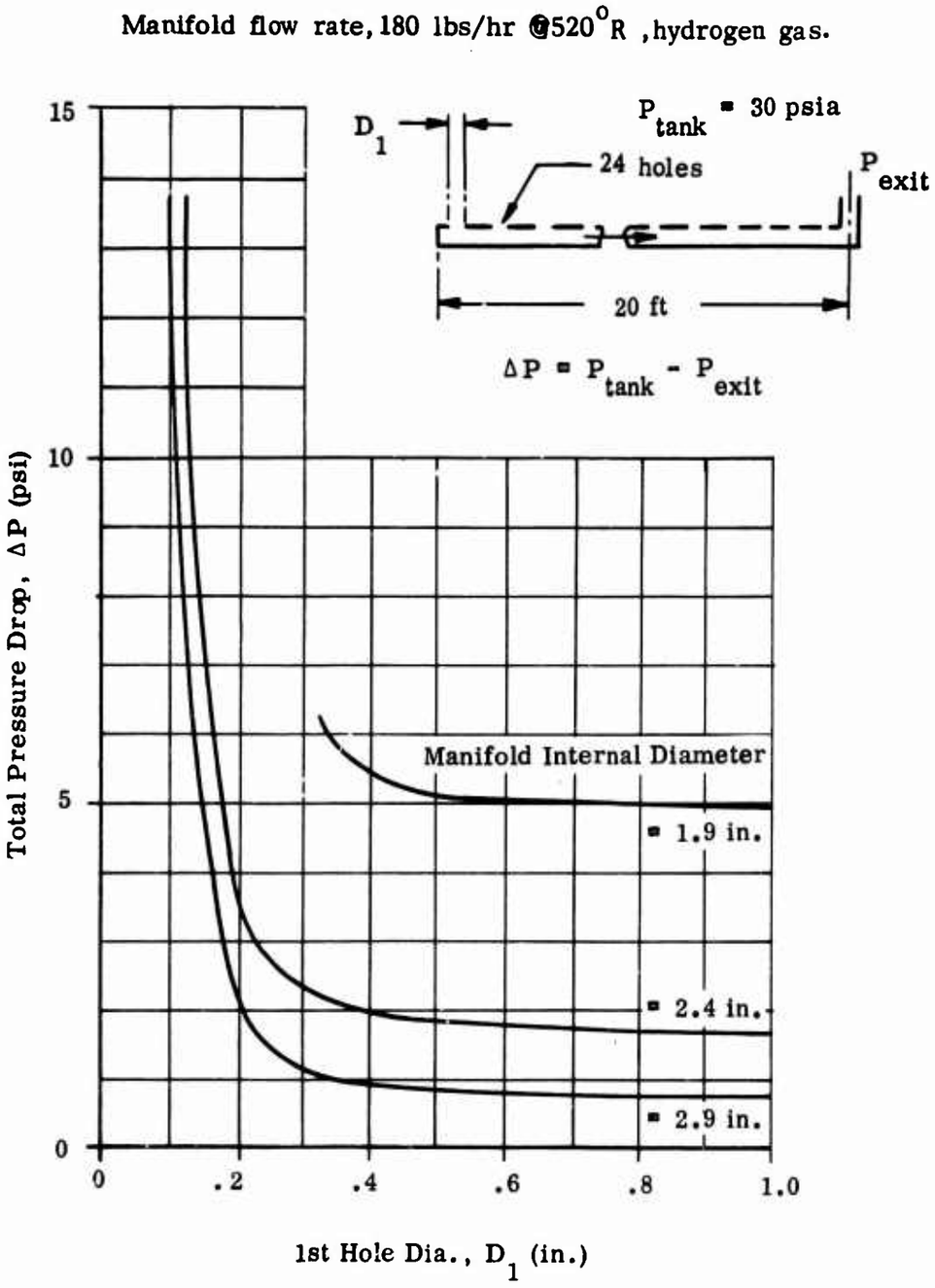

Figure 41. Pressure Drop in Vent Manifold vs. First Hole Diameter

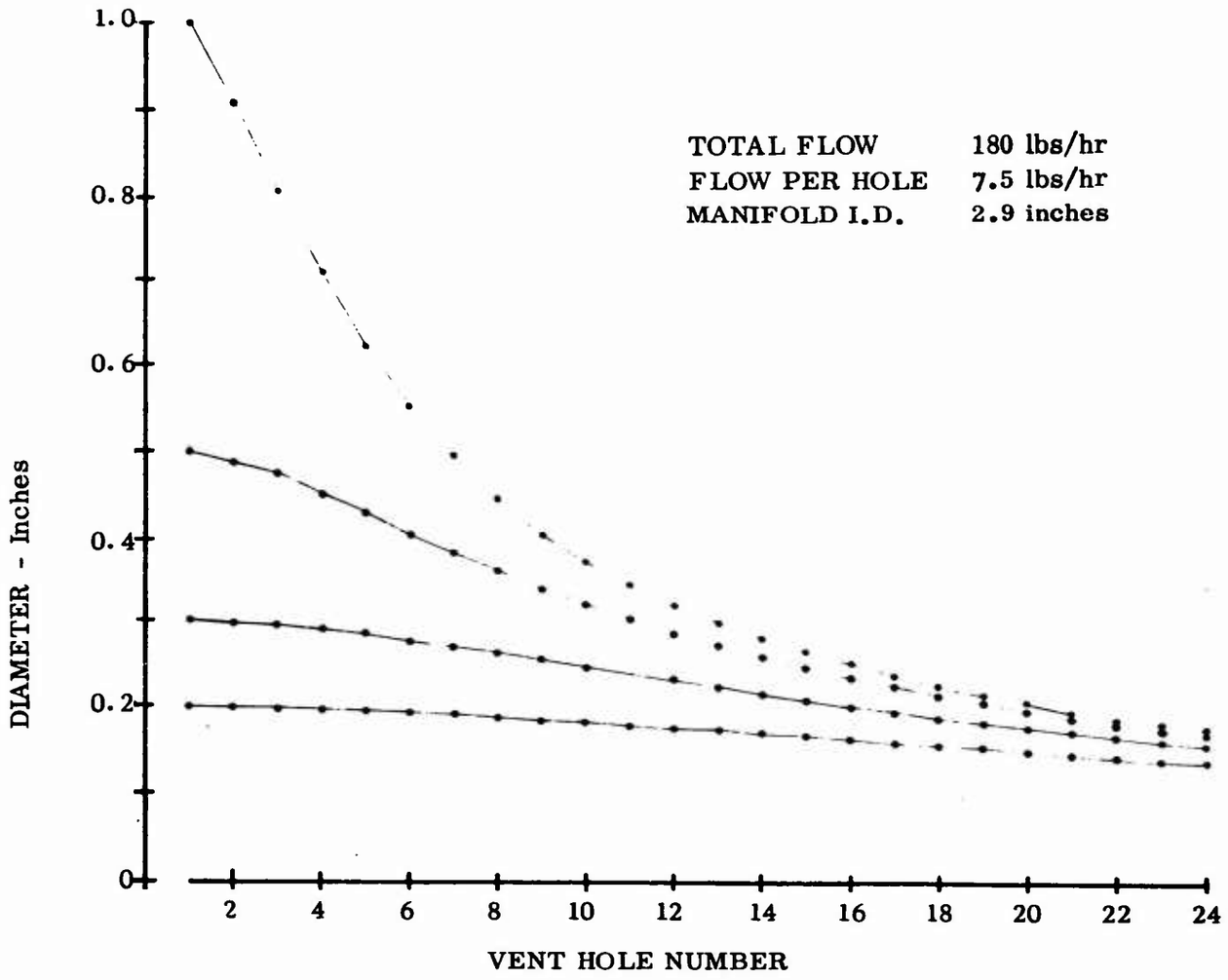

Figure 42. Hole Sizes Required For Uniform Vent Flow

The 2.9 inch manifold was checked for flow distribution at an off-design flow of 50 lbs/hour at 200°R and 650°R vent gas temperature. The resulting flow distribution along the manifold is shown in Figure 43 . The flow distribution is shown for a first hole diameter of 0.2 and 1.0 inch. The variation in flow distribution is negligible, except for the upstream holes in the manifold, with a first hole diameter of 1.0 inch.

The liquid level at tanking and ground hold should not exceed the bottom of the vent manifold. If the liquid contacts the vent manifold, it will boil off. The vent manifold with "warm" vent gas will act as a heat exchanger. Thus, a minimum vent manifold diameter is desirable. The volume penalty at the top of the tank and equivalent liquid mass is illustrated in Figure 44. The vent is mounted on .frames one inch below the top of the tank. Thus the maximum allowable liquid level is one inch plus the vent pipe outside diameter.

The vent manifold selected for the large scale tank is 2.9 inches I.D. with a first hole diameter 0.3 inch. The selection was made on the basis of a reasonable compromise betweeen pressure loss (~ 1.0 psi at design flow), off-design flow distribution, and vent manifold diameter (volume loss at tanking). The ports in the tank through which the vent manifold passes were designed and released at 2 inches diameter. A bellmouth entrance at this 3 inch to 2 inch transition was used to minimize the contraction pressure loss.

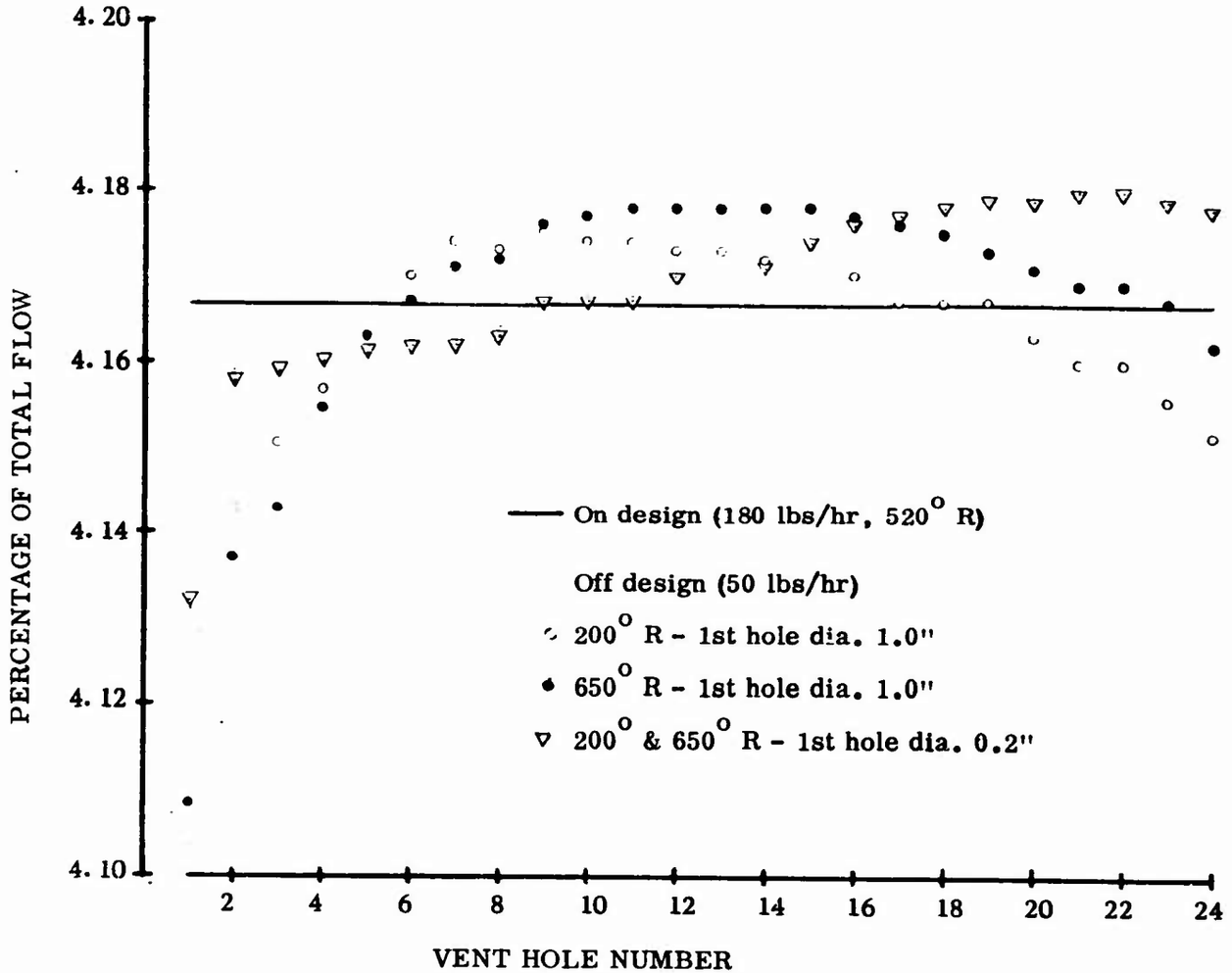

Figure 43. Piccolo Vent Off-Design Performance

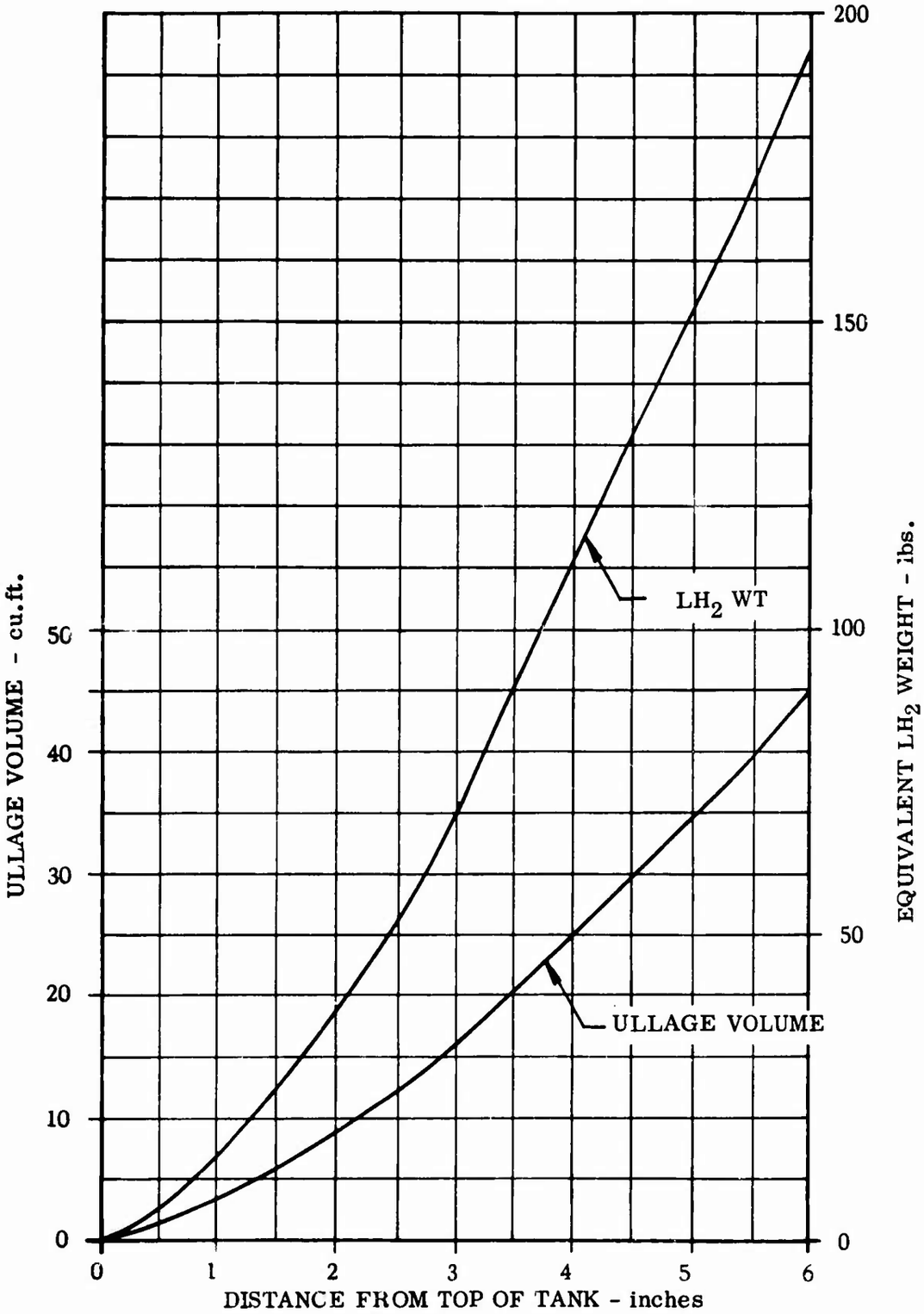

Figure 44. Tank Volume Loss vs. Liquid Level

APPENDIX III

SLUSH HYDROGEN

A comparison has been made between propellant tank installations containing 50% slush hydrogen and liquid hydrogen tanked at atmospheric pressure. The comparison is based on mission parameters used for the large scale test tank optimization. The environmental pressures and temperatures, and the fuel flow rates are given in Figure 45 . It is assumed that the slush can be tanked and pumped as a homogeneous mixture and that "liquid" stratification results from density gradients due to heating of the thermodynamic fluid. The density of slush and saturated liquid hydrogen as a function of enthalpy is shown in Figure 46. Saturation temperature is also shown for reference.

Two tanks sized for 50% slush hydrogen are compared with the optimum installation for liquid hydrogen in Table V. The optimized liquid hydrogen tank is discussed in Reference 2 . Case 1, 50% slush, has the same insulation thickness (1.3 inch top, 4.0 inch bottom) and the same operating pressure (30 psia) as the optimum liquid hydrogen tank. Case 2, 50% slush, has 1.3 inch top and 2.8 inch bottom insulation and 20 psia operating pressure. The weight of both slush tanks is about 8 percent less than the liquid tank. The difference in installed equivalent weight is somewhat greater because the installed volume of the slush tanks is about 180 cubic feet less than the liquid tank; the numerical values of the installed volume penalty in Table V were computed with a weight to volume sensitivity of 7.0 pounds per cubic foot.

The tank installations all require the use of a boost pump which will pump boiling fluid so that pressurization is not used for propellant transfer. However, the tank structure cannot accept a negative pressure differential so that pressurization for the slush tanks is probably required. The fluid vapor pressure and the required minimum pressure to maintain a 2 psi positive differential are illustrated in Figure 47. The 2 psi positive differential would be used, as a safety factor, for a tank designed for unpressurized operation. Operating pressure would be used for a tank design requiring pressurized operation. Two flight conditions are shown in Figure 47: (1) the normal cruise mission, and (2) an abort and 30 minute fly around at low altitude. When the fluid vapor pressure at take-off is equal to or greater than the required pressure, the fluid can boil and prevent a drop in ullage pressure below the vapor pressure. This is the case with the liquid hydrogen tank consequently no pressurization is required. The fluid vapor pressure in the slush tanks is less than the required pressure indicating a probable need for pressurization. Slush tanks will be topped off to operating pressure with helium and under certain conditions ullage expansion below the required pressure might not occur. An accurate internal energy balance is required to determine actual tank pressures as a function of time.

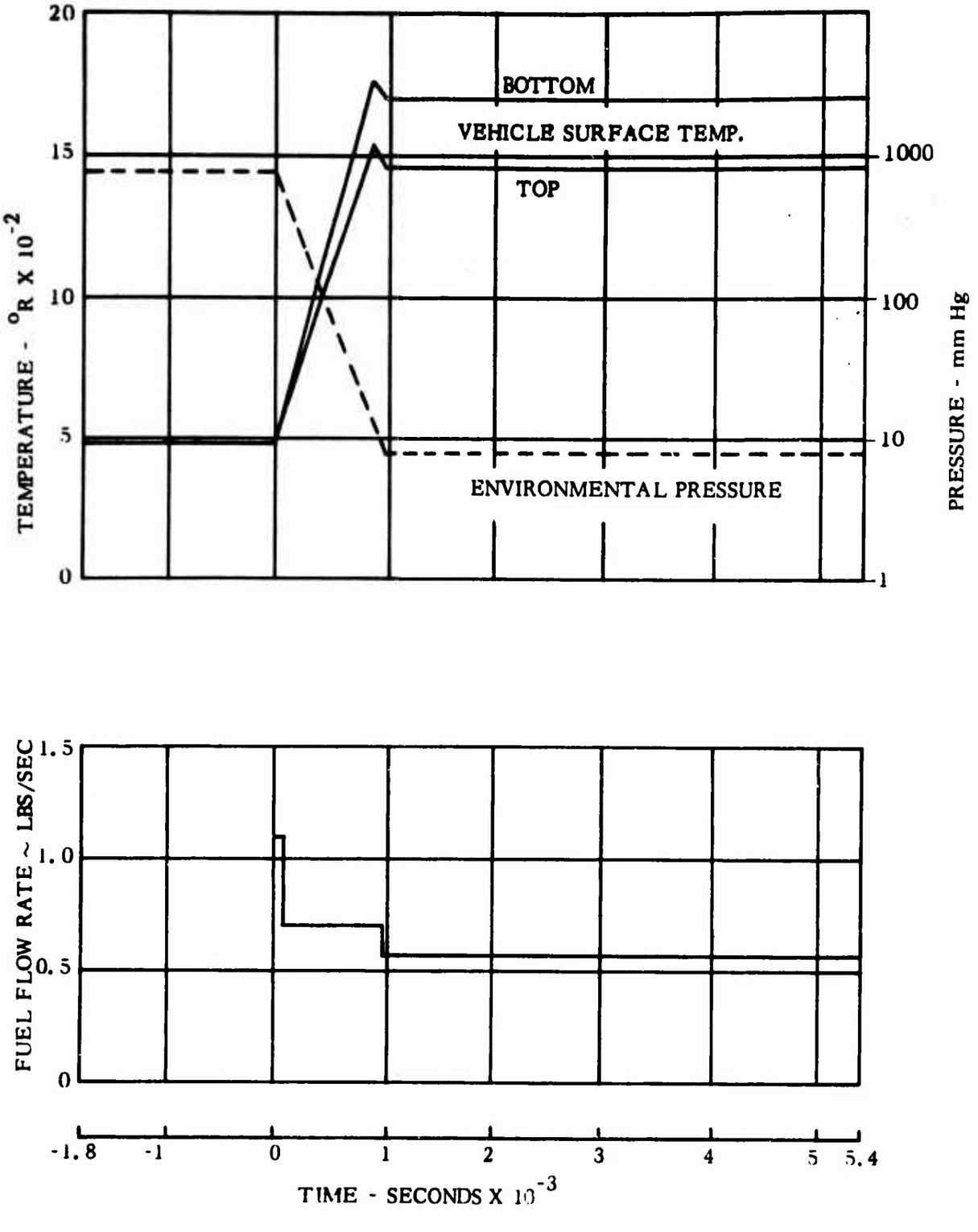

Figure 45. Trajectory/Mission Parameters

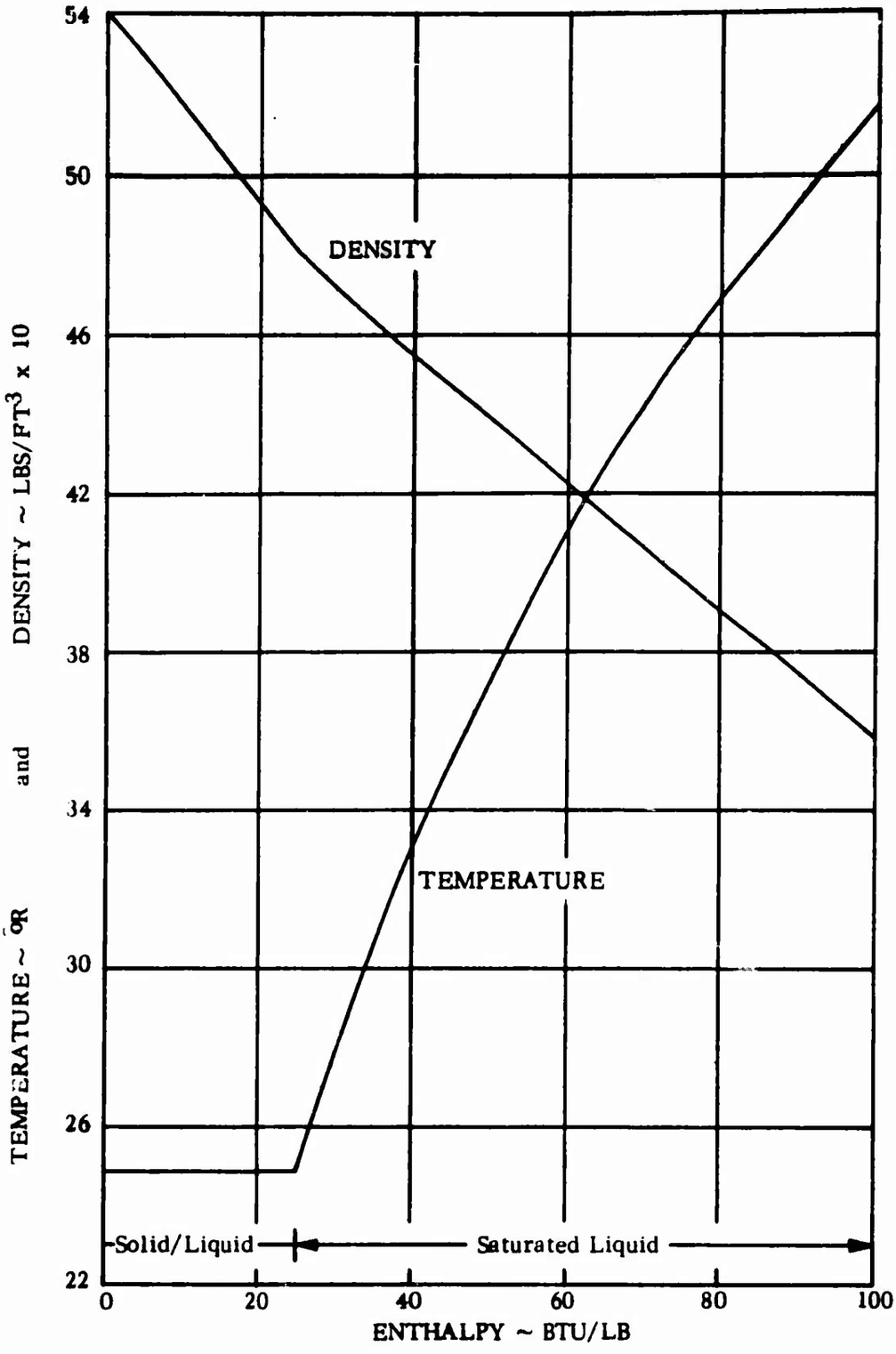

Figure 46. Properties of Slush and Liquid Para-Hydrogen

Table V. LH_2 Tankage - Thermal Performance, Size and Weight.

Intersecting cylinder tank with center-to-center spacing, one radius. Ellipsoidal dome ends.

Radius = 2.67 ft.
Vent height = 5.25 ft.
Maximum liquid level = 5.00 ft.
Unusable liquid level = 0.44 ft.

	Liquid	Case 1 50% Slush	Case 2 50% Slush
Tanking pressure, psia	16.7	1.02	1.02
Operating pressure, psia	30.0	30.0	20.0
Tanking liquid level, ft.	4.868	4.846	4.829
Length (overall), ft	25.16	20.77	21.60
Length (cylinder), ft.	21.37	17.00	17.83
Installed volume, ft^3	1060	877	883
Heat input to liquid, BTU.			
Insulation	67118	56257	97389
Radiation from top, ϵ = 0.2	3291	38406	28974
Internal (pump)	1262	1262	1262
Turbulent liquid surface	852	27	635
Supports and penetrations	383	384	391
Total	72906	96336	128651
Design pressure, psig	31.5	31.5	21.0
Design (Max.) tank skin temp., °R	578.	890.	890.
		Weights	
Tank structure (Inconel 718, min. gage = 0.010 in.)			
Cylinder shells	245.0 (.012 in.)	194.7 (.012 in.)	170.2 (.010 in.)
Hatches and domes	62.6 (.010 in.)	62.6 (.010 in.)	57.9 (.010 in.)
Main frames	37.8	35.9	36.0
Intermediate frames	83.7	59.6	62.4
Y-section	69.5	49.4	45.4
Truss	72.0	55.6	42.3
Supports and doublers	25.1	22.9	17.6
Total	595.7	480.8	431.8
Insulation (Microquartz/Helium)			
Top (60° angle from top)	153.4 (1.3 in.)	126.4 (1.3 in.)	131.5 (1.3 in.)
Side	214.2	183.8	155.1
Bottom (60° angle from bottom)	360.8 (4.0 in.)	297.3 (4.0 in.)	228.5 (2.8 in.)
Total	728.4	607.5	515.1
Subsystems			
Fuel	37.8	37.8	37.8
Vent	46.6	42.4	61.1
*Pressurization	0	46.4	46.4
Total	84.4	126.6	145.3
Propellant			
Boil-off	200.3	42.7	168.7
Unusable	162.2	130.7	140.8
Usable	3240.9	3240.9	3240.9
Total	3603.4	3415.3	3549.4
Total weight, lbs.	5011.9	4630.4	4641.6
Installed volume penalty, lbs.	2285.0	1006.0	1048.8
Installed equivalent weight	7296.9	5636.4	5690.4
Mass fraction = $\frac{\text{usable fuel}}{\text{total weight}}$	0.647	0.700	0.698

NOTE: *Pressurization subsystem, hand calculation, see Table III. All other calculations made by thermal performance and weights analysis computer program.

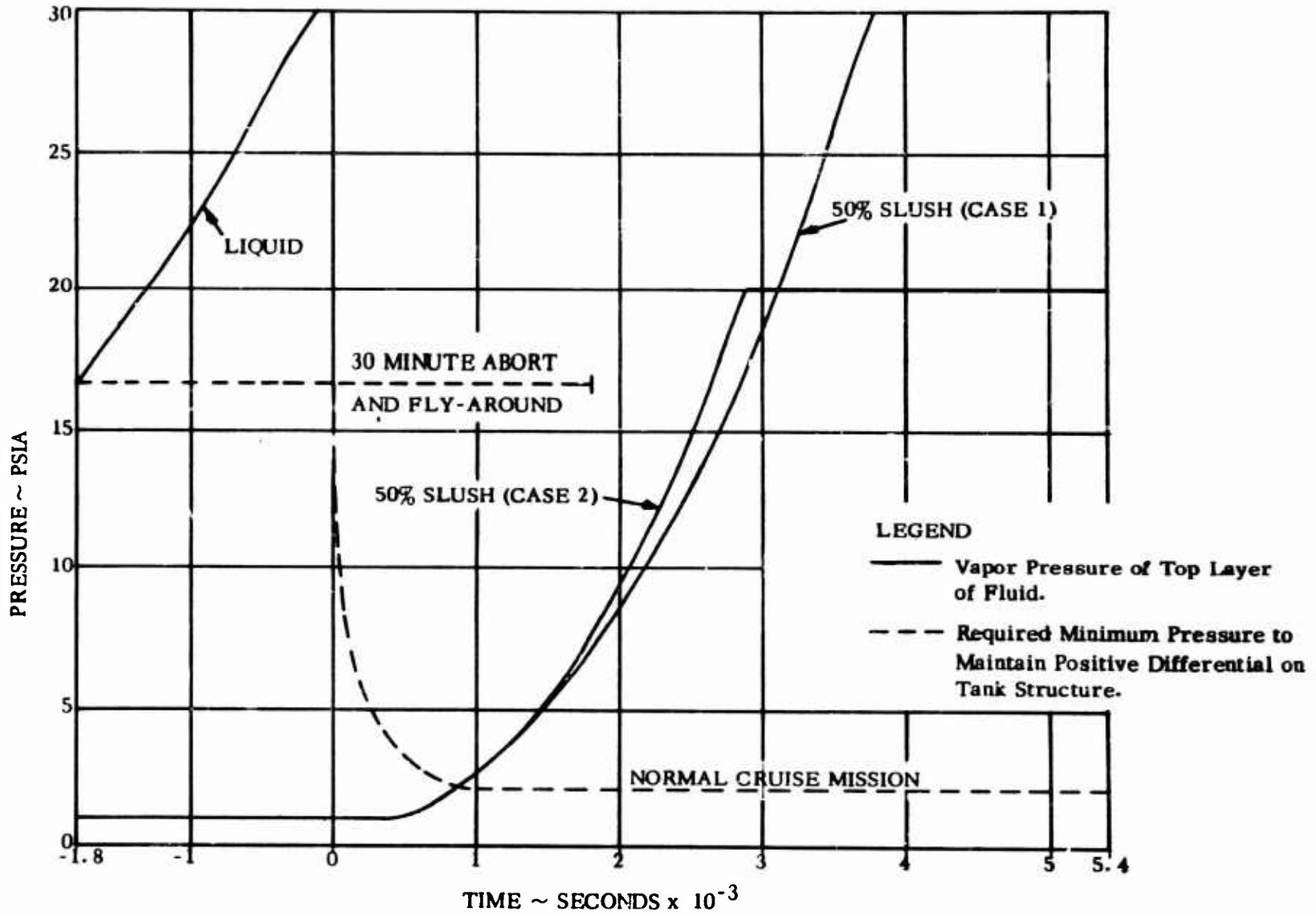

Figure 47. Hydrogen Vapor Pressure and Required Tank Pressure

The requirement for and selection of a pressurization system is influenced by many factors some of which are listed below:

Mission:	Normal cruise Abort
Tank Design:	Pressurized operation required Unpressurized operation permitted
Pressurant Gas:	Vaporized propellant Helium
Pressurant Storage:	Cryogenic (inside propellant tank) Ambient (outside propellant tank)
Pressurant Use Temp:	Cryogenic Ambient Hot

The quantities of pressurant gas (hydrogen or helium) required to pressurize the two slush hydrogen tanks for various design and operating conditions are listed in Table VI. The quantities shown were determined by simple mass addition due to liquid displacement at the specified ullage condition. An internal energy balance is required to completely specify the pressurant requirement. The table is, however, a good indication of the relative quantities needed and will be used to make a preliminary selection of pressurization conditions. This particular tank has been designed for unpressurized operation. Only that condition will be considered here. Both the normal cruise and the abort mission must be satisfied and the abort mission from Table VI, requires the most pressurant. It will be considered the design condition.

The pressurant, storage temperature and use temperature are considered in more detail for the design condition. Weights of individual pressurization system components are listed in Table VII. Both vaporized hydrogen and helium at cryogenic and ambient temperature are shown. Ambient temperature here is $450^{\circ}R$. This is the approximate internal temperature of the vehicle fueled with hydrogen during ground hold and low altitude flight. When hydrogen is used as a pressurant it is assumed to be bled from the boost pump discharge line and then through a vaporizer and for ambient temperature use through an additional heat exchanger. An electrical heater, hot gas from the engine or other heat sources are required in this case. Helium stored at cryogenic temperature is assumed to be located in a long cylinder at the bottom of the tank in the space occupied by unusable fuel.

The actual quantity of pressurant required, as noted previously, must be determined by an internal energy balance in the tank. In its simplest form the energy balance should account for pressurant mixing, gas and liquid stratification, ullage expansion as the liquid is expelled, wall to gas heat transfer, and gas-liquid interface heat and mass transfer. Sloshing, liquid surface turbulence, and droplet injection due to bulk boiling also affect ullage pressure and can cause implosive depressurization. An analysis of this type is beyond the scope of this evaluation. Existing techniques will be used to estimate pressurant quantities. A moderate amount of testing and analysis has been done

Table VI. Mass Required for Pressurization, 50% Slush Hydrogen
(See Table I for Tank Sizes)

CASE 1 30 psia op. press. 1.3/4.0 in. insulation		Time Seconds	Ullage Condition		Mass Required	
			Temp. R	Press. psia	Hydrogen	Helium
	Take-Off	0	450	30.	.264	.526
Tank Design, Unpressurized Operation	Normal Mission	870	27	2.3	.198	.447
			450	2.3	.136	.269
			875	2.3	.070	.139
	Abort/ Fly-around	1800	37.25	16.7	23.85	40.10
			450	16.7	1.66	3.32
Tank Design, Pressurized Operation	Normal Mission	3780	41.4	30.	74.2	122.70
			450	30.	5.66	11.28
			875	30.	2.92	5.80
	Abort/ Fly-around	1800	41.4	30.	39.1	64.60
			450	30.	2.98	5.94

CASE 2 20 psia op. press. 1.3/2.8 in. insulation		Time Seconds	Ullage Condition		Mass Required	
			Temp. R	Press. psia	Hydrogen	Helium
	Take-Off	0	450	20.	.185	.367
Tank Design, Unpressurized Operation	Normal Mission	870	27	2.3	.197	.445
			450	2.3	.135	.268
			875	2.3	.069	.138
	Abort/ Fly-around	1800	37.25	16.7	23.32	39.20
			450	16.7	1.62	3.24
Tank Design, Pressurized Operation	Normal Mission	2880	38.4	20.	37.8	66.2
			450	20.	2.84	5.65
			875	20.	1.46	2.91
	Abort/ Fly-around	1800	38.4	20.	25.90	45.40
			450	20.	1.95	3.87

Table VII. Pressurization Systems, Weight and Volume.

PRESSURANT →		HYDROGEN		HELIUM		
STORAGE TEMPERATURE →		VAPORIZED PROPELLANT		CRYOGENIC	CRYOGENIC	AMBIENT
USE TEMPERATURE →		CRYOGENIC	AMBIENT	CRYOGENIC	AMBIENT	AMBIENT
1. Pressurant (displacement)	lb	23.85	1.66	40.1	3.32	3.32
2. Collapse factor		1.0	10.0	0.5	4.0	4.0
3. Pressurant (required)	lb	23.85	16.6	20.05	13.28	13.28
4. Storage bottle, titanium (1000 psi)	lb	--	--	19.4	12.6	162.0
5. Added tankage weight to contain pressurant	lb	5.7	4.0	-10.2@	-6.8@	--
6. Heater or heat exchanger, regulator, plumbing, supports	lb	35	55	17	36	36
7. Total weight 3. + 4. + 5. + 6.	lb	64.6	75.6	46.4	55.1	211.3
8. Installed volume	ft^3	6	6	0	1	15
9. Installed volume penalty	lb	42	42	0	7	105
				ⓑ		

@ Cryogenic helium storage bottles are long, small diameter cylinders in the unusable propellant at the bottom of the tank. The negative quantity is the displaced weight of unusable propellant.

ⓑ Helium stored and used at cryogenic temperature is the minimum weight pressurization system completely contained within the fuel tank at no added volume.

on missile type tankage with relatively large ullage space compared to the gas-liquid interface area. The Centaur hydrogen fueled upper stage uses a boost pump. It is topped off with helium on the ground. A small quantity of He pressurant is used to suppress boiling at engine start-up, otherwise, no pressurization is required. The two hydrogen fueled Saturn stages use vaporized propellant for essentially continuous pressurization. Pertinent test data for missile type tanks has been conveniently summarized and correlated by Epstein, Reference 15. He has introduced a collapse factor which can be considered a simplified representation of an energy balance. The collapse factor is the ratio of actual pressurant mass required to the pressurant mass determined for conditions of zero heat and mass transfer in the ullage. After evaluating the test results summarized in Reference 15 as well as some flight test data from the Saturn S-IV stage, collapse factors were estimated for this tank. In this case, the liquid surface area is large and slush hydrogen is at a considerably lower temperature than any test data yet taken. The collapse factor of 0.5 for cryogenic helium is used because it will be stored at slush hydrogen temperature then introduced into a warm ullage compared to storage temperature. This will increase the helium temperature and reduce the actual amount required compared to the displacement mass.

The minimum weight pressurization system, Table VII, is helium stored and used at cryogenic temperature. It utilizes no additional volume and is the simplest system because no hardware external to the propellant tank is required (assuming that a cryogenic pressure regulator and control can be mounted in the ullage at the top of the tank). The results of this hand calculation are included in the overall tank installation summary in Table V.

APPENDIX IV

VEHICLE TANK OPTIMIZATION

1.0 INTRODUCTION

Cryogenic tank design depends on the conventional interrelating factors of temperature, stress, and pressure. The degree of dependency is great when the tankage system has to operate over wide environmental extremes associated with high speed flight up to high altitudes. Optimization techniques must be employed to assure minimum weight. A computer program has been written to calculate the installed size and weight of a cryogenic propellant, LH_2, tank for a manned hypersonic flight vehicle. The tank configuration is a horizontal "double bubble" intersecting cylinder with dome ends. The purpose of the computer program is to permit selection of an optimum tank installation. Two flight weight insulated tanks were tested with liquid hydrogen under simulated environmental flight conditions. The test articles included a cylindrical 130 gallon subscale tank with cone ends (Reference 2) and a "double-bubble" 6,000 gallon tank with elliptical dome ends. Both tanks were fabricated from thin gauge Inconel 718 alloy and insulated with quartz fiber. This computer program has been correlated with the thermal performance results of these tests.

The selection of an optimum tank installation requires that all the parameters which affect the installed weight and volume be either consistently controlled or independently varied. A basic requirement is that the tank contain a specified quantity of propellant to accomplish a particular mission. Propellant density varies with temperature and may decrease significantly due to melting slush or contained vapor bubbles when boiling. The minimum ullage space and the quantity of unusable fuel are generally specified as geometrical distances from the top and bottom of the tank, thus their volume and mass are dependent on tank radius and length dimensions. Boil-off losses vary with heat flux (insulation thickness), operating pressure and mission time. Spray cooling losses are dependent on the specified tank structure temperature limit. The program automatically accounts for these variables and sizes the tank to contain the total required propellant mass and ullage space.

Time dependent trajectory parameters and independent variables affecting installation weight are input to the program. The output includes thermal performance and propellant level as a function of time, tank size and propellant and hardware weights. The computation is based on a non-integrated finite time interval calculation where time dependent parameters are specified or selected at the beginning of a time interval and held constant through the interval.

In general, the program input is:

Fluid thermal properties

Tank geometry characteristics and limiting propellant levels

Transient heat flux through the insulation, penetrations and supports

Propellant flow schedule and internal heat flux

Tanking and operating pressure

Structural upper temperature limit

Structural material properties and design coefficients

Insulation and subsystem weight coefficients

The program will then compute:

Thermal performance as a function of time

Propellant losses, boil-off and spray (if needed to maintain structural temperature limit)

Tanking or fill level so that propellant expansion while heating will not exceed specified maximum level

Tank size required to contain useful propellant plus losses and unusable fuel

Total propellant mass and inert weights of tank structure, insulation and subsystems

The tank is assumed to be chilled down and filled while being vented to ambient pressure then topped-off at a pressure (tanking pressure) slightly above ambient sufficient to suppress boiling. The computer calculation starts at the time when the tank is locked up and self-pressurized to operating pressure. The thermal performance analysis includes a simplified liquid stratification model based on local external heating of horizontal liquid nodes. The ullage heat balance includes radiation from the tank skin to the liquid and convection from the tank skin to the boil-off gas. The thermal environment on the top and bottom of the tank will differ because of differences in aerodynamic heating and the variable environment at different locations within the vehicle. Provision has been made to have different heat fluxes and insulation thickness at the top and bottom of the tank with the remaining insulation tapered through any desired angular sector on the side.

The weights computed include the propellant (usable, unusable, boil-off, and spray), insulation, fuel system, vent system and tank structure. Most aerospace vehicles are both weight and volume sensitive. Preliminary design of a vehicle usually involves a synthesis analysis which gives a weight to volume sensitivity or payload (weight) gain per cubic foot decrease in volume. Two tank installations with the same total weight and useful propellant may differ only in installed volume. The one with the least volume is obviously better. The weight/volume sensitivity is a measure of "how much better". Provision is made in the program to input this sensitivity. The program computes installed volume and an equivalent weight. Thus the optimization can be based on either actual weight or an equivalent installed weight.

The program will compute the thermal performance, weights (except tank structure), and installed volume of any horizontal cylindrical tank configuration, either single or intersecting cylinders. Any flat or dome end geometry can be input. The tank structure weight calculation is limited to an intersecting cylinder configuration with a center-to-center spacing of one radius and elliptical dome ends.

2.0 LIST OF SYMBOLS

A	heat transfer area (ft^2)
a	coefficient, flight heat flux, equation 2 ($BTU/hr\text{-}ft^2$)
Ac	cross-sectional area (ft^2)
b	exponent, flight heat flux, equation 2 (radians)
Cp	specific heat of hydrogen gas ($BTU/lb\text{-}^\circ R$)
f	factor or coefficient
F	strength of material (lb/in^2)
G	ultimate vertical load factor (g's)
H	enthalpy (BTU/lb)
h	heat transfer coefficient ($BTU/hr\text{-}ft^2\text{-}^\circ R$)
j	total number of liquid nodes
k	thermal conductivity ($BTU/hr\text{-}ft\text{-}^\circ R$)
K	coefficient, turbulent liquid column, equation 17 (ft)
L	length (ft)
Ld	structural load (lb)
M	bending moment (in-lb)
m	mass of fluid (lb)
$\dot{m}$	mass flow (lb/hr)
n	number liquid nodes in mixed layer
P	pressure (psia)
Q	heat flux (BTU/hr)
q	heat flux density ($BTU/hr\text{-}ft^2$)
R	tank radius (ft)
Sc	section modulus (in^3)
Sp	intermediate frame spacing (in)
T	temperature ($^\circ R$)
t	thickness (in)
V	volume (ft^3)
$\dot{V}$	gas or vapor velocity (ft^3/hr)
v	bubble velocity (ft/hr)
Vs	vertical shear load (lb)
W	weight of hardware (lb)
w	weight per unit length (lb/ft)
Wa	unit area weight (lb/ft^2)
x	height (ft)
y	thickness turbulent liquid column (ft)
z	exponent, convective heat flux, equation 25
α	angle from bottom of tank (radians)
ϵ	surface emissivity
θ	time (hour)
ρ	density (lb/ft^3)
σ	Stefan-Boltzmann constant, 0.173×10^{-8} ($BTU/hr\text{-}ft^2\text{-}^\circ R^4$)

Operators

d	differential
Δ	incremental

Subscripts

1	bottom of a node
2	top of a node
b	bottom of tank
bo	boil-off or boiling
bos	boil-off required to cool top of tank
bu	burst pressure
c	convection
cb	buckling
cor	turbulent liquid column
crf	flange crippling, frames
cry	flange crippling, Y-section
cyl	cylinderical section of tank
d	dry
des	design
dbl	doublers
dg	diagonal members of truss
dom	dome end of tank
e	end of flight
f	constant or fixed value (see Table I)
g	vapor or gas
i	insulation
if	intermediate frame
ℓ	liquid or liquid node
ℓf	liquid fill height
m	structural material
max	maximum
mix	mixed liquid layer at bottom of tank
mf	main frame
o	outside the insulation
op	operating
p	pump
p1	penetration, #1
p2	penetration, #2
pr	proof pressure
r	radiation
ref	reference
s	side of tank
sk	tank skin
s1	support, #1
s2	support, #2
sat	saturated fluid
spr	spray cooling
str	forming or stretch
sup	supports
T	total
t	top of tank
tk	tanking
tr	truss
tu	ultimate
ty	yield
u	ullage or ullage node
up	upright members of truss
un	unusable liquid
us	usable liquid
v	variable value (see Table I)
vp	volume penalty
vt	vent
w	wet
y	Y-section

3.0 ANALYTICAL MODEL DEVELOPMENT

The computer program performs a heat balance in the liquid based on the incoming heat flux at each time interval. Using the boil-off from the liquid calculation it performs a heat balance in the ullage. Radiation from the top of the tank, calculated as part of the ullage heat balance, is added to the liquid heat balance. The overall calculation is repeated and converged to a numerical solution. The heat balance is based on a constant pressure single gas (propellant vapor) ullage. A tank mounted boost pump capable of pumping boiling propellant is assumed to be part of the fuel system and was used in the performance verification tests of the large scale tank.

The program computes the propellant fill level so that a minimum specified ullage space is maintained while the propellant expands due to heating. The calculation continues through the trajectory, using an input estimate of tank size, until the unusable propellant level is reached. The propellant used is compared with that required and, if necessary, a new tank size is computed to contai . the required propellant and the thermal performance analysis is repeated.

The propellant, insulation, and subv tem weight are computed based on tank size. The final calculation is the tank structure and support weights which are dependent on pressure differential, maximum tank skin temperature and, insulation and propellant weight.

An analytical model of the tank is shown in Figure48. Illustrated are the liquid and ullage nodes used in the heat balance, limiting liquid levels, and the provisions for variable thickness insulation.

3.1 HEAT FLUX INTO THE TANK

Transient heat flux density through the insulation to the top, q_t, and the bottom, q_b, of the tank are input in table form as a function of flight time starting with the beginning of flight. The first value in the table is considered the steady state heat flux for ground hold. Heat fluxes are used, as tabulated, for the constant insulation thicknesses top and bottom. Heat flux through the tapered side insulation is handled differently during ground hold and flight. Figure 49 illustrates the form of heat flux distribution for the two operating conditions. Insulation taper is assumed to vary linearly with circumferential distance or swept angle. Angular position is the independent variable used to define local heat fluxes through the tapered side insulation.

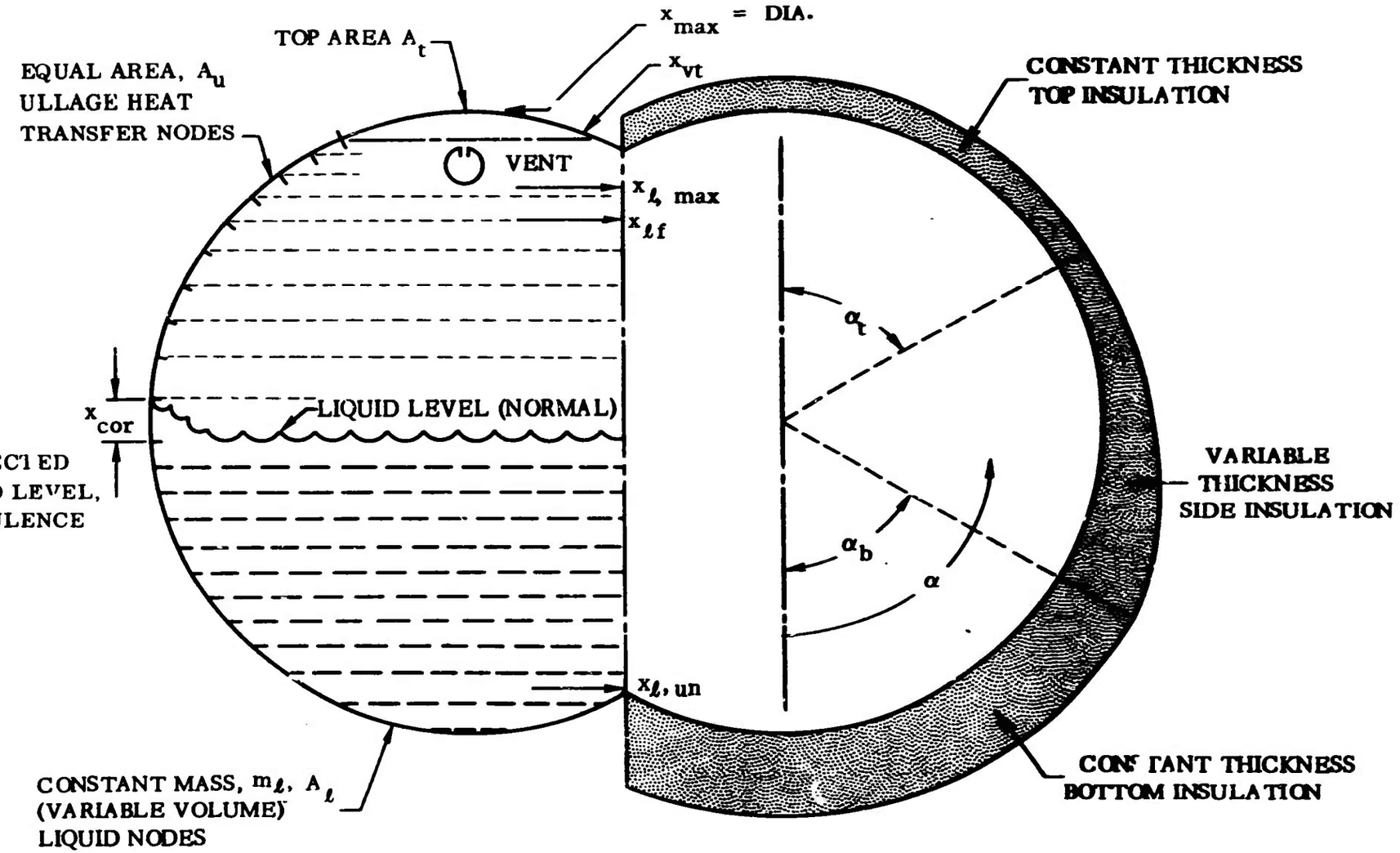

Figure 48. Analytical Model of Insulated Tank

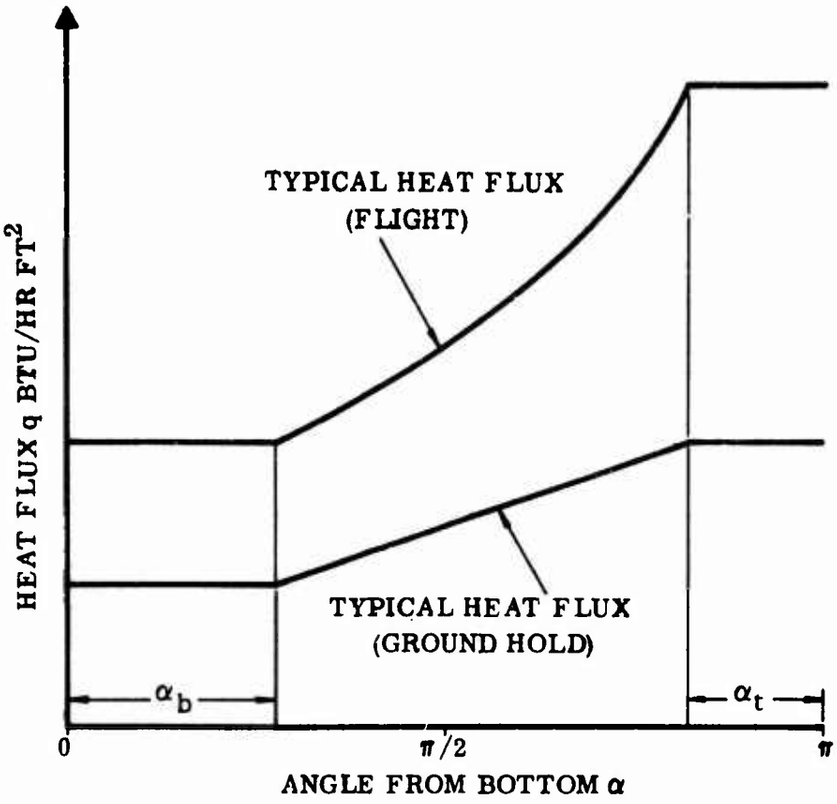

Figure 49. Heat Flux Through Variable Thickness Insulation

3.1.1 GROUND HOLD INSULATION - Heat fluxes at ground hold are assumed to vary linearly with insulation thickness as shown in the lower curve, Figure 49. The local heat flux at any given position, $\alpha_b \leq \alpha \leq \pi - \alpha_t$, is given by

$$q(\alpha) = q_b + (\alpha - \alpha_b)(q_b - q_t) / (\alpha_b - \pi + \alpha_t) \quad (1)$$

The heat transfer areas at ground hold are the actual wetted areas of the tank including end domes.

3.1.2 FLIGHT INSULATION - Heat fluxes in flight are assumed to vary exponentially with insulation thickness as shown on the upper curve, Figure 49. The equation used is of the form

$$q = a\, e^{b\alpha} \quad (2)$$

The form of this equation was obtained by plotting heat flux as a function of insulation thickness using the actual external environmental temperatures for the vehicle geometry

and trajectory stipulated for this experimental program. The maximum temperatures were 1460°R top, 1580°R side, and 1700°R bottom. Variation in fuselage configuration, trajectory parameters and tank location in the vehicle will result in different heat flux distributions. However, it is typical of this type vehicle that there can be significant temperature differences between top and bottom and that the top of the tank (not being wetted) will require the least insulation. Thus the exponential heat flux distribution evolved from this program should be representative of other insulation systems and trajectories. Substituting in limiting conditions and integrating equation (2) between two angular positions α_1 and α_2 gives a local mean heat flux

$$q = \frac{q_b}{\ell n\,(q_b/q_t)} \left[(q_b/q_t)^{\frac{\alpha_2 - \alpha_b}{\alpha_b - \pi + \alpha_t}} - (q_b/q_t)^{\frac{\alpha_1 - \alpha_b}{\alpha_b - \pi - \alpha_t}} \right] \left[\frac{\alpha_b + \alpha_t - \pi}{\alpha_2 - \alpha_1} \right] \quad (3)$$

The heat transfer areas used in flight assume a flat ended cylindrical or 'double-bubble' tank with an effective length equal to the actual tank length including dome ends. During flight the sides of the tank, adjacent to the aerodynamically heated surfaces of the vehicle, will be subjected to a higher heating rate than the ends. The effective heated area in flight is used to compensate for this difference in heating rate.

3.1.3 SUPPORT AND PENETRATION HEAT LEAKS - Provision has been made to introduce additional heating into the liquid through supports and/or penetrations at four different locations (heights) on the tank. This is illustrated in Figure 50 for the large scale 6000 gallon test tank. Heating rates may be variable with time and are input in

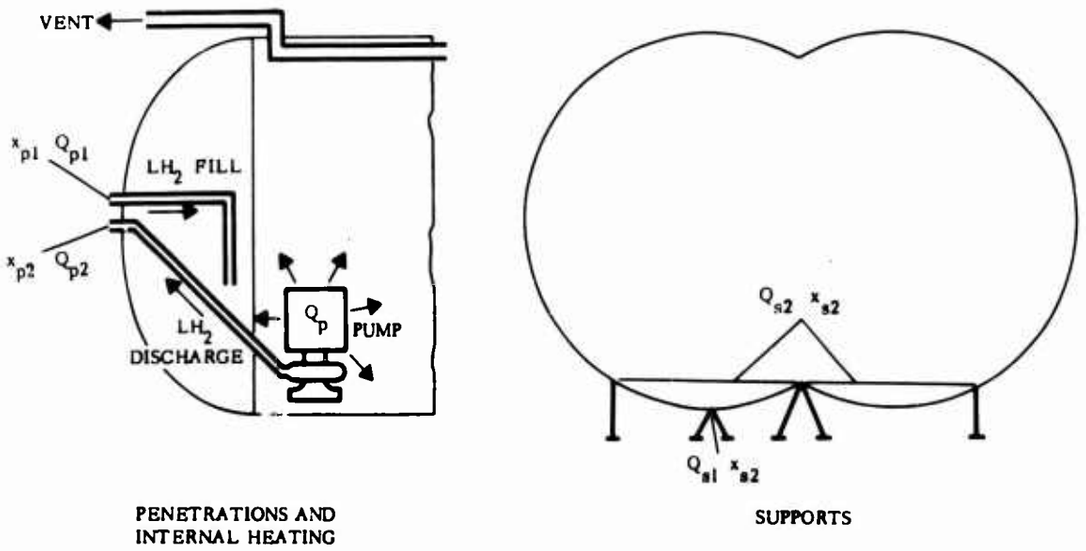

Figure 50. Typical Support, Penetration, and Internal Heat Sources

tabular form. Heat from the supports and penetrations is introduced uniformly into all liquid nodes at or above the support or penetration height. Heat fluxes through penetrations and/or supports all at the same height can be input as a single set of values. During the trajectory calculation heat input is discontinued when the liquid level drops below the given height.

3.1.4 INTERNAL HEATING - Provision has been made to introduce an internal heat source, Q_p. Heat from this source is introduced uniformly into all liquid in the tank. With high power input and only moderate efficiency a considerable amount of heat input to the liquid and boil-off will result from boost pump operation. Internal power is input into the program along with propellant flow rate.

3.2 LIQUID THERMAL ANALYSIS

3.2.1 LIQUID NODES - The liquid thermal analysis is performed using constant mass nodes, m_ℓ, illustrated in Figure 48. At the start of the calculation (beginning of ground hold) the liquid is assumed to be at a uniform density and temperature equal to the equilibrium temperature at tanking pressure. If the operating pressure is greater than the tanking pressure then the liquid is subcooled. Each node at this point has an equal volume and mass. The number of liquid nodes is reduced as the calculation progresses through the trajectory. Boil-off mass, m_{bo}, and spray cooling mass, m_{spr}, are taken from the top node and liquid pumped from the tank is taken from the bottom node. All other nodes retain a constant mass. The thermodynamic properties, liquid density and enthalpy as a function of temperature, are input to the program. The density of the liquid when boiling is reduced 2.5% from the quiescent or input value ($\rho_{\ell, bo} = \rho_\ell / 1.025$). This is based on measurements made on Centaur LH_2 tanks at heat flux densities comparable to those likely to be experienced on hypersonic vehicle tanks. The volume, V_ℓ, density, ρ_ℓ, temperature, T_ℓ, and enthalpy of each node is computed at each time interval. Using the volume of each node and the geometrical characteristics of the tank (area and volume as a function of height) the heated, A_ℓ, and the height, x_ℓ, of each node is computed. The liquid calculation for each time interval consists of:

heat input per node

$$m_\ell \Delta H_\ell = \left[q_\ell A_\ell + V_\ell \left(\frac{Q_{s1}}{V_{T,\ell,s1}} + \frac{Q_{s2}}{V_{T,\ell,s2}} + \frac{Q_{p1}}{V_{T,\ell,p1}} + \frac{Q_{p2}}{V_{T,\ell,p2}} + \frac{Q_r + Q_p}{V_{T,\ell}} \right) \right] \Delta\theta \qquad (4)$$

where

$V_{T,\ell,s1}$ = volume of liquid above level, x_{s1}, of support #1

$V_{T,\ell}$ = total liquid volume

enthalpy increase per node

$$H_{\ell,\,\theta+\Delta\theta} = H_{\ell,\,\theta} + \Delta H_{\ell} \tag{5}$$

The wetted area/volume ratio of each node varies continuously in the cylindrical tank geometry; maximum at the bottom, decreasing to minimum at the side then increasing toward the top. This results in high temperature low density liquid nodes in the bottom of the tank. A mixed layer in the bottom is computed such that the enthalpy of this layer is less than the next adjacent node above. All nodes in the mixed layer are at

$$H_{mix} = \left[\sum_{\ell=0}^{n} H_{\ell}\, m_{\ell}\right] \Big/ \left[\sum_{\ell=0}^{n} m_{\ell}\right] \quad ; \; H_{mix} < H_{n+1} \tag{6}$$

equal temperature (enthalpy). The enthalpy of each node is checked and where $H_{\ell} > H_{sat}$ the excess energy is boil-off.

boil-off per node

$$m_{\ell,\,bo} = \frac{(H_{\ell} - H_{sat})\, m_{\ell}}{\Delta H_{vp}} \tag{7}$$

$$\dot{m}_{\ell,\,bo} = m_{\ell,\,bo} / \Delta\theta \tag{8}$$

total boil-off rate

$$\dot{m}_{bo} = \sum_{\ell=0}^{j} \dot{m}_{\ell,\,bo} \tag{9}$$

The boil-off rate also incudes an amount due to liquid surface turbulence which is discussed below in Section 3.2.2. This is added to equation (9) to obtain the boil-off rate.

The heat input to the liquid, equation (4), includes radiation, Q_r, from the top of the tank. The heat input calculation is iterative and the first computation is made with $Q_r = 0$. This gives a boil-off rate, $\dot{m}_{bo}$, which is used in the ullage heat balance to obtain a value for Q_r. The calculation is repeated starting with equation (4) using Q_r. This iterative procedure is converged to an overall heat balance solution.

The liquid heat balance is based on a non-integrated finite time interval calculation. An integrated calculation would cost too much in computer time. The heat input to the liquid is based on heat fluxes taken at the beginning of the interval. If the heat fluxes and liquid level are changing rapidly with time and/or a long calculation time interval

is selected the resulting error could be appreciable. An estimated error at each time interval is computed and printed by the program. This error can be reduced at the expense of increased computer time by reducing the calculation time interval. The computed error is the ratio of (1) the difference in total heat flux to the liquid at succeeding time intervals and (2) the average total heat flux at the two intervals.

3.2.2 CORRECTED LIQUID LEVEL - A form of liquid surface turbulence was postulated, although not observed or measured directly, from the test results. Surface agitation caused by convective liquid motion and/or local boiling at the tank skin/ullage/liquid interface is believed to have caused an effective increase in wetted area. An increase in liquid level has been developed according to the model illustrated in Figure 51. All heat entering the bulk, Δx_{cor}, above the normal liquid level results in boil-off.

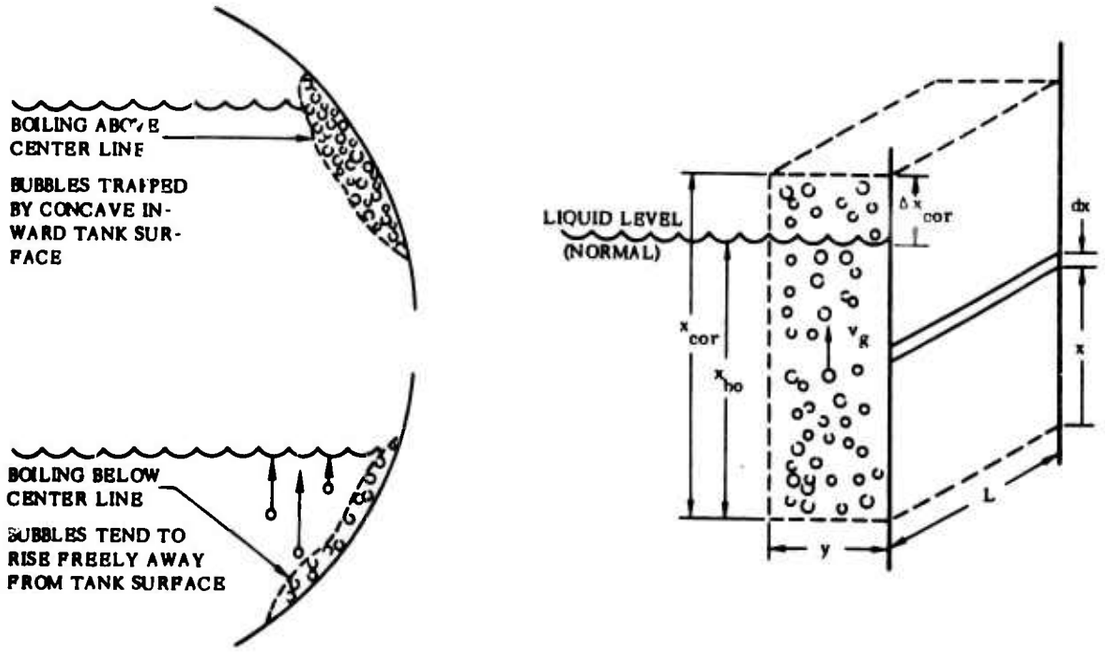

Figure 51. Turbulence at the Tank Skin/Ullage/Liquid Interface

Vapor bubbles are assumed to be introduced into an arbitrary volume of liquid along the skin based on the heat flux at the interface. This increases the volume by the amount of vapor introduced, thus column height rises above the normal liquid level.

$$V_{T,cor} = V_{\ell,cor} + V_{g,cor} \qquad (10)$$

The depth of the column, x_{bo}, below the liquid level is assumed to be the depth of the boiling liquid or an arbitrary depth before boiling starts. The volume of liquid, $V_{\ell,cor}$ and the total volume $V_{T,cor}$ is

$$V_{\ell, cor} = y\, x_{bo}\, L \tag{11}$$

$$V_{T, cor} = y\, x_{cor}\, L \tag{12}$$

The volume rate of vapor entry into the column at height x is

$$\dot{V}_{g, cor} = \frac{q\, L\, dx}{\rho_g\, \Delta H_{vp}} \tag{13}$$

The time that the vapor remains in the column is

$$\theta = \frac{x_{cor} - x}{v_g} \tag{14}$$

Multiplying equations (13) and (14) and integrating from $x = 0$ to x_{cor} gives the total vapor volume

$$V_{g, cor} = \int_0^{x_{cor}} \frac{q\, L\, (x_{cor} - x)\, dx}{v_g\, \rho_g\, \Delta H_{vp}} \tag{15}$$

$$V_{g, cor} = \frac{q\, L\, x_{cor}^2}{2\, v_g\, \rho_g\, \Delta H_{vp}} \tag{16}$$

Substituting the volumes into equation (10) and equating to zero gives

$$x_{cor}^2 - 2\, K\, x_{cor} + 2\, K\, x_{bo} = 0 \tag{17}$$

where

$$K = y\, v_g\, \rho_g\, \Delta H_{vp}/q$$

the height of the vapor/liquid column is

$$x_{cor} = K\, (1 - \sqrt{1 - 2\, x_{bo}/K}\,) \tag{18}$$

and the increased liquid level is

$$\Delta x_{cor} = x_{cor} - x_{bo} \tag{19}$$

Boiling hydrogen bubble rise rates, v_g, have been measured, Reference 16 under one 'g' conditions. Values ranged from 5 to 20 inches per second. A basic value of one foot per second is used for this analysis.

Tank curvature will influence the bubble rise rate in the column along the skin. When the liquid level is above the center line bubbles will tend to be slowed and accumulate as they attempt to rise parallel to the gravity field and are forced sideways by the tank wall. When the liquid level is below the center line the bubbles will rise freely and will not tend to accumulate in a boiling layer (Figure 51). To compensate for this tank geometry characteristic, the velocity is adjusted according to the angular position of the liquid level in the tank.

$$v = v_g (1 + \cos \alpha) \tag{20}$$

3.3 ULLAGE THERMAL ANALYSIS

The ullage heat balance is made progressively upward through the tank starting with the node just above the corrected liquid level. The ullage and tank skin temperatures are computed for approximately equal area skin nodes illustrated in Figure 48. The top area of the tank above the level of the vent is considered separately. Heat flux through the insulation, q_w, is input to the program. The local heat flux to a particular node at any given time is computed according to the procedure given in section 3.1. Heat is transferred from a tank skin node by convection to the ullage and by radiation to the liquid according to the equations

$$q_c = h (T_{sk} - T_u) \tag{21}$$

$$q_c = (\dot{m}_{bo} Cp/A_u) (T_2 - T_1) \tag{22}$$

$$q_r = \sigma \epsilon f_r T_{sk}^4 \tag{23}$$

The temperature difference between the ullage gas and the tank skin is defined as the log mean temperature difference and is given by

$$T_{sk} - T_u = \frac{(T_{sk} - T_1) - (T_{sk} - T_2)}{\ell n \left(\frac{T_{sk} - T_1}{T_{sk} - T_2} \right)} \tag{24}$$

Substituting equation (24) into equation (21) then combining and rearranging equations (21) and (22) gives are expression for the convective heat flux, q_c, as a function of T_{sk}

$$q_c = (\dot{m}_{bo} Cp/A_u) (1 - e^{-z}) (T_{sk} - T_1)$$

$$\text{where } z = h A_u / \dot{m}_{bo} Cp \tag{25}$$

The internal tank emmissivity, ϵ, is input to the program. The radiation shape factor, f_r, used in the program is given by

$$f_r = .5\left[1 + \sin(\alpha - \pi/2)\right] \tag{26}$$

The free convection heat transfer coefficients obtained from the tank tests varied from about 10 BTU/hr ft^2 °R at 40°R to about 1 BTU/hr ft^2 °R at 580°R. Thus h is assumed to vary linearly up to 580°R and is constant above that temperature.

$$\begin{aligned} h &= 10.67 - T_u/60 \qquad T_u \leq 580 \\ h &= 1.0 \qquad\qquad\quad T_u > 80 \end{aligned} \tag{27}$$

The top area of the tank above the level of the vent (x_{vt} in Figure 48) was consistently hot during the tests where the ullage gas tended to stagnate. Correlating this with free convection heat transfer phenomena resulted in a Nusselt number, $h/(k_g/\Delta x)$, near unity when the distance $\Delta x_t = x_{max} - x_{vt}$ was used. Thus the heat balance on the top of the tank assumes thermal conduction in gaseous hydrogen plus radiation to solve for the ullage and top tank skin temperature. h is replaced with $k_g/\Delta x_t$ for the heat balance at the top of the tank otherwise the equations are identical. The heat transfer coefficient, h, and a typical conductance, $k_g/\Delta x_t$, at the top of the tank as a function of temperature are shown in Figure 52.

The ullage heat balance assumes steady state conditions for the computation at each time interval. The input heat flux, q_w, to the liquid should, however, be based on a proper transient analysis which accounts for (1) the thermal inertia of the entire external system of insulation and airframe structure and (2) the effect of varying environmental temperature and pressure on the conductivity of the insulation.

3.3.1 ULLAGE HEAT BALANCE - CONSTANT Q_w - The transient heat flux through the insulation to the tank skin at liquid temperature is input to the program. This heat flux is assumed to be constant (independent of temperature) for a given time interval calculation. The ullage heat balance equation is

$$q_w = q_c + q_r \tag{28}$$

Substituting equations (23) and (25) into equation (28) and rearranging gives a polynomial which can be solved numerically for T_{sk}.

$$\sigma \epsilon f_r T_{sk}^4 + (\dot{m}_{bo} Cp/A_u)(1 - e^{-z})(T_{sk} - T_l) - q_w = 0 \tag{29}$$

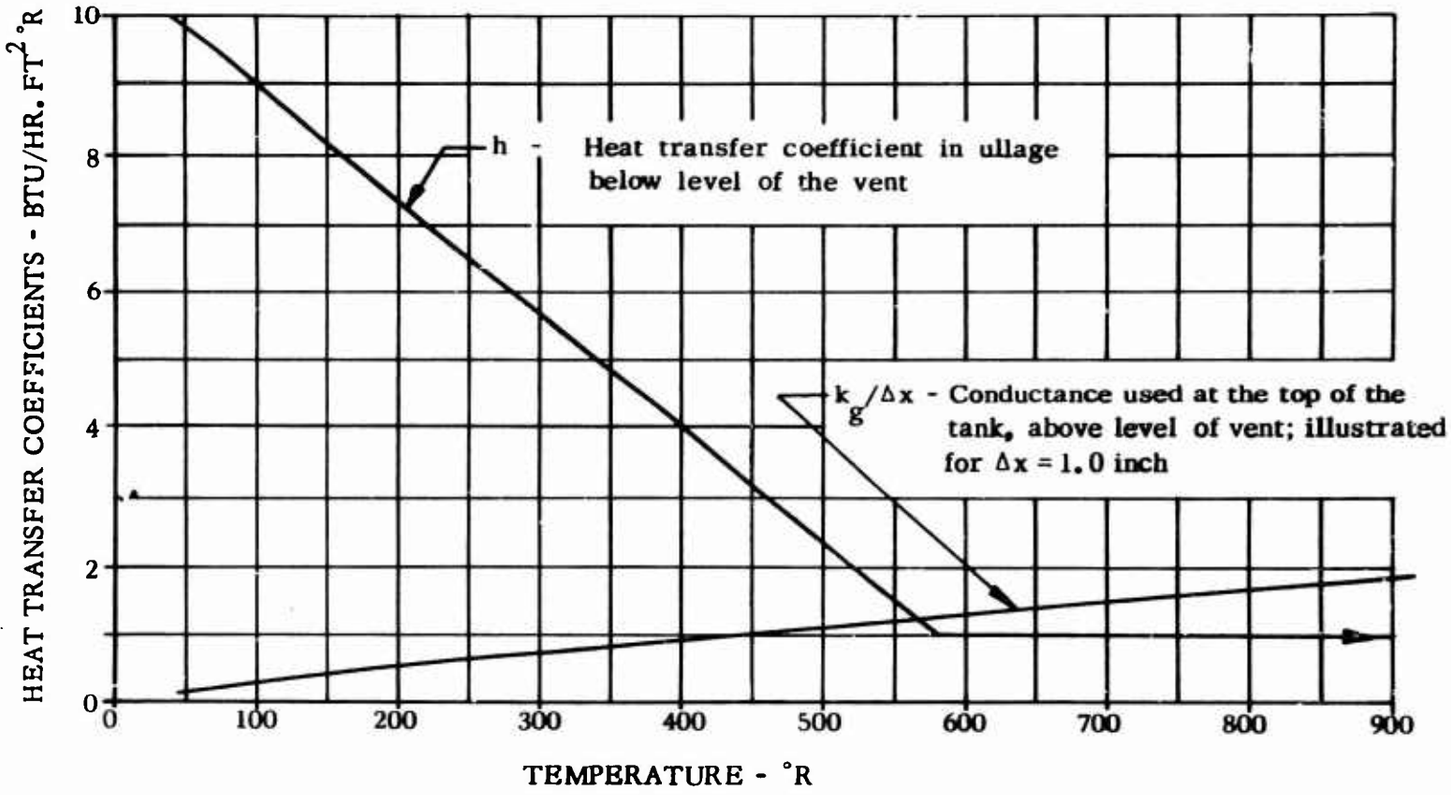

Figure 52. Ullage Heat Transfer Coefficients

The ullage temperature at the bottom of a node, T_1, is known. The convective heat flux, q_c, is calculated from equation (25) using the computed value of T_{sk} from equation (29). The temperature rise of the ullage gas across the node is calculated by solving equation (22) for T_2.

This is the most simple solution to the ullage heat balance. However, it should be noted that no specific bounds are placed on the calculated tank skin temperature. As a result it is possible to compute a tank skin temperature which is greater than the real external surface temperature of the insulation especially when the heat flux is high and the boil-off rate is low. The ullage heat balance is deleted when $T_{sk} > 490°R$ at ground hold and when $T_{sk} - T_{vt} < 0.1$ in flight. A deleted ullage heat balance is noted in the output.

3.3.2 ULLAGE HEAT BALANCE - VARIABLE Q_d - An option is provided in the program to compute the heat flux based on the temperature difference across the insulation. In this case it is necessary to input the external surface temperature, T_o, of the insulation as a function of time along with the heat flux, q_w.

The heat flux through a conducting material is proportional to the temperature difference, ΔT, across the material,

$$q = \left[\frac{k_i}{t_i}\right] \Delta T \tag{30}$$

where k_i/t_i is the constant of proportionality. The heat flux to the liquid is

$$q_w = \left[\frac{k_i}{t_i}\right] (T_o - T_\ell)$$

thus

$$\left[\frac{k_i}{t_i}\right] = \frac{q_w}{T_o - T_\ell} \tag{31}$$

If the thermal conductivity of the insulation is constant then the heat flux, q_d, though the insulation to the dry tank skin can be expressed as

$$q_d = \left[\frac{q_w}{T_o - T_\ell}\right] (T_o - T_{sk}) \tag{32}$$

The thermal conductivity of most materials varies with temperature. This variation is quite large over a temperature range from cryogenic to the maximum for hypersonic vehicle flight. The thermal conductivity of helium purged microquartz (the material used on the test tanks) as a function of temperature at two representative pressures is given in Figure 53. In order to compute the correct heat flux as a function of temperature, the mean conductivity of the material over the temperature interval, $T_o - T_{sk}$ should be used. The mean conductivity is also shown on Figure 53. Since the thermal conductivity typically varies with both temperature and pressure, it would

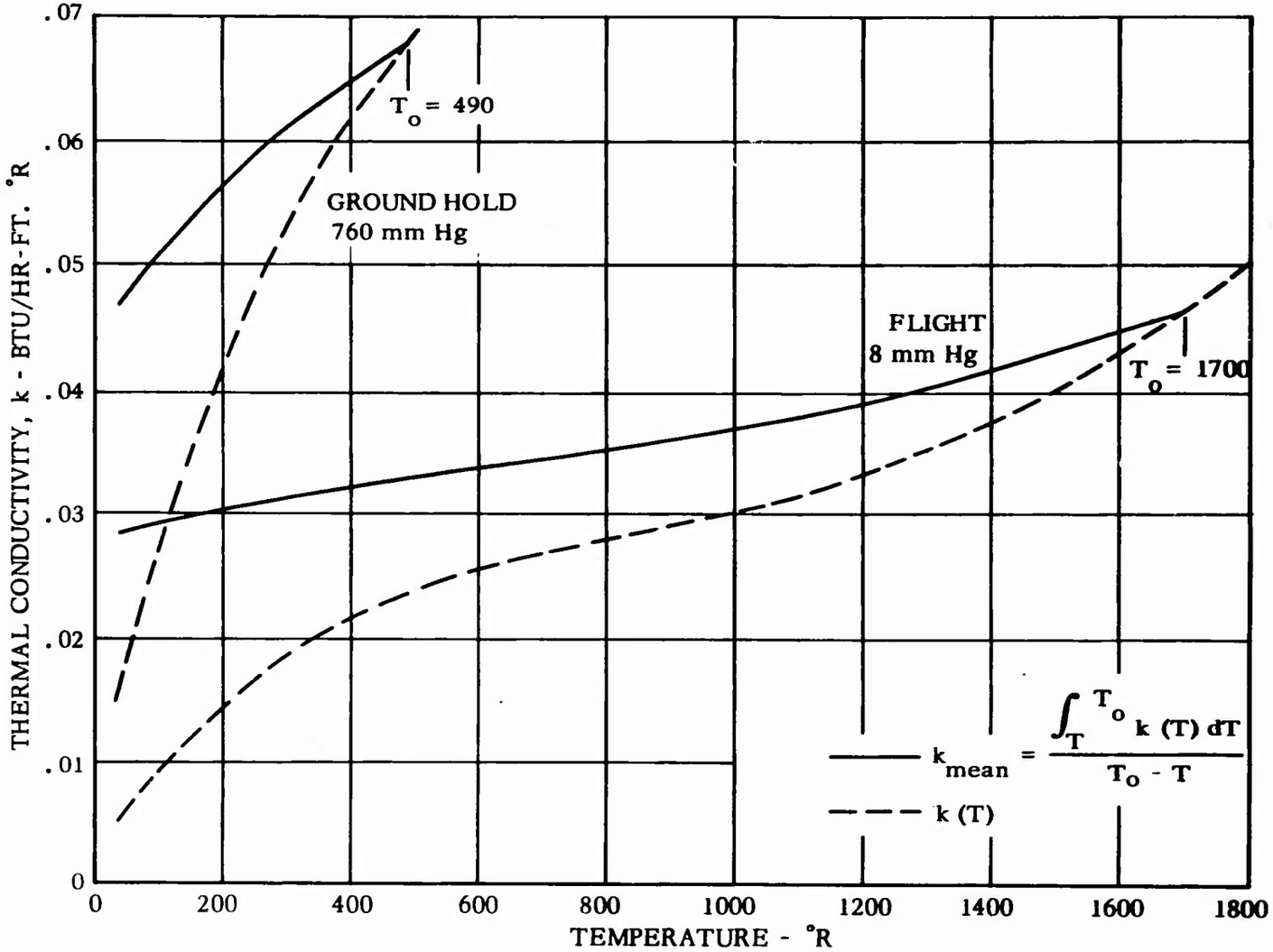

Figure 53. Thermal Conductivity of Microquartz, Helium Purged

be necessary to input to the computer program a rather complex and unwieldy set of expressions or tables to properly describe the thermal conductivity of the material. Therefore an approximation has been developed for this program which accounts for the variation in thermal conductivity as a function of temperature. The variation of thermal conductivity with pressure is accounted for through the use of, q_w, which should include the effects of a varying environmental pressure on the performance of the insulation. The heat flux as a function of tank skin temperature is illustrated in Figure 54. The true variation in heat flux as a function of the integrated mean thermal conductivity from Figure 53 is shown. Also shown is the heat flux assuming a constant conductivity, equation (32), and the heat flux approximation used in this program. Using this approximation the heat flux is held constant over the interval $T_{sk} = T_\ell \longrightarrow T_\ell + 0.15\,(T_o - T_\ell)$ and then varies linearly up to the maximum temperature, T_o. The expression for heat flux is

$$q_d = \frac{q_w\,(T_o - T_{sk})}{0.85\,(T_o - T_\ell)} \tag{33}$$

and the ullage heat balance is

$$q_d = q_c + q_r \tag{34}$$

Substituting equations (23), (25) and (33) into equation (34) and rearranging gives a polynomial which can be solved numerically for T_{sk}

$$\sigma \epsilon f_r T_{sk}^4 + \left[\frac{\dot{m}_{bo}\,Cp}{A_u}(1 - e^{-z}) + \frac{q_w}{0.85(T_o - T_\ell)}\right] T_{sk} - \tag{35}$$

$$\frac{\dot{m}_{bo}\,Cp}{A_u}(1 - e^{-z})\,T_1 + \frac{q_w}{0.85\,(T_o - T_\ell)} = 0$$

The constant 0.15 used above to describe the temperature interval for constant heat flux is arbitrary and represents a best approximation for this particular insulation. It is characteristic of most insulations that there is a significant drop in thermal conductivity as the temperature approaches liquid hydrogen, ~40°R. Thus this approximation should be representative of other insulating materials for an LH_2 tank.

3.3.3 SPRAY COOLING HEAT BALANCE - Provision is made in the program to limit the top tank skin temperature to any desired value $T_{sk,max}$. This done by first computing the normal ullage heat balance with current boil-off rates, $\dot{m}_{bo}$. If the tank skin temperature exceeds the limit, the boil-off rate is increased, $\dot{m}_{bos}$, and the ullage heat balance recomputed to reduce the temperature to $T_{sk,max}$. This is converted to spray rate according to the equation

$$\dot{m}_{spr} = \left[\frac{\dot{m}_{bos} - \dot{m}_{bo}}{\Delta H_{vp}}\right]\left[\Delta H_{vp} + \int_{T_\ell}^{T_{vt}} Cp\,dT\right] \tag{36}$$

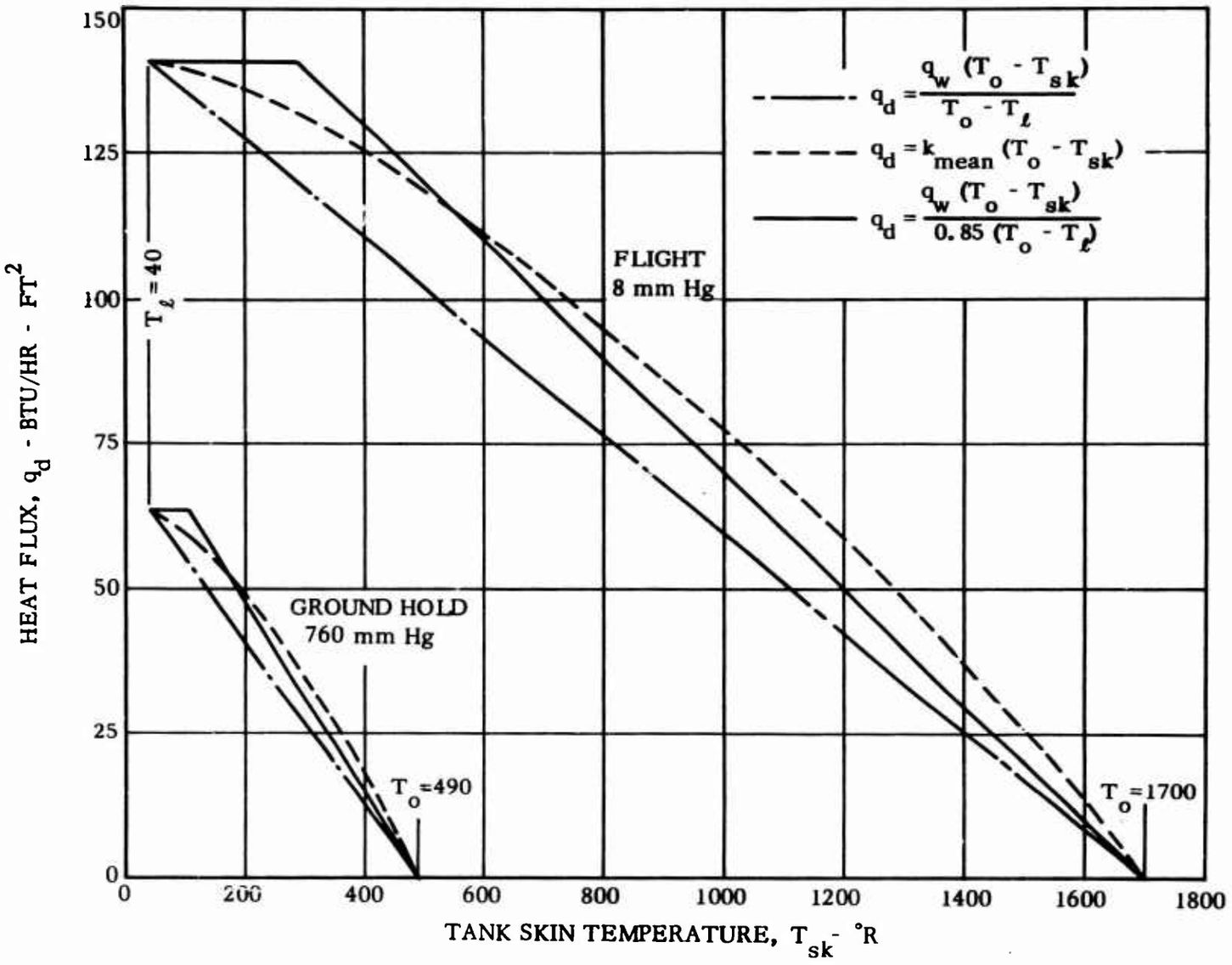

Figure 54. Heat Flux Through 4 Inches of Microquartz, Helium Purged

3.3.4 VENT INSTALLATION - Ullage gas tends to stratify and stagnate in the top of the tank. Only a minimum amount of convective cooling results. A horizontal piccolo vent, illustrated in Figures 48 and 50 is recommended in this type tank to obtain more uniform and predictable cooling of the tank structure. The height, x_{vt}, of the holes in the vent pipe are input to the program to specify the level of ullage stagnation. Above this level heat conduction through the gas is assumed. Most horizontal tanks will have frame stiffening which will block lateral movement of the ullage gas even if internal venting is not provided. The depth of these frames should be specified as the vent height in this case.

The maximum allowable liquid level, $x_{\ell,max}$, the limiting level to which the liquid is allowed to expand while heating, should be no higher than the bottom of the internal vent pipe. If the liquid is in contact with the vent pipe it will become a liquid/vent gas heat exchanger. No provision is made in the program for this type heat transfer.

3.4 TANK SIZING ANALYSIS

The computer program sizes the tank to contain the total required propellant mass and ullage space by varying the length of the cylindrical section of the tank. It is assumed that radius constraints on the installation will be accounted for by proper input to the program. It should be noted that if a specific set of vertical and lateral dimensional contraints exist for a particular vehicle then tank radius and insulation thickness should change simultaneously to make optimum utilization of vehicle volume.

The criteria for determining the correct tank size is that the liquid reach the unusable level, $x_{\ell,un}$, simultaneously with the mission (flight) time, θ_e, expiration. If the unusable liquid level is reached at a time θ before the mission time expiration, a volume correction is computed based on the propellant flow, boil-off, and spray cooling rates.

$$\Delta V = \frac{(\dot{m}_{p,\theta} + \dot{m}_{bo,\theta} + \dot{m}_{spr,\theta})}{\rho_\ell} (\theta_e - \theta) \tag{37}$$

The length correction based on equation (37) is

$$\Delta L_{cyl} = - \Delta V/(Ac_{\ell f} - Ac_{un})_{cyl} \tag{38}$$

If the mission time expires before the unusable liquid level is reached the length correction is

$$\Delta L_{cyl} = (V_{T,\ell,\theta_e} - V_{un})/(Ac_{\ell f} - Ac_{un})_{cyl} \tag{39}$$

The revised length is

$$L\,(new) = L\,(current) - \Delta L_{cyl} \tag{40}$$

These correction factors are not necessarily exact and the calculation may be repeated. It converges to within ±0.2 percent of the required tank volume. The tank to be sized must have a finite cylindrical length. Input parameters should be checked to assure that the sizing calculation will not result in a calculated value of $L_{cyl} < 0$.

Liquid hydrogen density decreases approximately 34 percent while being heated from 50% slush to a boiling condition at 60 psia. This may be an extreme for an operating tank but it illustrates the fact that expansion can utilize a considerable amount of volume. An amount which may be comparable to the ullage space. In order to be consistent in sizing tanks for a particular mission, the minimum ullage volume should be a constant for each tank sized. The maximum liquid level, $x_{\ell, max}$, is specified in the input to the program. The liquid first expands and the level increases due to heating until boil-off and/or propellant outflow through the pump start reducing the level. The tanking or fill level, $x_{\ell f}$, is computed such that the maximum level reaches but does not exceed the specified value.

3.5 WEIGHTS ANALYSIS

The weights analysis is based on actual designs of a large scale 6000 gallon test tank. The inert weights computed by the program are illustrated in Figure 55. They include the subsystems, insulation, and tank structure components. In addition the program computes propellant mass and an equivalent installed weight or volume penalty.

3.5.1 PROPELLANT - The propellant mass includes usable, unusable, boil-off and spray.

$$m_{T,\ell} = m_{us} + m_{un} + m_{bo} + m_{spr} \tag{41}$$

3.5.2 SUBSYSTEMS - The subsystem weight include the fuel, vent and spray cooling. Typical input weight coefficients for these subsystems are listed in Table VIII. Weight coefficients should be input to the program as though the tank were a single cylinder. Appropriate corrections are made within the program for dual hardware in an intersecting cylinder tank.

Fuel Sybsystem - The fuel subsystem includes the internal boost pump, pump discharge lines and fill-drain lines. The weight of this system will be primarily a function of the maximum required mass flow rate.

$$W_p = W_{f,p} + \frac{\dot{m}_{p,\,max}}{3600.} W_{v,p} \tag{42}$$

Vent Subsystem - The vent subsystem includes an internal piccolo vent pipe to distribute the ullage boil-off gas for maximum cooling, the penetration through the tank skin and a pressure regulator valve. This system will be sized primarily to minimize pressure losses. The parameter most closely related to pressure loss is vent velocity. The vent velocity for hydrogen vapor is computed with equation (43).

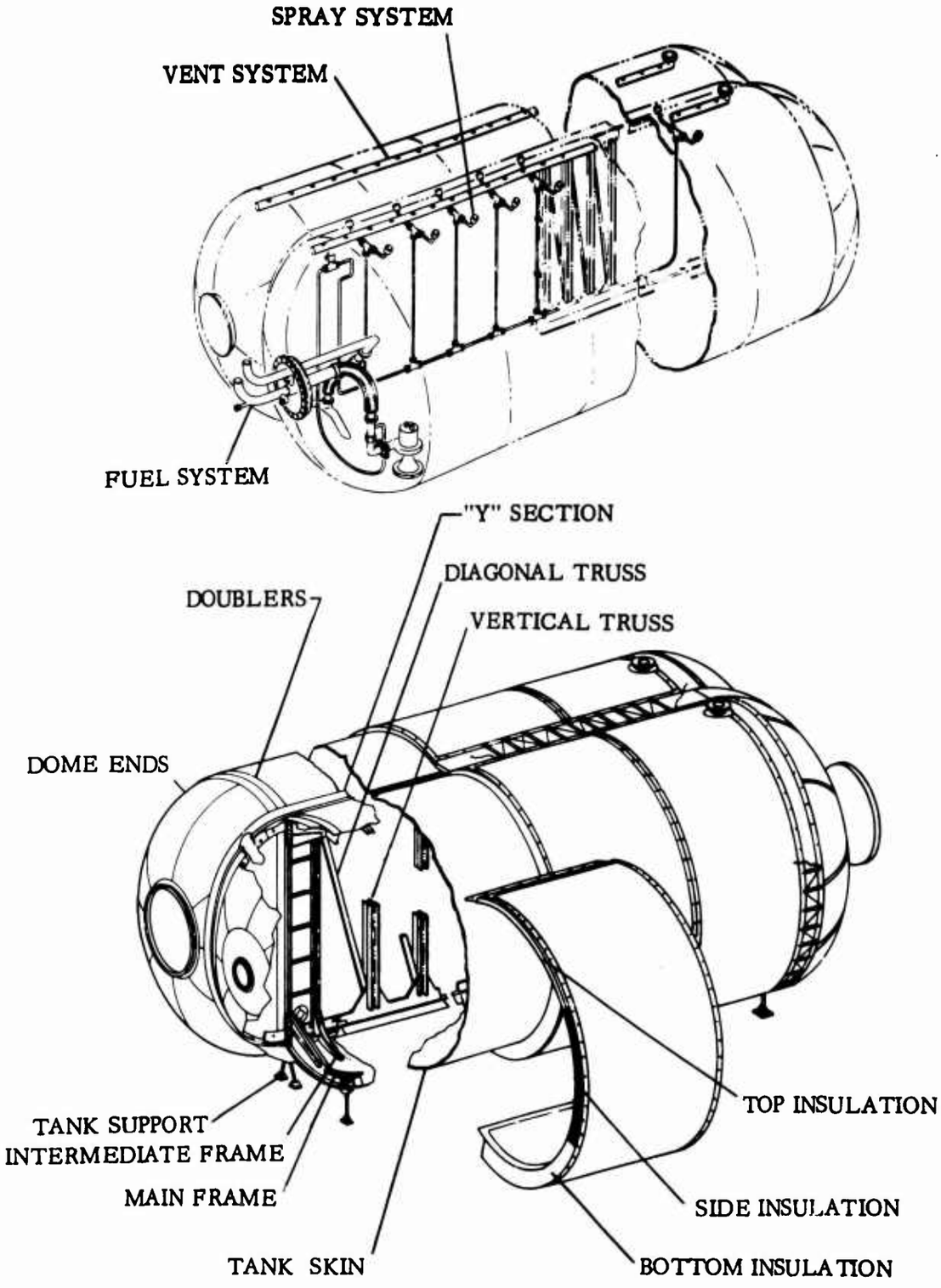

Figure 55. Propellant Tankage System

Table VIII. Weights Analysis Coefficients

Insulation and subsystem weights subscripted with f are fixed values and those subscripted with v are variable with respect to some parameter as noted below.

Top insulation	$Wa_{f,t,i} = 0.2450$ lb/ft^2	$Wa_{v,t,i} = 0.3753$ lb/ft^2/(inch insulation)
Side insulation	$Wa_{f,s,i} = 0.2450$ lb/ft^2	$Wa_{v,s,i} = 0.3753$ lb/ft^2/(inch insulation)
Bottom insulation	$Wa_{f,b,i} = 0.2230$ lb/ft^2	$Wa_{v,b,i} = 0.3753$ lb/ft^2/(inch insulation)
Vent subsystem	$W_{f,vt} = 23.0$ lb	$W_{v,vt} = 10.0$ lb/(ft^3/sec, vent flow)
Fuel subsystem (pump)	$W_{f,p} = 30.0$ lb	$W_{v,p} = 7.0$ lb/(lb/sec, fuel flow)
Spray cooling subsystem	$W_{f,spr} = 5.0$ lb	$W_{v,spr} = 0.25$ lb/(ft, tank length)

Structural design coefficients

Proof pressure factor	$f_{pr} = 1.33$
Burst pressure factor	$f_{bu} = 2.0$
Buckling factor	$f_{cb} = 0.64$
Flange crippling factor, frames	$f_{crf} = 0.5$
Flange crippling factor, Y-section	$f_{cry} = 0.065$
Forming or stretch factor	$f_{str} = 1.2$

Point design parameters

Radius	$R = 8/3 = 2.67$ ft
Cylinder length	$L_{cyl} = 20$ ft
Skin thickness	$t_{cyl,sk} = 0.016$
Material density	$\rho_m = 513$ lbs/ft^3
Design pressure	$P_{des} = 30$ psid
Ultimate vertical load factor	$G = 3.0$ g's

Values in this table are based on the large scale test tank design concepts.

$$\dot{V}_{vt} = \frac{\dot{m}_{bo} + \dot{m}_{spr}}{P_{op} / 5.324\, T_{vt}} \tag{43}$$

The maximum vent velocity during the mission is used to compute the vent subsystem weight.

$$W_{vt} = W_{f,p} + \frac{\dot{V}_{vt,\,max}}{3600.}\; W_{v,\,vt} \tag{44}$$

Spray Cooling Subsystem - The spray cooling subsystem will include a spray bar with nozzles and a shut-off valve. Liquid is assumed to be sprayed from the system. Excess liquid will be flowed through the spray bar and returned to the tank to keep liquid at all nozzles. The weight will be independent of flow rate and dependent primarily on installed length. The weight is represented by the expression,

$$W_{spr} = W_{f,\,spr} + L_{cyl}\, W_{v,\,spr} \tag{45}$$

This weight is computed only if spray cooling is required, i.e., a quantity of spray cooling mass is used.

3.5.3 INSULATION - The insulation weight coefficients used in the program are listed in Table VIII. All values are for a unit area of tank surface. The numerical values are based on quartz fiber insulation with metal screen covers. A metal foil convection shield is installed under the first layer of insulation on the top and side. Fixed weights include the metal screen covers and convection shield. Variable weights as a function of thickness include the insulating material and thread or wire which holds the insulation blankets together. The insulation weight equations are

top
$$W_{T,\,t,\,i} = A_{t,i}\,(Wa_{f,t,i} + t_{t,i}\; Wa_{v,t,i}) \tag{46}$$

side
$$W_{T,s,i} = A_{s,i}\left(Wa_{f,s,i} + \frac{t_{t,i} + t_{b,i}}{2}\; Wa_{v,s,i}\right) \tag{47}$$

bottom
$$W_{T,b,i} = A_{b,i}\,(Wa_{f,b,i} + t_{b,i}\; Wa_{v,b,i}) \tag{48}$$

total
$$W_{T,i} = W_{T,t,i} + W_{T,s,i} + W_{T,b,i} \tag{49}$$

3.5.4 TANK STRUCTURE - The structural weights analysis is based on an intersecting cylinder tank configuration with elliptical dome ends. The center-to-center spacing of the cylinders is one radius and the major/minor axis ratio of the dome ellipsoid is 1.38. An optimized stress analysis was performed on the large scale test tank design. Appropriate ratios and curve fits from this point design stress analysis were used to develop the weight equations. The structural design coefficients and the principal point design parameters used in the weight equations are listed in Table VIII.

Other point design values are indicated in the discussion of specific structural components. Factors of 1.2 and .833 (= 1/1.2) are used in some cases to increase margins of safety. An inch is the standard unit of length in stress analysis. Conversion in some of the equations to the unit of feet has been made for consistency in the nomenclature.

The design pressure used in the structural weight analysis is given in equation (50). The

$$P_{des} = 1.05\, P_{op} \tag{50}$$

operating pressure, P_{op}, a thermodynamic value used for boil-off and liquid stratification calculations. The design pressure is 5 percent greater than operating to provide for vent valve control tolerances. The operating pressure is input to the program.

Cylinder Skins - Three pressure vessel design conditions are evaluated to determine the cylinder skin thickness; two room temperature conditions to meet structural proof test requirements and one maximum temperature condition to meet operational requirements. The skin thickness equations are

$$t_{cyl,sk} = 12.(f_{bu}\, P_{des}\, R/F_{tu}) \qquad F_{tu} @ 540^{\circ}R \tag{51}$$

$$t_{cyl,sk} = 12.\,(f_{pr}\, P_{des}\, R/F_{ty}) \qquad F_{ty} @ 540^{\circ}R \tag{52}$$

$$t_{cyl,sk} = 12.\,(P_{des}\, R/F_{ty}) \qquad F_{ty} @ T_{sk,max} \tag{53}$$

No safety factor is used at the maximum temperature condition, equation (53), because this temperature occurs only on the top of the tank while it is operating at design pressure. Thus the maximum skin thickness is required only at the top. Equation (53) represents an average value for weight purposes. The maximum of the three thicknesses above is used.

$$t_{cyl,\,sk,\,max} = \text{maximum of } t_{cyl,sk} \text{ from equations (51),(52),(53)}$$

A minimum gage is specified in the program input and is used if calculated values are lower.

$$t_{cyl,sk,des} = \text{maximum of } t_{cyl,\,sk,\,max} \text{ and } t_{min,m}$$

The weight of the cylinder section skins is

$$W_{cyl,sk} = 2\,(\tfrac{4}{3}\,\pi\, R\; L_{cyl}\; t_{cyl,sk,des}\; \rho_m)/12. \tag{54}$$

Dome Ends - The load intensity ratio from the dome to the cylinder skins for this particular ellipsoid is 0.69. This factor is applied along with a stretch factor to determine the dome skin thickness.

$$t_{dom,\,sk} = .69\ f_{str}\ t_{cyl,\,sk,\,max} \tag{55}$$

The minimum gage is used if the calculated skin thickness is lower

$$t_{dom,\,sk,\,des} = \text{maximum of } t_{dom,\,sk} \text{ and } t_{min,\,m}$$

The surface area of domes is

$$A_{dom} = 15.96\ R^2 \tag{56}$$

The weight of the dome skin is

$$W_{dom,\,sk} = (A_{dom}\ t_{dom,\,sk,\,des}\ \rho_m)/12. \tag{57}$$

The weight of the hatch rings on the point design tank was 13.4 lbs. The hatch sizes should remain essentially constant on any size tank. Thus weight changes will result primarily from either a material or a pressure change from the point design. The dome end weight is

$$W_{dom} = W_{dom,\,sk} + 13.4 \left(\frac{\rho_m}{513}\right)\left(\frac{P_{des}}{30}\right) \tag{58}$$

Intermediate Frames - The intermediate frames are equally spaced through the cylinder section of the tank. The frame spacing is assumed to be proportional to R/L_{cyl}. The point design frame spacing is 10 inches. The frame spacing for a different size tank is

$$Sp = 10. \left(\frac{R}{8/3}\right)\left(\frac{20.}{L_{cyl}}\right) \tag{59}$$

The general bending moment equation for the intermediate frames is

$$M_{if} = G\ Sp\ f_{cb}\ \frac{R}{8/3}\ X\ (\text{unit bending moment}) \tag{60}$$

A factor, f_{cb}, is used to proportion the shear load between the center beam (Y-section and truss) and the nacelles (cylinder sections). The tank design is based on an unpressurized condition with nacelle skin buckling. The buckling factor developed from the point design analysis, $f_{cb} = 0.64$, is recommended for this design concept.

Intermediate frame bending moments result from inertia loading due to tank skin, insulation, and propellant weight; the point design unit bending moments were 2.9, 4.1

and 21. in-lb/in respectively. The unit bending moment due to tank skin will vary with thickness, material density, and radius.

$$M_{if,m} = G\ Sp\ f_{cb}\ \frac{R}{8/3}\left[2.9\left(\frac{t_{cyl,sk,des}}{0.016}\right)\left(\frac{\rho_m}{513}\right)\left(\frac{R}{8/3}\right)\right] \tag{61}$$

The unit bending moment due to insulation will vary with insulation weight. The point design insulation weight is 620 lb.

$$M_{if,i} = G\ Sp\ f_{cb}\ \frac{R}{8/3}\left[4.1\ \frac{W_{T,i}}{620}\right] \tag{62}$$

The unit bending moment due to propellant weight will vary with tank radius.

$$M_{if,\ell} = G\ Sp\ f_{cb}\ \frac{R}{8/3}\left[21.\ \frac{R}{8/3}\right]$$

The intermediate frame section modulus is

$$Sc_{if} = (M_{if,m} + M_{if,i} + M_{if,\ell})/(.833\ f_{crf}\ F_{tu}) \qquad F_{tu}\ @\ 540°R \tag{63}$$

The required cross-sectional area of an intermediate frame was plotted versus section modulus for several frame sizes in the point design. The resulting curve fit is used to compute the area.

$$Ac_{if} = (.42\ Sc_{if})^{.6}/144 \tag{64}$$

The intermediate frame weight is increased by 30 percent to provide for gussets to connect the frame into the center beam.

$$W_{if} = 2\left(\frac{4}{3}\pi R\ Ac_{if}\ \rho_m\ 1.3\right) \tag{65}$$

The total intermediate frame weight is

$$W_{T,if} = W_{if}\ \frac{L_{cyl}}{Sp/12.} \tag{66}$$

Main Frames - The vertical shear load on the main frames is given by

$$Vs = 1/2\ (W_{T,i} + W_{T,if} + W_{cyl,sk} + m_{T,\ell})\ G\ f_{cb}$$

The bending moment on the main frames varies with tank radius and shear load. The

point design bending moment was 25000 in-lb and the vertical shear load was 4000 lb.

$$M_{mf} = 25000\left(\frac{R}{\delta/3}\right)\left(\frac{Vs}{4000}\right) \tag{67}$$

The main frame section modulus is

$$Sc_{mf} = M_{mf}/f_{crf}\ F_{tu} \qquad F_{tu}\ @\ 540^{\circ}R \tag{68}$$

The required cross-sectional area of the main frame was plotted versus section modulus for several frame sizes in the point design. The resulting curve fit is used to determime the area

$$Ac_{mf} = (.40\ Sc_{mf})^{.6}/144 \tag{69}$$

The main frame weight is increased 66 percent to provide for gussets to connect the frames into the center beam.

$$W_{mf} = 2(\frac{4}{3}\ \pi R\ A_{mf}\ \rho_m\ 1.66) \tag{70}$$

Truss - The truss consists of vertical and diagonal members. The weight analysis for the upright members is

$$L_{up} = 1.732\ R \tag{71}$$

$$Ld_{up} = 12(f_{bu}\ P_{des}\ R\ Sp) \tag{72}$$

$$Ac_{up} = (1.2\ Ld_{up}/F_{tu})/144 \qquad F_{tu}\ @\ T_{sk,\,max} \tag{73}$$

$$W_{up} = Ac_{up}\ L_{up}\ \rho_m\left(\frac{L_{cyl}}{Sp/12}\right) \tag{74}$$

The weight analysis of the diagonal members is

$$L_{dg} = \sqrt{(Sp/12)^2 + L_{up}^2} \tag{75}$$

$$Ld_{dg} = Vs\ L_{dg}/L_{up} \tag{76}$$

$$Ac_{dg} = (1.2\ Ld_{dg}/F_{tu})/144 \qquad F_{tu}\ @\ 540^{\circ}R \tag{77}$$

$$W_{dg} = Ac_{dg}\ L_{dg}\ \rho_m\left(1.0 + \frac{L_{cyl}}{Sp/12}\right) \tag{78}$$

The total truss weight is

$$W_{tr} = W_{up} + W_{dg} \tag{79}$$

Y-Section - The Y-section size can be critical to any of three conditions:

1) Manufacturing constraints for machining the Y and doubler buildup for welding require that a minimum cross-sectional area given by equation (80) be maintained.

$$Ac_y = (34\ t_{cyl,sk,des})/144 \tag{80}$$

2) The beam action of the tank in bending results in the Y-sections acting as major longerons which must not buckle. The design for this condition is

$$w_{cyl} = (W_{T,i} + W_{cyl,sk} + W_{T,if} + W_{tr} + m_{T,\ell})/L_{cyl} \tag{81}$$

$$M_{cyl,max} = 12\left[(G\ w_{cyl}/8.0)\ L_{cyl}^2\right] \tag{82}$$

$$Ac_y = M_{cyl,max}\ f_{cb}/(12\ L_{cyl}\ f_{cry}\ F_{tu}) \qquad F_{tu}\ @\ T_{sk,max} \tag{83}$$

3) The design must provide for local bending of the Y-section between truss uprights.

$$M_{y,max} = f_{bu}\ P_{des}\ R\ Sp^2 \tag{84}$$

$$Ac_y = \frac{3t_{cyl,sk,des}}{144}\sqrt{\frac{2M_{y,max}}{t_{cyl,sk,des}\ f_{crf}\ F_{tu}}} \qquad F_{tu}\ @\ T_{sk,max} \tag{85}$$

The maximum required cross-sectional area is used for the design.

$$Ac_{y,max} = \text{maximum of } Ac_y \text{ from equations (80), (83), (85)}$$

The Y-section weight is

$$W_y = 2(Ac_{y,max}\ L_{cyl}\ \rho_m) \tag{86}$$

Doublers and Supports - The doubler weight is a percentage of the total installation weight based on point design values. A sensitivity to pressure change is also included.

$$W_{dbl} = .0034(W_{cyl,sk} + W_{T,if} + W_{mf} + W_{tr} + W_y + W_{dom} + W_{T,i} + m_{T,\ell})\left(\frac{P_{des}}{30}\right) \tag{87}$$

The support weight is proportional to the total load.

$$W_{sup} = .00155 \left(W_{cyl,sk} + W_{T,if} + W_{mf} + W_{tr} + W_{y} + W_{dom} + W_{T,i} + m_{T,\ell}\right)\left(\frac{G}{3}\right) \quad (88)$$

3.5.5 VOLUME PENALTY - A volume to weight sensitivity is input to the program. This must be established for each individual vehicle being studied. It represents a payload gain per unit decrease in volume, lbs/ft^3. The penalty is obtained by comparing the actual installed volume of the tank to an arbitrary reference volume. The difference between these volumes times the coefficient gives the volume penalty

$$W_{vp} = f_{vp} \left(V_T - V_{ref}\right) \quad (89)$$

W_{vp} has no particular meaning for a single tank calculation but can be used to select an optimum installation when an array of parameters is being investigated for a given vehicle installation. The sum of the actual weight and the volume penalty can be plotted parametrically to determine the optimum. The installed tank volume is illustrated in Figure 56. It is a flat ended can which covers the tank, insulation and end domes. The reference volume is assumed to be the actual volume of useful fuel (@ standard density) or an arbitrary reference volume, can be input to the program. For the volume penalty to be meaningful this value should be held constant for a given tank evaluation.

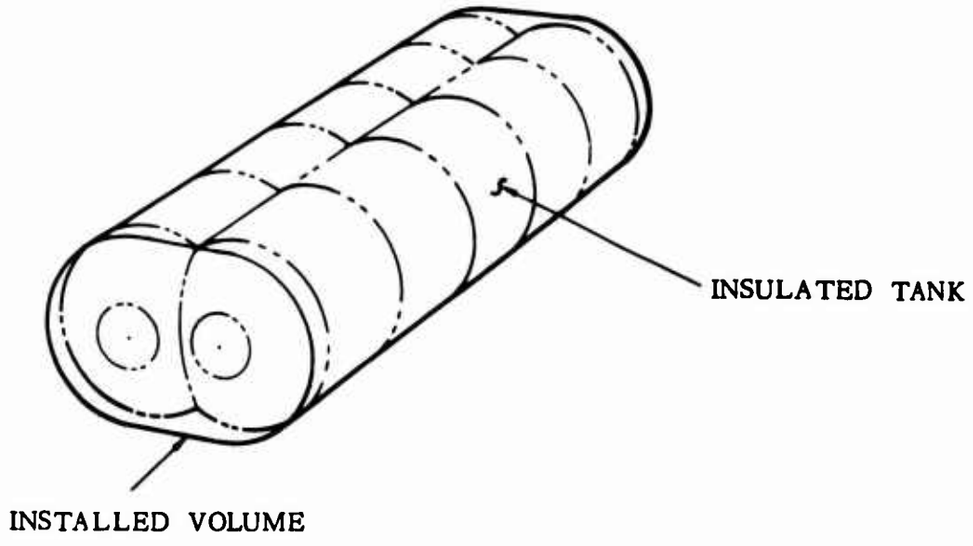

Figure 56. Installed Tank Volume

4.0 OPTIMIZATION PARAMETERS

The full scale tank size selected for the optimization is a nominal 50,000 gallons. The radius and center-to-center spacing of the intersecting cylinders is 5.33 feet. The cylinder section length is approximately 40 feet. The usable fuel quantity is held constant while the tank length varies as a function of the optimizing parameters.

The basic mission parameters include a 30 minute ground hold and 90 minute hypersonic flight. The environmental temperature on the top and bottom of the vehicle and the environmental pressure schedule are given in Figure 57. The fuel flow schedule scaled from the total vehicle fuel flow requirements given by the contract work statement is shown in Figure 57. This fuel flow schedule gives a usable fuel quantity of 26,985 lbs. Also shown on Figure 57 is the heat rejection rate to the fuel from the submersible boost pump. The heat rejection rate was scaled from the operating efficiency data on the pump used in the large scale tank test program.

The unusable fuel depth was assumed to be 4 inches. The minimum ullage space was assumed to be 6 inches. The tanking liquid level varied as a function of the optimizing parameters and was computed so that this minimum (6 inch) ullage space was not exceeded as the liquid expanded due to heating at ground hold. The tanking and chilldown is assumed to be done with the tank vented to atmospheric pressure (14.7 psia). Top-off is assumed to be at 16.7 psia. This is sufficient to surpress boiling during top-off and to provide a pressure differential for vent control during topping. The operating pressure was one of the optimizing parameters and was evaluated over the range 17 to 40 psia.

The tank structural material is aged and 30% cold rolled Inconel 718. The minimum gage is 0.010 inches. The yield and ultimate strength of the material used in the optimization analysis is shown in Figure 58. Cryogenic allowables were not used. This is illustrated in Figure 58 where allowables are constant below room temperature. The tank design coefficients used to determine weights were discussed in Section 3 and are listed in Table VIII.

The insulation system is helium purged quartz fiber. This is the same system used on the large scale test tank. The weight coefficients for this insulation system are given in Table VIII. The weight coefficients for the subsystems are also given in Table VIII. The insulation system was optimized for both top and bottom thickness. The bottom thickness was evaluated over a range of 3 to 5 inches. The top thickness was evaluated over a range of 0.5 to 2.0 inches. The transient heat flux through the insulation is illustrated in Figure 59 for the range of insulation thicknesses evaluated. Heat flux through the supports and penetrations is shown in Figure 60. These values were scaled from the large scale test tank support and penetration heat leak data.

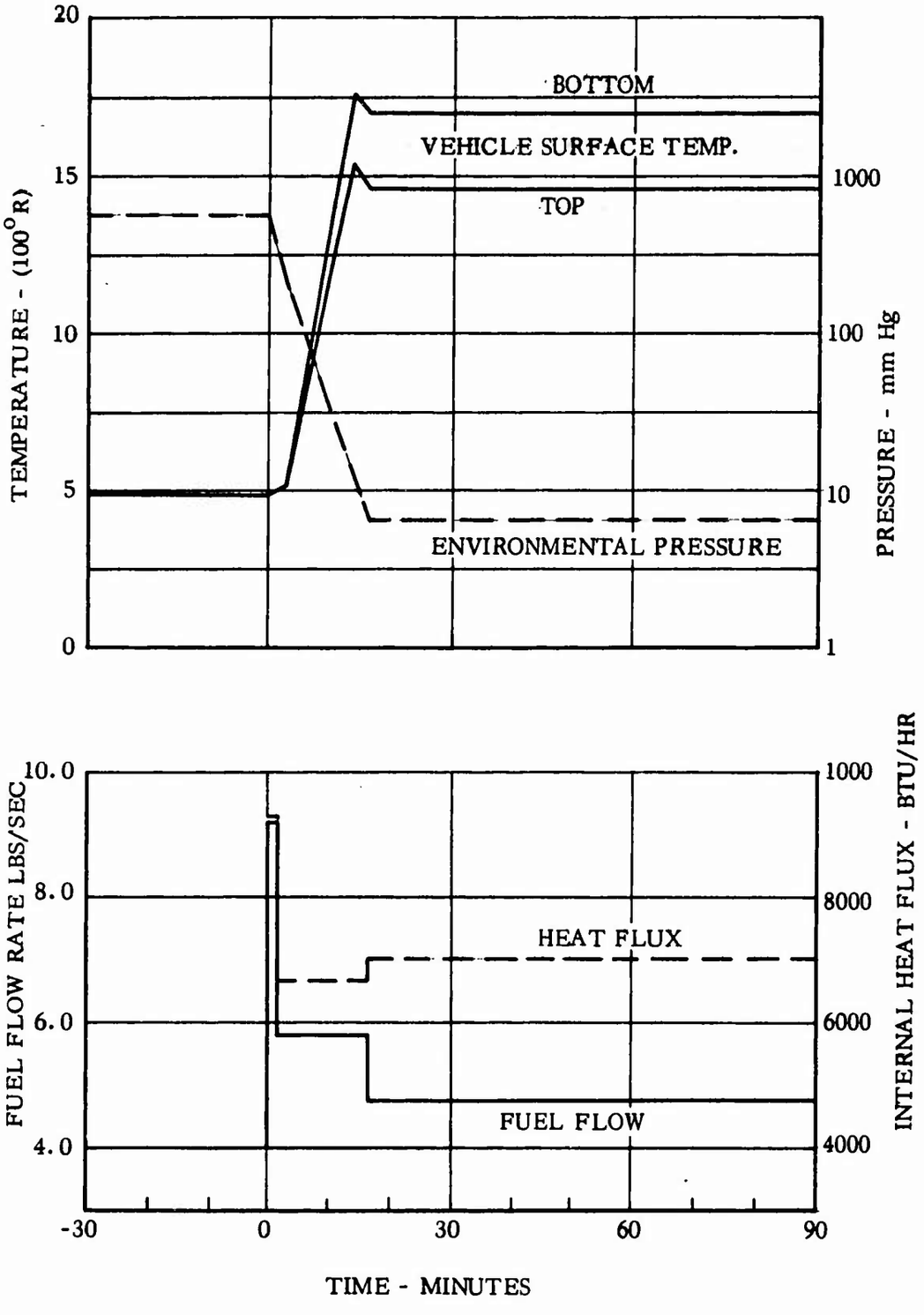

Figure 57. Trajectory/Mission Parameters for Full Scale Vehicle Tank

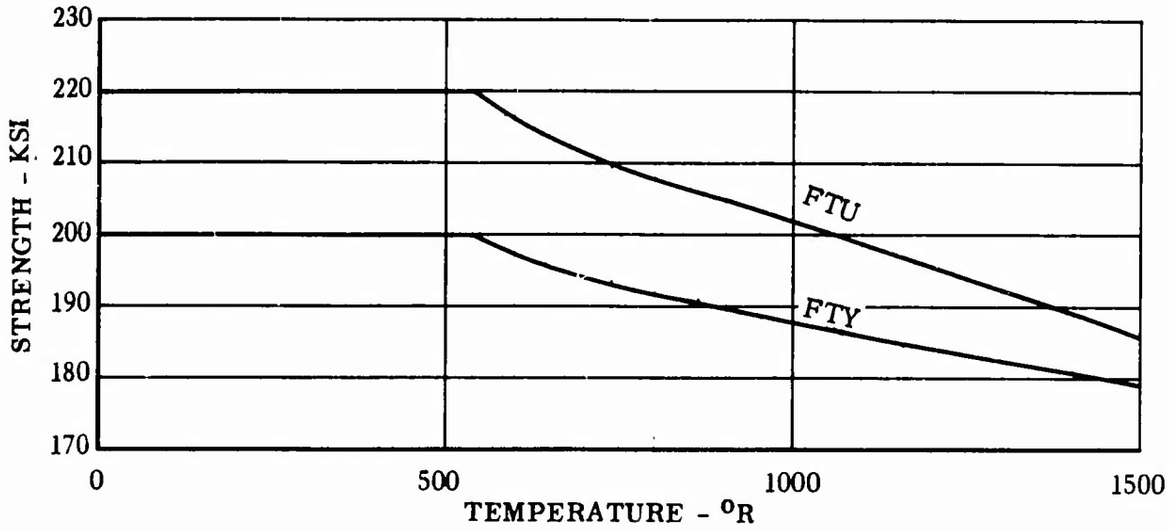

Figure 58. Yield and Ultimate Strength of 30% Cold Worked and Aged Alloy 718.

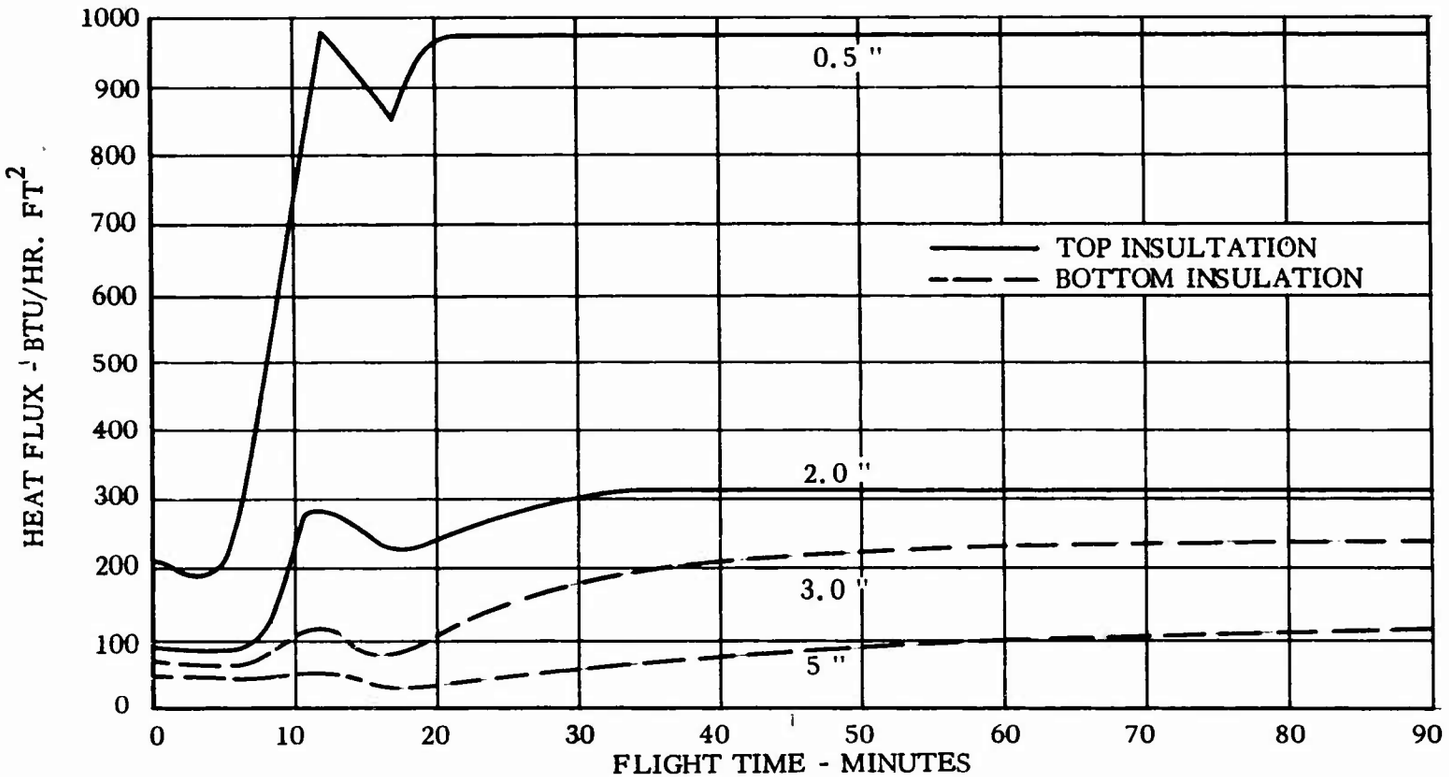

Figure 59. Heat Flux Through Quartz Fiber Insulation in Helium

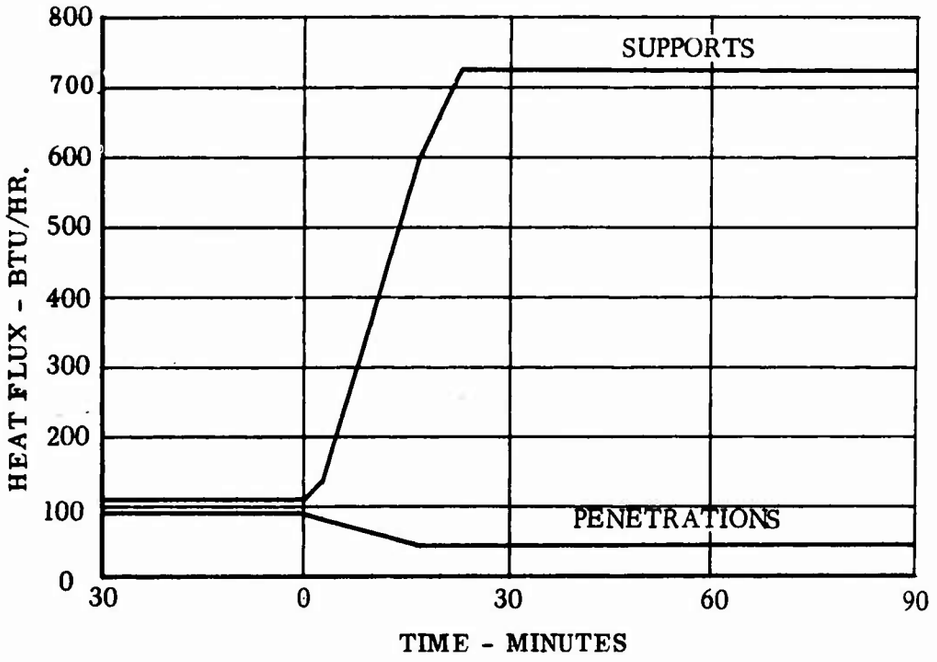

Figure 60. Heat Flux Through Supports and Penetrations.

The independent variables used to optimize were operating pressure, top insulation thickness and bottom insulation thickness. An additional variable or limit is maximum tank structure temperature. This variable is used when there are required temperature limits on tank structure or insulating materials. It can also be used as an optimizing parameter. Generally the tank structure weight and the boil-off can be reduced by lowering the maximum operating temperature. This is done, of course, at the expense of spray system and sprayed fuel weight for cooling. The temperature of the tank structure for the optimum tank in this analysis was 660°R (200°F). This is well within the operating limit of both the structural material and the insulation. The structural material is within 3% of its maximum allowable at this temperature. Thus the optimization did not include temperature as a parameter.

5.0 OPTIMIZATION RESULTS

The tank installation was optimized to obtain a minimum total take-off weight. The component weights which make up the take-off weight are tank structure, insulation, subsystems and fuel. The fuel weights consist of boil-off, unusable and usable (26,985 lbs). The magnitude of these variable weights is illustrated in Figure 61. The weights are shown as a function of operating pressure with bottom insulation thickness as a parameter for a top insulation thickness of one inch. The boil-off weight varies significantly with both pressure and insulation thickness. The boil-off is greatest at low operating pressure. The lower the operating pressure, the sooner the bulk liquid starts boiling. Thus the liquid level is higher in the tank when bulk boiling starts so that an increasingly larger amount of boil-off results as the operating pressure is reduced. The boil-off represents 1 to 8 percent of the total take-off weight. The insulation weight varies primarily as a function of insulation thickness. The small weight change with pressure is the result of increasing tank size at lower pressures due to increased boil-off. The insulation represents 6 to 9 percent of the total take-off weight. The tank structure is the largest inert weight and varies predictably with pressure. The increase in tank structure weight with decreasing insulation thickness is the result of an increasing tank size. With less insulation the boil-off is greater thus a larger tank is required to contain the total propellant. The tank structure represents 10 to 15 percent of the total take-off weight. The unusable fuel is relatively constant and is less than one percent of the total take-off weight. The subsystem weight consists of the fuel system (95 lbs) and the vent system. The vent system weight varies with maximum venting rate so that this weight is generally proportional to boil-off. The vent system represents less than one percent of the total take-off weight.

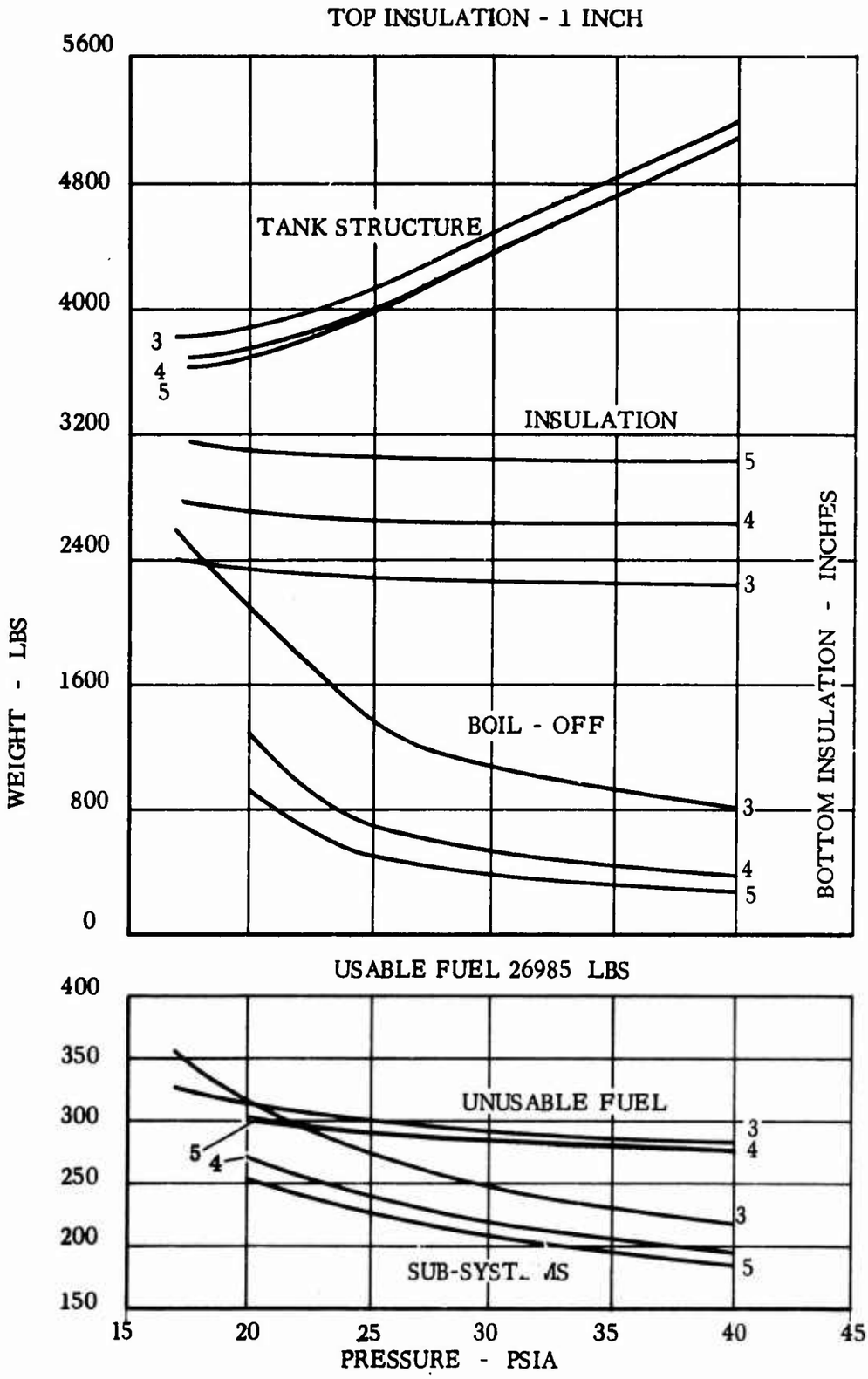

FIGURE 61. Full Scale Vehicle Tank Weight Breakdown

The optimum take-off weight was determined by parametrically plotting total weight as a function of top and bottom insulation thickness and operating pressure. The minimum weight points from these parametric plots are cross-plotted to obtain the value of each parameter at the overall minimum (optimum) weight. Plots of total weight at three top insulation thicknesses are shown in Figure 62. The weights are plotted as a function of bottom insulation thickness at various pressures. Plots of total weight at three bottom insulation thicknesses are shown in Figure 63. The weights are plotted as a function of pressure at various top insulation thicknesses. Plots of total weight at four pressures are shown in Figure 64. The weights are plotted as a function of top insulation thickness at various bottom insulation thicknesses. This set of parametric plots are cross-plotted to obtain a set of minimum values. The minimum weight points at each pressure for the three top insulation thicknesses in Figure 62 are plotted in Figure 65. This gives a set of minimum weight curves as a function of pressure for the three top insulation thicknesses. The minimum weight points from Figure 63 are plotted in Figure 66 to give a set of minimum weight curves as a function of top insulation thickness for three bottom insulation thicknesses. Figure 67 is cross-plotted the same way from Figure 64 to give a set of minimum weight curves as a function of bottom insulation thickness for four pressures. The minimum points from Figures 65, 66 and 67 are cross-plotted again in Figure 68 to obtain the optimum value of each of the independent variables. The optimum values are 24.5 psia operating pressure, 1.05 inches of top insulation and 4.1 inches of bottom insulation.

The optimization discussed above is based on actual total take-off weight of the tankage installation. The values are optimum for a vehicle which is insensitive to volume variation. Most aerodynamic vehicles are volume sensitive and generally both weight and volume must be simultaneously optimized to achieve a true optimum. The sensitivity of vehicle performance to changes in volume can be expressed as an equivalent weight. The addition of a unit volume to the vehicle requires additional airframe weight to contain the volume and additional propulsion weight to compensate for added aerodynamic losses. Lifting entry vehicles have a weight to volume sensitivity of 6 to 10 lbs/ft^3; hypersonic cruise vehicles have a weight to volume sensitivity of 5 to 8 lbs/ft^3. Supersonic vehicles have a weight to volume sensitivity of 1 to 4 lbs/ft^3.

The installed volume of this particular tank is discussed in Section 3.5.5 and illustrated in Figure 56. The installed volume of the tank for the range of parameters evaluated in this analysis is shown in Figure 69. The installed volume variation of the tank considered here is quite large and ranges from 7400 to 8000 cubic feet. It is interesting to note that the volume increases rapidly with decreasing pressure below 25 psia. The tank with a weight to volume sensitivity of zero optimizes at 24.5 psia and a volume of 7517 cubic feet.

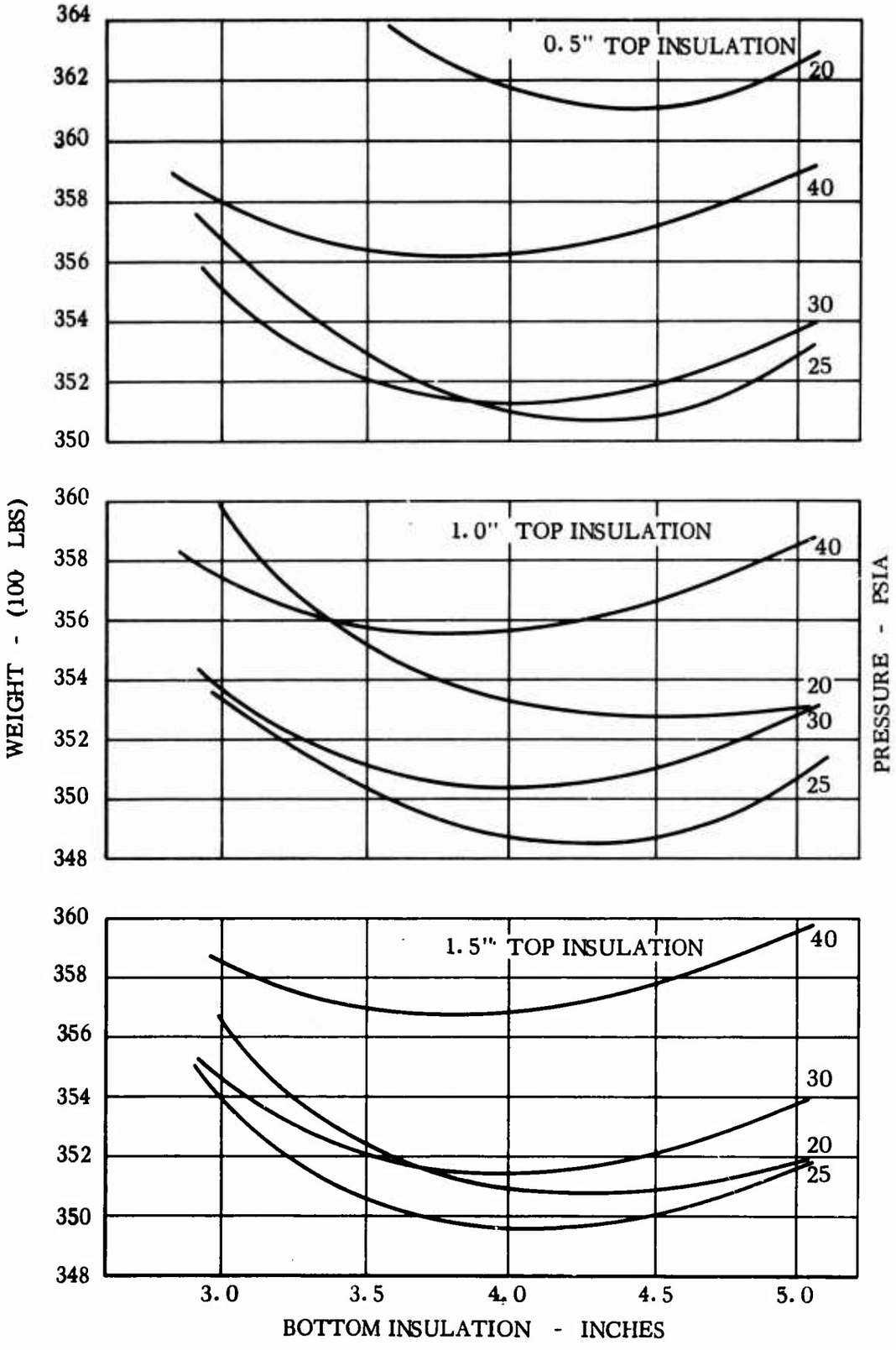

Figure 62. Total Tankage Weight vs. Bottom Insulation Thickness

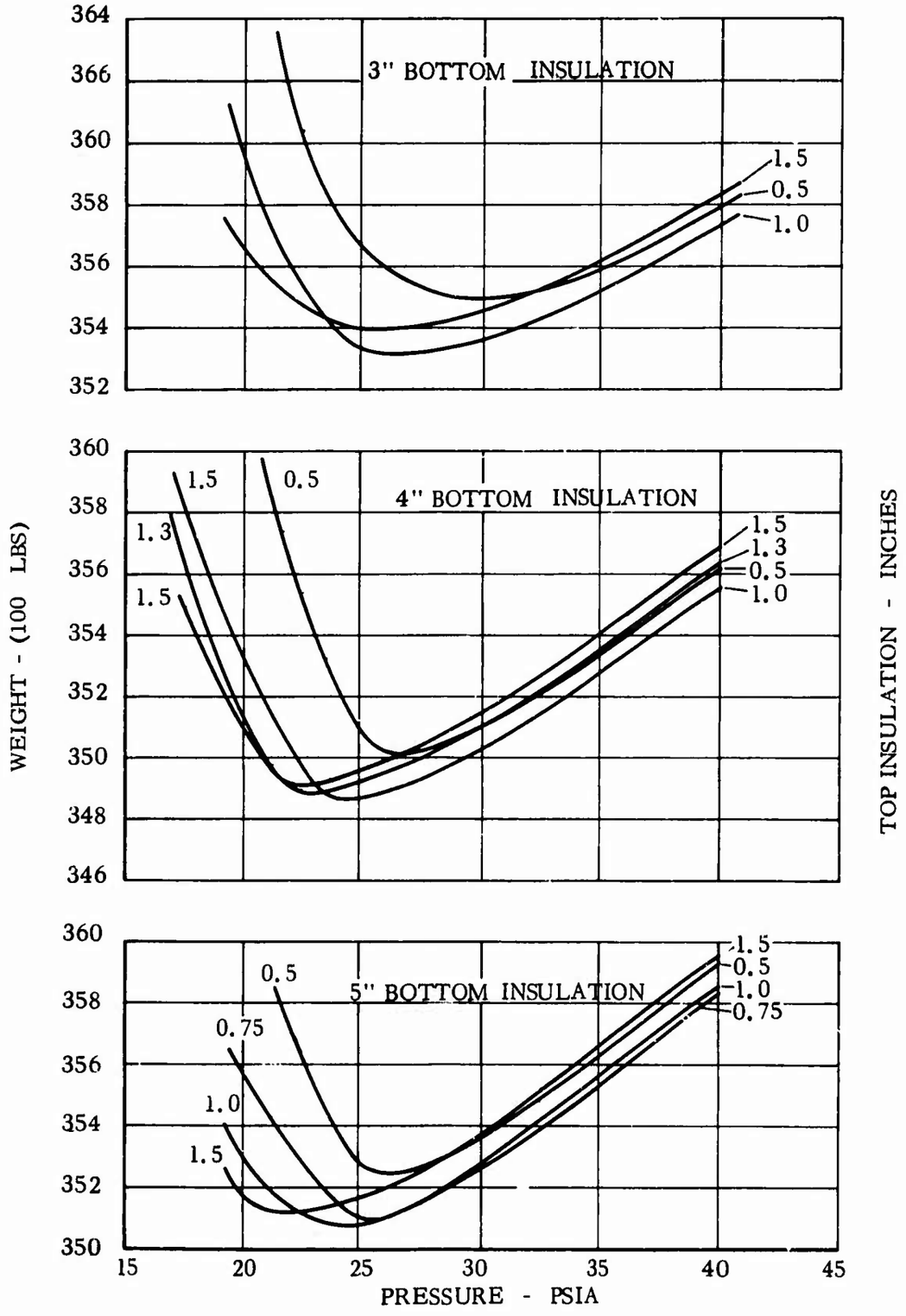

Figure 63. Total Tankage Weight vs. Operating Pressure

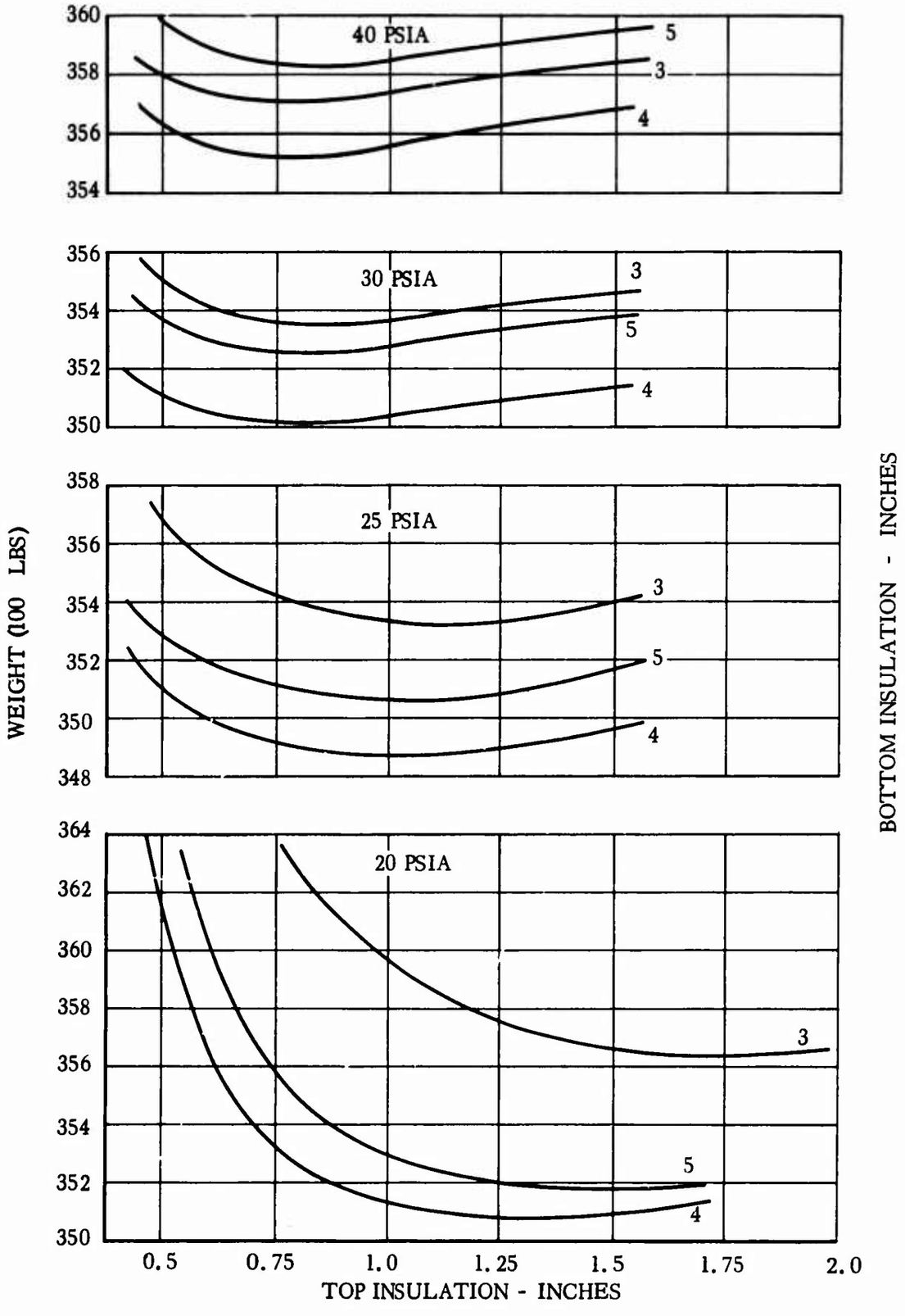

Figure 64. Total Tankage Weight vs. Top Insulation Thickness

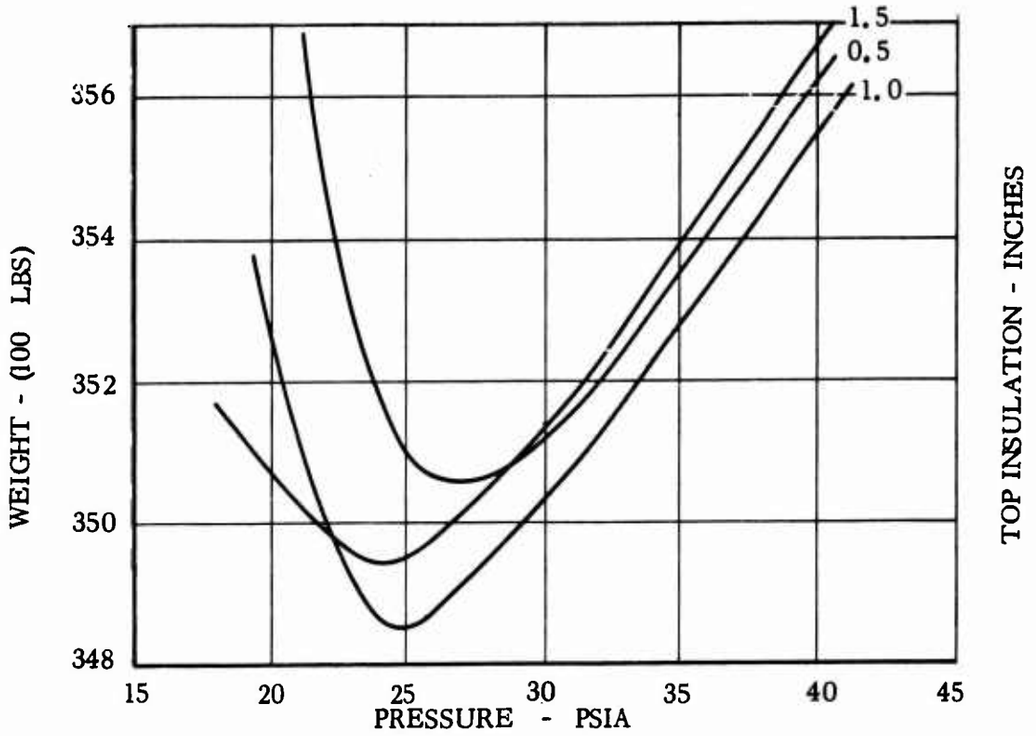

Figure 65. Minimum Tankage Weight vs. Operating Pressure

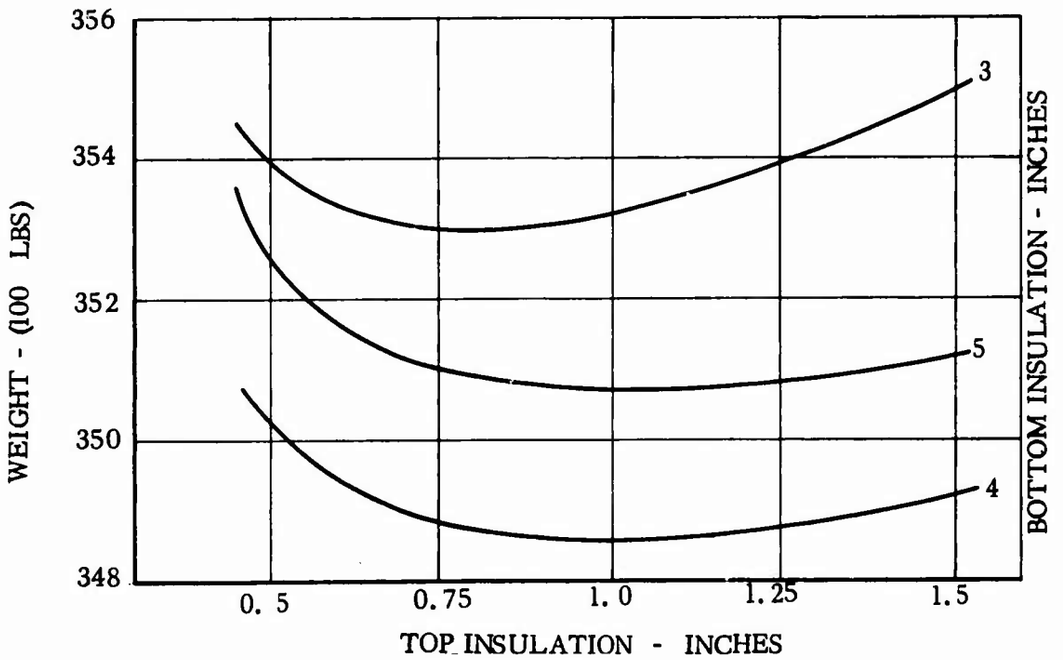

Figure 66. Minimum Tankage Weight vs. Top Insulation Thickness

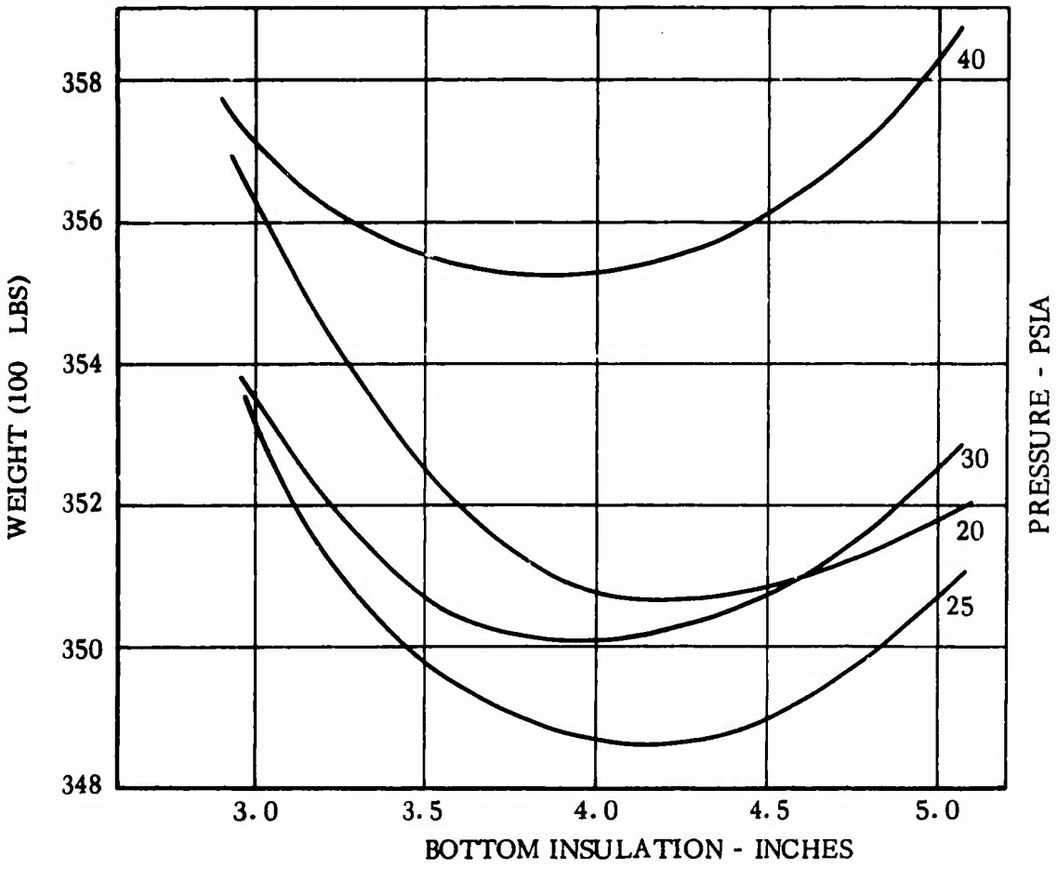

Figure 67. Minimum Tankage Weight vs. Bottom Insulation Thickness

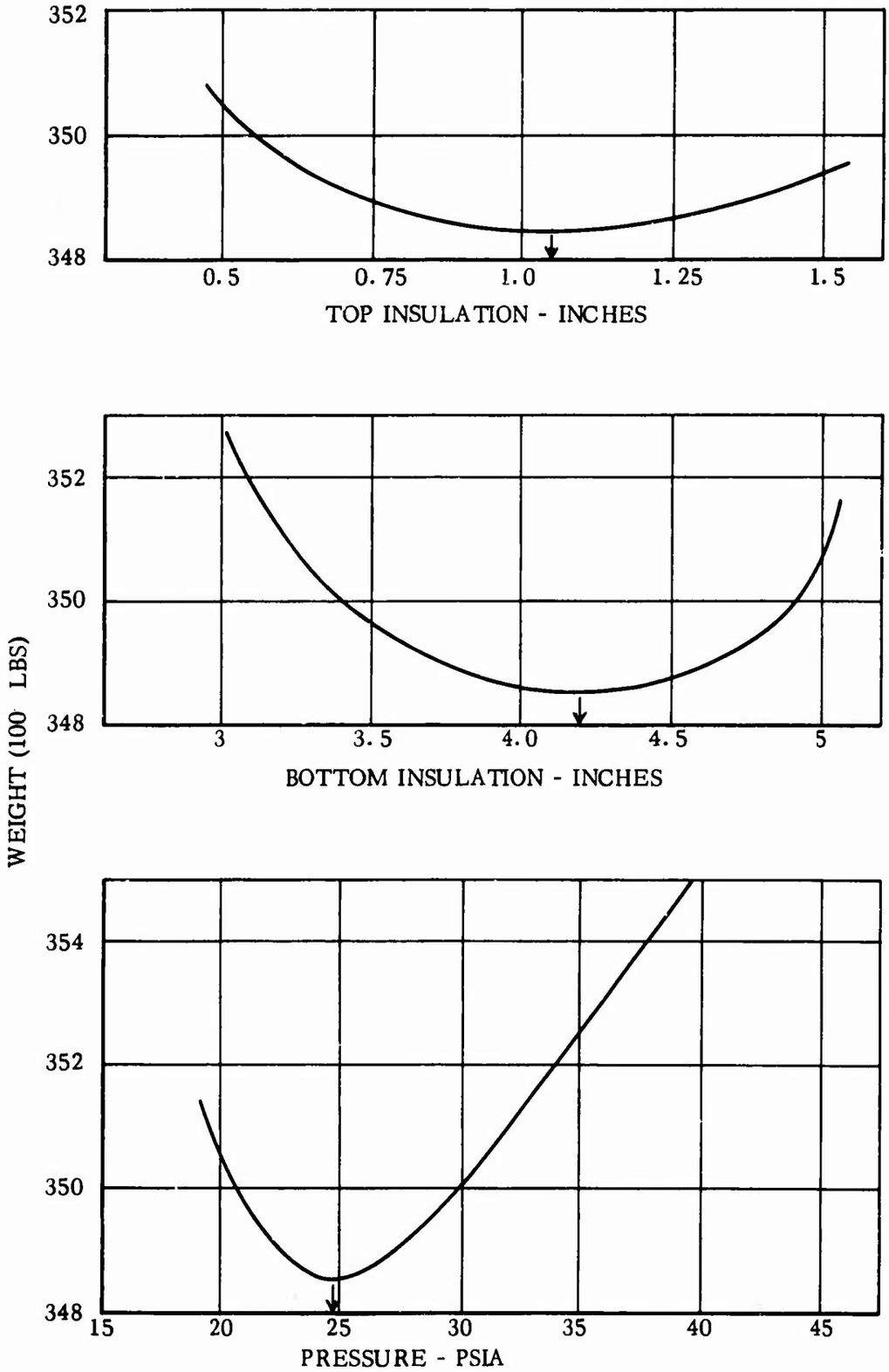

Figure 68. Optimum Full Scale Tank Parameters

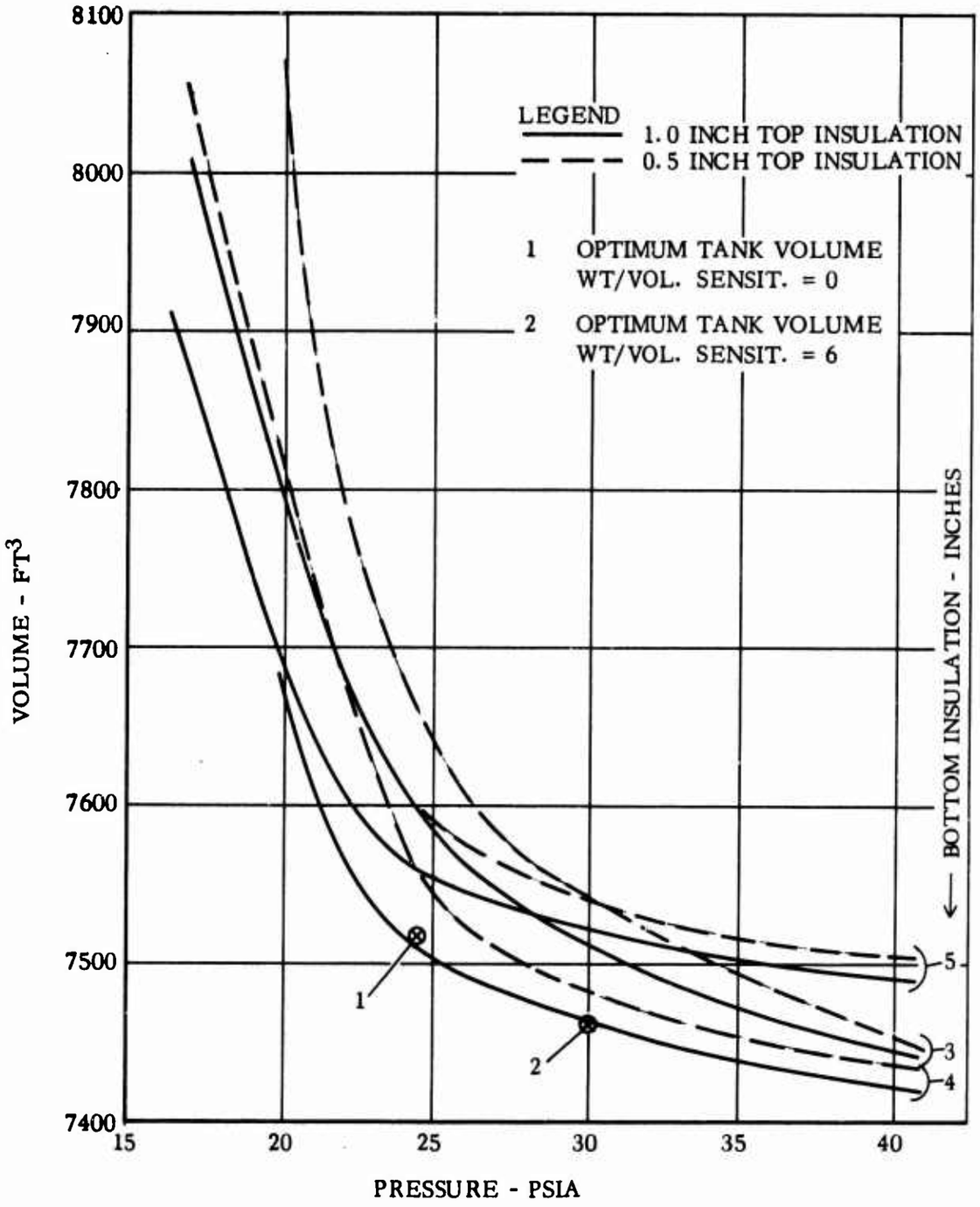

Figure 69. Tankage Installed Volume

The tank has also been optimized for a weight to volume sensitivity of 6. An equivalent weight for each tank is computed using the volume penalty correction, equation (89). In this case reference volume has been arbitrarily chosen as 7517 cubic feet, the volume of the previously optimized tank. The actual weight of each tank is corrected to an equivalent weight by algebraically adding the volume penalty correction to the actual tank weight.

For tanks with a volume less than the reference volume the correction is negative and the equivalent weight is less than the actual weight. This shifts the optimum equivalent weight to a lower volume tank. The total equivalent weights are parametrically plotted in Figures 70, 71 and 72 for a weight to volume sensitivity of 6. The minimums from these curves are cross-plotted as in the previous optimization to obtain the final minimum equivalent weight parameters shown in Figure 73. The optimum parameters in this case are 0.86 inches top insulation, 3.95 inches bottom insulation and 30 psia operating pressure. The optimum volume is 7462 cubic feet and is shown on Figure 69. The volume is 55 cubic feet less than the optimum tank with a weight to volume sensitivity of zero. The variation in optimum conditions as a function of volume to weight sensitivity is shown in Figure 74. Insulation thicknesses vary only a small amount and tend to decrease as weight to volume sensitivity increases. The optimum operating pressure increases with weight-to-volume sensitivity. Increasing the operating pressure decreases the volume of the tank by reducing the amount of boil-off. The actual take-off weight is increased from 34805 pounds to 35033 pounds; an increase of 228 pounds. The volume, however, has been reduced by 55 cubic feet. This represents an airframe weight savings of 6 x 55 = 330 pounds. The net reduction then in overall airframe weight is 102 pounds when the weight-to-volume sensitivity is considered in the optimization. Computer runs were made at the optimum parameters for weight-to-volume sensitivities of zero and six. The results are tabulated in Table IX to illustrate the thermal performance and weight data generated by the computer program. The mass fraction of these 50,000 gallon tanks is 0.77, usable fuel to total take-off weight ratio. This compares to a mass fraction of 0.65 for an optimum 6000 gallon tank with the same insulation and tank structural material. The larger tank is considerably more efficient. When considering a total vehicle, tank sizes will become an additional parameter to be considered in the optimization.

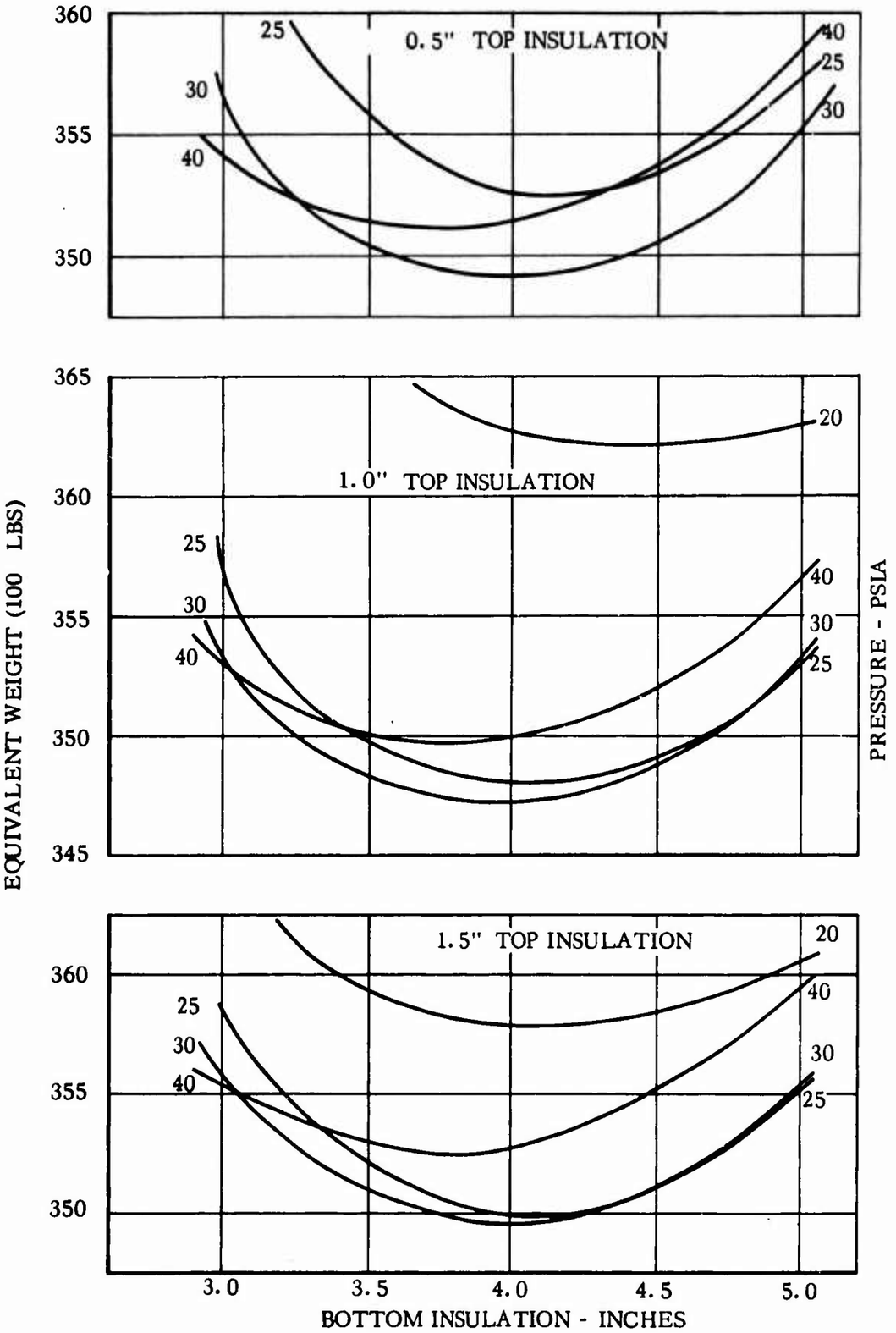

Figure 70. Equivalent Tankage Weight vs. Bottom Insulation Thickness (Weight-to-Volume Sensitivity = 6)

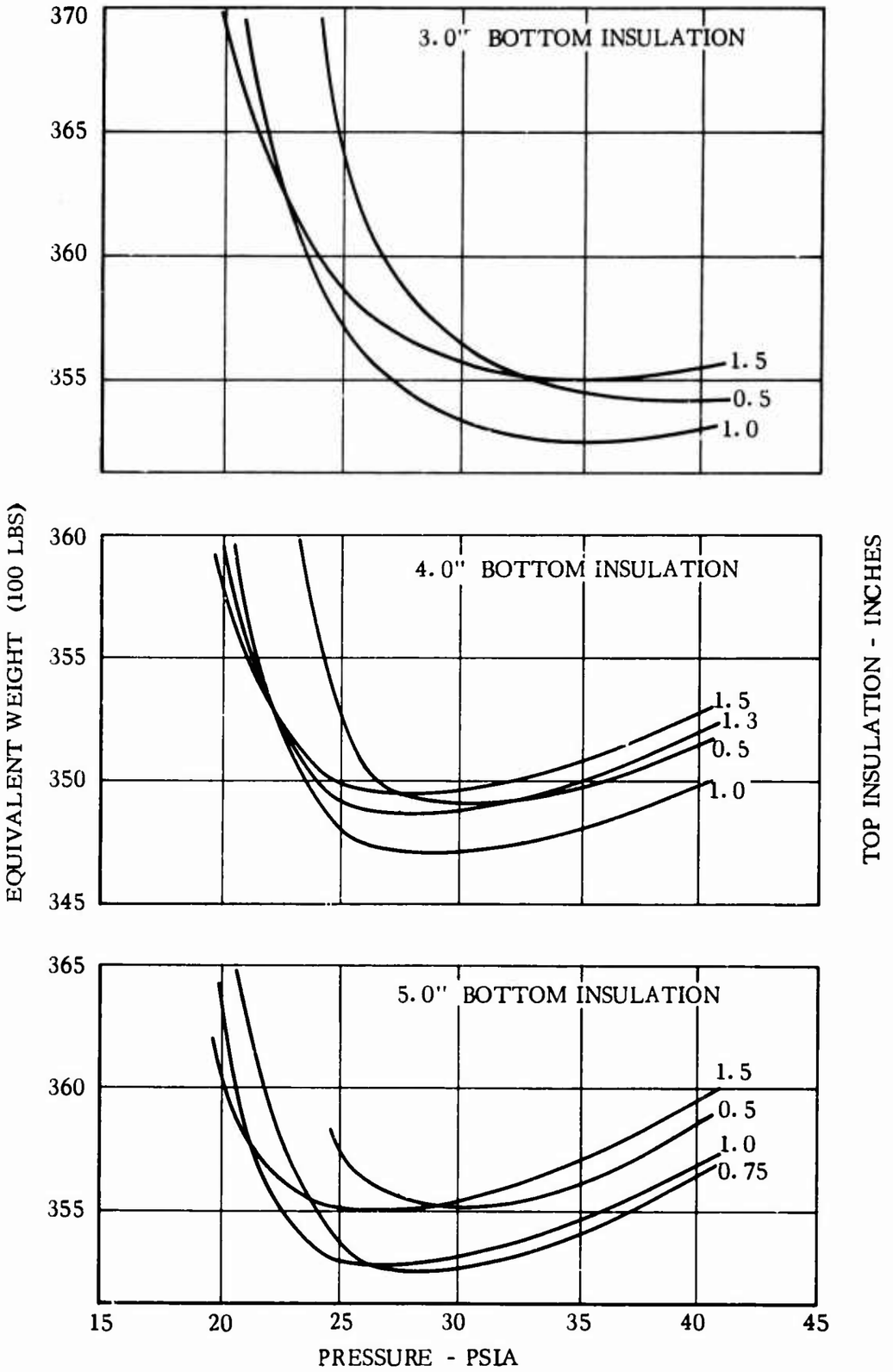

Figure 71. Equivalent Tankage Weight vs. Operating Pressure (Weight-to-Volume Sensitivity = 6)

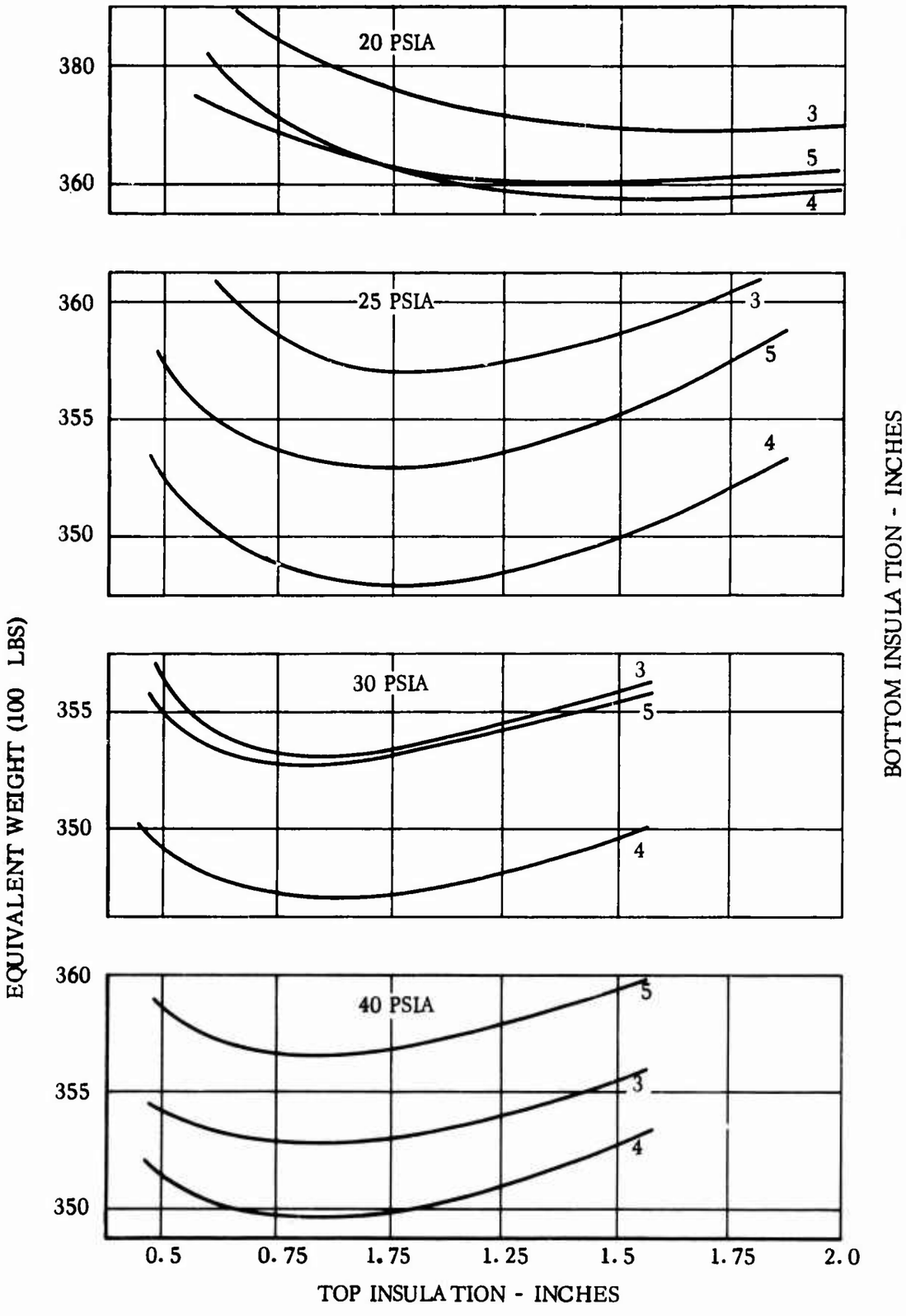

Figure 72. Equivalent Tankage Weight vs. Top Insulation Thickness (Weight-to-Volume Sensitivity = 6)

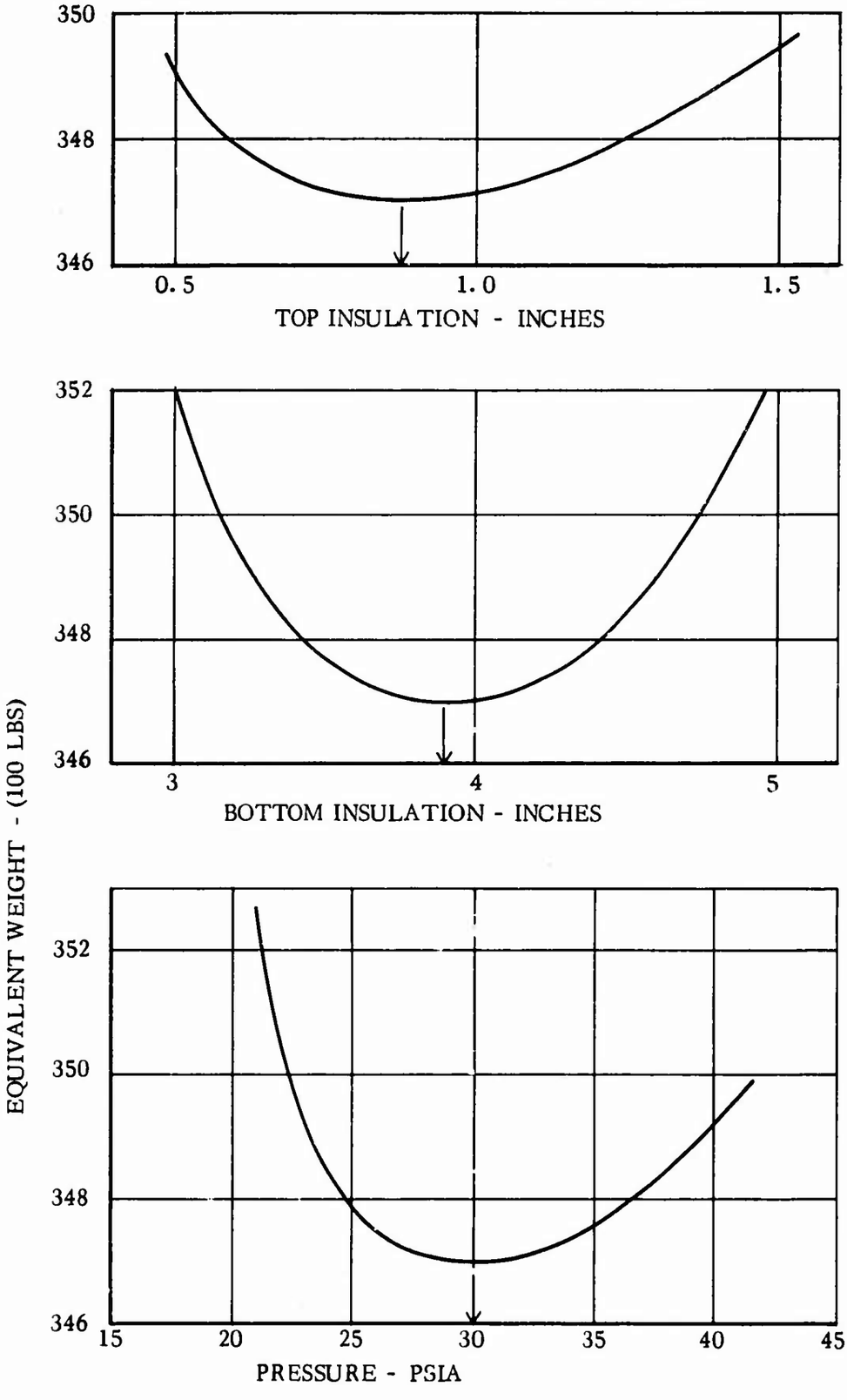

Figure 73. Optimum Full Scale Tank Parameters
(Weight-to-Volume Sensitivity = 6)

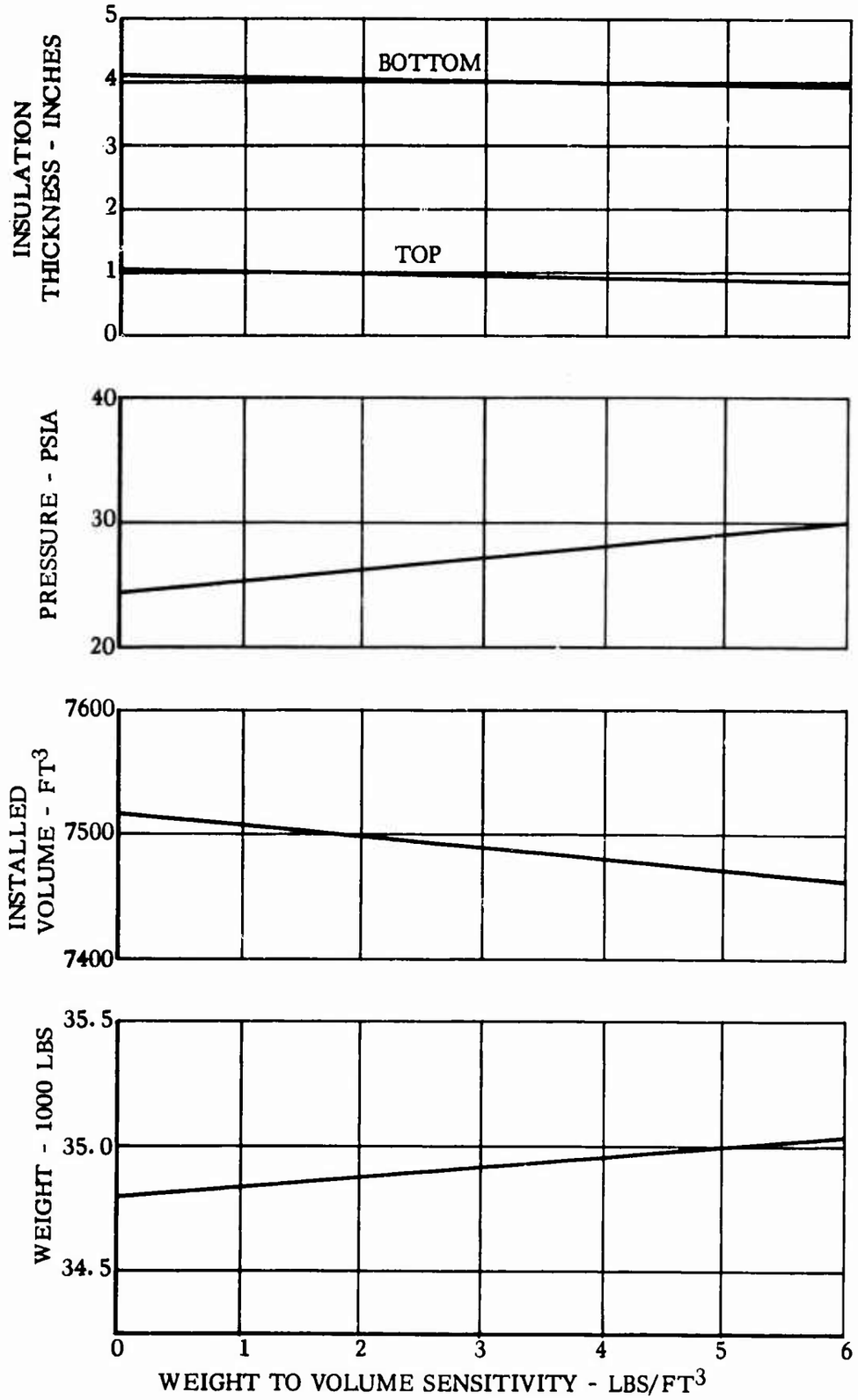

Figure 74. Optimum Parameters of Full Scale Vehicle Tank as a Function of Vehicle Weight to Volume Sensitivity

Table IX. Full Scale Vehicle Tank - Thermal Performance, Size and Weight

Intersecting cylinder tank with center-to-center spacing, one radius. Ellipsoidal dome ends.

Diameter = 128 in. Maximum liquid level = 122 in.
Vent height = 127 in. Unusable liquid level = 4 in.

	Optimum Weight Tank	Optimum Tank, Wt/Vol Sens. = 6
Tanking pressure, psia	16.7	16.7
Operating pressure, psia	24.5	30.0
Tanking liquid level, in.	120.15	120.0
Length (overall), ft.	47.92	47.79
Length (cylinder), ft.	40.38	40.25
Tank volume, ft^3	6564	6545
Heat input to liquid, BTU		
Insulation	255952	278826
Radiation from top, $\epsilon = 0.2$	16124	46610
Internal (pump)	10509	10509
Turbulent liquid surface	936	398
Supports and penetrations	1101	1101
Total	284621	337444
Design pressure, psig	25.7	31.5
Design (Max.) tank skin temperature, ^oR	661.	882.
	Weights	
Tank structure (Inconel 718, min. gage = 0.010 in.)		
Cylinder shells	1156.3 (.015 in.)	1459.9 (.019 in.)
Hatches and domes	263.9 (.013 in.)	324.7 (.016 in.)
Main frames	325.8	326.1
Intermediate frames	690.7	690.4
Y-section	720.8	746.4
Truss	577.6	655.2
Supports and doublers	153.7	177.3
Total	3888.8	4380.0
Insulation (Microquartz/Helium)		
Top (60^o angle from top)	509.2 (1.05 in.)	451.1 (0.86 in.)
Side	805.0	760.9
Bottom (60^o angle from bottom)	1403.7 (4.1 in.)	1355.1 (3.95 in.)
Total	2717.9	2567.1
Subsystems		
Fuel	94.7	94.7
Vent	143.2	135.2
Total	237.9	229.9
Propellant		
Boil-off	682.9	586.2
Unusable	292.7	287.1
Usable	26985.3	26985.3
Total	27960.9	27855.5
Total weight, lbs.	34805.4	35032.7
Installed Volume, ft^3	7517	7462
Installed volume penalty, lbs	0	-330
Installed equivalent weight	34805.4	34732.7
Mass fraction = $\frac{\text{usable fuel}}{\text{total weight}}$	0.7753	0.7703

GENERAL DYNAMICS

Convair Division

UNCLASSIFIED

Security Classification

DOCUMENT CONTROL DATA - R & D

(Security classification of title, body of abstract and indexing annotation must be entered when the overall report is classified)

1. ORIGINATING ACTIVITY (Corporate author)	2a. REPORT SECURITY CLASSIFICATION
Convair Division of General Dynamics Corp. San Diego, California	UNCLASSIFIED
	2b. GROUP

3. REPORT TITLE

HYDROGEN TANKAGE APPLICATION TO MANNED AEROSPACE SYSTEMS, PHASE II & III
Volume I. Design and Analytical Investigations

4. DESCRIPTIVE NOTES (Type of report and inclusive dates)
Phases II & III, Final Technical Report, November 1965 to April 1968.

5. AUTHOR(S) (First name, middle initial, last name)
Heathman, John H., et al

6. REPORT DATE	7a. TOTAL NO. OF PAGES	7b. NO. OF REFS
April 1968	166	16

8a. CONTRACT OR GRANT NO.	9a. ORIGINATOR'S REPORT NUMBER(S)
AF33(615)-2048 b. PROJECT NO. 651G	AFFDL-TR-68-75, Volume I
c.	9b. OTHER REPORT NO(S) (Any other numbers that may be assigned this report) GDC-DCB68-008, Volume I
d.	

10. DISTRIBUTION STATEMENT
This document is subject to special export controls and each transmittal to Foreign governments or Foreign Nationals may be made only with prior approval of the AFFDL/FDTS.

11. SUPPLEMENTARY NOTES	12. SPONSORING MILITARY ACTIVITY
	AF Flight Dynamics Laboratory FDTS Wright-Patterson AFB, Ohio

13. ABSTRACT

This volume of the final report presents the designing criteria and groundrules, design of the tankage systems structure, insulation and fuel system together with analytically investigations supporting these designs. The design of this 6,000 gallon liquid hydrogen tank is representative of a half-scale version of that which might be employed for a Mach 6 hypersonic cruise vehicle application and incorporates most of the significant aspects of the tankage system which have influence on its overall performance. The structure is of pressure membrane construction, aligned to a maximum operating pressure of 30 psig, with frame stiffening of cylindrical shells to prevent collapse under the unpressurized condition. Skins are allowed to buckle elastically. The tank support system, located at the main frames, allows for the movement of the tank around a single fixed point within the vehicles hot structure. The tanks thin gage, 0.016, structural material is Alloy 718, a nickel-base heat resistant superalloy, employed primarily in the aged condition. The insulation employed is an all-Micro-Quartz system in a helium environment, distributed around the tank in such a manner as to provide maximum protection of the fuel. The fuel system employs a booster pump to handle saturated fuel conditions and a vent manifold system to ensure good distribution of the boiloff gas for upper tank wall cooling. A thermal performance and weight synthesis computer program was updated and used to provide evaluation of slush-hydrogen, thermal performance of the designed tank, and optimization of a vehicle-size tankage system.

DD FORM 1 NOV 65 1473

UNCLASSIFIED

Security Classification

14. KEY WORDS	LINK A		LINK B		LINK C	
	ROLE	WT	ROLE	WT	ROLE	WT
HYPERSONIC VEHICLE (U)						
HYDROGEN TANKAGE (U)						
SIAMESE CONFIGURATION (U)						
ALLOY 718 MATERIAL (U)						
INSULATION SYSTEM (U)						
MICRO-QUARTZ INSULATION (U)						
FUEL SYSTEM (U)						
HYDROGEN BOOST PUMP (U)						
THERMAL PERFORMANCE (U)						
WEIGHTS SYNTHESIS (U)						